Novel aspects of blood platelet function and biology measured by fluorescent flow cytometry.

Matthew Shaun Hindle

Submitted in accordance with the requirements for the degree of
Doctor of Philosophy

The University of Leeds
Faculty of Medicine and Health
Leeds Institute of Cardiovascular and Metabolic Medicine

November, 2019

The candidate confirms that the work submitted is his own and that appropriate credit has been given where reference has been made to the work of others.

Acknowledgements

Abstract

Fluorescent flow cytometry (FFC) is an accessible, high-throughput and sensitive technique that is well suited to analysis of cells suspended in complex heterogeneous media. Using a wide variety of live, fixed, extracellular, intracellular, dye/antibody/peptide based FFC assays, multiple and novel aspects of platelet biology including; activation, inflammation and mitochondrial function were examined.

Through the examination of platelet activation with multiparameter and multidimensional analysis three platelet subsets in PAR1/GPVI activated whole blood samples were described. This same assay in the presence of PGI_2 suggested a dichotomy in inhibition when comparing fibrinogen binding, phosphatidylserine (PS) exposure and CD62P. Using novel phosphoflow protocols the inhibition resistant expression of CD62P was shown to be independent of robust cAMP signalling. This CD62P expression was then shown to mediate platelet monocyte interactions – in the presence of inhibition.

Caspase-1 cleavage as a marker of NLRP3 inflammasome activity was measured using fluorescent peptide dyes. Activation was induced by canonical activators of the complex, but it was observed that this was significantly potentiated by oxidised LDL (oxLDL). ROS and calcium were also shown to have a vital role in activation of platelet NLRP3 and scavenging or chelation of either induced a loss of signal. Furthermore, active caspase-1 signal also correlated with PS exposure.

Finally, mitochondrial function in response to oxLDL *in vitro* and in the context of murine hyperlipidaemia *ex vivo* was measured using live cell dyes. *In vitro* stimulation with oxLDL drove an increase in both mitochondrial superoxide production and mitochondrial membrane potential. However, this was demonstrated to be important *in vivo,* as transgenic models of hyperlipidaemia showed a significant increase in basal mitochondrial superoxide compared to wild type control. This was recapitulated diet-induced obesity murine models and a trend towards increased mitochondrial superoxide and membrane potential was described.

Table of Contents

List of Tables

List of Figures

Publications

Oral presentations

ECTH, October 2019. Glasgow. <u>Oral presentation</u>: Multicolour flow cytometry reveals platelet subpopulations that are regulated by prostacyclin.

Platelet Society meeting, September 2019. University of Cambridge. <u>Oral presentation</u>: Multicolour flow cytometry reveals novel platelet subpopulations that are remodelled by cAMP signalling.

Poster presentations

CYTO, June 2019. Vancouver. <u>Poster presentation</u>: t-Distributed Stochastic Neighbourhood Embedding (Flt-SNE) and multicolour fluorescent flow cytometry identify novel context dependent platelet subpopulations. (Received a travel award)

Platelet Society early career research meeting, July 2018. Manchester Metropolitan University. <u>Poster presentation</u>: Multicolour whole blood platelet flow cytometry demonstrates functional differences in response to prostaglandin.

Journal articles

Berger M., Wraith K., Woodward C., Aburima A., Raslan Z., **Hindle MS**., Moellmann J., Febbraio M., Naseem KM. (2018). Dyslipidemia associated atherogenic oxidized lipids induce platelet hyperactivity through phospholipase Cγ2-dependent reactive oxygen species generation, *Platelets*, PM: 29733744

Berger M., Raslan Z., Aburima A., Magwenzi S., Wraith KS., Spurgeon BEJ., **Hindle MS**., Yusuf M., Law R., Febbraio M., Naseem KM. (2019). Atherogenic lipid stress induces platelet hyperactivity through CD36-mediated hyposensitivity to PGI$_2$ – the role of PDE3a, *Haematologica*, PM: 31289200

Hindle MS., Spurgeon BEJ., Cheah LT., Webb BA., Naseem KM. (2019). Multidimensional flow cytometry reveals novel platelet subpopulations in response to prostacyclin, <u>in submission</u>

Chapter 1
Introduction

1.1 PLATELETS

1.1.1 Platelet production and death

Platelets are anucleate cells that have been shown to have roles in haemostasis, thrombosis, innate immunity, wound healing and angiogenesis (Gibbins, 2004, Koupenova et al., 2018, Golebiewska and Poole, 2015, Blair and Flaumenhaft, 2009). They circulate in the body at a clinical reference range of 150-400 x 10^9 cells/L of blood (Bonaccio et al., 2016) and have a lifespan in circulation of approximately ten days. They are removed via Ashwell-Morrell receptors, in the hepatic vasculature, which recognise the desialyted surface proteins aged platelets display (Hoffmeister and Falet, 2016). As part of the apoptotic pathway in platelets, several key events occur which include; mitochondrial depolarisation, cytochrome C release, activation of apoptotic caspases culminating in caspase-3, exposure of phosphatidylserine and finally cellular blebbing and fragmentation (Gyulkhandanyan et al., 2012). Ageing of platelets is controlled by the major anti-apoptotic protein BCL-XL (Vogler et al., 2011) and this is suggested to be further regulated by cAMP-PKA activity (Zhao et al., 2017). The majority of platelets are produced within the bone marrow by the platelet pre-cursor cell, megakaryocytes (Parise, 2016), however, there is also evidence of a megakaryocyte population within the pulmonary system (Lefrancais et al., 2017). Megakaryocytes are large diffuse cells which exhibit polyploidy with many copies of nuclear DNA, often 64 copies at maturity (Italiano and Battinelli, 2009). Megakaryocytes trail filopodia into the circulation which shed pro-platelets. Pro-platelets undergo maturation in the vasculature and further break apart in their final discoid mature platelet morphology (Italiano and Battinelli, 2009). Megakaryocytic platelet production is mostly driven by the hormone thrombopoietin and a steady

platelet count is maintained within the body, although certain conditions may predispose individuals towards changes in the number of platelets produced such as in acute coronary syndrome (Martin et al., 2012), while pathogenic disease such as sepsis can result in consumption of platelets (Guclu et al., 2013).

1.1.2 Platelet structure

Platelets are small discoid cells with a diameter between 2-4 µm and despite their size they are complex cells with over 4,191 proteins listed on a recent proteomic study (Burkhart et al., 2012). These proteins may be membrane bound, cytosolic or within secretory α- or δ-granules (Figure 1). Platelets have evolved for rapid haemostatic function and are able to respond rapidly to stop haemorrhage at vascular sites of both arterial and venous shear, including; tethering against shear forces, degranulation, spreading over a damaged site and binding to and recruiting other platelets and facilitating the coagulation cascade.
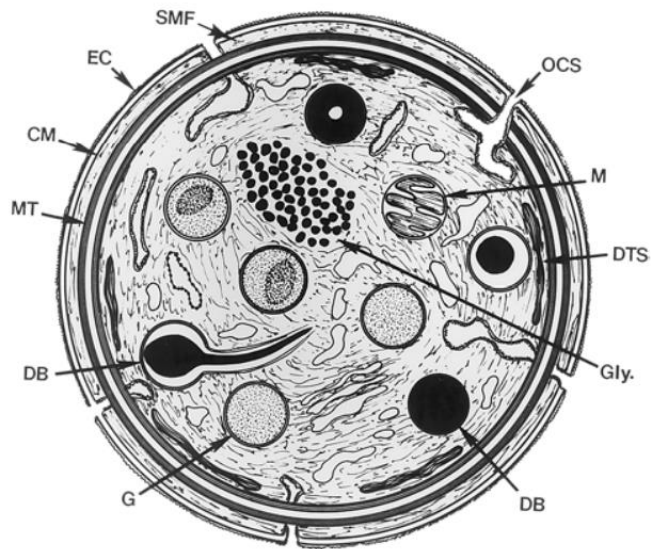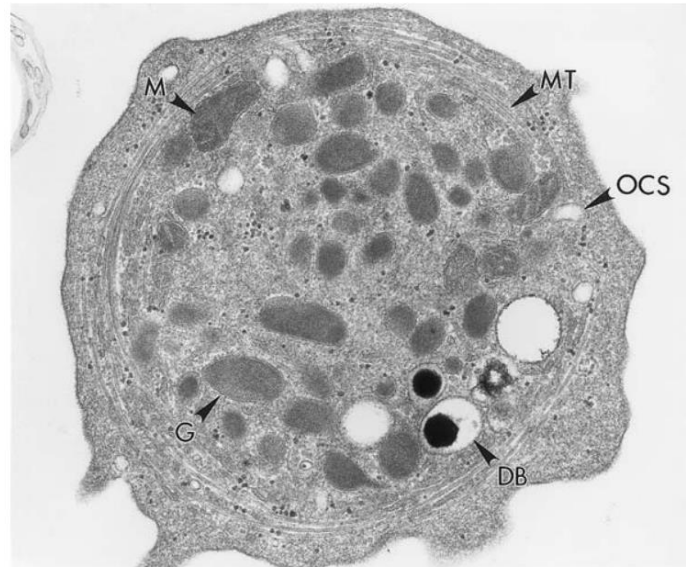
Figure 1. Platelet structure and typical contents. (Upper) Equatorial section of a resting human platelet taken by transmission electron microscopy (x36,000). (Lower) Ultrastructural features of resting human platelets. Abbreviations in each area of the cell include peripheral zone; Exterior coat (EC), trilaminar unit membrane (CM), submembrane (SMF) and open canalicular system (OCS). Sol-gel zone; microtubules (MT) and glycogen (Gly). Organelle zone; mitochondria (M), alpha granules (G), dense bodies (DB) and dense tubular system (DTS). Adapted from (White, 2004).

1.1.2.1 Membrane

The platelet membrane is a typical cellular phospholipid bilayer, presenting

phosphatidylcholine on the exterior and phosphatidylserine on the interior, which is

regulated by flippase and scramblase enzymes (Lhermusier et al., 2011). However when platelets are activated, some platelets present phosphatidylserine (PS) on the surface of the cell (Agbani and Poole, 2017), with these negatively charged phospholipids facilitating coagulation (Hoffman and Monroe, 2001). Outside of the platelet lipid bilayer is the polysaccharide rich glycocalyx, in which the glycoprotein surface receptors sit (Bennett, 1963). Platelets also demonstrate a phenomenon of folding of the membrane, suggested to be important for quickly increasing the platelet surface area on activation and spreading, this is termed the open canalicular system (OCS) (Escolar and White, 1991). More recently, changes of the OCS in disease has been suggested to play a role in platelet activation (Selvadurai and Hamilton, 2018). The platelet lipid membrane is a dynamic environment which has been shown to undergo extensive remodelling, allowing receptor recycling and localisation, this is facilitated by cholesterol rich lipid rafts (Lopez et al., 2005). Lipid rafts are suggested to form islands of lipids within the phospholipid bilayer, presenting a fluid mosaic structure which can readily move and rearrange to facilitate membrane bound protein reorganisation. The islands are cholesterol sphingolipid rich domains and can, therefore, remain distinct from phospholipid lipid rich regions, which allows them to move independently of the total membrane (Lopez et al., 2005). These rafts, carrying receptors, are thought to play an important role in allowing receptors to cluster, which is a central requirement for signalling in the case of Immunoreceptor Tyrosine-based Activation Motifs (ITAMs), notably platelet GPVI clustering and signalling (Locke et al., 2002). Lipid rafts have also been linked to roles in compartmentalisation of inhibitory cAMP signalling, which may control spatial inhibition (Raslan and Naseem, 2015).

1.1.2.2 Cytoskeleton

The platelet cytoskeleton is vital to the ability of platelets to rapidly change morphology on activation and their role in driving clot retraction. The cytoskeleton in resting platelets is apparent as a cell spanning coil of microtubules (Figure 1), which support the resting discoid cell shape of platelets (Behnke, 1965). Upon activation the coil of microtubules are contracted and the platelets lose their discoid shape (Menche et al., 1980). Platelets also contain an active actin cytoskeleton controlled by a wide variety of kinases which is also mobilised on activation driving formation of filopodia, lamellipodia and finally stress fibres (Atkinson et al., 2018, Yusuf et al., 2017). Together these two processes result in the collapse of the platelet discoid shape and the ability to rapidly spread over a large surface area.

1.1.2.3 Cytosol and granules

Like other cells, the platelet cytosol contains many of the typical eukaryotic organelles, although it also contains platelet specific granules (Figure 1). In similarity to all other cells (excluding red blood cells), in the cytosol platelets carry mitochondria for the efficient production of ATP (Zharikov and Shiva, 2013). A platelet specific organelle termed the dense tubular system (DTS) is also present, and this stores intracellular Ca^{2+} (Ebbeling et al., 1992). Platelets contain three types of granules, of which the α-granule is the most numerous, this is followed by δ-granules and lysosomal granules. There are ~65 α-granules per platelets and they are roughly 0.2 – 0.5 µm in diameter (Blair and Flaumenhaft, 2009). The contents of each granule type vary. In general, α-granules contain adhesion proteins, chemokines, coagulation factors, fibrinolytic enzymes and growth factors. The function of α-granules, therefore, spans haemostasis, thrombosis, repair/growth and immunity (Golebiewska and Poole, 2015). The role of α-granules is diverse. They not only release haemostatic modulators such as; thrombospondin-1 (TSP-1), fibrinogen, von

Willebrand factor (vWF), but also contain growth factors such as; vascular endothelium, platelet-derived, fibroblast, epidermal, hepatocyte and insulin-like growth factors (Blair and Flaumenhaft, 2009). Further to this α-granules also play a role in immunity through the release of soluble chemokine factors; CXCL4, CXCL7, CXCL12, CCL2 and CCL3 and the surface presentation of CD62P and CD154 from within the granules (Blair and Flaumenhaft, 2009). This led to discussion over the wide-ranging roles of platelet α-granules and whether they may be distinctly sorted into subsets of granules, such as "haemostatic" or "inflammatory" granules (Italiano and Battinelli, 2009). Classically, the role of secreted chemokines and growth factors has been suggested to facilitate thrombus resolution and subsequent wound healing, however, the platelet: immune cell interactions facilitated by α-granules proteins has also been reported to be important to atherosclerotic plaque development (Golebiewska and Poole, 2015).

In contrast, δ-granules contain primarily small molecules such as polyphosphates, ADP, ATP, Ca^{2+} and serotonin, all of which support coagulation or directly promote further platelet activation through the P2X1, P2Y1/12 and 5-HT2A g-coupled receptors respectively (Stalker et al., 2012).

1.2 HAEMOSTATIC FUNCTION

1.2.1 Platelet activation at the site of injury

The initiation of haemostasis is a major function of platelets in the vasculature. Platelets circulate the body in a state of tonic inhibitory quiescence, which is maintained by endothelial derived nitric oxide and prostacyclin. This inhibitory state is rapidly overcome at sites of injury, which is vital to fast cessation of bleeding. Platelet activation and subsequent thrombus formation consists of several distinct stages; rolling, tethering, spreading, recruitment and finally resolution (Figure 2). Blood flow forces platelets to the periphery of vessels due to their relatively small size, which places them near walls of the vessels, allowing them to rapidly detect vascular injury. When the vasculature is damaged the sub-endothelial matrix is exposed and the fibrillar protein collagen is exposed. von Willebrand factor (vWF), which circulates in the blood in a conformation unable to bind collagen, binds to collagen when shear induces a conformational change in the protein. This vWF can then ligate GP1b/V/IX receptor complex on the platelet surface. Ligation of the receptor acts to slow circulating platelets, allowing them to roll and come into further contact with the exposed surface. This initiates a major haemostatic activation of blood platelets, where the receptor GPVI can interact with collagen.

The platelet receptors facilitating adhesion to collagen are $\alpha_2\beta_1$ integrins and GPVI. When bound to GPVI, collagen stimulates signalling events that lead to platelet activation. Collagen cross-links GPVI resulting in tyrosine phosphorylation of immunoreceptor tyrosine-based activation motifs (ITAMs) on Fc receptor γ-chains (FcRγ) which is co-expressed and physically associated with GPVI at the platelet membrane. These phosphorylation events are mediated by Src-family kinases, Lyn and Fyn, and lead to the recruitment of the tyrosine-kinase Syk to phosphorylated FcRγ ITAMs where it becomes activated by autophosphorylation. This leads to the activation of phospholipase γ 2 (PLCγ2) and phosphatidylinositol 3-kinase (PI 3-K).

PLCγ2 hydrolyses membrane phosphatidylinositol-4,5-bisphosphate (PI(4,5)P$_2$) into diacylglycerol (DAG) and inositol-1,4,5-triphosphate (IP$_3$). DAG activates the serine-threonine kinase protein kinase C (PKC). This leads to the mobilisation of intracellular calcium through IP$_3$ binding to its receptors on the DTS. This rapid activation cascade drives conformational changes in platelet integrins. The integrin α2β1 binds firmly to collagen and allows firm tethering on the endothelial matrix. The integrin α$_{IIb}$β3 also undergoes a conformational change through its controlling proteins, including talin. The conformational change exposes the site of the integrin which binds to the RGD domain on the bivalent ligand fibrinogen. As a single platelet expresses over 50,000 copies of this integrin, and can, therefore, bind to many fibrinogen monomers, this bridges many platelets into a platelet rich aggregate. The platelets then spread across this three-dimensional matrix and recruit further platelets from the blood by secretion of additional mediators. The binding of fibrinogen to integrin α$_{IIb}$β3 not only provides a mechanical attachment, but also causes outside-in signalling when ligated and this drives further activation. Simultaneously, the localised release of both α- and dense granules and the synthesis of eicosanoids (thromboxane A2 (TxA2)) acts to further drive platelet activation. Platelet α-granules contain many inflammatory and haemostatic mediators, and those which support haemostasis include fibrinogen, factor XIII and vWF. The release of ADP from dense granules activates platelets through binding to the P2Y1 and P2Y12 receptors, which drive further activation and inhibit adenylyl cyclases. The synthesis of thromboxane A$_2$ (TxA$_2$) through cyclo-oxygenase 1 (COX1) drives further secondary activation through the thromboxane receptor (TP). A subset of these robustly activated platelets express phosphatidylserine on their surface through enzymatic activation of flippases. The expression of phosphatidylserine supports coagulation through the recruitment of factor X. The factor Xa complex drives the activation of pro-thrombin (factor II) to thrombin (factor IIa). Thrombin cleaves fibrinogen into fibrin monomers, which can polymerise into vast interlinked webs of protein that form the major protein net-like

structure of a clot. Thrombin also further potentiates platelet activation through the protease activated receptors 1 and 4 (PAR1/4). Platelets are also able to begin the resolution of thrombus formation. Firstly, platelets induce clot and thrombus retraction by pulling on the fibrinogen network (Tucker et al., 2012). Secondly, within the α-granules are many chemokines; PF4, CXCL7 and SDF-1, cytokines; TGF-β and MIP-1α and growth factors; PDGF and VEGF (Golebiewska and Poole, 2015). These factors all play an important role in the recruitment of neutrophils to remove cellular debris and in the development of an healing response.
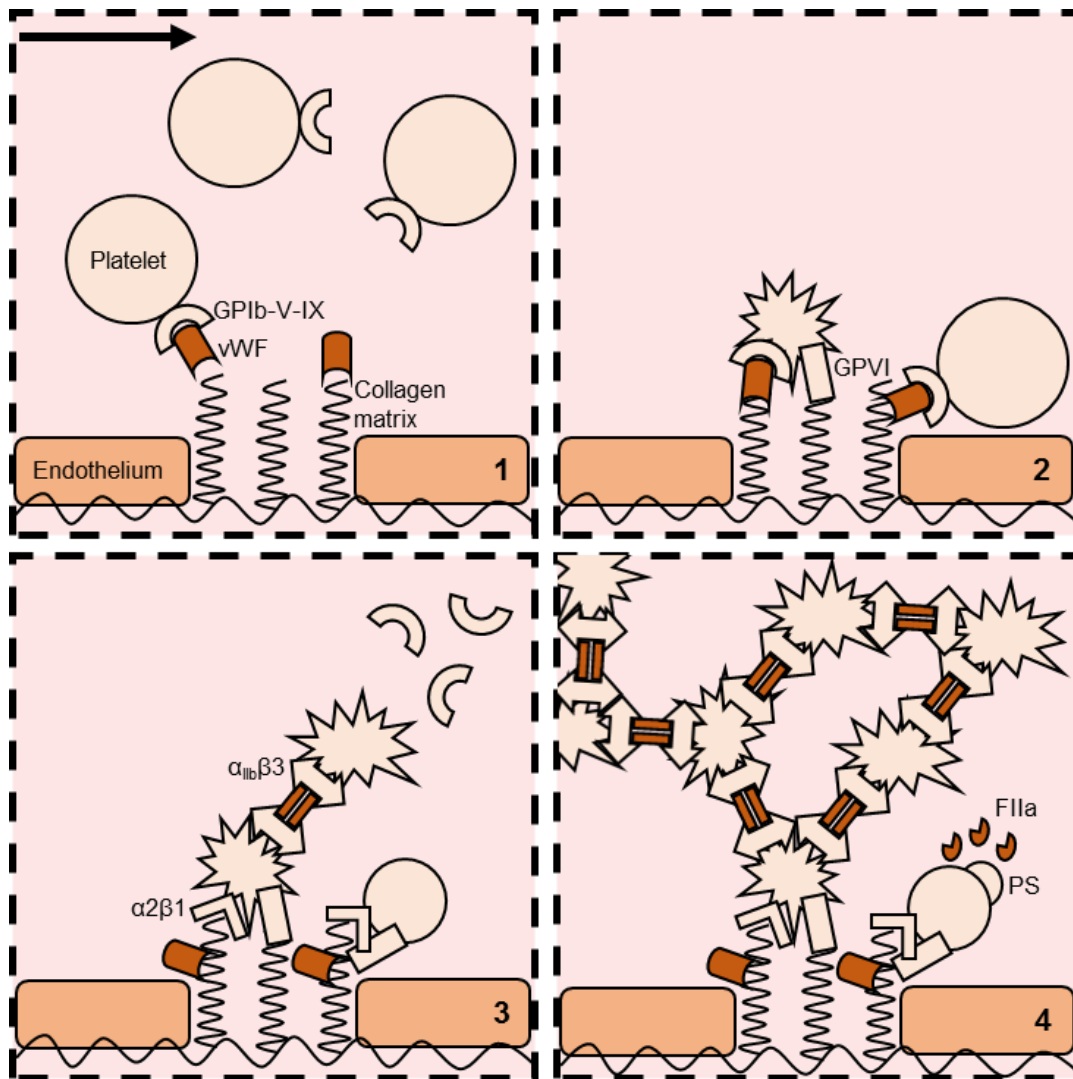
Figure 2. Schematic of platelet activation induced by exposure of a vascular wound. Tethering occurs through GPIb-IX-V binding to vWF which in turn interacts with exposed collagen. Robust activation can occur when GPVI is able to cluster on collagen inducing ITAM signalling motifs. This leads to activation of the integrin αIIbβ3 which facilitates platelet: platelet interactions through the bivalent ligand fibrinogen. Further platelet recruitment is mediated by ADP release, thromboxane synthesis and granule secretion. Finally, full thrombus formation occurs, procoagulant platelets are formed and thrombin (FIIa) is produced leading to fibrin mesh production. (Left to right, upper then lower).

1.2.2 Procoagulant activity

Alongside typical platelet-platelet homotypic interactions driven by integrin $\alpha_{IIb}\beta3$ binding the bivalent ligand fibrinogen, vital for clot retraction and platelet-rich thrombus formation (Tucker et al., 2012), an alternative mode of platelet function is supported through their procoagulant function (Heemskerk et al., 2013).

Procoagulant platelets externalise PS on their outer leaflet membrane, a phospholipid whose expression is normally conserved to the inner leaflet of the cell membrane. Exposure of PS plays a vital role in the support of the coagulation cascade and thrombin generation (Hoffman and Monroe, 2001). The procoagulant platelet phenotype has been described for many years under a variety of pseudonyms (COATED, collagen and thrombin activated-activated; FIB-CAP, fibrinogen-capped platelets; SCIP, sustained calcium-induced platelet morphology; and BNS, balloon non-spread), however, many of these suggested subpopulations have now been unified as all falling within the procoagulant super-family (Agbani and Poole, 2017). Studies have identified key roles for the externalised PS on the surface of procoagulant platelets in the recruitment of coagulation factors (Podoplelova et al., 2016). It is also widely accepted that for the procoagulant platelets to form, a robust stimulus of dual PAR1 and GPVI ligation is key (Agbani and Poole, 2017) and that these platelets likely form at the core of a thrombus where both thrombin and collagen (respective to the above receptors) will be present (Stalker et al., 2013).

Procoagulant platelets have been described by many methods including fluorescent flow cytometry using primarily annexin V and lactadherin conjugates (Sodergren and Ramstrom, 2018), fluorescent imaging cytometry (Reddy et al., 2018) and *ex vivo* flow models (Kuijpers et al., 2005). However, procoagulant activity can also be measured through thrombin generation assays both directly in PRP and in PPP which contain platelets and platelet microparticles respectively, although for direct measurement fluorescent flow cytometry remains the gold standard. This thorough phenotyping has helped describe some of the pathways vital to procoagulant platelet activation and formation. Primarily a sustained calcium flux has been shown to be vital (Choo et al., 2012), which is driven by the simultaneous activation of both PAR1 and GPVI. In addition, mitochondrial depolarisation has been shown as a key event prior to PS exposure (Choo et al., 2017). While a consensus on the overall description of procoagulant platelets in the literature has now been reached (Agbani and Poole,

2017), there are still several open questions regarding roles they may play *in vivo*, how number of procoagulant platelets may change in disease and further understanding of the regulation and activation of procoagulant platelets. A key argument for the important role of procoagulant platelets in *in vivo* haemostasis is illustrated in Scott syndrome patients whom demonstrate no scramblase activity, and cannot expose PS and as a result show a strong bleeding phenotype (Lhermusier et al., 2011). In disease, initial observations suggest that PS exposing platelets are formed in individuals who have Wiskott-Aldrich syndrome, at a greatly increased rate (Obydennyi et al., 2019) and it has also been shown that in individuals who have suffered an ischaemic stroke, PS positive platelets can be detected in the blood (Pretorius et al., 2012). The first definitive description of procoagulant platelets were described in trauma patient undergoing haemorrhage by imaging cytometry, further validated by transmission electron microscopy (Vulliamy et al., 2019). These procoagulant platelets were stimulated by histone H4 and shown to release PS positive microparticles that interacted with leukocytes (Vulliamy et al., 2019). These studies propose that PS platelets may well play a role in platelet-pathogenesis in disease or act as sensitive biomarkers of disease.

1.2.3 Platelet heterogeneity

Platelet heterogeneity has been a widely discussed topic for several years, with several suggested sources of heterogeneity within the platelet population. A widely accepted source of heterogeneity within the total platelet population is the procoagulant subset (Agbani and Poole, 2017), however it must be noted that this heterogeneity only emerges on activation. To date there have been no pre-activation features identified to recognise which platelets may assume a procoagulant phenotype on stimulation, if discovered this may prove to be a valuable biomarker of the future of propensity to form the procoagulant subset. Beyond the previously described 1/3 of platelets becoming procoagulant, in recent years the procoagulant

subset has been described to contain further heterogeneity. Initially procoagulant platelet subsets were suggested to be distinguished by calcium signalling and modulation of the integrin αIIbβ3 (Topalov et al., 2012), however this was later refuted as a result of erroneous flow cytometry gating (Choo et al., 2017), the study described herein goes further to describe heterogeneity within the procoagulant platelet subset. Platelet size has also been shown as another feature of platelet heterogeneity associated with procoagulant exposure. It was described that platelet size correlated very closely with procoagulant activity, where it was small cells that primarily expressed PS (Sodergren and Ramstrom, 2018).

In addition to the platelet heterogeneity characterised by procoagulant formation, which only emerges on activation, platelet age can also be used to describe heterogeneity within the platelet population, vitally in resting platelets. Young platelets which have been recently released from the megakaryocytes and carry more vestigial mRNA are described as reticulated platelets (Harrison et al., 1997) and are typically enumerated by their thiazole orange staining intensity (Bonan et al., 1993). Many studies have since pursued these immature cells and they have been characterised *in vitro* which has shown they exhibit a phenotype of hyperactivity in comparison with aged platelets (Lador et al., 2017), furthermore reticulated platelets have also been shown to be clinically relevant *in vivo* and potentially prognostic of cardiovascular disease (Lev, 2016).

1.3 REGULATION OF PLATELET FUNCTION

Platelet activation is a rapid process which if uncontrolled can lead to pathological thrombosis. Therefore, it is vital that platelets are maintained in a sensitive but quiescent state of inhibition in circulation. Endothelial derived PGI_2 and NO are the two major endogenous inhibitors of platelet function (Mitchell et al., 2008). These inhibitors are both synthesised by the vascular endothelium in response to the pulsatile flow of blood which ensures that circulating platelets are maintained in an inhibitory state throughout circulation. These inhibitors regulate platelets through cyclase mediated production of cyclic nucleotides, and activation of downstream inhibitory protein kinases.

1.3.1 Nitric oxide

NO is a potent vasodilator that relaxes vascular smooth muscle and diffuses across platelet membranes to activate intracellular soluble guanylyl cyclase (sGC) to produce cyclic guanosine monophosphate (cGMP) which activates a dependent serine/threonine kinase, protein kinase G (PKG), which in turn mediates various inhibitory phosphorylation events (Mitchell et al., 2008, Stalker et al., 2012) (Figure 3). Notable among these are inhibition of Rap1b, TxA_2 receptors, RhoA and IP_3 receptors on the DTS, which result in inhibition of the integrin $\alpha_{IIb}\beta3$, secondary activation, actin remodelling and calcium mobilisation respectively. Moreover, PKG activates sarcoendoplasmic reticulum calcium ATPase (SERCA) which pumps cytoplasmic calcium back into the DTS, returning its concentration to basal levels.

1.3.2 Prostacyclin

PGI_2 is a prostanoid which is derived from arachidonic acid freed by phospholipase A (PLA). PGI_2 is secreted by the endothelium and has a short half-life in the blood (Cho and Allen, 1978). It binds to the prostacyclin $G\alpha_s$-linked IP receptors on

platelets. $G\alpha_s$ activates adenylyl cyclase, which converts adenosine triphosphate (ATP) to cyclic adenosine monophosphate (cAMP). High intracellular levels of cAMP signal within the cell driving activation of protein kinase A (PKA), which drives the inhibitory effects within the cell (Figure 3).

Similar to cGMP via PKG, cAMP targets several key pathways in the cell to mediate inhibition via PKA. In terms of receptors and their immediate signalling, PKA controls several routes of activation. PKA modulates GPIb-V-IX by phosphorylation of GPIbβ which reduces vWF binding (Bodnar et al., 2002). PKA is able to further target GPVI dimerization (Loyau et al., 2012), which is vital to GPVI signal transduction (Locke et al., 2002), thereby reducing collagen mediated signalling. It also modules $G\alpha_{13}$ thereby blocking signal transduction from both TP receptors and PAR (Manganello et al., 1999, Manganello et al., 2003). The major integrin $\alpha_{IIb}\beta3$ is also blocked from activation by phosphorylation of Ca^{2+} dependent Rap1b (Lapetina et al., 1989). In combination, these demonstrate that PKA can modulate the major activatory platelet receptors via a combination of direct or indirect phosphorylation of related components. Calcium mobilisation is, as described, a major outcome of platelet activation and is vital to almost all aspects of activity (Varga-Szabo et al., 2009). cAMP-PKA inhibitory signalling also modulates calcium signalling via targeting IP_3 receptors which would, in turn, prevent the release of internal stores of calcium downstream of PLCγ2 (Quinton et al., 1996). More recently, however, aspects of calcium signalling via $P2X_1$ calcium entry have been shown to remain independent of cAMP-PKA activity, which suggests that cAMP does not result in the complete shutdown of platelet activity (Fung et al., 2012). An additional key aspect of platelet activity is shape-change and spreading, primarily mobilised by the highly active actin cytoskeleton. PKA phosphorylates several actin binding proteins including LASP (LIM and SH3 protein), HSP27 (heat-shock protein 27) and vasodilator-stimulated protein (VASP) (Butt et al., 1994, Butt et al., 2001, Butt et al., 2003). VASP is heavily phosphorylated on two serine residues, 157 and 239 (Benz et al., 2009), and provides

a valuable readout of cAMP-PKA activity by immunoblot and phosphoflow (Spurgeon et al., 2014).

1.3.3 Regulation of inhibitory signalling

Given the potent inhibitory effects of cAMP signalling, levels must be maintained within the cell to ensure that activation of platelets can take place when required. Phosphodiesterases (PDEs) can terminate PGI_2- and NO-stimulated signalling events and are thus important regulators of platelet function and many other cells. PDEs form a large group of enzymes that hydrolyze the 3' cyclic phosphate bond of either cAMP or cGMP, yielding their inactive 5' metabolites. Although cyclic nucleotides can be transported across the platelet membrane, the catalytic action of PDEs represents the only known mechanism for rapidly lowering platelet cyclic nucleotide contents and thereby controlling signalling events. Platelets contain at least three different PDE isozymes including cGMP-stimulated PDE2, cGMP-inhibited PDE3A and the cGMP-specific PDE5. Binding of cGMP to an allosteric binding site leads to the PDE2-catalysed degradation of both cAMP and cGMP. Binding of cGMP to PDE3A, on the other hand, inhibits the preferential hydrolysis of cAMP. The second messenger, cGMP, can, therefore, attenuate or enhance the level of intraplatelet cAMP. Indeed, significant cross-talk exists between the cAMP and cGMP signalling cascades. PDE3A is phosphorylated and activated by cAMP-dependent protein kinase in a negative feedback loop that eventually restores basal levels of cAMP. There is also evidence that the transporter ABCC4 (Cheepala et al., 2015), can drive efflux of cAMP out of a platelet to rapidly diminish the inhibitory burden, although phosphodiesterases are currently considered the major regulator of cAMP levels.
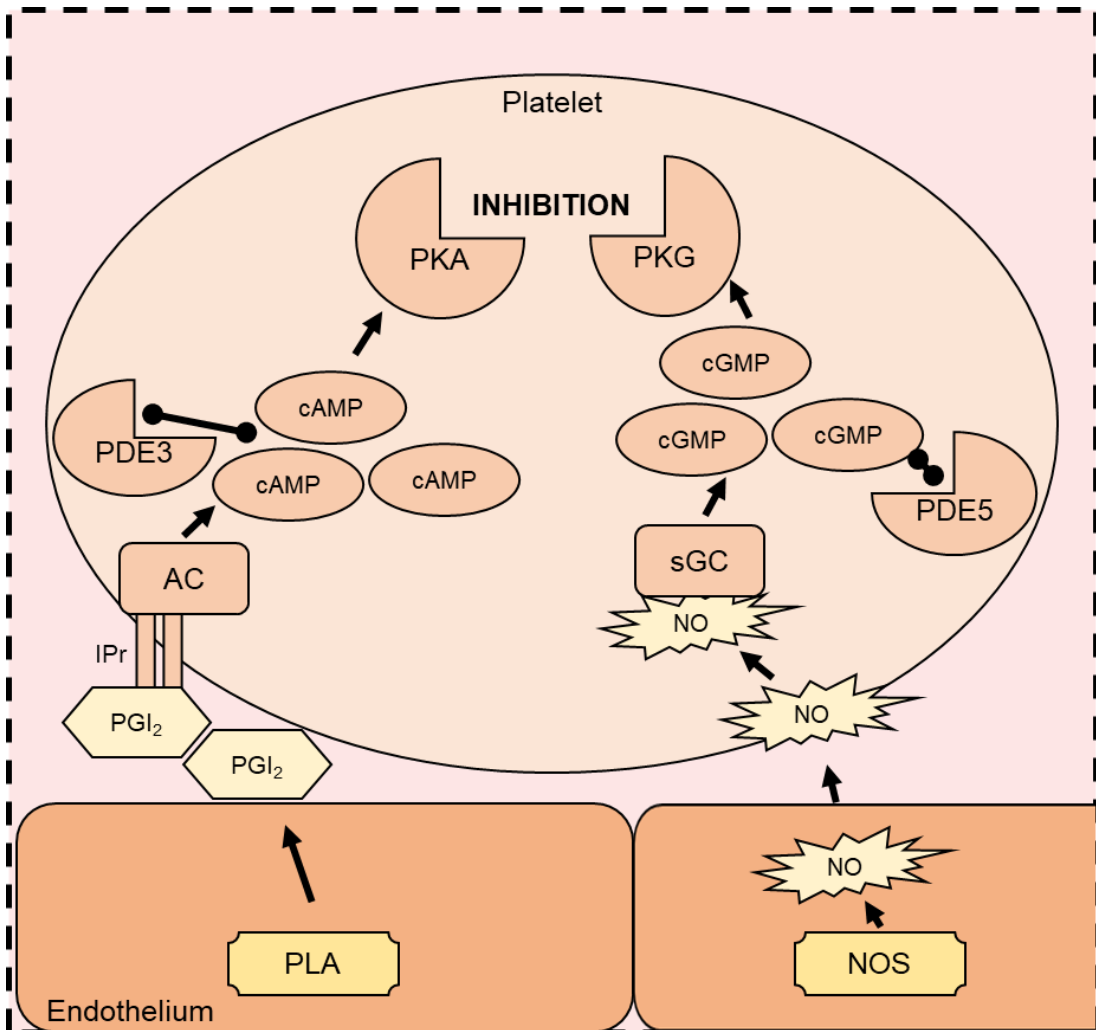
Figure 3. Overview of platelet inhibitory signalling mediated by prostacyclin and nitric oxide. Prostacyclin (PGI_2) and nitric oxide (NO) are synthesised in endothelial cells by phospholipase A (PLA) and nitric oxide synthetase (NOS) respectively. They are then subsequently released in the cytoplasm. PGI_2 binds to the platelet prostacyclin receptor (IP) which in turn activates adenylyl cyclases (AC) which produce cAMP in an ATP dependent manner. Intracellular pools of cAMP are regulated by phosphodiesterase 3A (PDE3A), but when production exceeds breakdown cAMP activates protein kinase A (PKA), which acts as the key effector of PGI_2-mediated inhibition and phosphorylates multiple targets within the platelet. NO does not require a receptor and diffuses across the phospholipid membrane where it activates soluble guanylyl cyclase (sGC) which produces cGMP. Phosphodiesterase 5a regulates intracellular levels of cGMP, but when levels are raised over breakdown rate protein kinase G (PKG) is activated. PKG acts as the effector of the NO pathway and phosphorylates multiple targets in the platelet.

1.4 PLATELET METABOLISM

1.4.1 Mitochondria and metabolism

Metabolism is a series of chemical processes which occur to support life, primarily to provide energy substrates for cellular processes. Eukaryotic cells carry mitochondria, which are organelles with a complex internal structure and defined external membrane. Mitochondria are vital to cellular homeostasis as they allow the more efficient aerobic respiration to occur rather than anaerobic glycolysis. Mitochondria are $0.5 - 1$ µm in length and are mobile organelles, continually undergoing fission and fusion. Structurally mitochondria have four regions (Figure 4); the internal matrix, which contains enzymes required for the citric acid cycle along with mitochondrial DNA (mtDNA), then surrounding this is the inner membrane which is folded into cristae that increase the intracellular membrane surface area in order to increase the number of proteins to drive oxidation in the electron transport chain (ETC). It is this membrane which the electrochemical gradient is maintained over. The intermembrane space is sandwiched between the inner and outer membranes and finally the outer membrane carries mitochondrial receptors and vitally the porin voltage-dependent anion channel (VDAC) which makes this membrane permeable to molecules <5 kDa (Alberts et al., 2008).

The core process of energy production relies on the harnessing of chemiosmotic coupling, namely chemical bond-forming reactions facilitated by changes in osmotic pressure and electric charge. In brief, electrons derived from oxidation are transported along the ETC embedded in the mitochondrial membrane in a process which liberates energy allowing H^+ to be pumped across the membrane, driving formation of an electrochemical gradient. This gradient is a form of energy, which when flowing back into the mitochondria via ATP synthase produces adenosine triphosphate (ATP) from adenosine diphosphate (ADP) and inorganic phosphate (P_i) (Alberts et al., 2008). ATP then acts as fuel within the cell for many processes.
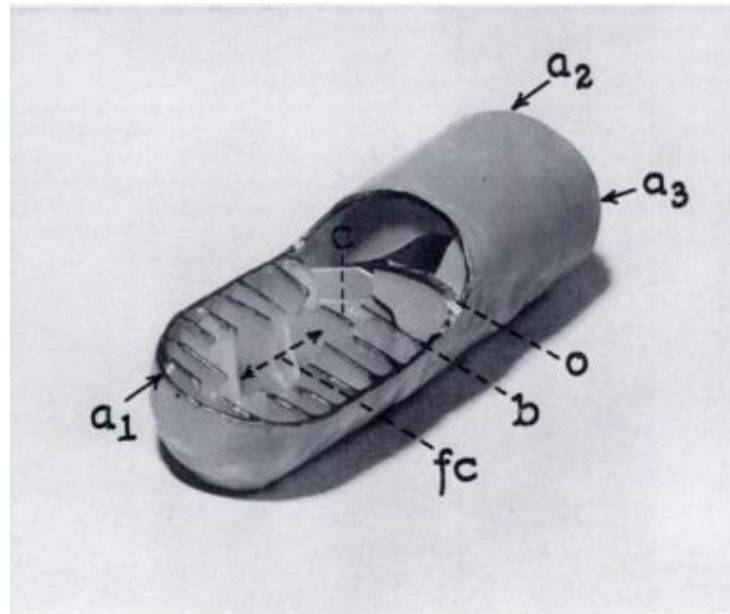
Figure 4. Mitochondrial structure. The complex internal structure of mitochondria is apparent in this three-dimensional model, with folded inner membrane forming cristae (*o, c* and *b*), the central free channel (*fc*) demonstrating increased surface area within the smaller confines of the outer membrane (*a1, a2, a3* demonstrate sites of section removal), adapted from (Palade, 1953).

1.4.2 Platelet metabolism and disease

Platelets are among the most numerous cells in the blood and are known to be very metabolically active. In recent years, studies have begun to assess how platelet mitochondrial dysfunction may be linked to changes in platelet function. A major part of this push, is the understanding that mitochondria are not only important for energy production (Alberts et al., 2008), but play a vital role in cellular signalling, predominantly through production of ROS (Tait and Green, 2012, Schulz et al., 2014). The important role of ROS in platelet biology, is easily summarised in the canonical spike in ROS (typically cytosolic not mitochondrial) when GPVI is activated (Walsh et al., 2014). Indeed, mitochondrial superoxide is readily produced from platelet mitochondria and it is converted to hydrogen peroxide where it may leave and act as a cellular messenger (Anand et al., 2013).

Platelets have a high energy consumption, and in circulation resting platelets derive 35% of their energy from oxidation phosphorylation and the majority (65%) from glycolysis (Zharikov and Shiva, 2013). When platelets are activated, they do not differentiate between the two sources of energy and the rate of both oxidative phosphorylation and glycolysis can be elevated relative to substrate availability (Aibibula et al., 2018). Studies have identified a role for mitochondrial function in several aspects of platelet biology. The formation of the mitochondrial permeability transition pore (MPTP) has been linked to platelet activation, notably the MPTP is formed on a subset of platelets on treatment with both thrombin and convulxin which leads to phosphatidylserine exposure, it was further suggested that mitochondrial cyclophilin D was regulating this (Jobe et al., 2008). Follow up studies later identified that it is specifically mitochondrial calcium and mitochondrial ROS which facilitated PS exposure (Choo et al., 2012). Highlighting an important role for mitochondria in regulating procoagulant platelet activity.

However, what is emerging, is that mitochondrial dysfunction likely plays an important role in modulating many aspects of platelet function (Wang et al., 2017a). To highlight several studies, in ageing mice mitochondrial membrane potential was suggested to be raised, hypothesising that this may lead to age associated degeneration of response (Xu et al., 2007). In the well-known disorder Wiskott-Aldrich Syndrome (WAS), the platelet thrombocytopaenia was recently shown to be dependent on mitochondrial dependent necrosis (Obydennyi et al., 2019). In several diseases there have also been observations of mitochondrial dysfunction noted specifically within platelets; in cardiovascular disease (CVD) there have been reports of increased mtDNA methylation (Baccarelli and Byun, 2015), in polycystic ovary syndrome (PCOS) AMPK and respiration rate are both decreased but rescued by metformin treatment (Randriamboavonjy et al., 2015), in sickle cell disease (SCD) complex V activity is reduced (Cardenes et al., 2014), in sepsis mitochondrial depolarisation correlates with disease severity (Grundler et al., 2014) and finally in diabetes mellitus

aldose reductase activity is reduced (Tang et al., 2014). Importantly all these conditions are also associated with platelet dysfunction; CVD increased thrombotic events and platelet transcriptional remodelling (Ramos-Arellano et al., 2014, Heffron et al., 2018), PCOS increased platelet hyperactivity (Aye et al., 2014), SCD increased platelet NLRP3 inflammasome activity (Vogel et al., 2018a), sepsis increased platelet activity and IL-1β production (Brown et al., 2013, Damien et al., 2015) and diabetes increased platelet activity and loss of inhibitory IP receptors (Angiolillo et al., 2005, Knebel et al., 2015). This suggests there may well be a link between mitochondrial dysfunction and platelet dysfunction in these conditions. Understanding what is driving these changes in platelet mitochondrial dysfunction will be key to development of pharmacological protection from these changes.

1.5 PLATELETS AND INFLAMMATION

The role of platelets in inflammation and immune response is a relatively new field of research, but there is now also evidence of platelet involvement in these responses (Vogel and Thein, 2018, Koupenova et al., 2018). There are indications of a concurrent role to thrombosis, of platelets as a blood-borne sentinel cell, and as such they are now thought to be involved in the development and progression of vascular inflammation, both sterile and unsterile (Koupenova et al., 2018). A growing body of evidence suggest that platelets are capable of mediating multiple immune responses (Morrell et al., 2014, Gaertner et al., 2017, Clark et al., 2007, Koupenova et al., 2018). This has been illustrated through showing their ability to respond to danger and pathogen-associated molecular patterns (D/PAMPs), which can be characterised into endogenous danger ligands such as oxidised LDL (oxLDL) and exogenous pathogenic ligands such a lipopolysaccharide (LPS) (Podrez et al., 2007, Damien et al., 2015). Platelet inflammatory responses can be manifested through many routes but key pathways include; direct synthesis of the cytokines IL-1β (Brown et al., 2013), and IL-18 (Allam et al., 2017), P-selectin mediated leukocyte recruitment, CD40L release or neutrophil extracellular trap (NET) activation (Morrell et al., 2014, Koupenova et al., 2018, Clark et al., 2007), and deposition and release of chemokines such as PF4 and RANTES (Golebiewska and Poole, 2015). These inflammatory mediators suggest platelets have the capacity to modulate all major immune cell classes within the vasculature, monocytes, lymphocytes and granulocytes.

1.5.1 Platelet-leukocyte interactions

A well described pathway which platelets modulate systemic inflammation through is heterotypic interactions with leukocytes. Platelets are demonstrated to have potent activatory checkpoint roles in the recruitment and activation of many white cell subsets including neutrophils, monocytes and lymphocytes. Numerous examples of

platelet leukocyte interactions have been described by both *in vitro* and *in vivo* with multiple partner cell types (Koupenova et al., 2018, Vogel and Thein, 2018, Morrell et al., 2014, Golebiewska and Poole, 2015, Li et al., 2017). Below, examples of how platelets interact with each major immune cell class are presented. Via CD62P-PGL1 interaction platelets activate neutrophils and receive eicosanoid precursors in return to drive thromboxane synthesis and stimulate inflammatory neutrophil extravasation (Rossaint et al., 2016). Platelets can also recruit monocytes via CCN1 and facilitate inflammatory monocyte patrolling in an animal model of inflammation (Imhof et al., 2016). Lymphocyte activation via platelet expressed CD40 ligand (CD154) has also been demonstrated (Stokes et al., 2009). However, beyond these studies the association between platelets and leukocytes primarily occurs through interaction of P-selectin and P-selectin glycoprotein ligand-1 (PSGL1).

1.5.2 CD62P-PSGL1

CD62P (P-selectin, granule membrane protein 140 or platelet activation-dependent granule to external membrane protein) is a platelet protein which is contained within α-granules, and as such is expressed on the surface of platelets when granule secretion is stimulated (Harrison and Cramer, 1993). The secretion of α-granules, as previously mentioned, will induce the release of many other chemokines and other recruitment mediators such as CD154 (CD40L) alongside CD62P. However, the interaction of CD62P with PSGL1 is among the most well described mediators of platelet: leukocyte interaction. CD62P is expressed in both platelet α-granules and also endothelial Weibal-Palade bodies and is also present as a soluble (cleaved) form in the blood as sCD62P, which can be cleaved from platelets (Andre, 2004). CD62P interacts with PSGL-1 (P-selectin glycoprotein ligand-1 or CD162) which facilitates both interactions between cells in suspension and rolling in vasculature as well as transducing activating signal, the partner for CD62P, PSGL1 is expressed on

monocytes, neutrophils and platelets themselves (Moore, 1998). Early descriptions of the CD62P-PSGL1 interaction were carried out *in vitro* and concentrated on the mediation of rolling, this study demonstrated that at a range of a shear rates neutrophils would roll on Chinese hamster ovary (CHO) cells which expressed CD62P (Moore et al., 1995). Further studies followed on and examined the affinity of the CD62P-PSGL1 interaction, the binding was highly specific and interestingly they demonstrated that sCD62P also binds with a high affinity, suggesting sCD62P may act as a regulator of the interaction or to drive signalling itself (Mehta et al., 1998). A reciprocal approach was later used, where PSGL1 was significantly increased on the platelet surface on activation, but treatment with an anti-PSGL1 antibody abrogated platelet-endothelial rolling when measured by *in vivo* intravital microscopy (Frenette et al., 2000). Although there had been a clear indication that the CD62P-PSGL1 axis may be important in disease, a consensus was reached that P-selectin played a vital role in the recruitment of leukocytes to the endothelial and that increased levels of sCD62P in CVD indicated it may play a role in the pathophysiology of atherogenesis (Blann et al., 2006). Alongside the indication of CD62P-PSGL1 playing a role in the modulation of vascular inflammation, there was also evidence emerging that it played a role in thrombosis as a stabilising agent between platelet-platelet interactions and the recruitment of leukocytes, which in turn facilitates a role in coagulation for CD62P-PSGL1, where it induces tissue factor expression on the monocyte surface (Andre, 2004). Clinical studies have also highlighted correlations between sCD62P and cardiovascular disease/events, which are vitally rescued in CD62P/PSGL1 knockout models (Wang et al., 2007, Ye et al., 2019). While the CD62P-PSGL1 interactions between platelets and monocytes and themselves vitally, important, they can lead to further interactions between the two cells. The major receptor on monocytes which is upregulated in response to CD62P/PSGL1 interactions is Mac-1 (integrin $\alpha_M\beta_2$ or CD11b/CD18) (Meerschaert and Furie, 1995). Mac-1 interacts with GP1bα on the platelet surface, which is a constitutive component of the GP1b-V-IX complex, and

this has been suggested to drive thrombosis (Wang et al., 2017b). In addition to this Mac-1 also binds to fibrinogen thereby driving heterotypic platelet-monocyte interactions via the integrin αIIbβ3 (Wright et al., 1988). These studies have continued to progress and the CD62P-PSGL1 axis is now understood to regulate many vascular events and drive the progression of atherogenesis, vascular inflammation, thrombosis and more recently described cancer (Kappelmayer and Nagy, 2017).

1.6 OXIDISED LOW-DENSITY LIPOPROTEINS AND PLATELETS

1.6.1 Low-density lipoprotein and atherosclerosis

Elevated plasma lipids, particularly cholesterol in the form of low-density lipoproteins (LDL), are correlated with increased CVD risk. However, the precise mechanisms of hyperlipidaemia mediated thrombosis are unclear. Lipoproteins are spherical rich particles, comprised of an 'outer shell', hydrophobic 'lipid core' and protein component that serve to transport lipids to the tissues. The outer shell is composed predominantly of a phospholipid monolayer, with traces of cholesterol and contains specialised apolipoproteins which act to direct the transport of lipoproteins. These proteins facilitate recognition of particles by cell surface receptors or enzymes. The lipid core contains triglycerides and cholesterol esters, but predominantly cholesterol esters in LDL, which are transferred to tissues during the lipoprotein's lifetime. There are several lipoprotein subtypes including; chylomicrons, vLDL, LDL and LP(a) which are atherogenic, and HDL which is anti-atherogenic, but it is LDL that is most strongly implicated in CVD (Feingold et al., 2000).

LDL are an intermediate size particle when compared with HDL, LDL, vLDL and chylomicrons, ranging from 18-25 nm in diameter with a molecular weight of ~2,300 kDa and density of 1.019 – 1.063 g/mL. In addition to their lipid content, the outer shell also contains a single apolipoprotein (Apo B-100). Apo B-100 is one of the largest proteins in the human genome and is comprised of 4,536 amino acid residues. Functionally, Apo B-100 is essential for the delivery of cholesterol by acting as a ligand for cells bearing the LDL-receptor (LDL-R) (Feingold et al., 2000). In patients with familial hypercholesterolemia, the amount of LDL increases due to mutations in the LDL-R, significantly increasing the risk of CVD (Defesche et al., 2017), clearly implicating excess plasma LDL with CVD. At sites of endothelial dysfunction, LDL can transverse the endothelial cell layer and accumulate in the *intima* layer of the blood vessel by binding to proteoglycans. Once retained in the *intima*, LDL undergoes

chemical modification resulting in oxidised LDL (oxLDL), a lipoprotein with distinct biological function and central in the pathogenesis of atherosclerosis. The degree of oxidation of LDL particles yields multiple species with different biological functions. The presence of oxLDL in the intima alters the local environment, causing changes to the secreted chemokine profile from activated EC and inflammatory cells, leading to the recruitment of monocytes to the area of inflammation, where they differentiate into macrophages and encounter oxLDL. Recognition of LDL, both native and modified, by LDL-R and scavenger receptors, causes unregulated lipid uptake into the macrophages and causes their phenotype to change, becoming 'foam cells' (Stocker and Keaney, 2004). In addition, internalised LDL can also be modified further due to the acidic conditions within the macrophage lysosome. Increased numbers of foam cells in the vessel wall manifests as a fatty streak, the earliest hallmark of pathological lesion formation in atherosclerosis (Wadhera et al., 2016).

More recently oxLDL has been shown to be increased in the circulation of subjects with atherosclerosis, early cardiovascular disease (obesity) and stroke (Kato et al., 2009, Ramos-Arellano et al., 2014, Wadhera et al., 2016). Circulating oxLDL functions as a vascular DAMP and is able to induce activation of both immune cells and platelets, which in turn drives vascular inflammation, endothelial dysfunction, and atherogenesis (Golia et al., 2014, Steinberg, 2009). Indeed, oxLDL has been shown to drive macrophage foam cell formation, specifically via the receptor CD36 (Podrez et al., 2002a), which further confirms that oxLDL plays a key role in the development of atherosclerotic plaque.

1.6.2 Oxidation of LDL

When oxidised, the LDL particle becomes highly atherogenic. Oxidation of LDL is a multi-step process which results in change to both surface phospholipids (oxPL) and protein modification (Apo B-100). This allows oxidised LDL to be recognised by

certain scavenger receptors (Levitan et al., 2010) which can drive monocyte polarisation, cytokine expression, expression of endothelial adhesion molecules and platelet hyperactivity among several characterised effects (Feingold et al., 2000).

Several cells in the atherosclerotic plaque/vessel wall have been shown to be able to oxidise LDL, notably endothelial cells, smooth muscle cells, macrophages (including foam cells) and lymphocytes (Wilkins and Leake, 1994a). Oxidation of LDL *in vivo* has been suggested to be predominantly via the production and release of reactive oxygen species into the locale, notably superoxide anion and hydrogen peroxide, which can interact with LDL in the extracellular matrix. Indeed, it has been demonstrated that superoxide dismutase regulates early stages of LDL oxidation, suggesting it is primarily the superoxide anion which controls the oxidation of LDL (Cathcart et al., 1988). Additionally, transition metal ions have been suggested to drive oxidation of LDL, while the zinc ion ($ZnSO_4$) was shown to protect LDL from oxidation – whereas copper ion and ferrous ions were not (Wilkins and Leake, 1994b). Myeloperoxidase (MPO) a ROS producing enzyme expressed in leukocytes produces hypochlorous acid (HOCl), which dissociates into the OCl^- hypochlorite anion and can oxidise LDL, however, other enzymes including lipoxygenase and nitric oxide synthase can also oxidise LDL *in vitro* (Carr et al., 2000).

To use oxLDL experimentally, it must be isolated directly from blood which contains modified LDL or produced by *in vitro* oxidation of native LDL (nLDL). Modified LDL has been successfully isolated from patients in the context of chronic kidney disease. isolating carbamylated LDL (cyanic acid adduct) (Holy et al., 2016) and from ST-segment elevation myocardial infarction (STEMI) patients isolated electronegative LDL (L5-LDL) (Yang et al., 2017b). However, typically LDL is modified *in vitro* to prevent multiple heterogenous modifications which may occur *in vivo* and to produce specifically oxidation, carbamylation, glycation or acetylation products which drive the phenotype. Of these varied species of modified LDL, oxLDL is the most researched modified LDL. Typically oxLDL is modified *in vitro* using well characterised oxidation

protocols, where oxidation is catalysed by the addition of copper ions (CuSO$_4$), although it is possible for other transition metal ions to replace copper in this model (Gerry et al., 2008). The output of this copper catalysed oxidation can be modified by the researcher through changes in temperature at which the oxidation is carried out, however, in all models oxidised LDL particles present a very heterogeneous particle with a variety of oxidation products, both phospholipids and modified Apo B-100 (Lenz et al., 1990). By oxidising LDL in the presence of copper ions at either 4∘C or 37∘C, the reactive species produced on the LDL can be manipulated. Through oxidation at 4∘C, LDL rich in hydroperoxides can be produced, at 4∘C the breakdown of these hydroperoxides is protected. Conversely if oxidised at 37∘C, an oxLDL of predominantly oxysterols is produced, as the hydroperoxides are fully broken down (Gerry et al., 2008). As the outer, and therefore accessible, surface of lipoproteins is formed of mainly phospholipids, therefore it is these which are most vulnerable to oxidative modification. In the presence of hydroxyl radicals (OH$^-$), lipid radicals are formed which react with molecular oxygen to form lipid peroxides (LOO$^-$). These LOO$^-$ further propagate the hydrogen abstraction from surrounding moieties or react with themselves to become oxidised phospholipids (Equation 1) (Feingold et al., 2000), such as KOdiA-PC, which is commonly used as an oxLDL mimetic (Biswas et al., 2017, Kar et al., 2008, Podrez et al., 2002a, Podrez et al., 2002b). Alongside production of oxPL, lipid aldehydes are also formed which modify surrounding proteins, notably Apo B-100 in the case of LDL (Feingold et al., 2000).

Equation 1. Copper mediated lipid peroxidation. Reaction 1 and 2, copper ions are involved in redox reactions with endogenous lipid hydroperoxides. Reaction 3 and 4, peroxyl and alkoxyl lipid radicals oxidised the parent polyunsaturated fatty acid by hydrogen abstraction. Reaction 5, oxygenation of lipids propagates reactions 3 and 4. Abbreviations; LOOH, lipid hydroperoxide, LOO∘ lipid peroxyl, LO∘ lipid alkoxyl, LH polyunsaturated fatty acid. Adapted from (Burkitt, 2001).

1 $Cu^{2+} + LOOH \rightarrow Cu^{+} + LOO\cdot + H^{+}$

2 $Cu^{+} + LOOH \rightarrow Cu^{2+} + LO\cdot + OH^{-}$

3 $LOO\cdot + LH \rightarrow LOOH + L\cdot$

4 $LO\cdot + LH \rightarrow LOH + L\cdot$

5 $L\cdot + O_2 \rightarrow LOO\cdot$
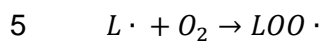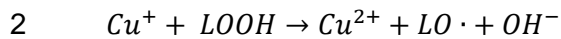
The understanding of specific oxPL which are produced on the surface of LDL on oxidation has allowed deeper characterisation of where precisely these adducts may bind to various receptors, including LOX-1 (Chen et al., 2001), SRB1 (Levitan et al., 2010) and CD36 (Podrez et al., 2002b, Kar et al., 2008).

1.6.3 Effects of oxLDL on platelets

Early evidence exists to show that human platelets are able to both bind and sequester labelled nLDL-Au (Zhao et al., 1994). Further studies then suggested that platelets recognise exclusively oxLDL, but not acetylated LDL, and that this was not via the typically described scavenger receptors A, but by CD36 (Volf et al., 1999). To provide further functional outcome of the platelet: oxLDL interaction, it was also shown that oxLDL induced platelet activation (Naseem et al., 1997). In studies similar to the initial LDL-Au study, oxLDL labelled with a fluorescent label was again shown to both bind and be internalised in platelets and these oxLDL positive platelets were shown to modulate endothelial inflammation *in vitro* (Daub et al., 2010). This study

was supported by a later *ex vivo* observation in patients with acute coronary syndrome (ACS), of increased oxLDL retention on circulating platelets paired with increased binding of platelets to the endothelium (Stellos et al., 2012). These initial studies have been followed by a comprehensive series of studies examining both the *in vitro* signalling biology of platelet: oxLDL and the translational aspects of this interaction *in vivo*.

oxLDL has been shown to drive many aspects of platelet function, indeed almost all facets of platelet function have been shown to be upregulated in some form by oxLDL. These include shape change in suspension and also static adhesion and spreading on immobilised oxLDL (Wraith et al., 2013), which in the context of immobilised oxLDL was shown to be accompanied by calcium flux, integrin activity and expression of CD62P (Nergiz-Unal et al., 2011). Other studies in response to modified electronegative LDL, which shares many hallmarks with oxLDL have shown platelet α-granule secretion, integrin activity, potentiation of aggregation and increased platelet-endothelium interactions, likely a result of increased platelet CD62P expression and endothelial activation (Chan et al., 2013). Alongside the described shape change, adhesion, calcium flux, α-granule secretion and integrin activity; δ-granule secretion has also been demonstrated as measured by ATP release (Nergiz-Unal et al., 2011), which suggests a model where oxLDL induces both cytoskeletal rearrangement and granule secretion, where dense granule secretion then releases ADP which provides an activatory feedback loop leading to complete platelet activation (Stalker et al., 2012), vitally all downstream of oxLDL (Nergiz-Unal et al., 2011).

Further studies began to interrogate the precise signalling events which led to oxLDL mediated platelet activation or hyperactivity, with a view to link these events to translational *in vivo* observations. A critical study in 2007 demonstrated that oxLDL could drive an *in vivo* prothrombotic phenotype via platelet CD36, demonstrated with murine models (Podrez et al., 2007). Many key studies emerged following this, which

began to elucidate the pathways by which oxLDL may drive platelet hyperactivity. Early work suggested that oxLDL, via CD36, signalled through a tyrosine kinase dependent pathway via Src family kinases Fyn and Lyn (Chen et al., 2008), a pathway common to several platelet signalling cascades, notably that of GPVI (Stalker et al., 2012). CD36: oxLDL induced signalling was further shown to drive cytoskeletal Rho-kinase, via tyrosine kinases, leading to platelet shape change and activation (Wraith et al., 2013). Further important roles for oxLDL *in vivo* were then described, where oxLDL was not only driving direct platelet activity but reducing tonic inhibition (disinhibition). Firstly, oxLDL, via CD36 and NOX2 was shown to reduce PKG activity – the key mediator of NO inhibitory signalling (Magwenzi et al., 2015). Following this, oxLDL were shown to activate PDE3a which regulates cAMP levels downstream of PGI_2, driving disinhibition of cAMP-PKA signalling in a CD36 dependent mechanism. Further to the involvement of CD36 and NOX2, a subsequent signalling study confirmed that this converged on the activatory kinase, ERK5, which was shown to regulate aspects of the oxLDL mediated platelet hyperactivity (Yang et al., 2017a). Finally, a new aspect of the CD36: oxLDL signalosome was suggested, which included toll-like receptors. Using a combination of murine models, it was demonstrated that TLR2 and TLR6 form a signalling complex with CD36 which then signals via the canonically described TLR-MyD88-IRAK pathway (Biswas et al., 2017).

1.7 INFLAMMASOMES

The inflammasomes are a broad group of large multimeric protein complexes with enzymatic activity. The complexes are related in their ability to drive an inflammatory response mediated by subsequent cytokine or interferon synthesis (Schroder and Tschopp, 2010). Inflammasomes respond to both DAMPs and PAMPs, although are often highly specific to a single ligand.

1.7.1 NLRP3 inflammasome

While NLRP3 is part of the larger family of inflammasomes, it remains distinct since it appears to play a role in many diseases, notably in multiple sterile inflammatory diseases including gout (Martinon et al., 2006), systemic lupus erythematosus (SLE) (Kahlenberg et al., 2013), cardiovascular disease (Yang et al., 2017b) and rheumatoid arthritis (Mathews et al., 2014). However, there is also evidence that the NLRP3 inflammasome is involved in systemic viral infections (Hottz et al., 2013) or bacterial sepsis (Dolunay et al., 2017). The multiple diseases NLRP3 is associated with, is likely due to the number of ligands it can be activated by. This is atypical of other inflammasomes, as the majority have a single specific agonist. This agonist specificity is vital to the tight regulation of inflammasomes, which when dysregulated drive severe inflammatory disease (Rowczenio et al., 2017). The NLRP3 inflammasome has been shown to respond to multiple ligands including the bacterial toxin nigericin, bacterial membrane component LPS, cellular stress signal ATP, gout monosodium urate crystals, atherosclerotic plaque cholesterol crystals, oxLDL and amyloid-β protein (Sheedy et al., 2013, Agostini et al., 2004). Conversely, the AIM2 inflammasome is only stimulated by viral double stranded DNA (dsDNA) presented when cells are infected by dsDNA viruses (Sagulenko et al., 2013), and the IPAF inflammasome is only stimulated by type III or IV secretion systems, commonly employed by gram negative bacteria to deliver toxins (Schroder and Tschopp, 2010).

The NLRP3 inflammasome is thought to respond to many ligands as they are assumed to converge on a common signalling pathway, where although they initiate from divergent points, there is a subsequent convergence on a shared node that has been suggested to be mitochondrial dysfunction paired with reactive oxygen species (ROS) production (Zhou et al., 2011, Ye et al., 2017, Murakami et al., 2012). This suggests that all the canonical agonists of the NLRP3 inflammasome are not yet known, but where mitochondrial ROS dysfunction is a result of the given ligand, NLRP3 inflammasome activation could be conjectured to occur.

The NLRP3 inflammasome has been comprehensively described in leukocytic models since the first report of the complex in 2004 (Agostini et al., 2004), and this has provided a robust understanding of the structure of the complex and each subunit of the multimer. The NLRP3 inflammasome when activated is comprised of the nacht-leucine rich repeat pyrin domain containing protein 3 (NLRP3) subunit, which binds to apoptosis-associated speck-like protein containing a CARD (ASC) via its pyrin domain. ASC subsequently recruits the thiol protease caspase-1 via its caspase recruitment domain (CARD). Once recruited, caspase-1 undergoes auto-cleavage and activation. The active caspase-1 tetramer is then able to cleave both gasdermin D and pro-interleukin-1β (IL-1β), which facilitate secretory pore formation and synthesis of IL-1β respectively (Figure 5).
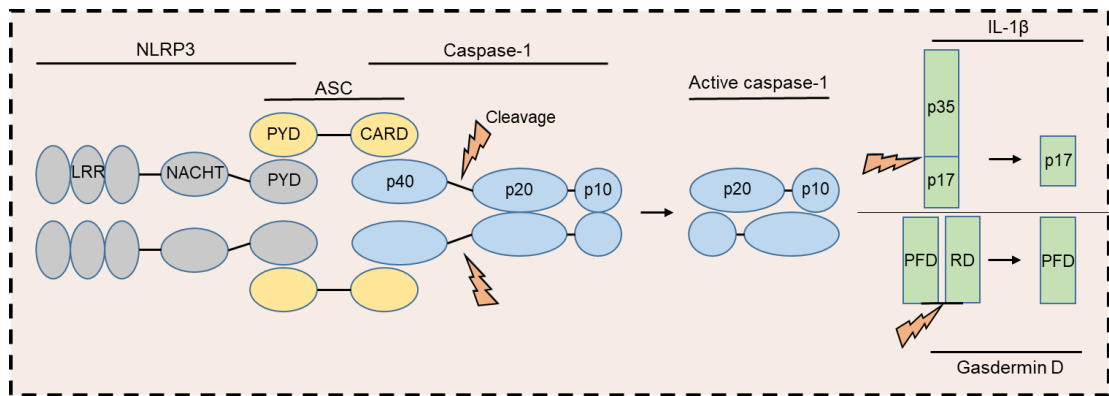
Figure 5. Molecular structure of the NLRP3 inflammasome. Upon activation, the NLRP3 inflammasome is recruited and oligomerises. This results in the recruitment and activation of caspase-1 which in turn cleaves pro-IL-1β and gasdermin D. Abbreviations; LRR – leucine-rich repeat, NACHT – nucleotide-binding and oligomerisation domain, PYD – pyrin domain, CARD – caspase recruitment domain, p20/p10 – active caspase-1 domains, p17 – mature IL-1β, PFD – pore forming domain, RD – repressor domain.

1.7.2 Activation and regulation of the NLRP3 inflammasome

For activation, the NLRP3 inflammasome must first undergo a priming event (Schroder and Tschopp, 2010). This is an intrinsic requirement of the complex, where it needs two distinct signals to permit activation. This two-step activation is a common feature of immune cell activation as it reduces aberrant activation which can drive severe inflammatory diseases. A classic example of this two-signal process is the memory B-cell class switch (Litinskiy et al., 2002), where a lack of dual signals, in this case, drives hypogammaglobinaemia (Salzer et al., 2005). In the context of the NLRP3 inflammasome, this requirement ensures careful regulation of the highly inflammatory IL-1β or IL-18 cytokines. The two-step activation is characterised firstly as a priming event which prepares the complex for recruitment and increases expression of constituent proteins, followed by a second signal that recruits the complex and drives activation (Schroder and Tschopp, 2010). It is now understood that priming is a combination of two concurrent events and can be further sub-divided into transcriptional and non-transcriptional priming. Transcriptional priming is transcription of inflammasome genes and translation of mRNA into inflammasome

component proteins – which of the five components, pro-IL-1β is required in particular abundance (Estruch et al., 2015). Non-transcriptional priming, is conversely regulatory events not driven by transcription, and has been shown to have several mediators including ubiquitination (Py et al., 2013, Rodgers et al., 2014, Song et al., 2016) and phosphorylation of multiple components including ASC (Lin et al., 2015) and NLRP3 (Song et al., 2017). This two-step model of NLRP3 inflammasome activation means that for a classical laboratory stimulation assay/experiment a two-step process of adding LPS followed by ATP or nigericin is required, to provide a priming and then an activating signal (Shi et al., 2016).

1.7.3 Platelets and the NLRP3 inflammasome

While several publications have demonstrated a role for the NLRP3 inflammasome in platelets, it is still an emerging field with many aspects of expression, regulation and function not yet understood. The NLRP3 inflammasome in platelets was first reported in 2013 and the authors described a role for platelets in the pathogenicity of viral haemorrhagic fever caused by dengue virus infection (Hottz et al., 2013). With the application of flow cytometry, this study demonstrated dengue virus driven shedding of IL-1β rich platelet microparticles which correlated with caspase-1 activation. Using pharmacological inhibitors against caspase-1, mitochondrial ROS and RIP1 kinase, these mediators were shown to be vital in the activation of NLRP3 (Hottz et al., 2013). Later it was reported that Brutons tyrosine kinase (BTK) caused the activation of the NLRP3 inflammasome downstream of the classical platelet agonists collagen and thrombin and it was proposed that NLRP3 had an important role in platelet haemostatic activation (Murthy et al., 2017). In 2018, NLRP3 inflammasome mediated regulation of platelet function was further explored and was shown to be key to the regulation of integrin outside-in signalling, and when tested in a NLRP3 knockout model (of note this was not a PF4/GP1b-cre model), platelet

thrombus formation was significantly reduced and bleeding times increased (Qiao et al., 2018). Although these two studies agreed on the importance of the NLRP3 inflammasome in platelet activation, they disagreed with respect to the existence of phenotypes associated with α-granule secretion. Murthy *et al.*, (2017) found no phenotype associated with α-granule secretion, whilst Qiao *et al.,* (2018) found an α-granule phenotype. Indeed, the role of the cytokine IL-1β itself on platelets and the effects it may have regarding function remains largely un-investigated.

The platelet NLRP3 inflammasome model has also been applied to a sickle cell disease (SCD) cohort and murine model (Vogel et al., 2018a). A series of experiments were performed concentrating on fluorescence measurements of caspase-1 cleavage with the fluorochrome labelled inhibitors of caspase (FLICA) (Bedner et al., 2000). Their data suggested that the platelet derived TLR4 ligand, high-mobility group box 1 (HMGB1) through BTK drives NLRP3 inflammasome activation. Furthermore, this ligand is present in the plasma of SCD patients, correlates with basal caspase activation and diseased plasma can also stimulate naïve platelets from healthy donors (Vogel et al., 2018a). This is consistent with work from the same group which showed that increased NLRP3 inflammasome activity drove platelet aggregation and thereby supports their previous findings (Murthy et al., 2017). A further short study again from the same group was published which reinforced their previously suggested aggregatory role of the platelet NLRP3 inflammasome in a murine model of hind limb ischemia downstream of platelet TLR4 ligation and caspase-1 cleavage (Vogel et al., 2018b). The same group then followed this up with a similar murine study which identifies that the platelet NLRP3 inflammasome plays a role in the development of pancreatic cancer in a murine model (Boone et al., 2019). While not directly referencing NLRP3, and as such not considered part of these core publications, in 2017 a group described a role for platelet secreted IL-1β in the stimulation of endothelial cells in the context of SLE (Nhek et al., 2017).

In summary of the NLRP3 inflammasome in platelets, these papers agree on the core hypothesis determined from the literature identified above, that the NLRP3 inflammasome plays an important role in platelet biology. However, they do not agree on the specific roles which the NLRP3 inflammasome may play, ranging from a systemic effect of secreted IL-1β driving vascular inflammation in dengue infection or SLE (Hottz et al., 2013, Nhek et al., 2017), to an autocrine effect which is vital for platelet activation (Brown et al., 2013, Qiao et al., 2018) or control of platelet activation (Murthy et al., 2017, Vogel et al., 2018a, Vogel et al., 2018b).

1.7.4 Expression of NLRP3 components in platelets

The current platelet NLRP3 inflammasome studies all provide convincing functional evidence of NLRP3 in platelets (Hottz et al., 2013, Murthy et al., 2017, Qiao et al., 2018, Vogel et al., 2018a, Vogel et al., 2018b), and in addition to this there is prior evidence that platelets can produce IL-1β (Brown et al., 2013, Nhek et al., 2017) and IL-18 (Allam et al., 2017) that is indicative of NLRP3 activity.

An additional valuable and comprehensive resource available to platelet researchers are transcriptomic or proteomic studies. In a brief overview of human and murine platelet proteomes and transcriptomes, the human proteome reports only ASC and gasdermin D, with copy numbers of both proteins predicted to be no more than 1500 per cell (Burkhart et al., 2012). In contrast, the transcriptome of both human and murine platelet RNA reports the presence of all components; NLRP3, ASC, caspase-1, IL-1β and gasdermin D, yet none are ranked within the 3000 most common transcripts (Rowley et al., 2011). The murine platelet proteome is identical to that for humans and suggests that only ASC and gasdermin D are present (Table 1) (Zeiler et al., 2014). These reports suggest that the presence of the complete NLRP3 inflammasome in healthy individuals is unlikely, as expression of NLRP3 was not detected within the healthy donors which the proteomic and transcriptomic studies

where performed, yet as previously described there is a functional role for platelet NLRP3 in the literature. This could be attributed to either low copy numbers of these proteins or transcripts below current detection thresholds. In support of this, the human proteome does not detect the presence of Toll-like receptors (TLR), but their expression has been evidenced by traditional biochemistry in multiple studies (Biswas et al., 2017, Fung et al., 2012, Rex et al., 2009, Damien et al., 2015, Vogel et al., 2018a, Vogel et al., 2018b). Alternatively, and discussed at greater length in the following section, within healthy naïve donors the complexes are not present until after an initial inflammatory insult.

Table 1. Relative expression or copy number of NLRP3 inflammasome components in human and murine platelets respectively (Rowley et al., 2011, Burkhart et al., 2012, Zeiler et al., 2014). Rowley et al., rank transcripts on assumed count from highest to lowest. Burkhart et al., and Zeiler et al., use an estimated copy number of each protein.

	Protein or transcript	Rowley, human rank	Burkhart, human copy number	Rowley, murine rank	Zeiler, murine copy number
Components	NLRP3	5913	-	10955	-
	ASC	3005	1000	4178	3743
	Caspase-1	3365	-	6354	-
	Interleukin1-β	4972	-	5773	-
	Gasdermin D	4114	1500	9645	308
Upstream	TLR2	5465	-	10865	-
	TLR4	7930	-	11414	-
	TLR6	11362	-	12714	-
	MyD88	3858	940	1906	1044
Controls	GPIX	48	32400	16	63503
	CD36	615	16700	6093	-
	GPVI	367	9600	155	7822
	BTK	599	11100	1590	12146
	Fyn	548	6800	490	4145

1.7.5 Priming of the NLRP3 inflammasome in platelets

The two-step model of NLRP3 activation of priming then activation is understood to be vital for robust synthesis of IL-1β via the NLRP3 inflammasome. However, no platelet NLRP3 inflammasome studies to date have explored this signalling dichotomy nor suggested it as necessary for NLRP3 activity. To date, the published work in this area agrees that platelets are able to demonstrate activation with only a single signal, but disagrees on whether this is inflammatory (Vogel et al., 2018a), pathogenic (Hottz et al., 2013), or thrombotic (Qiao et al., 2018). While this disagrees with current literature in nucleated cells, where the use of thrombotic ligands has been described, this is not surprising since platelets are unique cells and lack the capacity to undergo extensive transcriptional priming. They are instead more likely released from a megakaryocyte with the inflammasome component proteins; NLRP3, ASC, caspase-1, IL-1β and gasdermin D present in an inactive state. Therefore, it is possible to hypothesise that pre-programming is occurring, and it is the megakaryocyte which receives the transcriptional priming signal and the platelet the non-transcriptional priming and second activatory signal. This suggests there may be a complex cross-cellular process in place regulating this potent inflammatory event controlling a platelet population which is pre-programmed by megakaryocytes whom have adapted to the systemic environment and produced platelets tailored to requirement, not dissimilar to the model proposed by Davizon-Castillo et al., who propose that in ageing megakaryocytes produce inflammatory and metabolically defective platelets (Davizon-Castillo et al., 2019).

In support of platelet pre-programming by the megakaryocyte, the concept of disease altering the platelet proteome has already been demonstrated in severe obesity (Heffron et al., 2018). This would further suggest that the lack of inflammasome components in the Burkhart (Burkhart et al., 2012), Rowley (Rowley et al., 2011), and Zeiler (Zeiler et al., 2014) studies may be due to the use of naïve donors for analysis. It is tempting to suggest the pulmonary megakaryocyte subset (Lefrancais et al.,

2017), which it can be assumed are constantly bombarded with various airborne DAMPs, exhaust emissions or smoke, and PAMPs may be a source of early inflammatory platelets. Early work on this megakaryocyte subset suggested that the blood concentration of platelets was changing in response to respiratory insult (Sharma and Talbot, 1986), and it could be hypothesised that this increase in cell count was paired with a change in proteome. However this has not been further pursued to date.

Conversely or alongside this theory of platelet pre-programming, there is some evidence platelets have synthetic capacity and they are packaged with mRNA for pro-IL-1β (Brown et al., 2013), and pro-IL-18 (Allam et al., 2017), which has been shown to be spliced upon activation. This suggests there is flexibility within the platelets to splice selected mRNAs and upregulate proteins (Denis et al., 2005), therefore platelets may also inherently have the capacity for transcriptional priming and undergo post-megakaryocyte proteomic changes.

What remains clear is that where there are 150-400,000 platelets per microlitre of human blood, or ~75-200 x10^{10} platelets per individual, any inflammatory event they can initiate must be tightly controlled and aberrant activation avoided. It is the relationship between megakaryocytes and platelets in an inflammatory environment which undoubtedly remains vital to the pro-inflammatory platelet phenotype which the NLRP3 inflammasome evidences. This strongly suggests that understanding the changes which megakaryocytes undergo in inflammation will be just as vital as those which the platelets themselves demonstrate.

1.7.6 NLRP3 inflammasome and atherosclerosis

While the role of the NLRP3 inflammasome in platelets is not yet fully understood, it is possible to hypothesise a role for platelets in other systemic inflammatory diseases beyond the example of an acute dengue virus infection (Hottz et al., 2013), or the

more recently established role for platelets in chronic sickle-cell disease (Vogel et al., 2018a). While many chronic inflammatory roles for other cells via the NLRP3 inflammasome have been demonstrated, the blood borne inflammation that drives atherogenesis is an area which platelets could be proposed to play a key role (Sheedy et al., 2013). Particular clinical emphasis has recently been placed on the role of NLRP3 inflammasome produced IL-1β in the progression of atherosclerosis (Grebe et al., 2018, Baldrighi et al., 2017). The link between IL-1β and atherosclerosis has been proposed for several years and has been demonstrated in animal models by different research groups. Heijden et al. used the ApoE$^{-/-}$ murine model, which rapidly develops atherosclerosis, to demonstrate that pharmacological NLRP3 inhibition leads to reduced plaque size (van der Heijden et al., 2017). Similarly, van Hout et al. used a wild type porcine model and observed that with NLRP3 inhibition, and therefore reduced IL-1β synthesis, the severity of myocardial infarction was reduced (van Hout et al., 2017). Finally, the ApoE$^{-/-}$/ IL-1β$^{-/-}$ double knockout murine model has been shown to present with reduced atherosclerotic plaque size compared to ApoE$^{-/-}$/IL-1β$^{+/+}$ (Kirii et al., 2003). These all identify a key role for IL-1β in atherosclerotic development and progression of cardiovascular disease.

Further to these observations, clinical studies have begun to explore the relationship between the NLRP3 inflammasome and atherosclerosis. A recent human study has associated genetic polymorphisms in the genes which code for NLRP3 and caspase-1 with increased risk of developing acute coronary syndrome (Gonzalez-Pacheco et al., 2017). These studies and others have prompted the clinical trial into the effectiveness of canakinumab, a monoclonal antibody targeting IL-1β, as a therapy to target atherosclerotic disease (Ridker et al., 2011). Early results have indicated that anti-IL-1β therapy leads to a significantly reduced rate of cardiovascular events against the control group (Ridker et al., 2017a). A further studies outcomes of note included that canakinumab also appeared to exert protective effects in lung cancer incidence, considering the pulmonary megakaryocyte/platelet pool this could be

considered as another proposed role for platelet inflammatory function (Ridker et al., 2017b). Importantly for platelet researchers, these studies are global knockouts or systemic non-targeted treatment, leaving the question as to which cells contribute to these overt atherosclerotic phenotypes open.

OxLDL has been shown to modulate cellular function in many ways (Levitan et al., 2010), however, an implication in driving vascular inflammation and atherogenesis suggests it is a potential clinical target. OxLDL has been implicated in driving atherogenesis through activation of the NLRP3 inflammasome in macrophages and monocytes (Sheedy et al., 2013, Estruch et al., 2015, Yang et al., 2017b), which is likely via CD36 in a heteromeric signalling platform with TLRs 2/4/6 (Chavez-Sanchez et al., 2014, Stewart et al., 2010). OxLDL has also been shown to modulate endothelial cell biology, mostly by driving production of ROS which in turn impacts cell viability and lifespan (Touyz, 2014, Vindis et al., 2005, Zmijewski et al., 2005). The majority of the ROS produced in endothelial cells downstream of oxLDL have been functionally linked to mitochondrial dysfunction (Giovannini et al., 2002). This is likely via the LOX1 receptor (Christ and Latz, 2014, Touyz, 2014, Yang et al., 2017b), although CD36 also mediates cellular dysfunction (Sheedy et al., 2013) and can also be found directly on the mitochondrial surface (Smith et al., 2011). Taking all of these points in other cell types together and the functional expression of the NLRP3 inflammasome in platelets, it is possible to hypothesise a role for oxLDL and platelet NLRP3 in atherogenesis and vascular inflammation (Figure 6).
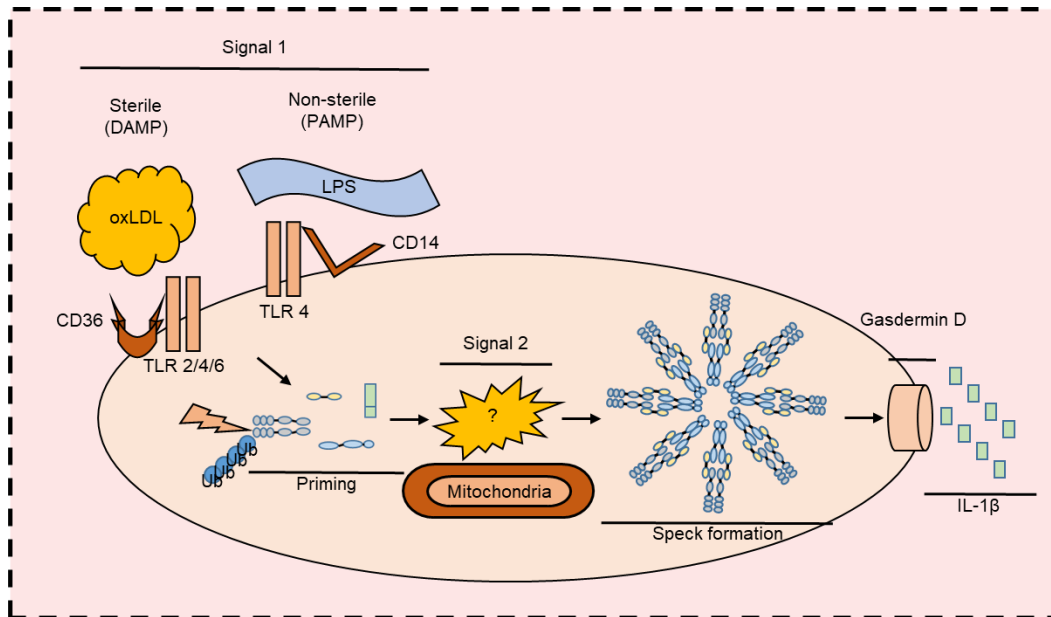
Figure 6. Proposed model of NLRP3 activity in platelets. DAMPs or PAMPs ligate their appropriate receptor which drives (post-)transcriptional priming of the NLRP3 inflammasome, followed by a second signal which drives recruitment, speck formation and cleavage of gasdermin D and IL-1β

1.8 AIMS OF STUDY

-Understand how platelet regulation may determine novel platelet subpopulations

-Explore the function of the NLRP3 inflammasome in platelets downstream of oxLDL

-Determine the role of oxLDL in driving platelet mitochondrial dysfunction

Chapter 2
Materials & Methods

2.1 REAGENTS

2.1.1 Chemicals & reagents

Sodium Citrate (367691), ACD-A (8304451), Sodium Heparin BD Vacutainer Tubes (8516324), BD DC Protein Assay Kit (5000112) and BD Phosflow Lyse/Fix Buffer 5X (558049) were from BD Biosciences. TMRE-Mitochondrial Membrane Potential Assay Kit (113852) was from Abcam. SFLLRN (Thrombin Receptor Activating Peptide) (58927) was from Anaspec. Collagen-related peptide (CRP-XL) was from Collagen Toolkits. Prostaglandin I_2 (sodium salt) (61849-14-7) was from Cayman Chemical. VersaComp Antibody Capture Bead Kit (B22804) was from Beckman Coulter Life Sciences. 4% Paraformaldehyde Aqueous Solution (157-4) was from Electron Microscopy Sciences. All other reagents were from Sigma-Aldrich.

2.1.2 Antibodies

Annexin V APC Ready Flow Conjugate (R37176), CD63 Monoclonal Antibody (H5C6) eFluor 660 (50-0639-42), CD154 Monoclonal Antibody (24-31) FITC (11-1548-42), Mouse IgG1 kappa Isotype Control (P3.6.2.8.1) eFluor 660 (50-4714-82), Mouse IgG1 kappa Isotype Control (P3.6.2.8.1) FITC (11-4714-81), and Goat anti-Rabbit IgG (H+L) Highly Cross-Adsorbed Secondary Antibody Alexa Fluor 488 (A-11034) were from ThermoFisher Scientific. BB700 Mouse Anti-Human CD42b (742219), APC Mouse Anti-Human CD42b (551061), FITC Mouse Anti-Human PAC-1 (340507), PE Mouse Anti-Human CD62P (555524), PE Mouse IgG1 κ Isotype Control (556650), FITC Mouse Anti-Human CD14 (347493) and PerCP Mouse Anti-Human CD42a (340537) were from BD Biosciences. Anti-Human Fibrinogen/FITC (F0111) was from Agilent Technologies. Phospho-VASP (Ser157) Antibody (3111) was from Cell Signalling Technology.

2.2 METHODS FOR THE ISOLATION OF BLOOD CELLS

2.2.1 Isolation of human platelets

Platelets were isolated from whole blood obtained from healthy volunteers in accordance with the declaration of Helsinki. All donors were consenting and healthy on presentation and also confirmed they had taken no anti-coagulants or anti-platelet drugs. Careful isolation procedures were required since platelets are very sensitive to artefactual activation during handling. The first approach was to use prostaglandin I_2 (PGI_2) to inhibit activation during isolation (Vargas et al., 1982). However, when cAMP signalling was being studied, a second approach where the pH was lowered using citric acid, which also inhibits platelets, was used. The average yield from 16 mL of healthy human donor blood was 2.4 mL of cell suspension at 5 x 10^8 platelets/mL (Figure 7).
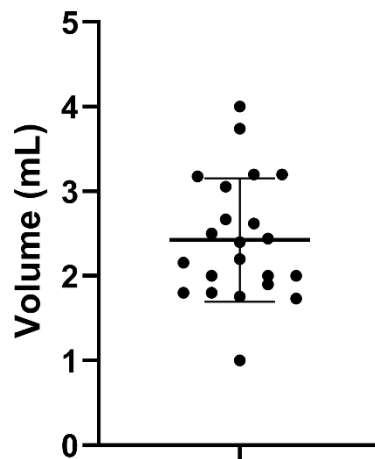
Figure 7. Average yield of washed platelets from 16 mL of whole blood. Platelets washed from 16 mL of whole blood drawn into ACD-A and resuspended to a final count of 5 x 10^8 platelets/mL and total volume measured. (Mean±SD, n=22)

2.2.2 Isolation methods

Blood was obtained from palpable veins located in the ante-cubital fossa through venepuncture with a 21g butterfly needle by trained phlebotomists. Blood was drawn into acid citrate dextrose (ACD, 2.9 mM citric acid, 29.9 mM sodium citrate, 72.6 mM NaCl, 113.8 mM glucose, pH 6.4) syringes at a 1:5 ratio with anticoagulant or into commercial ACD-A (BD) vacutainers at 1:5 ratio with anticoagulant (85 mM sodium citrate, 136 mM dextrose, 42 mM citric acid, 1 mM potassium sorbate), then transferred to a 50 mL falcon tube at a fill rate of 20 mL per tube, and centrifuged at 100 g for 20 minutes (no brake) to isolate platelet-rich plasma (PRP). PRP was removed using a 1.5 mL Pasteur pipette and equally distributed between two 15 mL falcon tubes.

In some cases, PRP was treated for 2 minutes with PGI_2 (200 nM) then centrifuged at 1000 g for 10 minutes (with brake) to pellet the cells. Supernatant plasma was removed, and the pellet was re-suspended in 5 mL of modified Tyrode's buffer (0.5 mM $MgCl_2$, 0.55 mM NaH_2PO_4, 2.7 mM KCl, 5 mM HEPES, 5.6 mM glucose, 7 mM $NaHCO_3$, 150 mM NaCl, pH 7.4), 0.5 mL of ACD and 200 nM PGI_2 and incubated for 2 minutes. This was then centrifuged at 1000 g for 10 minutes (with brake) to pellet washed cells. Supernatant wash buffer was removed, and the pellet was re-suspended in 1 mL of modified Tyrode's buffer, counted and rested at 37∘C for 20 minutes prior to assay initiation to allow for recovery from PGI_2 treatment.

As an alternative approach, a citric acid-based wash buffer, which both reduces pH and contains EDTA to chelate calcium ions, was used to inhibit platelet activation in the absence of PGI_2. Here PRP was treated for 2 minutes with citric acid (0.3 M) at a ratio of 20 μL/1 mL PRP. This was then centrifuged at 1000 g for 10 minutes (with brake) to pellet the cells. Supernatant plasma was removed, and the pellet was re-suspended in 5 mL of wash buffer (5 mM glucose, 5 mM KCl, 9 mM NaCl, 10 mM EDTA, 36 mM citric acid, pH 6.4) and centrifuged at 1000 g for 10 minutes (with

brake) to pellet washed cells. Supernatant wash buffer was removed, and the pellet was re-suspended in 1 mL of modified Tyrode's buffer, counted and rested at 37∘C for 20 minutes prior to assay initiation to allow for recovery from isolation.

2.2.3 Isolation of murine platelets

Murine blood was drawn from the exposed *vena cava* of isoflurane anaesthetised mice with a 25g needle into a 1 mL syringe pre-filled and coated with 200 µL of ACD. This was transferred to a 15 mL falcon tube and 200 µL of modified Tyrode's buffer was added prior to centrifugation at 100 g for 5 minutes (no brake) to isolate PRP. PRP was removed to a 15 mL falcon tube and the remaining blood cell pellet was remixed with an addition of 200 µL of modified Tyrode's buffer prior to a second centrifugation at 100 g for 5 minutes (no brake). The resulting PRP was combined with the previously isolated PRP. The PRP volume was then adjusted to 2 mL with modified Tyrode's buffer and PGI_2 (200nM). The PRP was centrifuged at 1000 g for 6 minutes (with brake), then the supernatant removed, and the isolated platelets resuspended in 500 µL of modified Tyrode's buffer, before counting and resting at 37∘C for 20 minutes prior to assay initiation to allow for recovery of cAMP levels.

2.2.4 Counting isolated platelets

Platelet counting was performed on a Beckman Coulter Z1 particle counter. The platelet suspension was diluted 1/2000 (5 µL in 10 mL) of isotonic count buffer (Beckman Coulter) and analysed for particles between 2 – 7 µm in diameter using a 50 µm aperture. This count was multiplied by 2000, to account for the dilution factor, giving a concentration per resuspended millilitre of cells. The count was adjusted to the desired concentrations for each assay using Equation 2. For example, concentrations of 2.5×10^8/mL, 5×10^8/mL and 10×10^8/mL were used for aggregation, flow cytometry and immunoblotting respectively.

$$\left(\frac{actual\ count}{target\ count}\right) - actual\ volume = adjustment\ volume$$

Equation 2. Used to calculate volume of buffer to add to adjust platelet count. Where adjustment volume is the volume of buffer to add to reach the desired concentration.

2.3 METHODS FOR STUDYING PLATELET FUNCTION

2.3.1 Fluorescent flow cytometry

Flow cytometry, as the name suggests is the measurement of cells under flow in suspension. This simple description hides the true power, which is the multiparameter analysis of single cells in complex media at a rate of >1000 cells/second. This allows not only descriptive characterisation of single cells, but vitally their comparisons within their given population, and subsequent division into phenotypically distinct subpopulations. However, given the current relative ease of accessibility, appropriate application of technical aspects and biological controls is key to the correct interpretation of data (Cossarizza et al., 2017).

Flow cytometry relies on several key principles, each of which feed into one another; (i) cells are in suspension at a suitably low concentration, (ii) the fluidic forces of sheath can push the sample into a sample core of single cells, (iii) lasers are able to excite each individual cell as it passes through and detectors collect the emitted and scattered light (Cossarizza et al., 2017).

The essential principle of a flow cytometer is the ability of a sheath of fluid under pressure to force a suspension of particles into a linear core, and this was first described and used for counting particles in suspension (Crosland-Taylor, 1953). This hydrodynamic focusing forces Brownian suspensions of particles into streams of single particles (Figure 8). Yet on some occasions events can pass through the flow cell simultaneously (swarming) or aggregates/agglomerates of cells/particles can form resulting in erroneous data as these are counted as single particles or events. Therefore, it is key that both, concentration of particles does not allow

swarming and the milieu in which the particles are suspended does not encourage precipitate or doublet formation, or commonly in the case of platelets, homotypic aggregate formation. Here we used a Beckman Coulter CytoFLEX, which uses a peristaltic pump as oppose to the more traditional syringe drive to maintain a consistent flow of sample through the flow cell (Beckman Coulter).

Typically, the digital information presented on an interface attached to a flow cytometer has gone through several transformations. Cells and fluorophores which are passed through the flow cell are excited by lasers and emitted light intensity is measured. This collected light, or photons, are routed to detectors after pre-processing in optical filters, which is a key step as the detectors are insensitive to the wavelength of light. In the CytoFLEX, avalanche photodiodes (APDs) are used rather than the more commonly used photomultiplier tubes (PMT), APDs have been shown to give a greater detection of near-infrared signals than PMTs (Lawrence et al., 2008), allowing greater flexibility in panel design. The detectors convert photons into photoelectrons which are then processed and amplified accordingly and then converted to a digital signal via an analogue digital converter (ADC) (Cossarizza et al., 2017). The optimal set up of the cytometer and performance of each component should lead to a low signal: noise ratio, which is the key determining factor of the sensitivity of a flow cytometer.
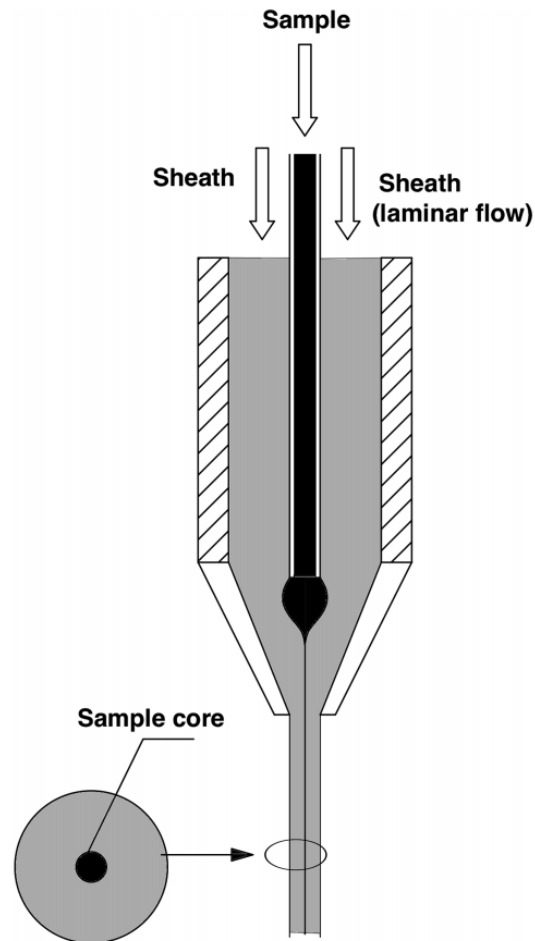
Figure 8. Fluidic system of a fluorescent flow cytometer. Sample is drawn into the flow cell and focussed into a beam of single cells by hydrodynamic focusing. These then pass through excitation lasers which drive emission of tagged fluorophores and allow physical light scattering to be collected. Adapted from (Cossarizza et al., 2017)

2.3.1.1 Applications of FFC to platelet biology

Flow cytometry has been used for the analysis of platelets for many years. It is a technique which is well suited for platelet research, since platelets typically exist within suspensions of complex media (blood or plasma) and express unique markers on activation which can be easily detected. Several major milestones of platelet flow cytometry have been reached. Firstly, the use of the peptide Glycine-Proline-Arginine-Proline (GPRP) was shown to allow activation analysis in thrombin stimulated whole blood to be carried out (Michelson, 1994). Secondly, the widespread use of the PAC1 antibody, which detects the conformational change in

the integrin $\alpha_{IIb}\beta3$, was presented as an alternative marker to fibrinogen binding (Frelinger, 2018). Thirdly the use of phosphoflow to detect intracellular changes to phosphorylation state in platelets (Spurgeon et al., 2014) Fourthly, the first six-parameter platelet panel was reported on in 2018 (Sodergren and Ramstrom, 2018), and finally the application of cytometry by time of flight (CyTOF) was applied to platelet biology (Blair et al., 2018). These milestones have all pushed the frontiers of platelet analysis by flow cytometry, and vitally have opened an important discussion on standardisation of technique and how these assays may be translated to clinics (Welch et al., 2018, Linden et al., 2004, Harrison, 2009, Harrison et al., 2011, Ramstrom et al., 2016, Spurgeon and Naseem, 2019). Based on the current progression of the cellular immunology field, platelet biology assessed by fluorescent flow cytometry is likely to continue to grow with an increased uptake of multiparameter assays with multidimensional analysis which will, in turn, drive the potential for discovery of rare cell subpopulations. Furthermore, the phosphoflow protocol has not yet been fully realised in the study of platelet biology, where the simultaneous measurement of multiple phosphorylation events paired with changes in surface marker expression (Leelatian et al., 2015), will provide a hugely powerful platform for the interpretation of platelet signalling in the future.

2.3.1.2 Multiparameter flow cytometry

As multiparameter flow cytometry becomes more routine, there is a requisite increase in demand for multidimensional analyses, which avoid the biased and time-consuming manual gating strategy in lieu of algorithm based deconvolution and clustering. There are several such variants now available for the researcher to use on an open access basis. The three most common variants currently in use are SPADE (Spanning-tree progression analysis of density-normalized events), flowSOM (Flow self-organising map) and tSNE (T-stochastic neighbourhood

embedding) and they can be applied from open-source GitHub resources or through packages such as FlowJo or Cytobank. A brief overview of the three main multidimensional analyses are as follows.

SPADE (2011), is a computational approach to analysis of flow cytometry data which is used to uncover cellular heterogeneity from multiparameter flow cytometry data sets. SPADE provides the researcher with a "tree" of clusters of cells which are grouped into major groups of related cells (branches), *i.e.,* granulocytes, and then within that will be individual clusters (leaves), *i.e.,* belonging to neutrophil, basophil and eosinophils – providing that the marker panel chosen distinguishes these cells.

FlowSOM (2015), analysis was developed as an alternative means of clustering and dimensionality reduction. FlowSOM produces a tree of related cells similar to SPADE, but has been shown to be roughly 100x faster in analysis as it does not require subsampling (Van Gassen et al., 2015). However, it is generally not compatible with less than 7-parameter cytometry as it loses power of resolution.

t-SNE (2008), is a visualisation tool which reduces the dimensionality of multiparameter data onto a 2-dimensional plot of arbitrary t-SNE axes (van der Maaten and Hinton, 2008). Unlike SPADE, which plots only clusters representative of cells as relatively size globes on a tree, t-SNE plots all cells/events analysed. Using a random seed and a series of exaggeration phases it pulls together related events and pushes apart non-related events giving rise to islands. t-SNE is used for both genomic data as well as flow cytometry data, although initially the algorithm struggled with very large (>1 x 10^6 events) datasets, several iterations have since been proposed to address these initial pitfalls. Further improvements include the development of optimal parameter t-SNE, opt-SNE (Belkina et al., 2018), which provided automated tools as part of the analysis package which deploy prior to tSNE analysis to determine optimal pre-t-SNE conditions. This demonstrated a significant improvement in the size of datasets which could be processed, allowing up to 20 x

10^6 events to be processed and populations resolved. In this study, we use fast Fourier transform-accelerated interpolation-based t-SNE, Fit-SNE (2019). This re-iteration of the original algorithm sped analysis time, reduced computational load and enhanced scaling to larger data sets through application of Fourier transform and using an ANNOY library lookup to calculate nearest neighbours as oppose to using vantage-point trees (Linderman et al., 2019). None of these methods of analysis have yet been applied to fluorescent flow cytometry data of platelets, while two papers using CyTOF analysis of platelets have used t-SNE (Blair et al., 2018) or both t-SNE and flowSOM (Blair and Frelinger, 2019) and have used these to describe differences in marker expression across the entire platelet population, although have not definitely identified subpopulations based on specific marker expression yet.

The following protocols focus primarily on human platelet analysis, although the assays are interchangeable with murine platelets providing an antibody that targets the murine platelets protein is available.

2.3.1.3 Platelet identification

Platelets can be identified on a flow cytometer based on their distinct physical characteristics of forward scatter (FSC) and side scatter (SSC), as they are considerably smaller than both red-blood cells and leukocytes. However, where possible and compatible with the assay, positive gating was used to confirm the gated population of cells are platelets. This uses the expression of platelet specific surface markers and excludes debris which may fall into the physical gate (Figure 9). In platelet activation assays, a further physical gate was analysed to ensure cellular doublets were not analysed.
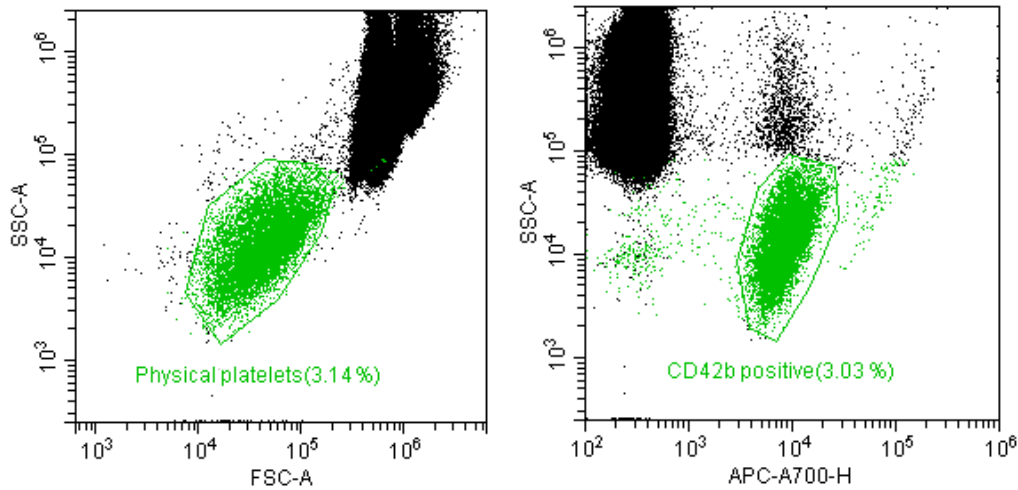
Figure 9. Platelet gating on a fluorescent flow cytometer. Platelets can be gated for using physical characteristics on FSC and SSC (left) or using CD42b positive events (right), where a small amount of debris (left shift) which positive gating omits can be seen, as can the platelet doublet events which are twice as bright for the platelet marker (right shift). Here a CD42b-BB700 was used to provide a platelet positive gate.

2.3.1.4 Platelet activation

Flow cytometric measurement of platelet activation utilises a variety of different antibodies or protein conjugates, which bind to either constitutive or inducible protein markers on the platelet surface. Typically, we used antibodies or conjugates raised against CD62P (P-selectin), fibrinogen, the active integrin $\alpha_{IIb}\beta3$ or annexin V which binds to PS in a calcium dependent manner.

Regardless of the antibody mixture used, platelet activation assays on the flow cytometer were performed under the following conditions. All reagents bar blood was added, and the tube was mixed thoroughly on whole blood addition, incubated for 20 minutes and then fixed in 10x volume of 1% paraformaldehyde/PBS. Table 2 provides an overview of the reagents required for a mock experiment comparing basal with stimulated and an isotype control tube. Where many conditions were being performed a 1.1 mL 96-well round bottomed plate was used to allow for high throughput processing of samples.

Table 2. A generic design of a platelet activation flow cytometry assay. Working with a total volume of 50 µL, whole blood, titrated antibodies and 10x agonists are added to an appropriate amount of modified Tyrode's buffer. There is flexibility in the additions as the volume of modified Tyrode's buffer can be adjusted to account for additional inhibitors or larger volumes of antibodies and agonists.

Condition	M. Tyrode's	Whole blood	Antibodies	Agonists	Control Antibodies
Basal	40	5	5	0	0
Stimulated	35	5	5	5	0
Control	35	5	0	5	5

Platelet activation can then be measured as median/mean fluorescence intensity (MFI), fold over basal or percent positive cells over control (Figure 10). MFI is a total reading of signal from the population of events and as such is quantitative for volume of antibody bound and therefore antigen exposed. Fold over basal also uses MFI, but all data is normalised to a basal signal, this eliminates a requirement for an IgG or fluorescence minus one (FMO) control. However, this approach prevents the researcher making any comment on basal activity. Percent positive cells is a qualitative readout, by setting a background fluorescence baseline of 2% on an IgG or FMO control, any fluorescence which exceeds this is determined to be positive signal, and the event is therefore considered positive for the marker. This measure is insensitive to quantity of antibody bound but can be very sensitive to subtle changes. Preferably, both quantitative MFI and qualitative percent positive are used when expressing data, as they present more fully the depth of data available and may provide insight into nuances which one data set alone would not illustrate.
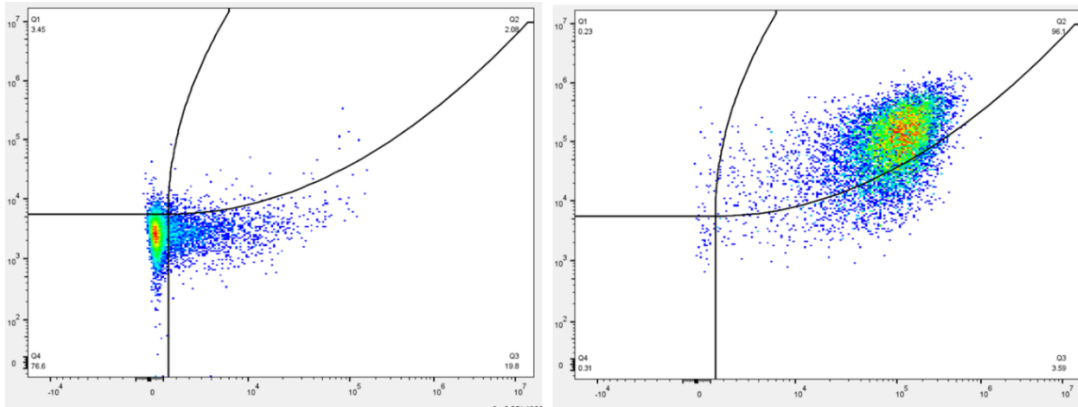
Figure 10. Two-parameter platelet activation. Fibrinogen-FITC (Y-axis) and CD62P-PE (X-axis) were measured in platelets at basal (left) and stimulated (right) with SFLLRN (5 µM). Gates were determined using EDTA and IgG-PE control which allows for percentage positive cells to be calculated.

In this study many antibodies were used to measure activation. They were often combined into panels (Table 3) to study activation and therefore compare markers and provide data for advanced analysis.

Table 3. Multicolour panels used to examine platelet activation. In combination these panels allow 7 markers to be compared for changes in expression upon activation. The breadth of markers was designed to allow several phases of platelet activation to be monitored including; aggregatory activation, degranulation of alpha and dense granules and procoagulant activity.

	Filter (band pass)			
Panel	525/40	585/42	660/10	712/25
1	Fibrinogen -FITC	CD62P -PE (AK-4)	CD42b -APC (HIP1)	-
2	Fibrinogen -FITC	CD62P -PE (AK-4)	Annexin V -APC	CD42b -BB700 (HIP1)
3	PAC1 -FITC	CD62P -PE (AK-4)	CD42b -APC (HIP1)	-
4	PAC1 -FITC	CD62P -PE (AK-4)	Annexin V -APC	CD42b -BB700 (HIP1)
5	CD154 -FITC (24-31)	CD62P -PE (AK-4)	CD63 -eF660 (H5C6)	CD42b -BB700 (HIP1)

2.3.1.5 Platelet counting in whole blood

In brief, by diluting 5 µL of blood within 45 µL of staining cocktail, that contained an antibody which targets a platelet marker such as CD41, CD42b or CD61, and then adding 450 µL of PBS a dilution factor of 1/100 was maintained. By running samples at a low acquisition rate (10 µL/minute) for 2.5 minutes, the events/µL and therefore cell count can be compared between donors, or transgenic murine strains.

2.3.1.6 Platelet leukocyte aggregates

Platelet-leukocyte aggregates are measured on a flow cytometer using a multi-fluorescence approach and through a gating strategy that uses cell specific surface markers to identify the leukocyte of interest (Figure 11). For example, in enriched

PBMC suspension monocytes are distinguished using gates set as SSC-A/CD14-FITC (CD45 positive) and lymphocytes with SSC-A/CD45-PE (CD14 negative).
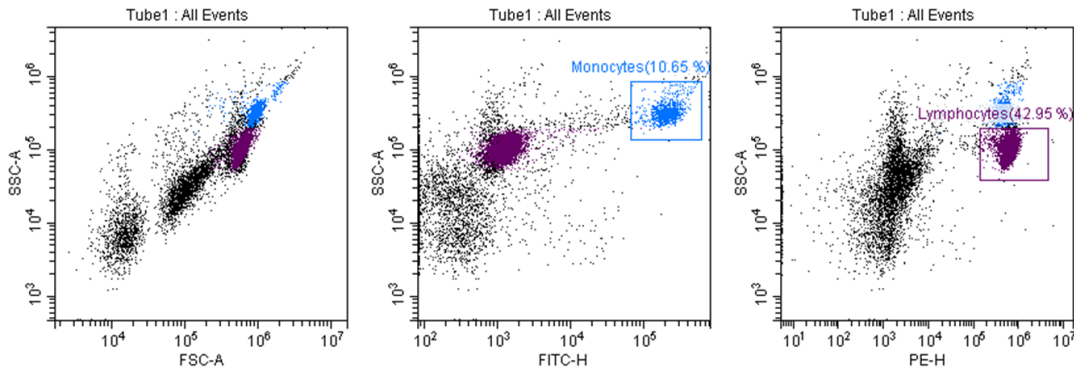
Figure 11. Monocyte and lymphocyte gating strategy in enriched PBMC suspension. Enriched PBMC suspension was probed with CD14-FITC and CD45-PE to allow for identification of monocytes (CD14-FITC, mid) and lymphocytes (CD45-PE, right) respectively.

Gating of the leukocyte of interest then allowed for platelet fluorescence to be measured from this gate, where signal for platelet specific markers indicated that platelets are bound to the leukocyte. For example, platelet monocyte interactions were measured using a CD14-FITC monocyte gate and then these cells were examined for CD42b-BB700 fluorescence. The basal sample exhibited little platelet monocyte aggregates and the stimulated sample (SFLLRN 10 µM, 20 minutes) demonstrated the majority of monocytes are bound to platelets (Figure 12).
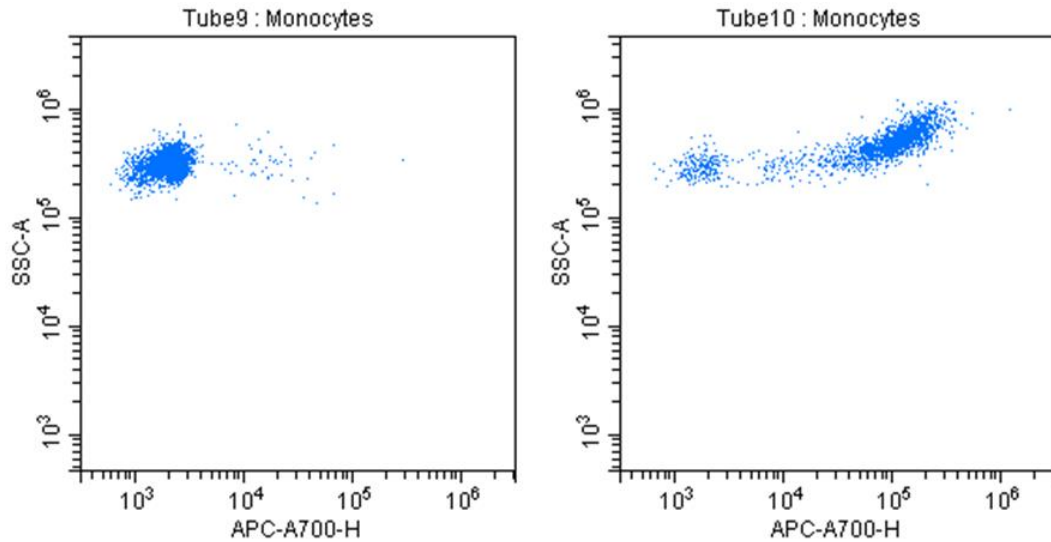
Figure 12. Platelet monocyte interactions. Whole blood is left at basal (left) or stimulated (right, SFLLRN 10 µM, 20 minutes) and probed with CD14-FITC and CD42b-BB700 (detected with the APC-A700 filter) to identify monocytes and platelets respectively.

In this study several antibodies were used to distinguish platelets, monocytes, lymphocytes and neutrophils. They include CD42b-APC, CD42b-BB700, CD42a-PerCP, CD14-FITC, CD16-APC, CD45-PE.

2.3.1.7 Technical development of assays

The use of multiple fluorophores allows the simultaneous acquisition of numerous markers on the cell surface. However, spectral overlap of fluorophores is considered the major issue with multi-colour fluorescent flow cytometry. With the Beckman Coulter CytoFLEX allowing up to 13 channels to be measured in a spectral range which covers only 330 nm, this means that panel design, fluorophore selection and compensation must all be used to eliminate the inclusion of false data.

2.3.1.8 Panel design

For the panel design used in this study, the targets were ranked by expression level and then by those markers which are used qualitatively for gating or those used

quantitatively for accurate measurement of expression. By arranging targets like this it was possible to assign appropriate fluorophores based on brightness, stability and the amount of spectral compensation each channel will require. For example, a target of interest which has low expression but is suspected to change only a small amount on activation is a good candidate for a bright fluorophore such as PE. However, if the target was simply a cell marker used for gating which is highly expressed and changes are not expected to occur, a less sensitive fluorophore could be used, such as far-red BB700.

2.3.1.9 Compensation

Compensation is the calculation of spectral overlap between fluorophores into adjacent channel bandpass filters, allowing the subsequent subtraction of fluorescence which is deemed to be from outside of the target fluorophores emission. It is performed with either antibody binding beads or cells. Several tubes of cells or beads are produced with each one stained with a single fluorophore and compared to an unstained tube. By analysing each tube individually, it is then possible to calculate the degree to which each fluorophore bleeds into each adjacent channel. Using software such as CytExpert or FlowJo, a compensation matrix can then be produced, an example of which is given (Table 4). A compensation matrix is specific to the fluorophores, gains and spectral characteristics for the specific cytometer on which it was acquired. Applied properly, a compensation matrix will subtract spectral overlap and allow multicolour fluorescent flow cytometry to be performed.

Table 4. An example compensation matrix. This matrix was produced using beads bound to antibodies with the appropriate fluorophore. It allows compensated four-colour measurement of Fibrinogen-FITC, CD62P-PE, Annexin V-APC and CD42b-BB700.

Channel	-FITC%	-PE%	-APC%	-APC-A700%
FITC		0.64	0.00	14.11
PE	27.62		0.00	42.67
APC	0.00	0.00		10.24
APC-A700	0.00	0.00	37.66	

In practice, compensation can be demonstrated using a population of three differently stained beads. Beckman Coulter VersaComp beads stained with FITC, PE and APC were run separately to produce a compensation matrix which was automatically calculated by the CytExpert compensation calculator, before running individually and the data was then compared for spectral overlap in both uncompensated and compensated data sets. FITC and PE were shown to overlap heavily as they are of similar emission and both excited by the 488 nm laser, while APC which is excited by the 638nm laser was not affected by either of these fluorophores. The matrix compensated the spill-over between FITC and PE, but it also induced an increase in spreading of the data around the median point (Figure 13). Which is the major caveat of compensation, which will result in a increase in data spread and therefore a small loss of a sensitivity, although often this caveat is outweighed by the increased power that multiple parameters bring to a cytometry assay.
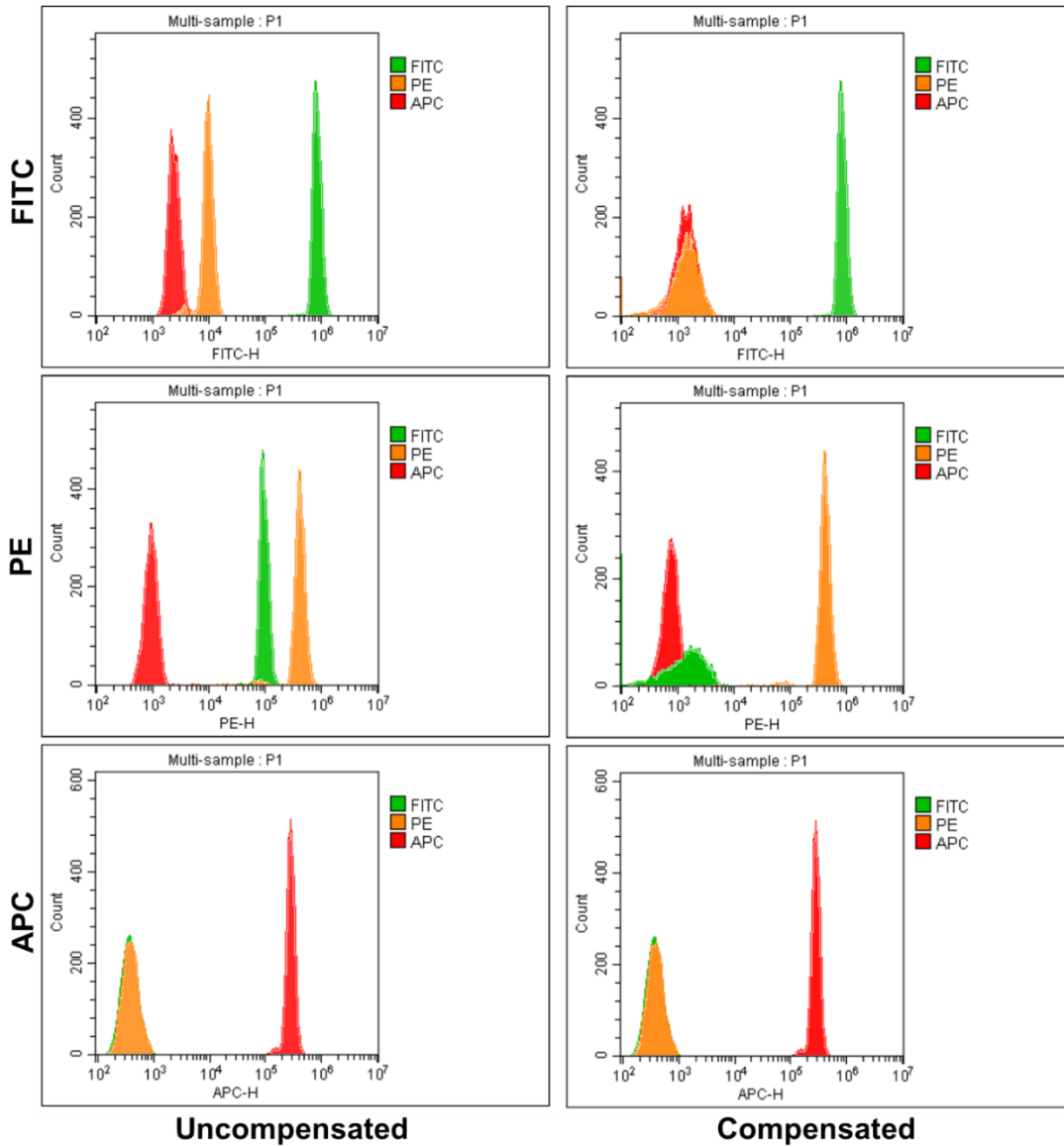
Figure 13. Three colour compensation in practice. Staining with FITC, PE and APC conjugated antibodies demonstrate the principles of spectral bleed from each channel in the uncompensated column (left), but when a compensation matrix is applied the spectral overlap is eliminated with some increased spreading of compensated parameters (right).

2.3.1.10 Phosphoflow

Phosphoflow is a novel method for analysing the phospho-proteome by fluorescent flow cytometry (Oberprieler and Tasken, 2011). Typically, phosphorylation events are measured through a combination of immunoblot and immunoprecipitation and this provides a bulk phosphorylation measurement for the entire population of cells. By flow cytometry each cell is analysed as an individual event, this allows phosphorylation of cellular subpopulations to be examined. Furthermore, flow cytometry is also high throughput and needs only small samples, whereas traditional immunoblot techniques take upwards of a day and require large sample volumes. The method is based on permeabilisation of cells to allow the entry of phospho-specific antibodies (Spurgeon and Naseem, 2018).

Whole blood (20 µL) was incubated with PGI_2 (1 – 1000 nM) for 2 minutes within the wells of 96-well plate. Each sample then had 10x volume of 1x BD fix/lyse at room temperature to fix and lyse RBC. This was centrifuged at 1000 g for 10 minutes with low brake to pellet cells and supernatant removed. The subsequent pellet was resuspended in 300 µL of ice-cold PBS/Triton-X100 0.1%, mixed by pipetting 20x avoiding aeration, incubated for 10 minutes and was followed by the addition 300 µL of ice-cold PBS then centrifuged at 1000 g for 10 minutes with low brake to pellet cells and supernatant removed. The pellet was then resuspended in 100 µL of ice-cold PBS/anti-phospho VASP s157 (1 µg/mL), and incubated for 30 minutes at 4∘C. This was followed by the addition 300 µL of ice-cold PBS followed by centrifugation at 1000 g for 10 minutes with low brake to pellet cells and supernatant removed. The pellet was then resuspended in 100 µL of ice-cold PBS/anti-rabbit-PE (1 µg/mL). At 30 minutes, 300 µL of ice-cold PBS was added and this was centrifuged at 1000 g for 10 minutes with low brake to pellet cells. The supernatant was removed, and the pellet was then resuspended in 150 µL of ice-cold PBS and analysed by fluorescent flow cytometry recording 10,000 platelet positive events. It is important that buffer post-fix is kept cold to prevent residual phosphatase activity reducing the

phosphorylation state of target proteins. Typically, IgG controls are not used in phosphoflow experiments and the increases in phosphorylation are expressed as fold over basal, however this does exclude the assays from commenting on changes in basal phosphorylation.

The basic protocol can be adapted to suit other phospho-site or protein specific antibodies which have been validated and optimised.

2.3.1.11 Surface staining and phosphoflow

A recent adaptation of phosphoflow developed here in platelets for the first time allows both intracellular phosphorylation and extracellular markers to be measured simultaneously. Here a novel protocol was developed to allow an intracellular signalling event to be compared directly to a change in expression of an activation marker. This protocol followed a simultaneous stimulate/probe (surface), fix, permeabilise, probe (intracellular), analyse approach, which allowed for simultaneous measurement of surface CD62P-PE and CD42b-APC with intracellular phospho VASP s157. The use of a probe, fix, permeabilise, probe was applied here as excessive fixation and permeabilisation would prevent the surface targeted antibodies from binding correctly due to loss of epitope. Permeabilisation also meaning that all CD62P would be measured, not just that expressed on the surface on activation, which would render the assay insensitive to changes if probed for CD62P post-permeabilisation.

For this assay whole blood was stimulated for 2 minutes with PGI_2 (10 – 1000 nM) followed by 20 minutes with SFLLRN (20 µM) in the presence of the surface staining antibodies. This is then fixed with 10x volume of 1x BD fix/lyse and then a standard phosphoflow protocol was used.

2.3.1.12 Application of novel dyes in platelet biology

The flow cytometry protocols described so far have relied primarily on the use of conjugated antibodies, aside from the annexin V-APC conjugate, as markers of changes to the platelet surface or signalling machinery. However, there are many other methods of staining markers which have no direct sites of recognition for antibodies to target. In this work three such dyes were applied.

2.3.1.13 Fluorochrome-labelled inhibitors of caspases

Fluorochrome-labelled inhibitors of caspases, or FLICA dyes are designed around an inhibitory motif specific to caspase enzymes (Bedner et al., 2000). Each caspase enzyme has a high affinity for four amino acid motifs, which can be used to target them with a relatively high specificity (Garcia-Calvo et al., 1998). Here FLICA was used to target caspase-1, and the motif applied was YVAD. The YVAD motif is sandwiched between FAM-YVAD-FMK where FAM is a carboxyfluorescein and FMK is a fluoromethylketone. An additional YVAD-FMK was used conjugated to a far-red fluorophore to validate findings with the FAM conjugate. When caspase-1 binds to the YVAD motif in attempt to cleave the moiety, it is covalently bound to the enzyme by the FMK group, this means that the fluorescent tag is directly bound to active caspase-1 (Figure 14).

Figure 14. Overview of method by which FLICA detects activated caspase-1. The fluorescently tagged peptide motif YVAD binds to the active site of caspase-1 and forms a covalent bond with the FMK moiety. This fluorescently tags active caspase-1 enzymes.

A protocol was developed to detect caspase-1 activity in platelets. Washed platelets (2×10^6) were suspended in a total volume of 50 µL of calcified modified Tyrode's buffer (2 mM) and the inflammasome activated by the bacterial potassium pore forming toxin nigericin (1-10 µM). If other agonists or inhibitors were used, they were added prior to nigericin to allow them to take effect. This activated suspension is mixed and incubated for 20 minutes and then 5.5 µL of 1x FLICA dye is added to this and mixed thoroughly. This is then incubated for a further 40 minutes to allow the dye to enter the cells and bind to active caspases. The samples are then fixed in 10x volume of 1% paraformaldehyde/PBS for 10 minutes prior to two washes in PBS at 1000 *g* for 10 minutes to remove unbound dye. The samples are then run and analysed for carboxyfluorescein fluorescence in the 525/40 bandpass filter or the far-red FLICA in the 660/10 bandpass filter. As there is no FMO, IgG or competitive control in this instance, MFI or fold over basal was used to present the data.

2.3.1.14 MitoSOX

MitoSOX is a mitochondrial superoxide dye, which is not fluorescent until it is oxidised by superoxide, for which it has a high specificity. The dye rapidly collects specifically within mitochondria, and when superoxide anions leak from the electron transport chain within the mitochondria, mitoSOX within the organelle will be rapidly oxidised and become fluorescent.
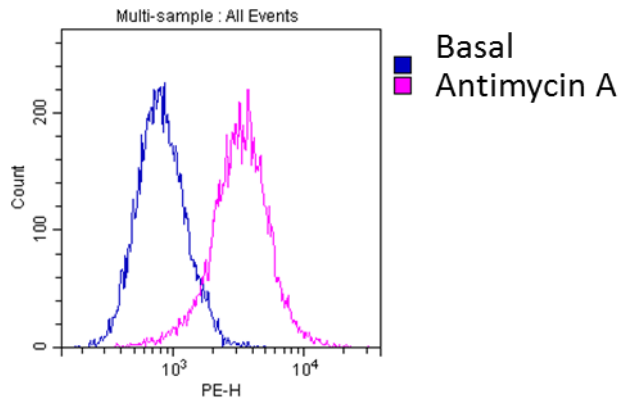
Figure 15. MitoSOX specificity for mitochondrial superoxide. Washed platelets (2 x 10^6) were suspended in a total volume of 50 µL and incubated with mitoSOX at basal and treated with antimycin A (100 µM). Fluorescent signal increases over basal (blue histogram) when treated and is measured in the 585/42 BP channel (pink histogram).

In this assay platelets (2 x 10^6) in a total volume of 50 µL of reaction mixture, containing modified Tyrode's buffer, mitoSOX (5 µM), agonists and inhibitors. Platelets in buffer are pre-incubated with MitoSOX for 10 minutes, to allow it to enter the mitochondria, and the reaction was started by the addition of agonists. However, where mitochondrial radical scavengers such as mitoTEMPO were used, these were pre-incubated for 20 minutes prior to mitoSOX. Agonists were then added and incubated at 37∘C for up to 180 minutes. At the endpoint, 10x volume of PBS was added and samples were then immediately analysed. As this was a live cell dye, it was important that cells were run immediately as the levels of reactive oxygen species may continue to change. Antimycin A was used throughout as a positive control to ensure cell viability and dye function (Figure 15). Although there was a negative control in the form of the mitochondrial superoxide scavenger it was most appropriate to express the data as total MFI or fold over basal.

2.3.1.15 TMRE

Tetramethyl rhodamine ethyl ester (TMRE) is a stain which collects specifically within the mitochondria of live cells, in the presence of polarised mitochondria which have

membrane potential. When mitochondria exhibit a loss of membrane potential, they also lose their capacity to be stained with TMRE. Furthermore, if mitochondria gain potential, they will accumulate more TMRE and therefore stain more brightly.
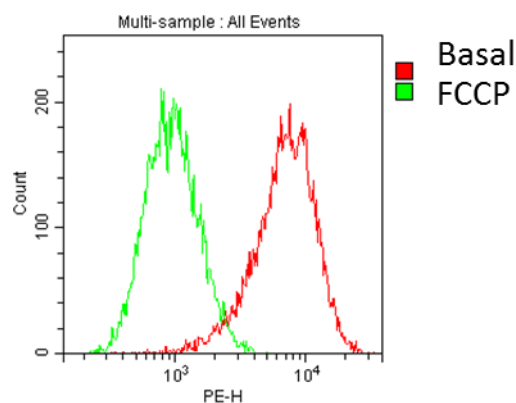
Figure 16. TMRE specificity for mitochondrial membrane potential. Resting platelets have active mitochondria and collect TMRE and therefore fluorescence in the 585/42 BP channel (red histogram). However, upon treatment with the negative control FCCP, fluorescence is lost (green histogram).

An assay to examine TMRE accumulation was established. Washed platelets (2.5 x 10^6) were suspended in 50 µL of 50 nM TMRE in modified Tyrode's buffer, mixed and left to stain for 20 minutes. The negative control, FCCP (20 µM), was added for 10 minutes prior to TMRE addition to fully depolarise the mitochondria (Figure 16). At 20 minutes, 10x excess of PBS was added and samples were immediately analysed. This assay was not fixative compatible, as this killed the cells and the mitochondria lost any mitochondrial membrane potential, as a result, alike to mitoSOX, there is no halt step so samples must be run as soon as possible.

2.3.2 Aggregometry

Light transmission aggregometry (LTA) was developed by Gustav Born in 1962 to examine platelet function (Born, 1962). The turbidimetric assay is based on changes

in light scattering through a platelet suspension which is detected by a photocell. It is assumed that when using small volumes with stirring that resting platelets are uniformly distributed in suspension and presented with shear stress. This forms an optically dense medium which is refractory to the passage of light. However, following their activation, platelets aggregate into clumps generating an increasingly transparent suspension that allow light to pass through (Figure 17). The extent of light transmission is proportional to the level of platelet aggregation which is in turn dependent on the degree of platelet activation.
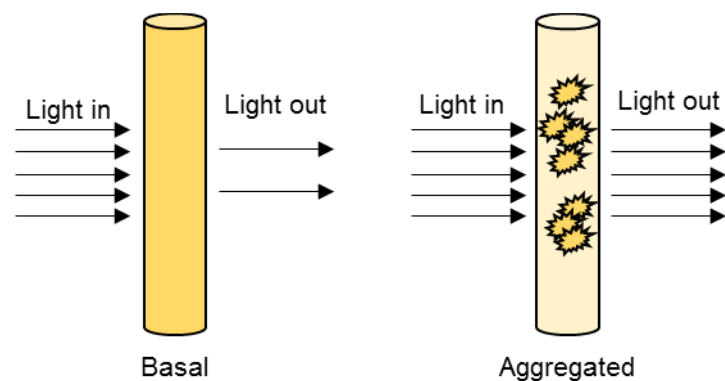
Figure 17. Principles of platelet light transmission aggregometry. Resting platelets in suspension show a turbid solution, however when stimulated, aggregation occurs then transmission of light increases and this correlates with level of aggregation and activation.

Aggregometry was performed on a Chrono-log aggregometer using washed platelets at 2.5×10^8/mL, stirred at 1000 RPM at 37°C. Activation was stimulated with collagen (1 - 10 µg/mL) or thrombin (0.01 - 0.1 U/mL) and recorded for 3 minutes. Aggregation traces were exported, and amplitude measured.

2.4 ISOLATION AND OXIDATION OF HUMAN LOW-DENSITY LIPOPROTEIN

LDL can be isolated from humans and oxidised, to produce oxLDL. In the laboratory LDL and oxLDL are stored at 4∘C, however shelf life is often limited to <12 weeks before native LDL becomes passively oxidised by environmental oxygen. Therefore, regular isolation and oxidation is a necessity.

2.4.1 Isolation

LDL has a density ranging between 1.019 and 1.063 g/mL and can therefore be isolated from other plasma lipoproteins based on density (Feingold et al., 2000). Here continuous density gradient isolation was used, although sequential density gradient ultracentrifugation is also appropriate (Wilkins and Leake, 1994a). Blood (40 mL) was drawn from the ante-cubital fossa through venepuncture with a 21g butterfly needle directly into EDTA (5 mM) and then centrifuged at 1500g for 20 minutes to allow for separation of acellular plasma. Plasma was placed into a 50 mL falcon tube in wet ice to preserve LDL and prevent any unwanted oxidation.

2.4.2 Density buffers

This protocol relies on the use of buffers of known densities. High (Table 5) and low-density (Table 6) buffers are first made and then buffers in the range between these can be made by mixing the 1.316 and 1.006 g/mL buffers at calculated ratios.

Table 5. Reagents for 1 L of high-density buffer (1.316 g/mL). 1 L of buffer is made, and pH is set at 7.4.

Reagent	Molarity (M)	g/L
KBr	2.97	354
NaCl	2.62	153
EDTA.Na$_2$2H$_2$O	0.297 mM	0.1105

Table 6. Reagents for 5 L of low-density buffer (1.006 g/mL). 5 L of buffer is made, and pH is set at 7.4.

Reagent	Molarity (mM)	g/5L
NaCl	150	43.83
EDTA.Na$_2$2H$_2$O	0.297	0.5645

A 2 L solution of 1.109 g/mL density was made by adding a 1.316 g/mL solution to a 1.006 g/mL solution using the following equation.

$$\left(\frac{0.013 * 2000}{1.316 - 1.019}\right) = volume\ of\ 1.316\ to\ add$$

The density of the resulting solution was then checked using a 100 mL volumetric flask weighed on a fine balance.

$$\left(\frac{weight - weight\ of\ flask}{100}\right) = density\ of\ 1\ mL\ of\ solution$$

If required, the density was then adjusted using appropriate volumes of either the 1.006 g/mL or 1.316 g/mL buffer calculated from the equation below if the density was too high, then the 1.006 g/mL solution was added, and conversely if is the density was too low then the 1.316 g/mL solution was added.

$$(current\ volume \times current\ density) + (x \times adjusting\ buffer)$$

$$= (volume + x) \times target$$

2.4.3 Continuous gradient ultracentrifugation

Continuous gradient ultracentrifugation has advantages over discontinuous gradient ultracentrifugation as it is far more time efficient and also requires a smaller starting volume of blood (Naseem et al., 1997). To carry out the procedure plasma density was adjusted through the addition of solid KBr, at a ratio of 0.44285 g/1 mL which was dissolved with gentle stirring. Beckman Coulter QuickSeal 13.5 mL tubes were pre-filled with 1.006 g/mL density solution (150 mM NaCl, 297 µM EDTA.Na$_2$2H$_2$O, pH 7.4) and underlaid with 5 mL of density adjusted plasma. Tubes were then balanced to +/- 10 mg on a fine balance and ultra-centrifuged at 200,000 g at 4◦C for 4.5 hours in a Beckman Coulter 70.1Ti rotor. This yielded a distinct band of LDL which could be removed by piercing the tube with a 21g butterfly needle and syringe, with an additional needle to release the vacuum (Figure 18).
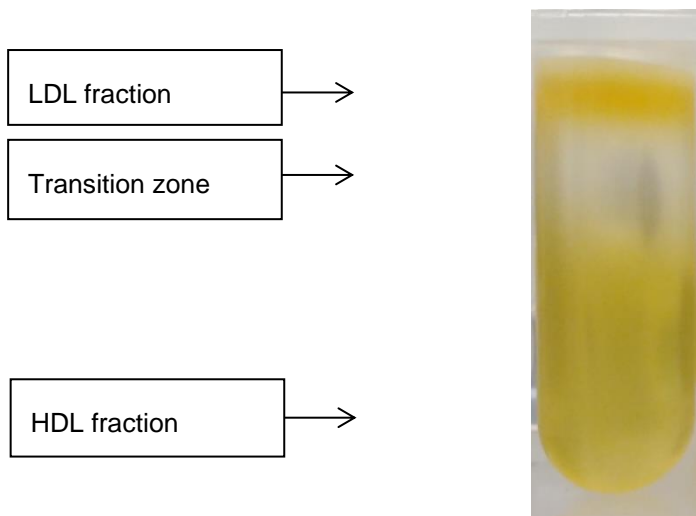
Figure 18. Adjusted plasma after the first stage of continuous gradient ultracentrifugation. A distinct LDL fraction rests in the middle of the tube and is distinct from other regions by clear zones of buffer, it can be isolated for further purification.

This preliminary LDL was then overlaid over 1.151 g/mL density solution into QuickSeal tubes before being itself overlaid with 1.063 g/mL density solution. This was then balanced to +/- 10 mg on a fine balance and ultra-centrifuged at 200,000 g at 4◦C for 16 hours in a Beckman Coulter 70.1Ti rotor. This yielded a clear bright yellow band at the top of the tube which was collected with a 21g butterfly needle as before. It was then dialysed for 24 hours with 10,000 molecular weight cut off dialysis tubing at 4◦C with 2 changes against phosphate-EDTA dialysis buffer (140 mM NaCl, 8.1 mM Na_2HPO_4, 1.9 mM NaH_2PO_4, 0.1 mM EDTA, pH 7.4) to remove the heavy salts and impurities. The LDL is then filtered through a 0.22 µm filter and stored in the dark at 4◦C prior to protein concentration and oxidation.

2.4.4 Oxidation of LDL

Unlike in the body, where oxidation predominantly occurs as a result of cellular ROS, *in vitro* oxidation is initiated with the addition of copper ions (Naseem et al., 1997). Oxidation at 37◦C was used as predominantly oxysterol-rich LDL is produced by that method, whereas at 4◦C primarily hydroperoxide-rich LDL is produced (Gerry et al., 2008).

In this work for LDL oxidation, LDL was first dialysed against phosphate buffer (140 mM NaCl, 8.1 mM Na_2HPO_4, 1.9 mM NaH_2PO_4, pH 7.4) for 4 hours at 4◦C with 3 changes of buffer. The LDL was then dialysed against MOPS-Chelex buffer to remove EDTA (150 mM NaCl, 10 mM MOPS, 0.1% Chelex-100 w/v, pH 7.4) for 24 hours at 4◦C with 2 changes of buffer. A small volume of MOPS-copper buffer was then added directly to the dialysis tubing (to ensure LDL concentration at oxidation was <2 mg/mL) and the LDL further dialysed against the MOPS-copper buffer (150 mM NaCl, 10 mM MOPS, 10 µM $CuSO_4$, pH 7.4) for 24 hours at 37◦C with 3 changes of buffer. Oxidation occurred within 4-6 hours indicated by a loss of yellow colouration of the LDL suspension as the β-carotene was broken down. Finally, oxidation was

halted through the addition of EDTA (1 mM) directly to the LDL. This was then dialysed against phosphate-EDTA dialysis buffer (140 mM NaCl, 8.1 mM Na_2HPO_4, 1.9 mM NaH_2PO_4, 0.1 mM EDTA, pH 7.4) for 24 hours at 4∘C with 2 changes, filtered through a 0.22 μm filter and stored in the dark at 4∘C.

2.5 **METHODS FOR THE STUDY OF PROTEINS**

2.5.1 Protein concentration

Protein concentration was measured in both LDL and platelet lysates. BioRad Detergent Compatible Protein assay is an adaptation of the Lowry assay (Lowry et al., 1951), and was used as per manufacturer's guidelines. In brief, protein standards were produced using BSA dissolved at a range of 0.2 - 2 mg/mL and loaded in triplicate in 96-well plates. The two-colour reagents, copper tartrate and Folin's reagent were added to each well and mixed, and a blue colour developed, the intensity of which was indicative of protein concentration, and is measured by a plate reader at 750 nm and a standard curve produced. The concentrations of protein, LDL or platelet lysates were calculated from these standard curves.

2.5.2 Relative electrophoretic movement assay

The relative electrophoretic movement (REM) was used to determine the overall surface charge of each LDL preparation. Since LDL becomes increasingly negatively charged during the oxidation process it leads to increase migration towards the anode. A ratio is calculated by comparing the distance migrated by ox and nLDL measured from the start point and can be used to determine the extent of oxidation, typically a ratio of >3 is considered appropriate (Figure 19). In addition, the REM assay can be used to confirm the purity of the LDL preparation, since LDL should have only a single protein band, Apo B-100. The presence of additional bands would suggest contamination with other lipoproteins.
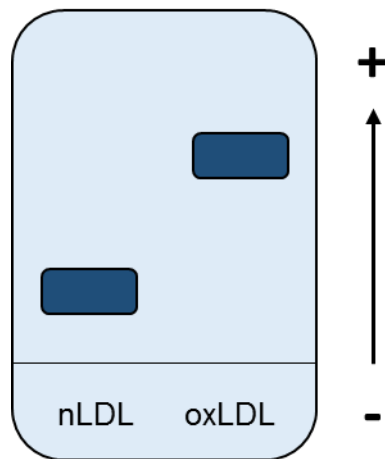
Figure 19. Schematic of relative electrophoretic movement assay. Differently treated LDL is loaded in an agarose gel and run towards the anode, the greater the level of oxidation the faster the speed of protein migration.

Native LDL and oxidised LDL were both loaded onto an agarose gel (1% agarose, TAE buffer w/v) in a tank of TAE buffer (Tris base 40 mM, glacial acetic acid 0.1% v/v, EDTA 1 mM) and ran at 100 volts for 60 minutes. The gel is then rinsed in dH$_2$O and proteins stained with Coomassie stain overnight. Excess stain is then washed off and the gel is imaged with a visible light scanner.

2.5.3 Dot blot assay

A dot blot is a simple but effective and high throughput method for assessing content of an antibody target within any suspension. In this case, it was used to detect oxidised phospholipids (oxPL) present in LDL preparations, as a marker of the levels of oxPL (Berger et al., 2019b). E06 is a murine IgM antibody raised against oxidised phospholipid (oxPL) and can therefore be used to differentiate between oxLDL and nLDL. A polyvinylidene fluoride (PVDF) membrane was activated in methanol and oxLDL and nLDL (2 µg) loaded. This was left to bind to the membrane (20 minutes) before blocking in BSA/Tris-base saline (5% BSA w/v, NaCl 150 mM, Tris-base 20 mM, pH 7.6) for 30 minutes at room temperature. The blocking buffer was removed,

and the membrane probed overnight at 4∘C with E06 (1/1000 in 2% BSA/TBS), an antibody that recognises oxPL. The membrane was washed three times in Tris-base saline-Tween 20 (TBS-T, NaCl 150 mM, Tris-base 20 mM, Tween 20 0.1% v/v, pH 7.6) and incubated with anti-mouse-HRP conjugate 1/10,000 TBS-T for 60 minutes at room temperature. Membrane was visualised by incubation with enhanced chemiluminescent (ECL) reagent for 90 seconds. For loading control, the membrane was counterstained with Coomassie stain and imaged on a visible light scanner.

2.5.4 Immunoprecipitation

Immunoprecipitation is used to isolate a protein from a mixture such as a cell extract. An antibody specific for a target protein is added to the mixture to form antibody-antigen complexes. The complexes are then precipitated by adsorbing the antibodies to an insoluble matrix such as agarose or sepharose beads conjugated to protein A or G. The latter two proteins derive from bacteria and are stably bound by antibody constant regions. Using centrifugation, the beads are sedimented into a pellet and the supernatant containing unwanted proteins is aspirated and discarded. After several washes, the antibody-antigen complex is liberated from the beads by boiling in lysis (Laemmli) buffer (Laemmli, 1970). The isolated protein may be studied further using SDS-PAGE and Western blotting or by mass spectrometry. In addition to enriching the concentration of proteins that would otherwise be too scarce to detect through normal immunoblotting, the technique enables biochemical analysis of single proteins and interactions or post-translational modification states.

Platelets were lysed with immunoprecipitation lysis buffer (150 mM NaCl, 10 mM Tris base, 1 mM EGTA, 1 mM EDTA, 1% Igepal (v/v)), which preserved protein: protein interactions and post-translational modifications. The lysed platelet suspension was then pre-cleared with protein A/G beads which were removed by centrifugation. The primary antibody targeted against the protein of interest was then added to the lysate

and incubated (4∘C, 60 minutes) prior to addition of protein A/G beads, which were then incubated overnight (4∘C). The lysate with beads now bound to antibodies which were bound to the desired protein were then isolated by centrifugation (1000 g, 10 minutes). The lysate supernatant was then removed, and the beads were resuspended in Laemmli lysis buffer which released the proteins from the beads and bound antibodies. This enriched lysate could then be processed by SDS-PAGE.

2.5.5 Gel electrophoresis and immunoblot

Immune-specific detection of proteins separated using SDS-PAGE allows accurate detection of selected proteins against which specific antibodies are used. Electrophoresis allows the separation of charged macromolecules in an electric field. When applied to a porous matrix such as a gel it can be used to separate molecules based on their size and charges. SDS-PAGE uses a combination of SDS and the polyacrylamide gels to separate proteins according to their molecular masses by electrophoretic migration. Acrylamide molecules polymerise into long linear chains which are cross-linked by bisacrylamide. This polymerisation is accelerated by the presence of free radicals. Hence, ammonium persulphate (APS) is added when casting gels as it decomposes to release SO_4^- radical anions. Tetramethylethylenediamine (TEMED) is also included to catalyse the decay of APS. The percentage of the acrylamide used in these solutions determines the pore size and therefore the relative separation of the proteins within the mixture.

To identify specific proteins separated from the mixture, Western blotting is routinely used. This involves transferring the proteins from a gel to an adhesive matrix such as nitrocellulose or polyvinylidene fluoride (PVDF) membranes under an electric field. Once transferred, the membranes are probed with specific primary antibodies against target proteins. A secondary antibody raised against the primary antibody species is

then added. Secondary antibodies are commonly conjugated to horseradish peroxidase (HRP) which allows visualisation of antibody detected protein bands.

2.5.6 Sample preparation

Platelet lysate was generated after treatment of washed platelets with the appropriate agonists or antagonists. Platelets (5-10 x 10^8/mL) were lysed with Laemmli buffer (4% SDS (w/v), 10% 2-mercaptoethanol (v/v), 20% glycerol (v/v), 50mM Tris base, trace bromophenol blue, pH 6.8) and boiled at 95◦C for 5 minutes (Laemmli, 1970). SDS is an anionic detergent that binds and denatures proteins leaving them with similar, rod-shaped tertiary structure. Furthermore, it confers equal negative charge per unit protein mass (1.4g SDS per 1g protein). In the presence of a reducing agent such as 2-mercaptoethanol, disulphide bonds are broken, and proteins become fully denatured.

All samples were run under discontinuous SDS-PAGE (Laemmli, 1970), using precast gels composed of a 4% stacking gel overlying a 10-18% gradient resolving gel. The more porous stacking gel containing wells for protein loading ensured that all the proteins entered the less porous resolving gel simultaneously. As the gels were buffered differently from each other and the running buffer, application of electric current caused a narrow band of high voltage to migrate down the stacking gel, compressing loaded proteins into a tight horizontal band. When the band reached the resolving gel, the proteins were dispersed as they passed through its pores. Protein lysates (30 µg) were loaded in each well and a biotinylated or visual molecular weight marker (Precision Plus) was also added. Gels were left to run at 120 V for 2 hours, after which proteins were transferred to PVDF membranes using a BioRad turbo blotter for 7 minutes at 2.5 A and 25 V. Where own cast gels were used, a 1.5 mm protocol was instead used which ran for 10 minutes to allow for the thicker gel's slower transfer.

The membranes were blocked with 5% (w/v) BSA dissolved in TBS-T BSA (bovine serum albumin) w/v or 5% milk w/v in Tris-base saline + Tween-20 0.1% v/v (TBS-T) for 30 min and subsequently probed with primary antibody (at noted dilution in figure legends) diluted in 2% (w/v) BSA/TBS-T overnight at 4°C. The next day, the membranes were rinsed with TBS-T for 10 minutes, probed with HRP-conjugated secondary antibodies; anti-rabbit or anti-mouse (as appropriate, both 1:10000) and anti-biotin (1:2000) for 1 hour, washed with TBS-T (4 washes, 15 minutes each) and developed with ECL solution.

2.5.7 Development of probed membranes

Development of membranes was performed by either near infra-red (nIR) fluorescence detection with a LiCor CLX or by enhanced chemi-luminescence (ECL) using film in a dark room. For fluorescence detection, after incubation with nIR-conjugated secondary antibodies, the membranes were further washed three times for 5 minutes each under orbital movement (30 $_{RPM}$) in TBS, rinsed in dH$_2$O and then imaged on a LiCor CLX system and analysed using Image Studio Lite (v.5.2.5). This system is a two-colour system and will allow multiplexed detection of two primary antibodies simultaneously provided they are from different species and therefore the secondary antibodies can distinguish between them.

For ECL detection, after incubated with HRP-conjugated secondary antibodies, the membranes were incubated with 1 mL of SuperSignal™ West Pico PLUS Chemiluminescent Substrate (ThermoFisher) for 1 minute, placed in a film cassette and developed under dark room conditions with exposures ranging from 0.2 – 30 minutes. Films were then developed using an automatic silver developing and acetic acid fixation system.

In either instance, membranes can then be washed for 5 minutes under orbital movement (30 RPM) in TBS-T and stored for repeat development, stripping or re-probing with further primary antibodies.

2.6 DATA PRESENTATION AND STATISTICAL ANALYSIS

2.6.1 Data presentation

Where raw value data was presented, GraphPad Prism (v.8) and/or Microsoft Excel (Office '16) were used. Where flow cytometry data was presented as histograms or scatter plots, FlowJo (v.10) or CytExpert (v.2) were used for analysis and graphics production. Data quoted in text is provided as *XX* ± standard deviation.

2.6.2 Statistical analysis

Statistical analysis was performed using GraphPad Prism (v.8). For single comparisons Students T-tests were used, however where multiple parameters were compared ANOVA tests were used.

Chapter 3
Platelet regulation and subpopulations

3.1 INTRODUCTION

Platelet activation results in a series of dramatic changes to the surface of the cell, which are required to facilitate haemostasis, coagulation and inflammation. Degranulation results in the increased expression of numerous ligands or receptors stored within the granules, primarily within α-granules. These include but are not limited to CD62P (P-selectin), CD154 (CD40L), CD63 (LAMP-3) and integrin αIIbβ3. Cellular activation also causes conformational changes in the integrins, notably integrin αIIbβ3, converting them from a cryptic form to one that can bind protein ligands. In addition to changes to the protein receptors and associated ligands there is also a change in the surface lipid profile, with the increased externalisation of phosphatidylserine required to support coagulation.

Fluorescent flow cytometry provides a platform for single cell analysis of multiple parameters. We sought to understand how multiple markers may be simultaneously changing across the platelet population and if the application of multiparameter assays in combination with multidimensional analysis could allow for identification of platelet subsets beyond the previously described procoagulant subpopulation and how the endothelial inhibitor PGI_2 may regulate these procoagulant platelets (Agbani and Poole, 2017).

3.2 AIMS OF CHAPTER

- Determine optimal conditions to measure platelet activity by flow cytometry

- Develop multiparameter flow cytometry panels and apply multidimensional analysis to identify platelet subpopulations

- Understand how PGI_2 regulates the formation of platelet subpopulations

3.3 OPTIMISATION OF ANTIBODY CONCENTRATIONS

Antibodies should be titrated to determine optimal doses. Correct titration can dramatically improve assay sensitivity and it can also allow for substantial reductions in antibody consumption per assay. In brief, each antibody dilution must be compared with a control or basal sample at a matched concentration, this comparison allows a comment on the sensitivity of each assay as opposed to simply the brightest stimulated condition, which will often be paired with excessive background binding and therefore anomalously high basal signal. Calculating fold over control allows the condition with the highest fold increase, and therefore optimal window for detection of changes, to be selected.

3.3.1 CD62P

CD62P was exposed on the platelet surface upon activation. Here we determined

that 1.25 µL of anti-CD62P-PE is the optimal titre (Figure 20).
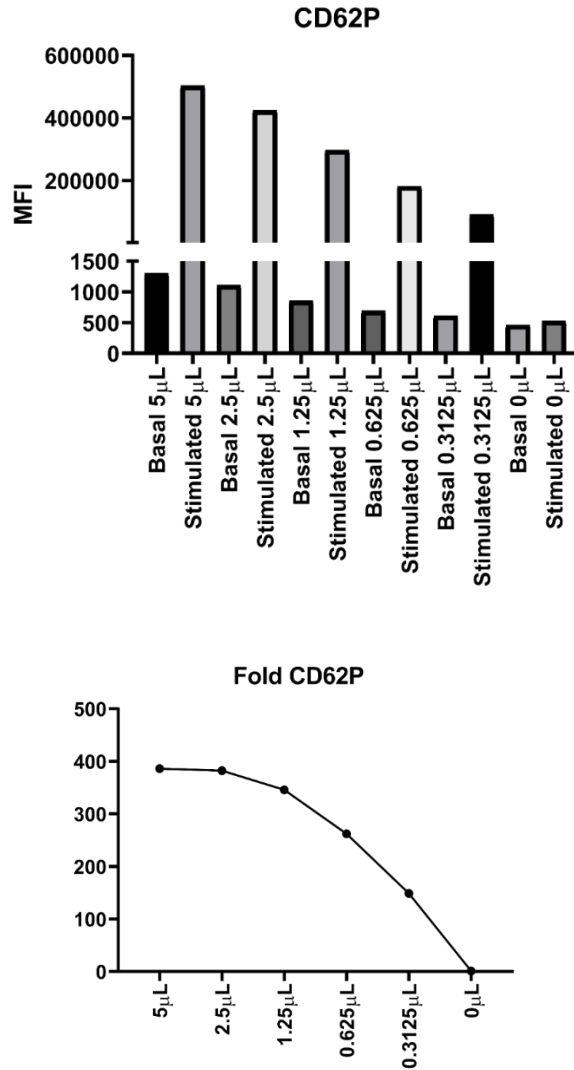
Figure 20. Titration of anti-CD62P-PE. In whole blood drawn into sodium citrate, CD62P-PE was added at 6 dilutions ranging from 5 to 0 µL of antibody. Each sample was made in duplicate and half were stimulated with SFLLRN (10 µM) for 20 minutes, and the other half were maintained at basal, prior to fixation (1% PFA/PBS). CD42b-APC was used as a platelet marker which did not spectrally interfere with CD62P-PE. Samples were analysed for 10,000 platelet positive events and MFI and fold over relative basal are presented.

3.3.2 Fibrinogen

Fibrinogen is a ligand of activated platelets. Because the conformational change of the αIIbβ3 integrin is dependent on calcium, EDTA is used as a background fluorescence control. Here we determined that 1.25 µL of anti-fibrinogen-FITC was the optimal titre (Figure 21).
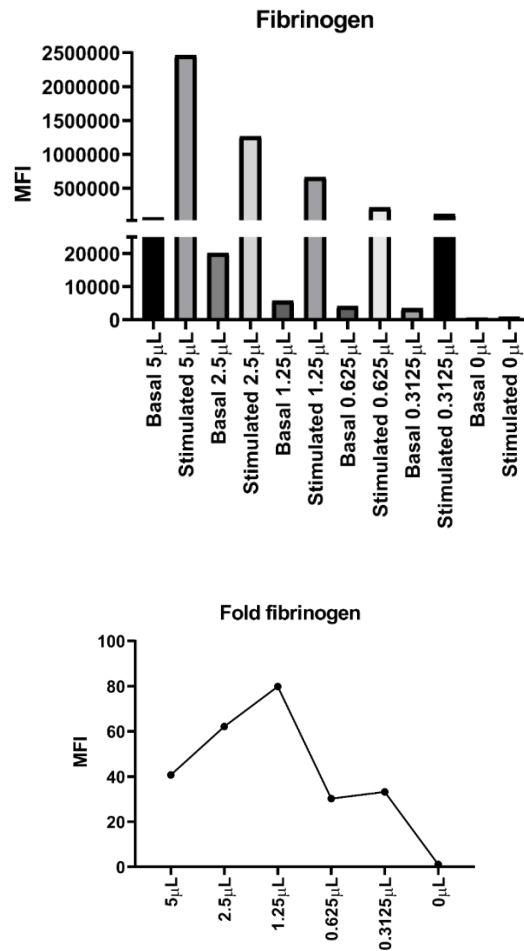
Figure 21. Titration of anti-fibrinogen-FITC. In whole blood drawn into sodium citrate, fibrinogen-FITC was added at 6 dilutions ranging from 5 to 0 µL of antibody. Each sample was made in duplicate and half were stimulated with SFLLRN (10 µM) for 20 minutes, while half were maintained at basal, prior to fixation (1% PFA/PBS). CD42b-APC was used as a platelet marker which did not spectrally interfere with fibrinogen-FITC. Samples were analysed for 10,000 platelet positive events and MFI and fold over relative basal are presented.

3.3.3 PAC1

The monoclonal antibody PAC1 measures the same activity as the anti-fibrinogen antibody. PAC1 recognises the activated, but not inactivated, αIIbβ3 integrin which is vital for platelet homotypic aggregate formation (Frelinger, 2018). EDTA is used as a background fluorescence control. Here we determined that 5 µL of PAC1-FITC was the optimal titration (Figure 22).
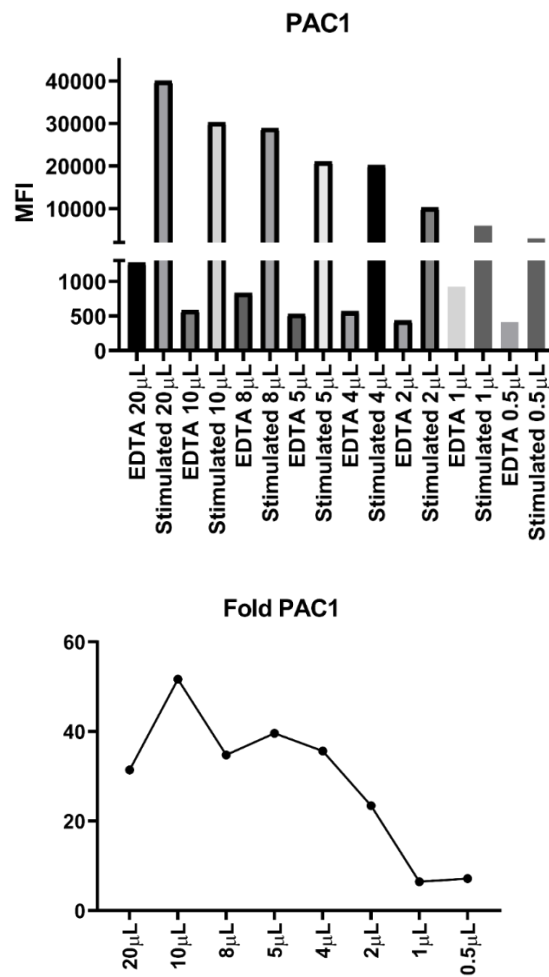
Figure 22. Titration of PAC1-FITC. In whole blood drawn into sodium citrate, PAC1-FITC was added at 8 dilutions ranging from 20 to 0.5 µL of antibody. Each sample was made in duplicate and half were stimulated with SFLLRN (20 µM) for 20 minutes prior to fixation (1% PFA/PBS). CD42b-APC was used as a platelet marker which did not spectrally interfere with PAC1-FITC. Samples were analysed for 10,000 platelet positive events and MFI and fold over EDTA control are presented.

3.3.4 CD63

CD63 (LAMP-3) is a lysosomal glycoprotein which is expressed in both platelet lysosomal and δ-granules and presented on the surface upon activation. Here we determined that 2 μL of anti-CD63-eF660 was the optimal dilution, where non-specific binding is at a minimum and the difference between IgG-eF660 control and CD63-eF660 is maximal (Figure 23).
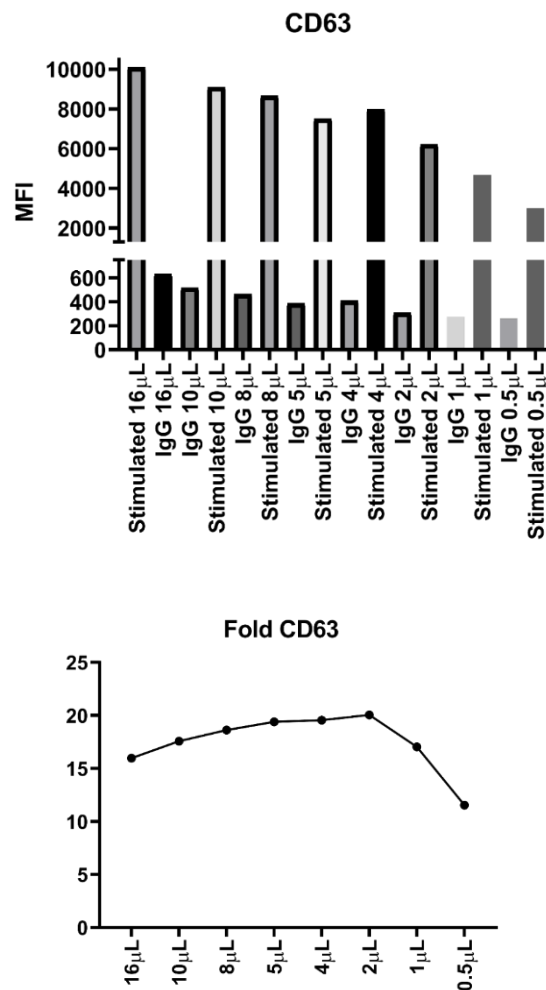
Figure 23. Titration of anti-CD63-eF660. In whole blood drawn into sodium citrate, CD63-eF660 was added at 8 dilutions ranging from 16 to 0.5 μL of antibody. Each sample was made in duplicate and all were stimulated with SFLLRN (20 μM) for 20 minutes prior to fixation (1% PFA/PBS). CD42b-FITC was used as a platelet marker which did not spectrally interfere with CD63-eF660. Samples were analysed for 10,000 platelet positive events and MFI and fold over matched IgG control are presented.

3.3.5 CD514

CD154 (CD40L) is expressed in platelet α-granules and is important for platelet-leukocyte interactions, when platelets degranulate some CD154 is maintained on the surface (Damien et al., 2015). Here we determined that 4 µL of anti-CD154-FITC was the optimal dilution over IgG-FITC control, although here all dilutions are similar, likely due to relatively low surface abundance of CD154 (Figure 24). As surface expression of CD154 was anticipiated to be low it was put in the relatively sensitive FITC channel.
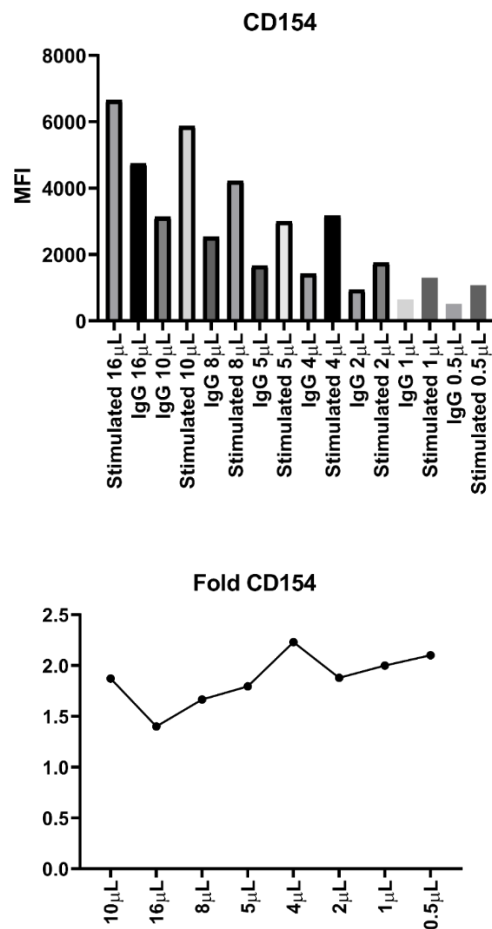
Figure 24. Titration of anti-CD154-FITC. In whole blood drawn into sodium citrate, CD154-FITC was added at 8 dilutions ranging from 16 to 0.5 µL of antibody. Each sample was made in duplicate all were stimulated with SFLLRN (20 µM) for 20 minutes prior to fixation (1% PFA/PBS). CD42b-APC was used as a platelet marker which did not spectrally interfere with CD154-FITC. Samples were analysed for 10,000 platelet positive events and MFI and fold over matched IgG control are presented.

3.3.6 TMRE

TMRE is a dye which collects within mitochondria against an electrochemical gradient and is used as a marker of mitochondrial hyperpolarisation or depolarisation. TMRE is incompatible with whole blood and must be used with washed cells. Here we determined that 50 nM of TMRE dye staining 2×10^6 washed platelets for 20 minutes was the optimal concentration over the mitochondrial uncoupler carbonyl cyanide-p trifluoromethoxyphenylhydrazone (FCCP) (20 µM) control (Figure 25).
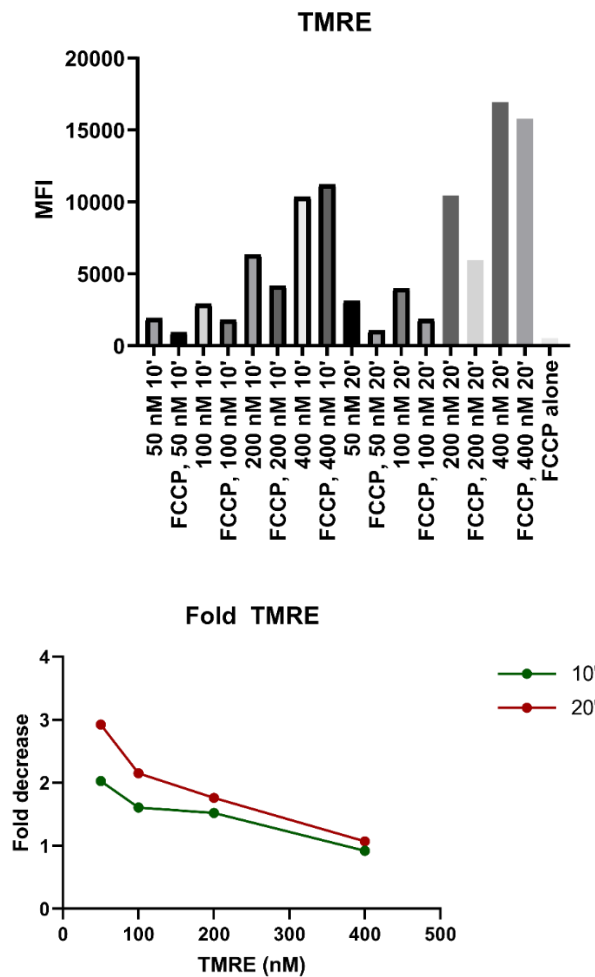
Figure 25. Titration of TMRE. 2×10^6 washed platelets were either treated or untreated for 10 minutes with FCCP (20 µM) and then duplicate pair was stained with TMRE (50 – 400 nM). At 10 (green) or 20 (red) minutes each sample was diluted 10x in PBS and analysed immediately for 10,000 platelet events and MFI and fold over matched FCCP control are presented.

3.4 PRE-ANALYTICAL CONDITIONS

The quality of a flow cytometry experiment is underpinned by three main aspects; appropriate pre-analytical conditions, assay design with appropriate controls and accurate analysis incorporating MFI, percent positive cells and appropriate gating. Here we sought to understand the impact of several different pre-analytical variables which can affect assay output. Platelet activation was analysed using a four-parameter assay for fibrinogen binding (FITC), CD62P (PE), annexin V (APC) and CD42b (BB700) under a variety of different conditions. Anti-coagulants were compared for; the effects of resting whole blood, reproducibility of the assay in different preparations of platelets and storage of samples for up to 4.5 hours. The four parameters which this assay measured provide a broad cross-section of the changes which platelet undergo upon activation, and therefore provides confidence that the pre-analytical conditions chosen as optimal, should be suitable for the measurement of many aspects of platelet biology.

For all experiments, blood was drawn into the appropriate vacutainer, after a discard of the first draw to prevent artefactual activation. Stimulation was then carried out for 20 minutes at 37∘C in the presence of calcium (1.8 mM) and Gly-Pro-Arg-Pro (GPRP; 500 µM). Calcium is required to support annexin V binding (Gyulkhandanyan et al., 2012) while GPRP is required to prevent fibrin polymerisation (Michelson, 1994). Activation was halted at 20 minutes by the addition of 450 µL of 1% paraformaldehyde/calcified modified Tyrodes buffer. Where storage was tested, samples were stored at 4∘C in the dark between re-acquisitions.

3.4.1 Optimal anti-coagulant

Three anti-coagulants were investigated to examine and compare their effects on platelet activation. Discerning the best anti-coagulant for platelet activation is likely the most important pre-analytical step. The three anti-coagulants compared were; sodium citrate, sodium heparin and potassium EDTA, all pre-loaded into commercial evacuated tubes. All three anti-coagulants are routinely used in clinical laboratories, and as such, platelet researchers in collaboration with a clinic could potentially receive, or request to receive patient samples in either of these three anti-coagulants. ACD is an anticoagulant which is used universally in the platelet research laboratory, however this is predominantly for isolation of platelets where the reduction in pH is beneficial. In the context of whole blood activation assays, it is unlikely to be suitable, so we did not test this anticoagulant. To assess each anti-coagulant we measured fibrinogen binding, CD62P expression and annexin V binding.

Platelets demonstrated the highest capacity for fibrinogen binding in citrate tubes and this was diminished in heparin and further diminished in EDTA (Figure 26a). CD62P expression was not affected by the anti-coagulants tested with both the capacity for expression and the number of positive events remaining the same for each anti-coagulant. However there was a difference in the basal expression; with the lowest basal expression observed in citrate, followed by heparin and the highest at 40% positive in EDTA (Figure 26b). The binding of annexin V to phosphatidylserine was the most sensitive in heparin, followed by citrate and finally EDTA. Although the brightness of positive events when measuring annexin V was reduced, the number of positive events was consistent across the anti-coagulants, which is an important observation when annexin V is used a qualitative as opposed to quantitative marker (Figure 26c). Collating this data, it was possible to determine that the optimal anti-coagulant to measure whole blood multiparameter platelet activation was determined to be sodium citrate as fibrinogen was most sensitive, CD62P basal was lowest and annexin V binding, as a qualitative marker, was effectively unchanged.
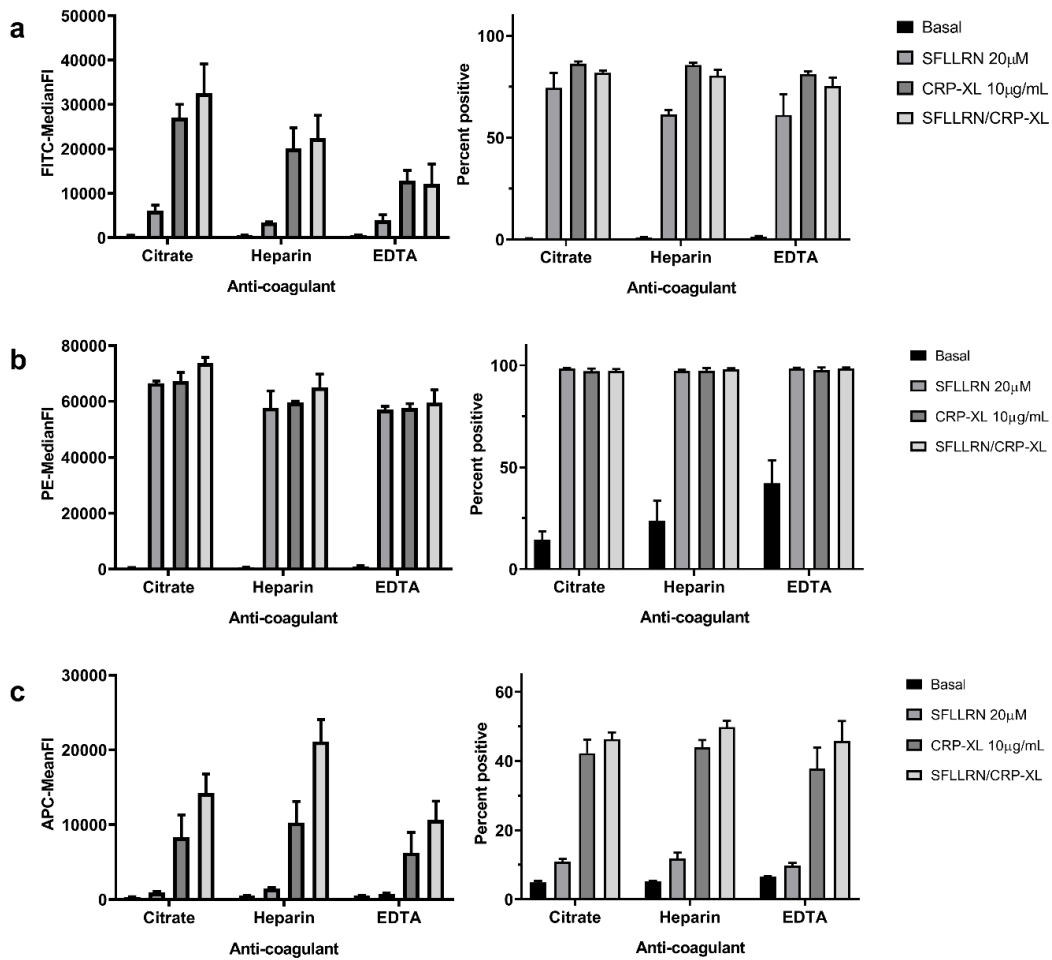
Figure 26. The major pre-analytical consideration for platelet activation assays is the anti-coagulant. Three anti-coagulants, sodium citrate, sodium heparin and potassium EDTA, were compared in whole blood for multicolour platelet activation and each is shown to affect activation markers differently. (A) Fibrinogen binding, MFI and percent positive over EDTA control. (B) CD62P, MFI and percent positive over IgG control. (C) Annexin V, MFI and percent positive over EDTA control. (n=3 for all experiments, error shown as standard deviation)

3.4.2 Optimal assay initiation

The second issue which researchers working on primary cells, or clinical samples, must contend with is delays in receipt of samples. Consequently, the impact of assay initiation at either 0, 1.5 or 4.5 hours after blood was drawn was tested.

Platelet binding to fibrinogen peaked at 0 hours, however this declined significantly after 1.5 hours and declined further still after 4.5 hours (Figure 27a). Although fluorescence intensity is reduced at 1.5 hours, percent positive cells retain some sensitivity but is severely compromised at 4.5 hours (Figure 27a). CD62P is a robust marker and is not significantly affected in terms of expression capacity or percent positive on stimulation, with only a minor decrease in capacity at the longest timepoint. However basal activation was shown to increase up to 2-fold across the time points tested, with the lowest at the immediate timepoint, and an increase in basal at 1.5 hours followed by further increases in basal degranulation at 4.5 hours (Figure 27b). Annexin V binding is a marker of cellular apoptosis as well as the procoagulant platelet subset. A longer rest increased the capacity for platelet annexin V expression with a small increase in basal expression (Figure 27c). The three studies would suggest that where possible, assays should be performed as soon as blood is drawn, however where this is not feasible, the degradation of sample quality over time must be appreciated during analysis of results and if carrying out multiple assay repeats these should be started at the same time point post-venepuncture wherever possible to eliminate artificial variation.
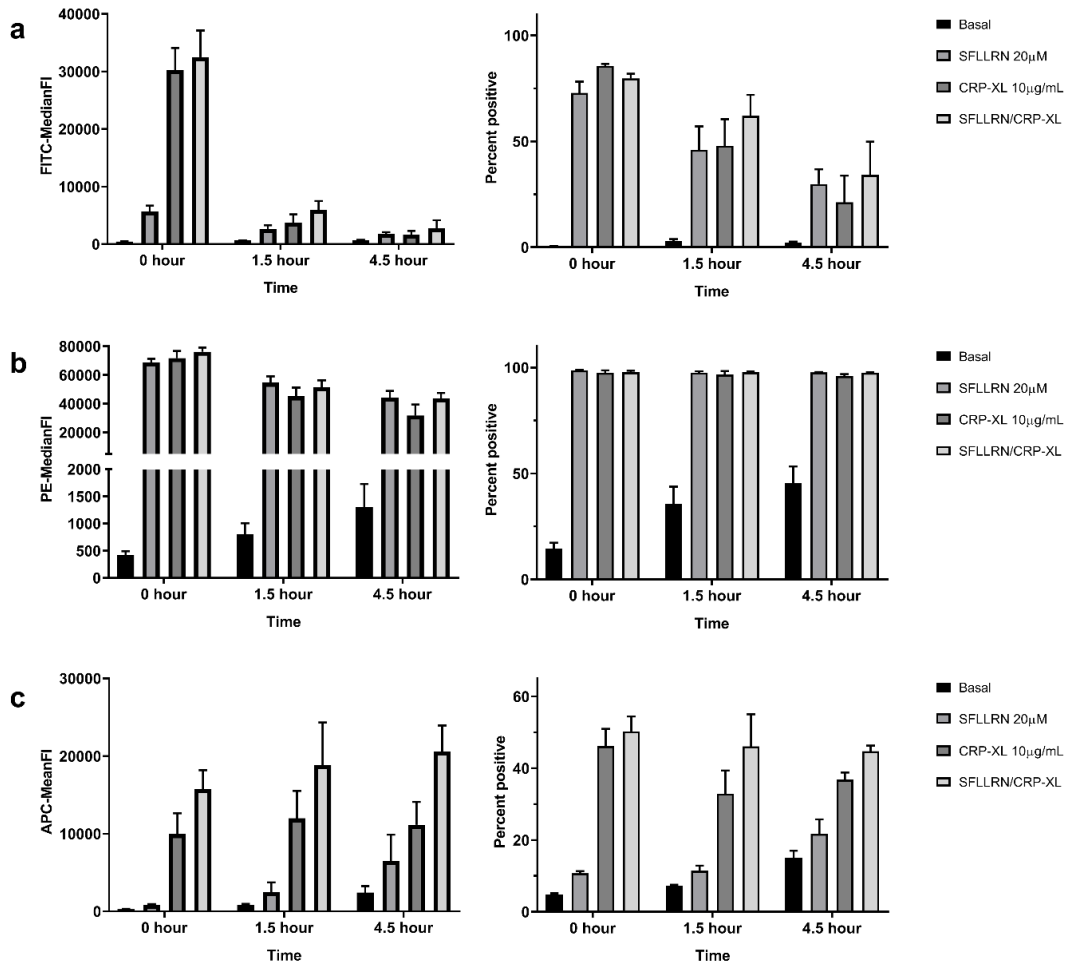
Figure 27. Resting citrated blood compromises assay sensitivity and drives basal expression of activation markers. Platelet activation was assayed in sodium citrated whole blood at 0 hours (freshly drawn), 1.5 and 4.5 hours. (A) Fibrinogen binding, MFI and percent positive over EDTA control. (B) CD62P, MFI and percent positive over IgG control. (C) Annexin V, MFI and percent positive over EDTA control. (n=4 for all experiments, error shown as standard deviation)

3.4.3 Optimal platelet preparation

The third pre-analytical consideration for the platelet biologist is the media the platelets are suspended in, either; whole blood, PRP or washed platelets. In many situations, whole blood is ideal, as this is the more physiologically relevant milieu to examine platelet activation. However, in certain experimental situations the use of whole blood is not feasible. This is likely in situations where a chemical reagent loses specificity or activity in whole blood, and therefore a depleted system of platelet-rich plasma or a buffered system of washed platelets would be used.

Whole blood and PRP from sodium citrate vacutainers were compared with ACD-A vacutainer washed platelets. Fibrinogen binding was most sensitive in whole blood, primarily as fibrinogen is removed in each stage of platelet isolation, presenting an anomalously high signal in washed cells. This anomalously high signal is represented by very bright MFI, indicative of strong antibody binding, but paired with low percentage positive, indicative of low antibody binding. As the percent positive cells is calculated over the EDTA control, and is low in signal, it suggests that the excess binding in MFI signal is likely non-specific (Figure 28a). The capacity for activation as measured by CD62P was again robust and not significantly affected by platelet isolation, although, the stress of isolation was indicated in the large increase in basal expression of CD62P, which correlated with longer isolation times and results in over 60% of washed platelets being pre-activated (Figure 28b). Finally, annexin V was shown to increase in sensitivity in PRP and washed platelets, however this is at the cost of a minor increase in basal expression of phosphatidylserine (Figure 28c). Where feasible, and assay reagents do not require PRP or washed platelets to be effective, whole blood should be used for platelet activation assays, particularly if fibrinogen binding is to be measured. However, CD62P and annexin V binding remain robust in other platelet preparations.
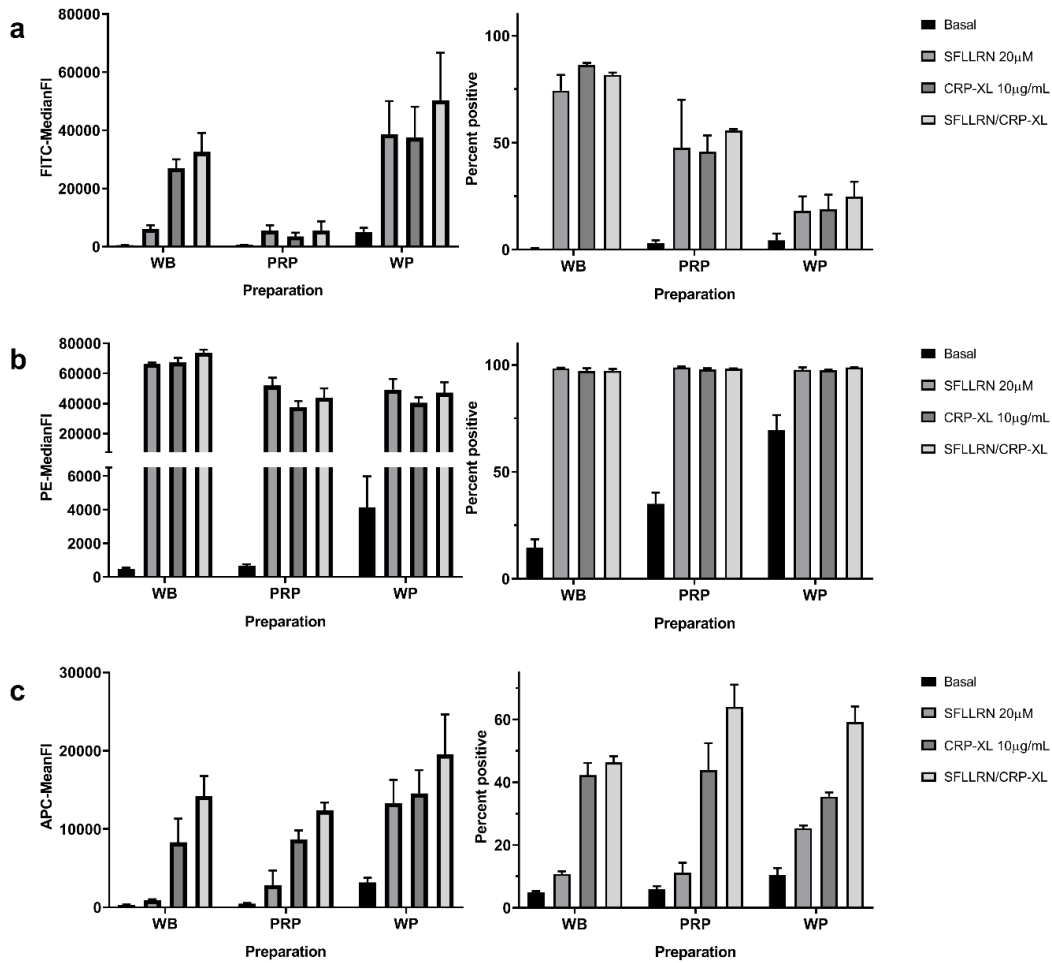
Figure 28. Different preparations of platelets either whole blood, platelet-rich plasma or washed platelets impacts assay sensitivity. Whole blood drawn into sodium citrate, PRP isolated from sodium citrated blood and washed platelets isolated from ACD blood were compared. (A) Fibrinogen binding, MFI and percent positive over EDTA control. (B) CD62P, MFI and percent positive over IgG control. (C) Annexin V, MFI and percent positive over EDTA control. (n=3 for all experiments, error shown as standard deviation)

3.4.4 Storage of samples

The final pre-analytical condition we considered was the durability of samples during routine 4◦C storage. Where feasible, it is expected that samples are processed for acquisition as soon as possible and then analysed. However, this is not always possible, therefore we re-ran selected samples at 90 minutes and again at 270 minutes, storing samples at 4◦C in the dark between acquisitions to observe any differences in assay results.

We compared the fluorescence intensity of the three activation markers from the initial processing with two later acquisitions of sample. Here we were able to show that fibrinogen binding remained robustly positive with no change in MFI (Figure 29a). However, both CD62P and annexin V binding demonstrated considerable decreases in fluorescence intensity in a time dependent manner (Figure 29b & Figure 29c). Whether this is due to degradation of the fluorophores, loss of epitope or antibody binding is unclear. Nevertheless, we can confirm that in the context of this four-colour assay, samples should be acquired as soon as possible, and it must be appreciated that any delay will result in a decrease in fluorescence intensity of both CD62P and annexin V.
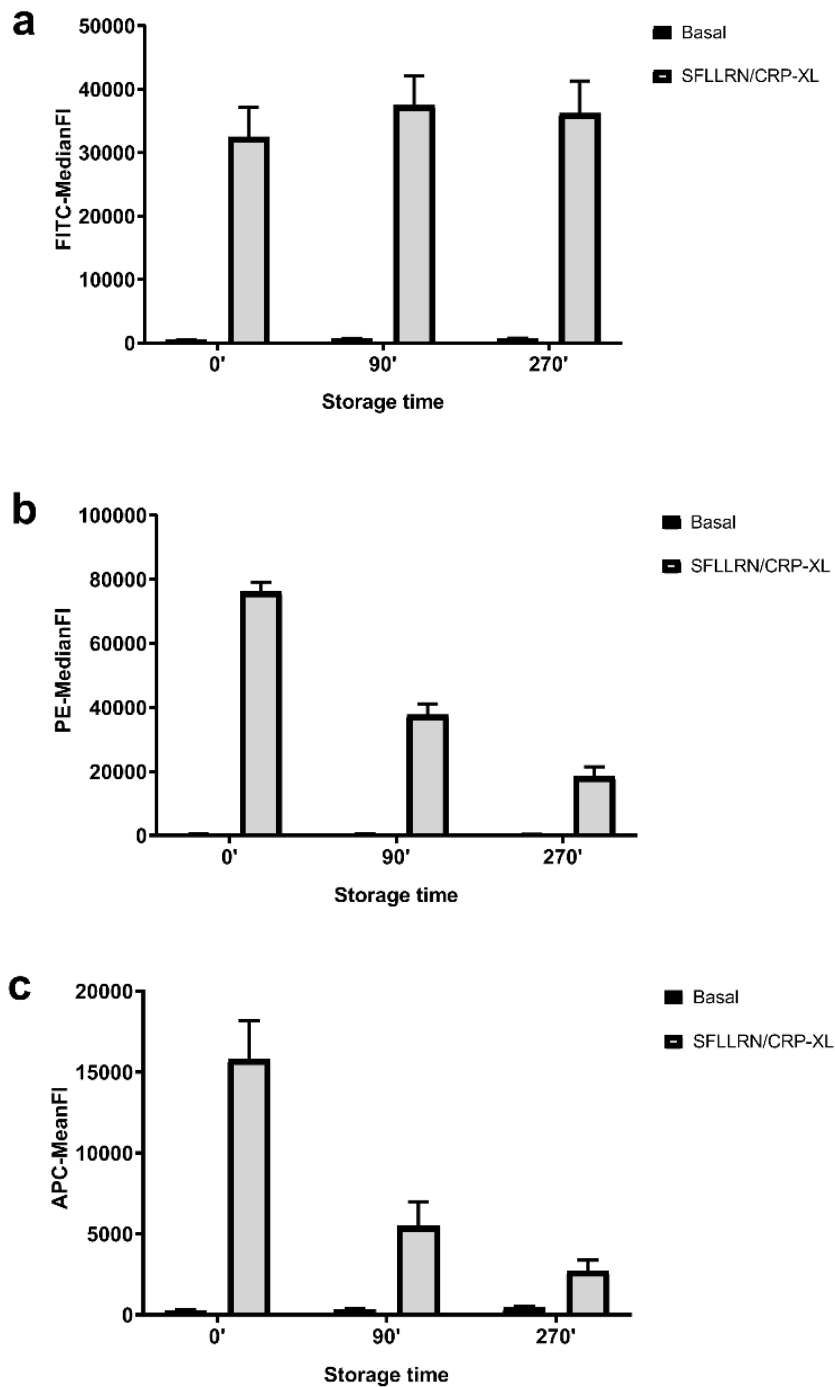
Figure 29. Storage time negatively effects CD62P and annexin V binding however fibrinogen binding remains consistent. The effect of storing blood at 4∘C for each demonstrated timepoint was compared. (A) Fibrinogen binding, MFI and percent positive over EDTA control. (B) CD62P, MFI and percent positive over IgG control. (C) Annexin V, MFI and percent positive over EDTA control. (n=4 for all experiments, error shown as standard deviation)

3.4.5 Activation induced intracellular phosphorylated ERK1/2

In conjunction with surface staining for activation markers, it is possible to link these changes in sensitivity in anti-coagulants to intracellular events by staining for key phosphorylation events using permeabilisation techniques (Spurgeon and Naseem, 2018). We used phospho-ERK1/2 as an intracellular marker of platelet activation (Stalker et al., 2012). Stimulation with SFLLRN (20 µM) for 10 minutes led to increased platelet ERK1/2 phosphorylation in whole blood. We compared ERK phosphorylation in whole blood using sodium citrate, sodium heparin and potassium EDTA as anticoagulants. As calcium flux is vital for platelet activation, the potent chelator EDTA prevents ERK phosphorylation (0.94). However, consistent with the surface marker expression, phosphorylation was still evident in citrate (1.64) and heparin (1.68) (Figure 30). Furthermore, in conjunction with the previous observation of diminished response over time (Figure 27), phosphorylation capacity was shown to decline over time in both citrate (0 1.64, 60 1.46, 300 minutes 1.01) and heparin (0 2.68, 60 1.63, 300 minutes 1.36) anticoagulants (Figure 30). This experiment was performed with a standard phosphoflow protocol (Spurgeon and Naseem, 2018), using an AF647 conjugated pERK1/2.
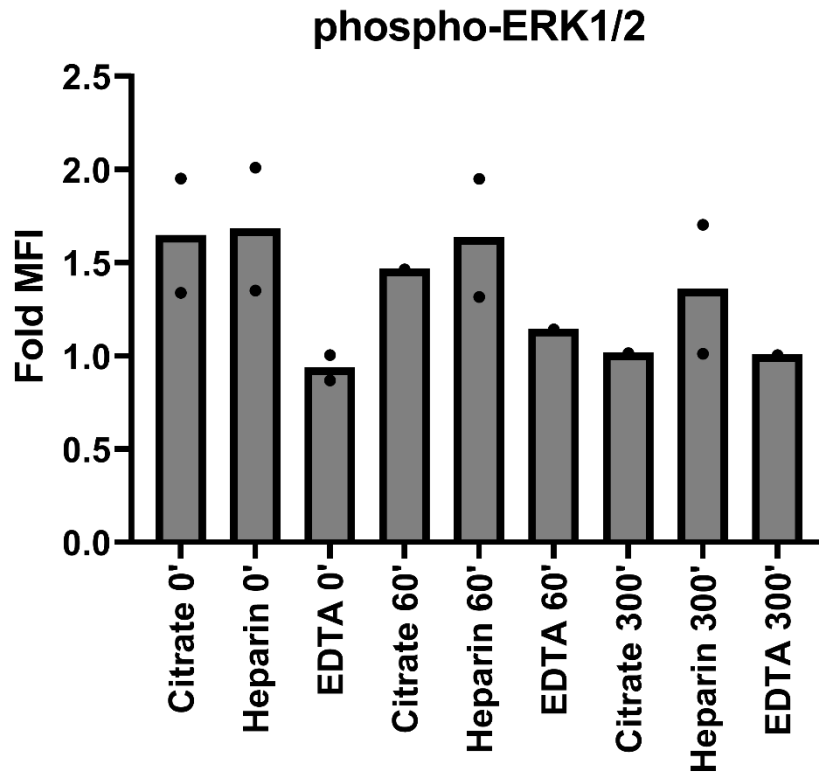
Figure 30. Phosphorylation of ERK1/2 on stimulation with 20 μM SFLLRN compared across anti-coagulants. Whole blood drawn from indicated anti-coagulants and at demonstrated time point was stimulated with SFLLRN (10 μM) for 10 minutes prior to fixation in BD fix/lyse, permeabilisation and staining with pERK1/2-AF647. (n=1-2)

3.4.6 Antagonist induced intracellular phosphorylated VASP

Platelet inhibition is a vital facet of platelet biology; however, it is more difficult to measure directly than activation, which can be measured by a multitude of surface markers. Although the effect of inhibition can be indirectly observed as a loss of activation, platelet inhibition can be directly measured through intracellular phosphorylation events which occur downstream of inhibition. The ability to measure platelet inhibition is a valuable tool in drug-screening studies (Spurgeon et al., 2014). Here we use the phosphoprotein VASP, an established target of both cAMP and cGMP signalling pathways (Butt et al., 1994).

In a mirror experiment to the identification of optimal anti-coagulant for intracellular pERK1/2 measurement, pVASP-s157 in response to PGI_2 was measured in sodium citrate, sodium heparin and potassium EDTA anticoagulated whole blood at multiple time points (0 – 300 minutes). The phosphorylation of VASP was not affected by anticoagulant choice (Citrate 8.69, Heparin 8.89, EDTA 8.31) (Figure 31). We found that after *in vitro* storage, platelet sensitivity to inhibition was diminished by 50% (Citrate 0 8.69, 60 6.47, and 300 minutes 4.47) (Figure 31). This experiment was performed with a standard phosphoflow protocol (Spurgeon and Naseem, 2018), using an AF647 secondary antibody against pVASP-s157.
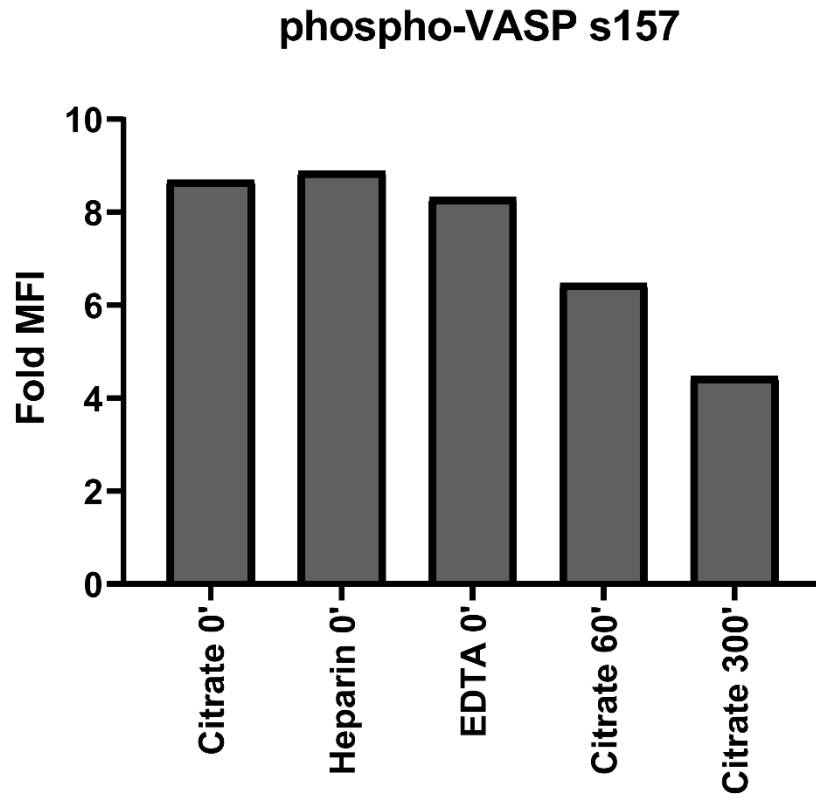
Figure 31. Phosphorylation of pVASP-s157 on stimulation with PGI₂ compared across time and anti-coagulants. Whole blood drawn from indicated anti-coagulants and at demonstrated time point was stimulated with PGI₂ (200 nM) for 5 minutes prior to fixation in BD fix/lyse, permeabilisation and staining with pVASP-s157. (n=1)

3.5 PLATELET ACTIVATION

Having previously determined that freshly drawn whole blood into sodium citrate, are the optimal conditions for measuring multiparameter whole blood platelet activation, we proceeded to develop panels of antibodies and fluorophores to examine platelet activation in different contexts. We demonstrate measurement of platelet activation by both agonists and antagonists by changes in the surface protein expression and by measurement of intracellular phosphorylation of activation transducing enzymes.

3.5.1 Activation induced surface antigens – fibrinogen, CD62P and CD42b

Initially a three-colour assay was developed using antibodies which targeted fibrinogen, CD62P and CD42b. This combination allows two distinct measurements of platelet activation, fibrinogen binding (integrin activity/aggregation) and α-granule secretion (degranulation), and a constitutively expressed marker for platelet identification. The antibodies were tagged with fluorescent conjugates; fibrinogen-FITC, CD62P-PE and CD42b-APC respectively. FITC and PE are both excited by the 488 nm laser and read in the 525/40BP and 585/42BP filters respectively and share overlapping spectral profiles. Due to this a compensation matrix was developed to allow for analysis of these parameters (Table 7).

Table 7. Compensation matrix for three colour panel.

Channel	-FITC%	-PE%	-APC%
525/40BP	-	0.64	0.00
585/42BP	27.62	-	0.00
660/10BP	0.00	0.00	-

The thrombin mimetic, SFLLRN (1 – 20 µM) induced a concentration dependent increase in both fibrinogen binding and CD62P expression (Figure 32). Where the data is analysed as percent positive cells, both markers reached near 100%

expression (fibrinogen 74.8±16% and CD62P 95.6±2%) at SFLLRN (5 μM) and do not increase significantly further as dose increased (fibrinogen 80.5±10% and CD62P 98.1±1%) at SFLLRN (20 μM). This means that all platelets expressed the marker of activation at a level above the detection threshold, which is determined by either the use of EDTA or isotype control for fibrinogen and CD62P respectively. This provides a valuable illustration where despite percent positive cells not increasing further beyond SFLLRN (5 μM), MFI continued to increase; in fibrinogen binding, this increased from 844.7±76 (basal) to 9332.6±5009 (5 μM) peaking at 11,057.4±4673 (20 μM). For CD62P expression, MFI increased dose dependently from 620.4±85 (basal) to 13,314.6±3170 (5 μM) peaking at 17,099.9±2273 (20 μM). This experiment was performed with a standard surface staining protocol.
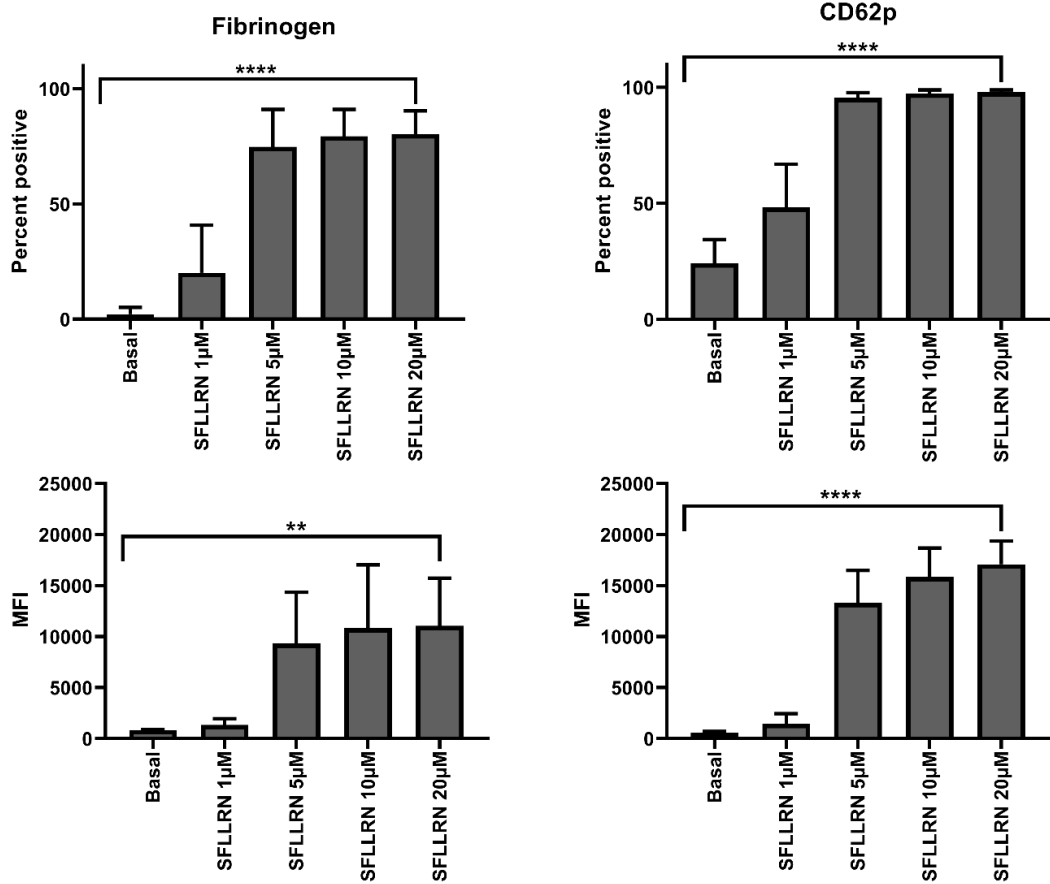
Figure 32. Platelet activation dose response to SFLLRN by three colour fluorescent flow cytometry. Whole blood was stimulated with SFLLRN (1 – 20 µM) for 20 minutes prior to fixation in 1% PFA/PBS and subsequent fluorescent flow cytometry acquisition and analysis. (unpaired T-test, n=5, **<0.01 and ****<0.0001, error shown as standard deviation)

3.5.2 The influence of PKA signalling on platelet activation

An outstanding caveat of most of the literature surrounding platelet activation, is that it is rarely carried out in the context of inhibition. Indeed, it is often measured in platelets which have been isolated from whole blood, plasma and any physiological milieu for some time. Work done in this hypo-inhibitory context suggests that platelets are hyper-sensitive to all stimuli, however, it must be considered that within the vasculature platelets are continually exposed to NO and PGI_2. Therefore, we sought to perform analysis of platelet activation in the physiological milieu of whole blood and in the presence of PGI_2, in order to more closely replicate activation in the blood to further understand how this affects the current beliefs surrounding the expression of markers of platelet activation. To do this, we applied fluorescent flow cytometry, as it allows an assessment of platelet function in whole blood without further sample processing.

We first performed a dose response of PGI_2 (1 – 100 nM) against a static dose of SFLLRN (5 µM) measuring fibrinogen-FITC, CD62P-PE and CD42b-APC simultaneously in the same samples (Figure 33). PGI_2 caused a concentration dependent inhibition of both fibrinogen binding and CD62P expression. However, this approach allowed us to observe a difference in sensitivity of the markers to PGI_2. Fibrinogen binding, and therefore integrin activation, was more sensitive to the effects of PGI_2 with the marker returned to basal (5.3±3%) at maximal PGI_2 (100 nM) treatment (5.9±3%). In contrast, CD62P remained significantly elevated over basal (10.1±6%) under the same conditions (33.1±18%) (Figure 33).

We sought to further characterise this apparent dichotomy and repeated this experiment using a static maximal dose of PGI_2 (1000 nM) against a dose response of SFLLRN (1 – 20 µM) (Figure 34). While kinetics of stimulation was similar across the two markers, with both fibrinogen and CD62P reaching near maximal percentage positivity at SFLLRN (5 µM) (74.6±16% and 95.6±2% respectively), the response to

activation in the context of inhibition was significantly different. Here, PGI_2 maintained fibrinogen binding at basal regardless of agonist concentration, at maximal SFFLRN (20 µM) with PGI_2, fibrinogen percentage expression was 3.7±3% and MFI was 966.6±72, in comparison with fibrinogen basal at 2.2±3% and 844.72±76 respectively. In contrast, CD62P expression remained elevated with PGI_2 and SFLLRN at maximal dose (20 µM), percentage expression was 72.3±4% and MFI was 2948.6±741, and this remained significantly increased over basal at 24.3±10% ($p<0.0001$) and 620.4±85 ($p<0.005$) respectively (Figure 34). This reinforces the earlier finding (Figure 33), where PGI_2 inhibited fibrinogen more than CD62P, and further confirms a dichotomy of response to PGI_2 between the two markers of platelet activation, fibrinogen binding (integrin activation) and CD62P expression (granule secretion).
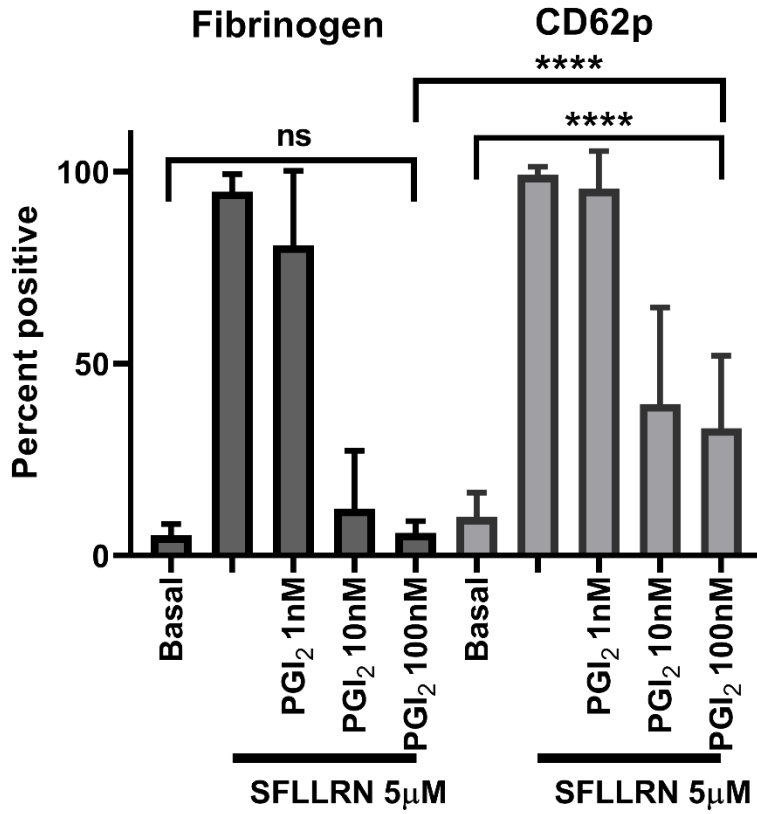
Figure 33. Dose response of PGI₂ against a static dose of SFLLRN. Whole blood probed with fibrinogen-FITC, CD62P-PE and CD42b-APC treated with PGI$_2$ (1 – 100 nM) for 2 minutes and then treated with SFLLRN (5 µM) for 20 minutes prior to fixation in 1% PFA/PBS and subsequent fluorescent flow cytometry acquisition and analysis. (n=42, unpaired T-test, ns=non-significant and ****<0.0001, error shown as standard deviation)
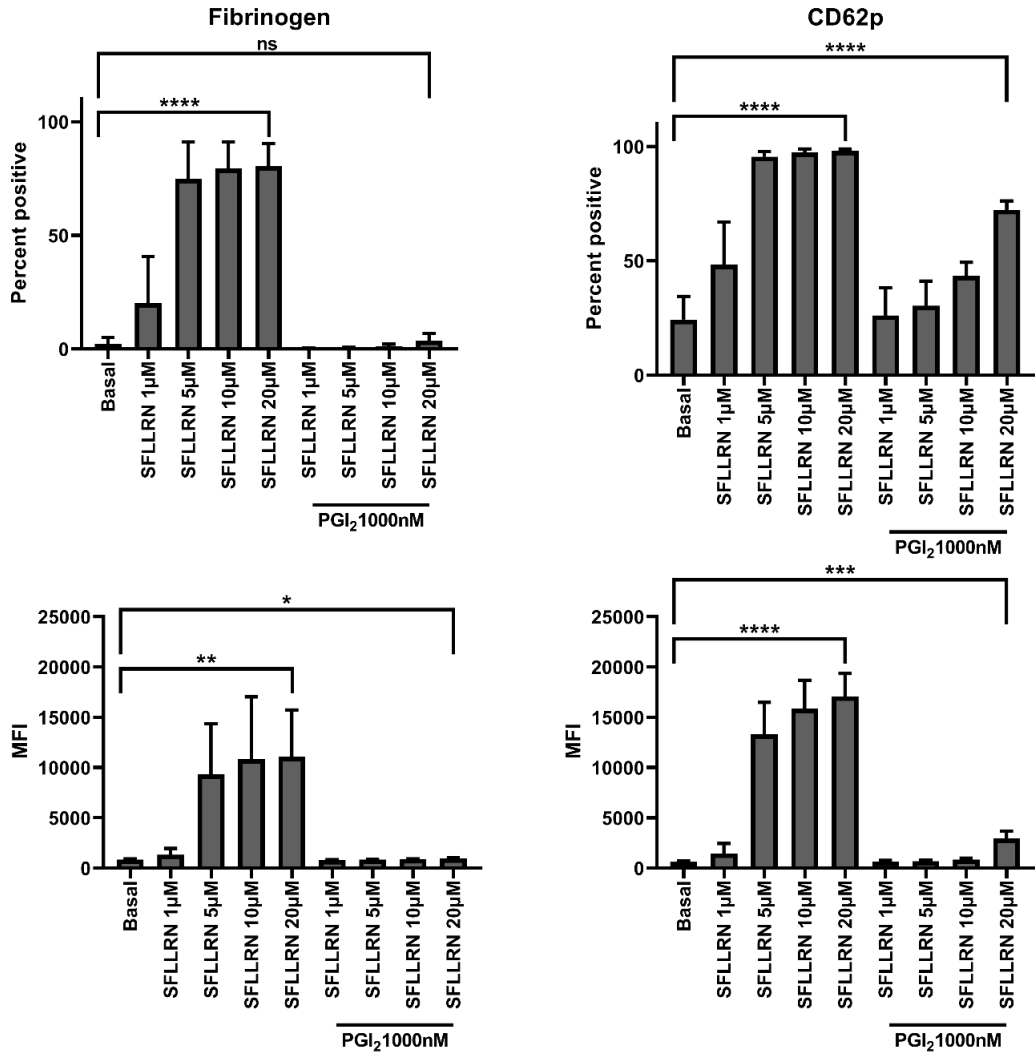
Figure 34. Dose response of SFLLRN against a static maximal dose of PGI$_2$. Whole blood probed with fibrinogen-FITC, CD62P-PE and CD42b-APC treated with PGI$_2$ (1000 nM) for 2 minutes and then treated with SFLLRN (1 – 20 µM) for 20 minutes prior to fixation in 1% PFA/PBS and subsequent fluorescent flow cytometry acquisition and analysis. (n=5, unpaired T-test, ns=non-significant, *<0.05, **<0.01, ***<0.005 and ****<0.0001, error shown as standard deviation)

3.5.3 pVASP-s157 phosphorylation is sustained

In order to confirm that inhibitory signalling induced by PGI$_2$ was sustained for the duration of the experiment (20 minutes) and these differences were not due to a significant loss of inhibitory signalling, we examined pVASP-s157. The levels of VASP phosphorylation at the initial time point of 2 minutes and the longer time point of 20 minutes were compared against a dose response of PGI$_2$. Although there was a small reduction in phosphorylation over time, vitally the phosphoflow data confirmed that inhibitory signalling was sustained above basal by >4-fold for the duration of the time course tested (Figure 35). Hence CD62P remains expressed on the majority of cells despite elevated cAMP.
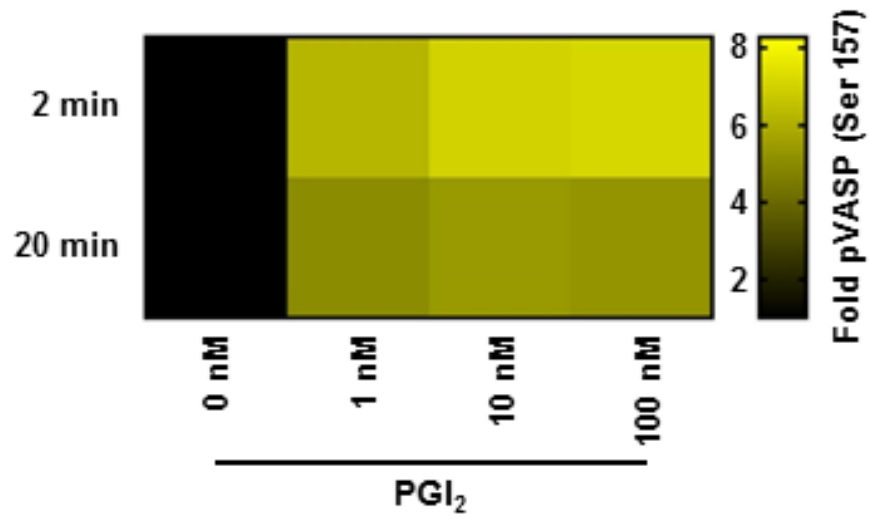
Figure 35. pVASP-s157 dose response of PGI₂ at 2 and 20 minutes. Whole blood treated with PGI₂ (1 – 100 nM) for 2 or 20 minutes prior to fixation in BD fix/lyse, permeabilisation, barcoding, washing and staining with pVASP-s157. (n=42)

3.6 MULTIPARAMETER SUBPOPULATION IDENTIFICATION

Given that previous data (Figure 33 and Figure 34) demonstrated that fibrinogen binding and CD62P showed differing sensitivity to PGI_2, we wanted to explore this concept of differential regulation using additional markers of platelet activation. The assay was adapted by adding in a fourth fluorescent parameter, annexin V-APC, which binds to phosphatidylserine (PS) and acts as a marker of platelet procoagulant activity (Gyulkhandanyan et al., 2012). In order to introduce this marker on an APC fluorophore, we used CD42b conjugated to a polymer BB700 dye, which is excited by the 488 nm laser and is detected in the 712/25BP channel. This increased the complexity of the compensation matrix required, as a greater number of fluorophores were emitting within a similar spectral range and overlapping within the detector bandpass array (Table 8).

Table 8. Compensation matrix for four colour panel.

Channel	-FITC%	-PE%	-APC%	-BB700%
525/40BP	-	0.64	0.00	14.11
585/42BP	27.62	-	0.00	42.67
660/10BP	0.00	0.00	-	10.24
712/25BP	0.00	0.00	37.66	-

3.6.1 Multiparameter analysis platelet activation in the presence of PGI_2

In the four-parameter fibrinogen, CD62P, PS and CD42b assay we provided robust SFLLRN mediated PAR1 activation and cross-linked collagen related peptide (CRP-XL) mediated GPVI activation. This dual stimulus drives platelet activation and phosphatidylserine exposure, which will induce the formation of the procoagulant platelet subpopulation (Sodergren and Ramstrom, 2018).

Data from the four-parameter assay is presented here as percent positive cells over EDTA or IgG control respective to the conjugate and as fold MFI over basal. Fibrinogen binding was significantly increased over basal when treated with SFLLRN

(20 µM)/CRP-XL (10 µg/mL) for both percent positive (0.5±0.3% to 67.6±13.5%, p<0.0001) and fold MFI (1 to 8.6±3.9, p<0.05). CD62P was also significantly increased over basal in the same samples after stimulation in both percent positive (20.4±9.3% to 96.9±2.6%, p<0.0001) and fold MFI (1 to 37.4±5.9, p<0.0001). Again from the same cells, PS exposure was measured, and this was also increased over basal after stimulation in both percent positive (7.7±7.8% to 43.5±13.6%, p<0.0001) and fold MFI (1 to 9.8±3.8, p<0.01). However, pre-treatment of the whole blood with PGI_2 (1 – 1000 nM) led to differences in sensitivity to inhibition becoming apparent in each marker measured on the same cells. In a recapitulation of previous data fibrinogen binding was shown to be significantly reduced in the presence of PGI_2 (1000 nM) in percent positive (67.6±13.5% to 10.62±6.9%, p<0.0001) and fold MFI (8.6±3.9 to 1.9±0.2, p<0.05). Again in support of previous findings, CD62P expression was shown to remain mostly independent of inhibition, with only a small reduction in percent positive (96.9±2.6% to 83.7±14.8%, p<0.05) and no significant reduction in fold MFI (37.4±5.9 to 23±13.6, ns). Finally, the third activation marker measured on these cells showed that PS exposure was also more sensitive to inhibition than granule secretion and demonstrated a significant reduction in percent positive (43.5±13.6% to 28.3±15.9%, p<0.01), although here percent positive cells appears to remain high the MFI data confirms that almost all signal is lost with a return to near basal (9.8±3.8 to 2.9±1.8, p<0.01). Furthermore, as a four parameter assay, CD42b expression was also measured here and shown to be decreased by stimulation (data not shown), but was protected from shedding by PGI_2 treatment. In total this experiment demonstrates that three of four markers measured here are sensitive to PGI_2 mediated inhibition of activation, but CD62P remains resistant to inhibition.

Here we demonstrated an extension of the dichotomy between different markers of platelet activation in response to PGI_2. Fibrinogen and phosphatidylserine both demonstrated markedly greater sensitivity to PGI_2 than CD62P, which demonstrated

a significant resistance to PGI_2. As this experiment was performed measuring four parameters simultaneously, this provides confidence in the dichotomy examined here between these markers as antagonists and agonists can be demonstrated to work in parallel markers, and further supports the previous observations made regarding the resistance of CD62P to inhibition.
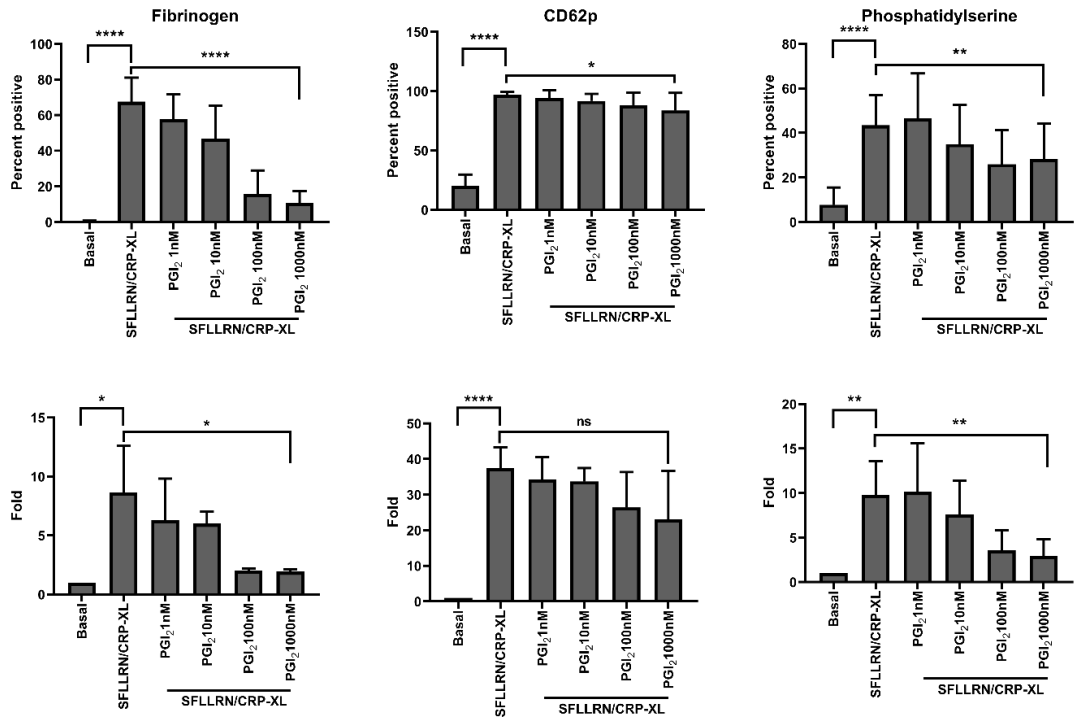
Figure 36. Four parameter dose response of PGI₂ against a static dose of SFLLRN/CRP-XL. Recalcified whole blood probed with fibrinogen-FITC, CD62P-PE, annexin V-APC and CD42b-BB700 treated with PGI₂ (1 – 1000 nM) for 2 minutes and then treated with SFLLRN (20 µM)/CRP-XL (10 µg/mL) for 20 minutes prior to fixation in 1% PFA/Ca²⁺ modified Tyrodes and subsequent fluorescent flow cytometry acquisition and analysis. (n=12 for percentage, 5 matched for fold MFI, paired T-test, ns=non-significant, *<0.05, **<0.01 and ****<0.0001, error shown as standard deviation)

3.6.2 FItSNE analysis of platelet subsets

Here we applied multidimensional analysis to the four-parameter fibrinogen-FITC, CD62P-PE, annexin V-APC, CD42b-BB700 panel to distinguish unique subsets of platelets with an impartial clustering strategy. We applied a variant of t-SNE, FIt-SNE (Linderman et al., 2019). tSNE allows multidimensional (4D) data to be expressed on a 2D plot by the formation of clusters of related cells. These resulting "islands" of cells are related by their unique receptor expression profile. This analysis was performed on concatenated FCS files with 30,000 platelet positive events in each treatment category, which was drawn from 3 biological repeats. The islands formed through the algorithm were then pseudo coloured for expression of each marker so we could further understand the defining characteristics of each group. Where islands were distinct, they are manually gated to provide relative fluorescence intensities and population size of each island. In this case, blue represents negative populations, green-yellow interstitial expression, while red is indicative of high levels of expression.

At basal we identified no distinct islands (upper, Figure 37), although the basal activity of CD62P was apparent. However this is a universally observed by platelet biologists (Frelinger et al., 2015), and is likely, but perhaps not exclusively, due to the physical trauma of venepuncture driving mild activation of platelets. When stimulated with SFFLRN (20 µM)/CRP-XL (10 µg/mL), 3 distinct islands emerged (mid, Figure 37). These cells were characterised primarily by distinct levels of PS exposure and fibrinogen binding. These are classified as; PS^{lo}/FB^{hi} (66.3%), PS^{hi}/FB^{lo} (23.3%) and PS^{hi}/FB^{hi} (9.5%). While the phenomena of PS+ and PS- platelet subpopulations have been previously described in many contexts, this is a novel observation suggesting that within PS+ platelets there are further unique subsets distinguished by a capacity to bind fibrinogen. In contrast to fibrinogen and PS, we found that within these populations there were minor differences in CD62P and CD42b expression.

However, as expected from our previous data, when pre-inhibited with PGI_2 (100 nM) and then stimulated with SFFLRN (20 µM)/CRP-XL (10 µg/mL), there was a dramatic remodelling of the subpopulations previously described. We now identify 4 unique islands which have all undergone large changes in the presence of inhibition (lower, Figure 37). These subsets are characterised as; $CD62P^{hi}/FB^{lo}$ (69.2%), $CD62P^{hi}/FB^{hi}$ (20.8%), $CD62P^{lo}/FB^{lo}$ (7.2%) and $CD62P^{hi}/PS^{hi}$ (2.9%). This is the first description of platelet subpopulations which emerge after potent stimulation in the physiological context of calcified whole blood and PGI_2.
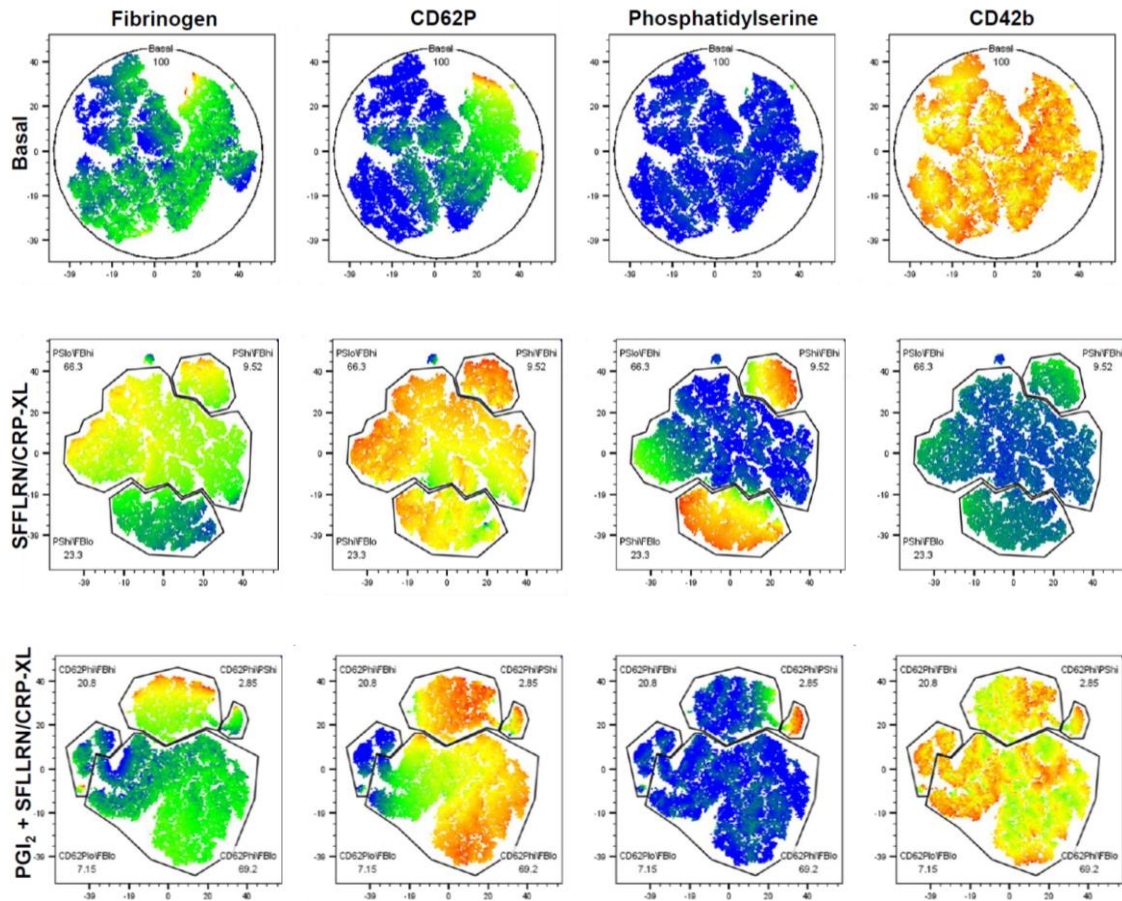
Figure 37. Static PGI$_2$ against static SFLLRN/CRP-XL analysed by Flt-SNE.
Recalcified whole blood probed with fibrinogen-FITC, CD62P-PE, annexin V-APC and CD42b-BB700 treated with PGI$_2$ (100 nM) for 2 minutes and then treated with SFLLRN (20 µM)/CRP-XL (10 µg/mL) for 20 minutes prior to fixation in 1% PFA/Ca^{2+} modified Tyrodes and subsequent fluorescent flow cytometry acquisition and analysis by Flt-SNE. (n=3)

3.6.3 PGI$_2$ protects mitochondria from depolarisation

TMRE collects within mitochondria against an electrochemical gradient and is used as a marker of mitochondrial (de)polarisation. It has been previously suggested that mitochondrial depolarisation is a key event in the process of phosphatidylserine exposure (Agbani and Poole, 2017, Choo et al., 2017). We wanted to use this as a basis for asking where in the pathway PGI$_2$ may target phosphatidylserine exposure. We demonstrate this data with fold MFI over controls (FCCP/EDTA respectively). Under basal conditions, TMRE measured 2.3±0.8, which was reduced to 1.1±0.1 after activation with SFLLRN/CRP-XL. This decrease is indicative of mitochondrial depolarisation. The loss of mitochondrial polarisation under these conditions was associated with increased PS expression from 1.0±0 to 41.2±4 (upper, Figure 38). This is visually demonstrated by the biaxial plots examining the relationship between TMRE and Annexin V. Here it can be seen that under basal conditions platelets were high in TMRE, but low in PS. Stimulation leads to a loss of TMRE and increase in PS (lower, Figure 38).

To understand if the inhibition of phosphatidylserine exposure was linked in any way to TMRE and the temporal order of events, we examined both markers in the presence of PGI$_2$. PGI$_2$ reduced annexin V events from 78.2% to 31.5%. The biaxial plots demonstrate that most of the platelet population (68.5%) that are PS negative also have normal TMRE staining (61.2%), this is an important observation, where a left shift alone would have shown that mitochondria are remaining depolarised, but PS is blocked from exposure. The shift is a return to polarised mitochondria, which confirms that depolarisation occurs upstream of PS exposure (Choo et al., 2017)and that PGI$_2$ is either targeting mitochondria and protecting them or inhibiting the event prior to depolarisation, which in turn blocks mitochondrial depolarisation to prevent PS exposure. There was a dose responsive recovery of mitochondrial depolarisation and inhibition of PS

expression in the presence of PGI$_2$, where at maximal dose mitochondria was rescued from depolarisation (TMRE, 1.1±0.1 to 2.0±0.7, SFLLRN/CRP-XL and PGI$_2$ 1000 nM respectively) (Figure 38).
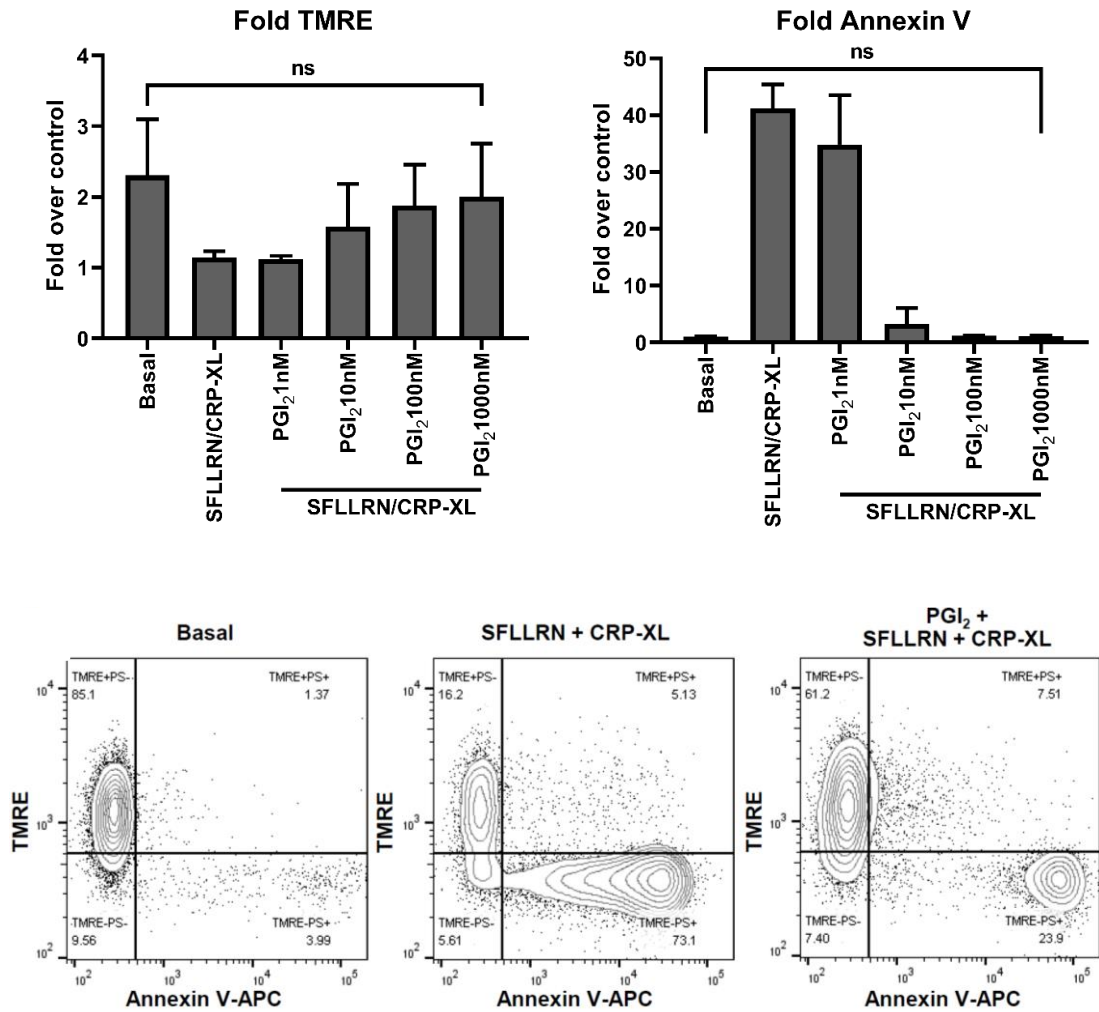
Figure 38. Dose response of PGI₂ against a static dose of SFLLRN/CRP-XL to examine mitochondrial membrane potential and phosphatidylserine. 2 x 10⁶ washed platelets were treated with PGI₂ (1 – 1000 nM) for 2 minutes and then treated with SFLLRN (20 µM)/CRP-XL (10 µg/mL) for 20 minutes while staining for TMRE (50 nM) and annexin V-APC. Each sample was diluted 10x in PBS and analysed immediately for 10,000 platelet events, biaxial contour plots and fold over matched FCCP/EDTA control are presented. (n=3, ns=non-significant, error shown as standard deviation)

3.6.4 Validation by PAC1 multiparameter panels

To validate the previous observation with a parallel marker of integrin αIIbβ3, we repeated these experimental conditions with the monoclonal antibody PAC1. This antibody targets the integrin αIIbβ3 specifically in its active conformation, as opposed to the anti-fibrinogen antibody which targets fibrinogen bound to the integrin αIIbβ3, or indeed elsewhere on the platelet surface, and acts as a proxy for receptor activation. This allowed us to cross-validate and confirm our previous observations which suggested that fibrinogen binding was more sensitive to PGI_2 mediated inhibition than CD62P expression.

We first compared PAC1 and CD62P in a three-parameter assay including CD42b (Figure 39). Here, to compare inhibitory response, the two parameters are compared on the calculated percent inhibition. This demonstrated that in response to increasing doses of PGI_2 (1 – 1000 nM), PAC1 inhibition was markedly more than that of CD62P and significantly increased when comparing minimal and maximal dose of PGI_2 (4.4±9% and 75.7±15%), whereas there was no significant difference when comparing CD62P (10.0±3% and 34.7±17%) (Figure 39).

To then further validate our findings regarding the two PS^{hi} subsets, we used PAC1 as an alternative marker of integrin αIIbβ3 activity and performed a four parameter assay also including CD62P, annexin V and CD42b. Here we could show that upon treatment with the dual stimulus of SFLLRN and CRP-XL, three subsets were formed; PS^-PAC1^+, PS^+PAC1^- and PS^+PAC1^+ (Figure 40). These corroborate with the three subsets formed when observed with fibrinogen as the primary marker of integrin αIIbβ3 activity (Figure 37).
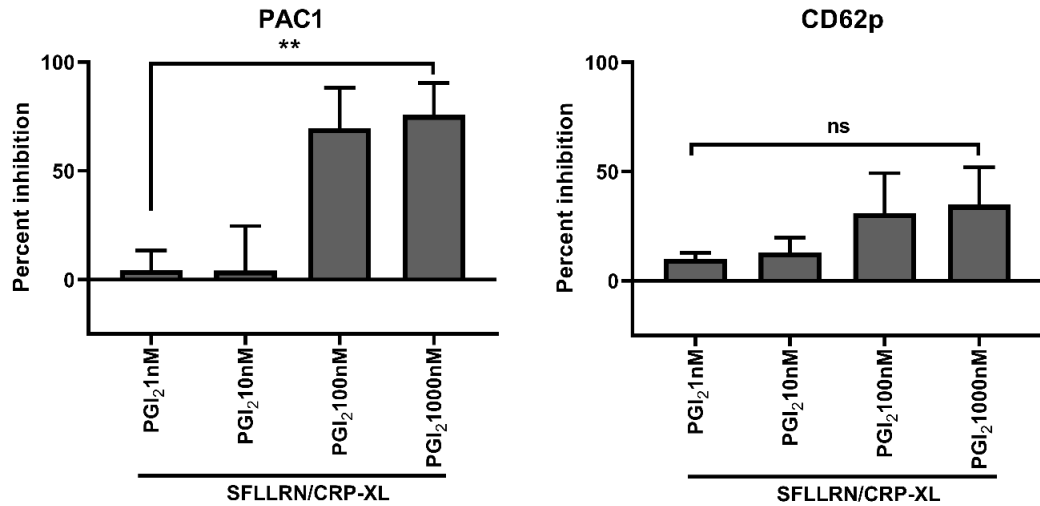
Figure 39. PAC1 and CD62P dose response of PGI$_2$ against a static dose of SFLLRN/CRP-XL. Whole blood probed with PAC1-FITC, CD62P-PE and CD42b-APC treated with PGI$_2$ (1 – 1000 nM) for 2 minutes and then treated with SFLLRN (20 μM)/CRP-XL (10 μg/mL) for 20 minutes prior to fixation in 1% PFA/PBS and subsequent fluorescent flow cytometry acquisition and analysis. (n=3, paired T-test, ns=non-significant and **<0.01, error shown as standard deviation)
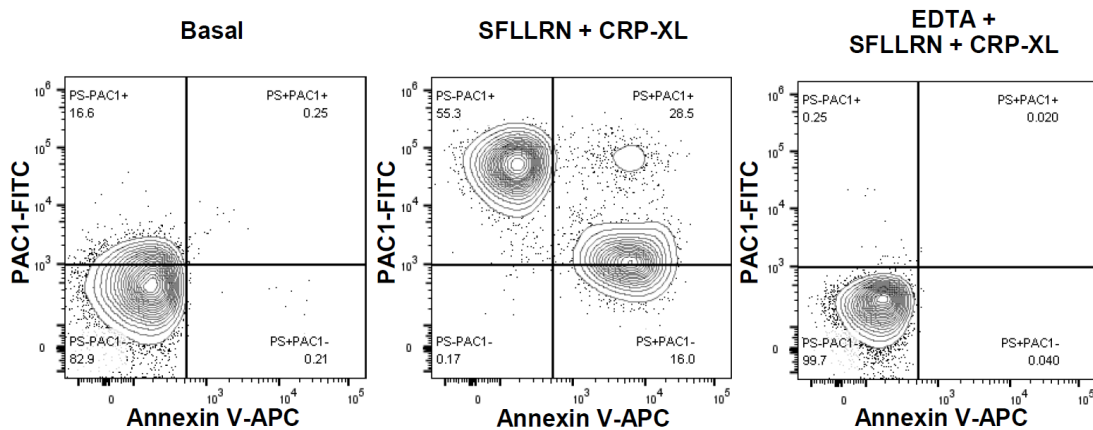
Figure 40. Four parameter PAC1 assay with a static dose of SFLLRN/CRP-XL for subpopulation identification. Recalcified whole blood probed with PAC1-FITC, CD62P-PE, annexin V-APC and CD42b-BB700 treated with SFLLRN (20 μM)/CRP-XL (10 μg/mL) for 20 minutes (+/- EDTA 10 mM) prior to fixation in 1% PFA/Ca^{2+} modified Tyrodes and subsequent fluorescent flow cytometry acquisition and analysis. (n=1)

3.6.5 Validation by multiparameter granule secretion panel

While we have been able to establish that CD62P demonstrates resistance to inhibition in the context of robust stimulation and show this in multiple assays, we sought to provide further validation and further explore this phenomenon. Here using an additional four-marker panel using CD154-FITC, CD62P-PE, CD63-APC and CD42b-BB700 we aimed to validate and explore our observations on these additional markers of platelet degranulation. By using 3 markers of granule secretion, we hoped to be able to confirm the resistance demonstrated to PGI_2 by CD62P would also be conferred onto other markers of granule secretion, thereby validating the independence of CD62P (and granule secretion) to cAMP-mediated inhibitory signalling.

These markers were all shown to be significantly increased in the presence of robust stimulation (SFLLRN/CRP-XL) (CD154 $28.1\pm7\%$, CD62P $98.7\pm0.2\%$, CD63 $98.5\pm0.3\%$), but also demonstrated significant resistance to inhibition, shown as a continued significant difference to basal in the presence of maximal PGI_2 (1000 nM) (CD154 $22.8\pm11\%$, CD62P $96.1\pm4\%$, CD63 $96.0\pm3\%$) (Figure 41). This validates our previous observations surrounding CD62P and further suggests that it is platelet degranulation itself that may retain resistance to cAMP signalling in the context of robust stimulation.
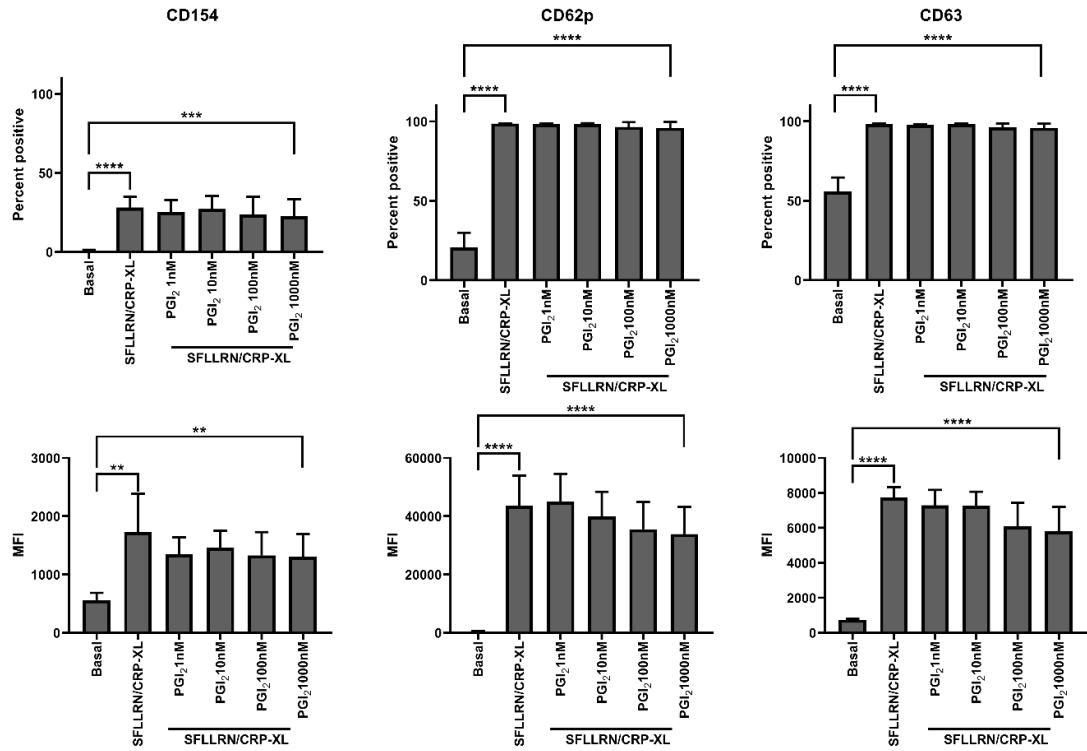
Figure 41. Dose response of PGI₂ against a static dose of SFLLRN/CRP-XL to measure granule secretion. Whole blood probed with CD154-FITC, CD62P-PE, CD63-eF660 and CD42b-BB700 treated with PGI₂ (1 – 1000 nM) for 2 minutes and then treated with SFLLRN (20 µM)/CRP-XL (10 µg/mL) for 20 minutes prior to fixation in 1% PFA/PBS and subsequent fluorescent flow cytometry acquisition and analysis. (n=5, unpaired T-test, **<0.01, ***<0.005 and ****<0.0001, error shown as standard deviation)

3.6.6 Inhibitory signalling by phosphoflow with surface CD62P

Having previously confirmed the partial resistance of agonist induced CD62P expression to PGI_2 through three different assays, we next wanted to further confirm that the resistance was not due to diminished cAMP signalling over the course of the experimental 20-minute incubation. To explore this, we developed a novel assay which for the first time in platelet biology combined intracellular phosphoflow with measurement of surface markers of activation. This assay requires a stimulation, surface probe, fix, permeabilise and intracellular probe protocol to allow for optimal recognition and detection of all markers.

Treatment with PGI_2 (10 – 1000 nM) resulted in a robust phosphorylation of pVASP-s157 (6.3±0.1, 7.5±0.5 and 7.6±1.1 at 10, 100 and 100 nM respectively), at higher doses of PGI_2 (100 – 1000 nM) this was not diminished in the presence of SFLLRN (20 μM) (8.3±1.8 and 9.0±3.0 respectively), but was reduced with weaker PGI_2 stimulation (10 nM) from 6.1±0.1 to 2.4±0.5 respectively (Figure 42). Examining CD62P on the same cells demonstrated that CD62P was expressed in the presence of both PGI_2 and SFLLRN, and SFLLRN alone at all doses, as prior, at the lower dose of PGI_2 (10 nM) the opposite observation than for pVASP-s157 was made where CD62P expression was greater than at higher doses of PGI_2 (100 – 1000 nM) 16,637.3±5495 vs. 8969.4±3613 and 8316.8±3007 at 10, 100 and 1000 nM respectively. This suggests there is some capacity for CD62P inhibition but it remains expressed independent of robust cAMP signalling driven by excess PGI_2 (Figure 42). By also demonstrating this data as a biaxial contour plot of pVASP versus CD62P, we can confirm that all cells positive for CD62P (97.1%) retain robust VASP-s157 phosphorylation and there is no subset of inhibition resistant platelets (Figure 42), therefore confirming that the CD62P expression is independent of intact inhibition signalling and is not due to diminished inhibition.
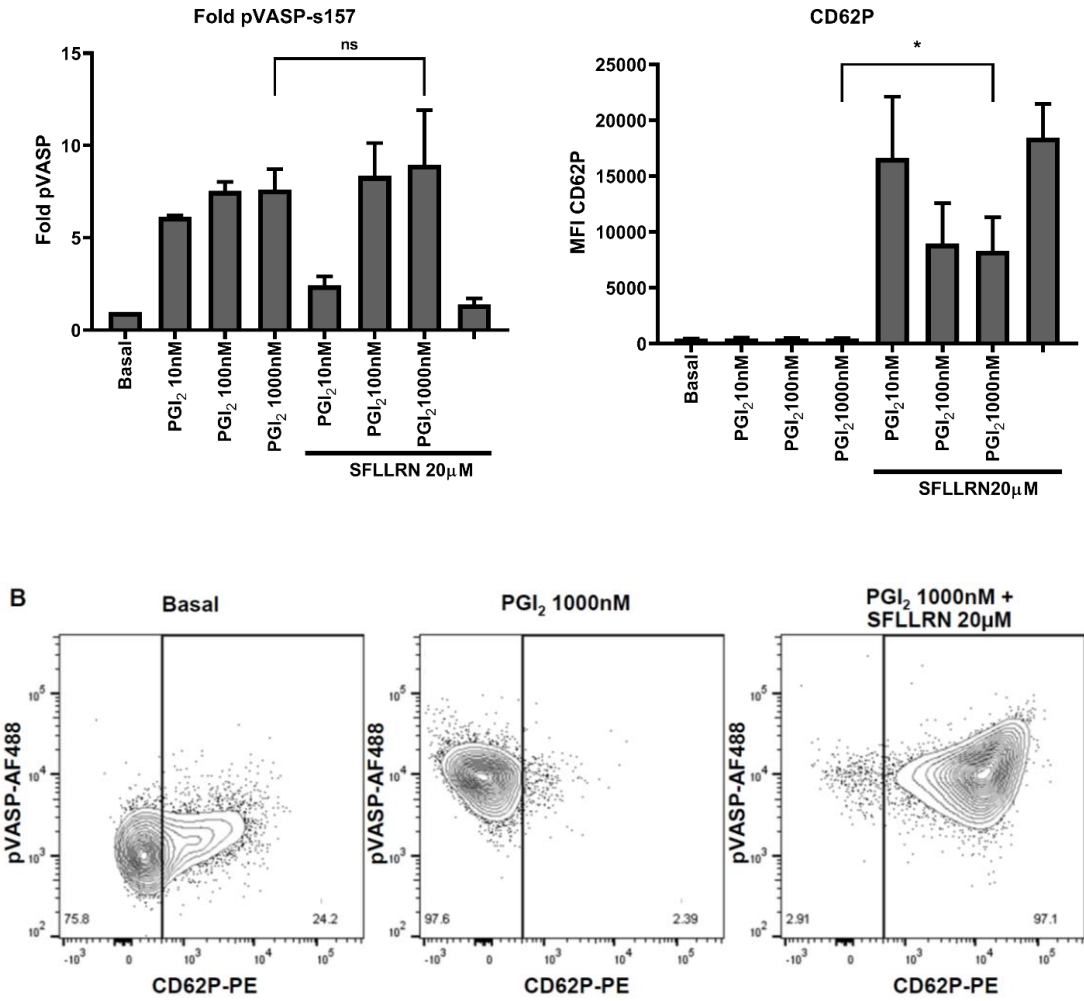
Figure 42. Dose response of PGI₂ against a static dose of SFLLRN/CRP-XL to measure inhibitory signalling. Whole blood probed with CD62P-PE and CD42b-APC treated with PGI₂ (10 – 1000 nM) for 2 minutes and then treated with SFLLRN (20 µM) for 20 minutes prior to BD fix/lyse, permeabilisation and staining with pVASP-s157 followed by fluorescent flow cytometry acquisition and analysis. Within biaxial contour plots, the line indicates IgG-PE background fluorescence. (n=3, unpaired T-test, ns=non-significant and *<0.05, error shown as standard deviation)

3.6.7 Platelet monocyte aggregates

Given that CD62P and CD154 are known to be as key mediators of platelet-leukocyte interactions (Rossaint et al., 2016, Stokes et al., 2009), and we had shown that these were independent of platelet inhibitory signalling, we assessed the effect of PGI_2 on platelet-monocyte aggregates (PMA). We hypothesised that PMA may be independent of PGI_2-cAMP signalling under the same experimental conditions of robust activation and inhibition where the previous observations had been made. Here, monocytes (CD14+) were analysed for expression of the platelet marker CD42a. PMA were significantly increased after co-stimulation of whole blood with SFLLRN (20 µM) and CRP-XL (10 µg/mL) from 1508.6±177 at basal to 6819.7±1835 when stimulated ($p<0.005$). Exposure of whole blood to PGI_2 prior to platelet activation led to a modest reduction in PMA (5093.6±705), but this was not statistically significant (Figure 43). To further confirm that fibrinogen binding was inhibited by PGI_2 and did not mediate PMA, we employed the specific $\alpha_{IIb}\beta3$ integrin blocker Tirofiban. We showed that Tirofiban did not potentiate PGI_2 (1000 nM) inhibition (4664.1) and that alone it could mimic the effects of PGI_2 alone (5673.4±1574) (Figure 43). This suggests that PMA do not depend on platelet-bound fibrinogen and can occur independently of fibrinogen binding and are probably mediated by platelet granule proteins which are resistant to inhibition. Therefore, residual PMA in the presence of the vascular inhibitor PGI_2 is independent of fibrinogen binding and occurs in a context where inhibition independent CD62P and CD154 expression is upregulated.
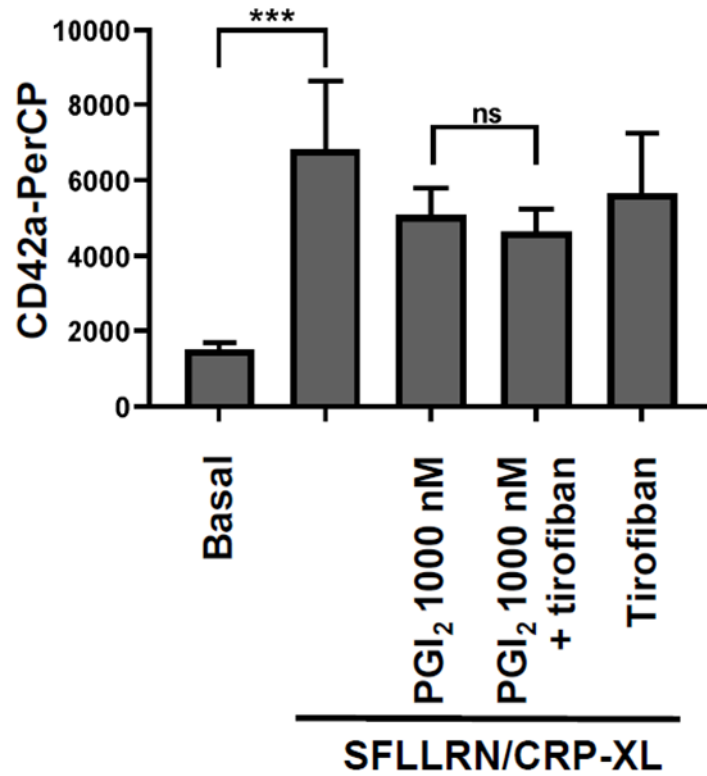
Figure 43. Platelet monocyte aggregates continue to form in the context of inhibition and are not dependent on fibrinogen. Platelet monocyte aggregates are induced by SFLLRN (20 µM) and CRP-XL (10 µg/mL) and in some cases pre-treated with PGI_2 (1000 nM) or Tirofiban (1 µg/mL). CD42a fluorescence measured with anti-CD42a-Peridinin Chlorophyll Protein Complex (PerCP). (n=5, Two-tailed unpaired T-tests; ns=non-significant and ***<0.005, error shown as standard deviation).

3.7 DE-ACTIVATION OF PLATELETS BY PROSTACYCLIN

Previously, we examined the effects of PGI_2 on platelet activation when added prior to stimulation, which most likely presents the real scenario *in vivo.* However, we also sought to understand if platelet activation markers could be modulated by PGI_2 post-stimulation, which had been shown previously in a static adherent model (Yusuf et al., 2017). *In vivo,* it is also likely that activated platelets may continue to be exposed to endothelial inhibitors. Our own data previously suggested there is some capacity for a reduction in activation markers, this was observed as part of the pVASP-s157/CD62P assay where basal expression of CD62P was shown to be lost when treated with PGI_2 (Figure 42). Therefore, we sought to specifically pursue this question.

3.7.1 Reversal of platelet activation

First, we designed a four-colour flow cytometry experiment to assess several aspects of platelet activation. Here we applied fibrinogen-FITC, CD62P-PE, CD63-EF660 and CD42b-BB700. whole blood was stimulated for 20 minutes followed by 2 minutes of PGI_2 treatment. Two matched controls were included, one of which was a mock treatment with 2 minutes of modified Tyrode's buffer and the second fixed at 20 minutes, which provided a snapshot of activation at both 20- and 22-minutes allowing comparisons to the effects of post-activation inhibition. Here mock treated then fixed is presented for comparison.

Remarkably, we were able to observe reductions in all examined markers of activation, although to different extents. Fibrinogen binding, CD62P and CD63 were all reduced by treatment with PGI_2 (1000 nM) and the effect was strongest on those samples which had been stimulated with the lower doses of SFLLRN (1 µM). At the lower dose of SFLLRN (1 µM) fibrinogen binding was reduced from 10,553.7 to 1465.4, CD62P from 25743.6 to 9965.4 and CD63 from 1825.8 to 1028.0 (Figure 44).

Again, in reference to our previous observation that fibrinogen binding/ integrin $\alpha_{IIb}\beta 3$ was more sensitive to PGI_2 than granule secretion, at maximal SFFLRN (10 µM), fibrinogen binding was reduced from 40,966 to 19,886.8 while the granule markers remained essentially unchanged; CD62P from 66,293.7 to 52,241.7 and CD63 from 6470.3 to 5571.1. CD42b presented an important control in this experiment. As previously shown (Figure 37), expression of CD42b was decreased by stimulation, from 11,375.7 to 4857.5 (basal and SFLLRN 10 µM respectively). Therefore, as CD42b was shed after stimulation, unlike the other markers, it could not be recovered (4407.6, SFLLRN 10 µM + PGI_2 1 µM) despite the post-activation inhibition.
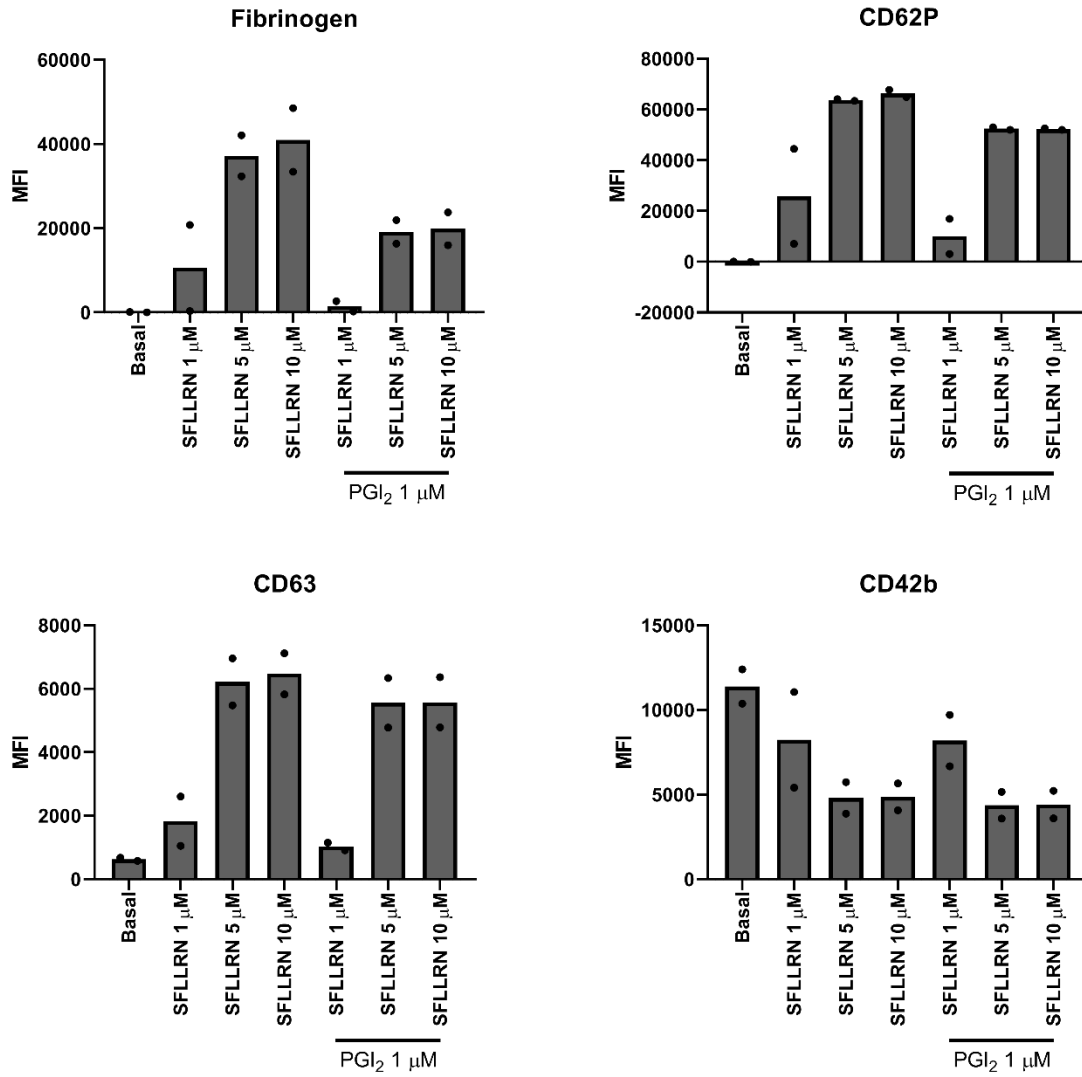
Figure 44. Dose response of SFLLRN against a static dose of PGI$_2$ added post activation. Whole blood probed with fibrinogen-FITC, CD62P-PE, CD63-eF660 and CD42b-BB700 treated with SFLLRN (1 – 10 µM) for 20 minutes prior to addition of PGI$_2$ (1000 nM) for 2 minutes or mock treated and then fixed in 1% PFA/PBS. (n=2)

3.8 DISCUSSION

Platelet activation and inhibition measured by fluorescent flow cytometry provides a platform for robust, reproducible and data rich interpretation of the platelet status. In this chapter, we have demonstrated the use of traditional surface markers of platelet activation, intracellular markers of inhibition and markers for surface phosphatidylserine and mitochondrial depolarisation. With the application of unique combinations of markers, we have been able to demonstrate the potential for discovery which this technique provides. We have revealed novel platelet subpopulations and shown how these are remodelled in the presence of activated PKA and also shown how fluorescent flow cytometry can be used to link surface markers to intracellular signalling events within platelets.

3.8.1 Pre-analytical considerations

Although there have been several platelet flow cytometry guidelines published to date (Spurgeon and Naseem, 2019, Harrison et al., 2011, Harrison, 2009, Linden et al., 2004) which comprehensively examine pre- and post-analytical considerations of platelet flow cytometry, they have not examined multicolour platelet flow cytometry in recalcified whole blood. Therefore, an important element of this chapter was to assess the major pre-analytical considerations which may impact this study. A four-colour assay was designed with the marker's fibrinogen-FITC, CD62P-PE, Annexin V-APC and CD42b-BB700, which allows the researcher to comment on $\alpha IIb\beta 3$ integrin activity, α-granule secretion and procoagulant activity on cells confirmed as platelets, all simultaneously. Applying this assay, we then examined and assessed the impact of the pre-analytical considerations including; anti-coagulant, assay initiation, platelet medium (whole blood, PRP or washed platelets) and impact of storage of samples post-fixation.

The three anti-coagulants tested here are all commonly used in clinical laboratories and all blood was drawn into vacutainers. The recent work of others on whole blood flow cytometry has confirmed the suitability of vacutainers for platelet biologists (Welch et al., 2018). The use of vacutainers carries several inherent advantages over manually prepared syringes. Primarily, it creates standardisation across laboratories, but it also allows rapid translation of assays to clinical samples, where the standard is evacuated tubes. We decided to determine the optimal anti-coagulant based on optimal sensitivity in each marker. We found that sodium citrate was the optimal anti-coagulant for platelet activation by flow cytometry. Previously, citrate, heparin and hirudin anti-coagulants were compared with markers PAC1, CD62P and LAMP1 (Ramstrom et al., 2016), or CD62P alone was assayed (Golanski et al., 1996) and in agreement with our study, citrate tubes were determined as optimal for platelet flow cytometry. We determined sodium citrate as optimal, as fibrinogen binding was most sensitive in this anti-coagulant, and CD62P remained sensitive and was not dependent on changes in anti-coagulant. Furthermore, in citrated blood fluorescence intensity of annexin V binding was reduced in comparison to sodium heparin, but as a qualitative marker, the percent positive remained unchanged and therefore sensitivity to determine the procoagulant platelet subset was not compromised. In support of this observation we were also able to measure ERK1/2 phosphorylation, which can be used as a marker of platelet activity (Stalker et al., 2012), and demonstrated that this was most sensitive in heparin and citrate, but not EDTA anti-coagulants. This signalling defect in EDTA mirrors the functional defects observed in EDTA anti-coagulated blood.

In a research laboratory prompt instigation of assays is optimum, however when working on clinical samples where medical intervention must be the first concern, delay in obtaining blood samples may be unavoidable. We rested blood at room temperature (Harrison et al., 2011), and compared results from each time point. Surprisingly we observed an almost total loss of fibrinogen binding at the longest time

point, with a large reduction in assay sensitivity. Work from others has suggested that this reduced fibrinogen binding is unlikely to be due to the αIIbβ3 integrin losing capacity to bind fibrinogen, as PAC1 binding does not significantly decrease over storage time (Huskens et al., 2018), nor is it likely degradation of the ligand, as fibrinogen levels have also been shown to increase at 8 hours of ambient temperature storage (Kemkes-Matthes et al., 2011). As part of assay design and to limit variation across time points, staining solutions were made up at 0-hours and stored on wet ice in the dark throughout the experiment. To eliminate the potential of this inducing error, duplicate samples with fresh stain at 4.5 hours were also analysed and the reduction in fibrinogen was again observed (data not shown). Therefore, it is probable that it is the addition of GPRP to the whole blood at 0 hours and subsequent storage with this peptide that caused this effect, indeed it has previously been shown that excess GPRP is able to block some fibrinogen binding to platelets (Plow and Marguerie, 1982). Nevertheless, the addition of GPRP is vital in a calcified whole blood system to prevent fibrin formation and clotting, but the consistent reduction in fibrinogen binding, suggests a long-term incompatibility with GPRP treated stored samples. Consequently either the addition of GPRP should be delayed, a non-calcified system used (meaning annexin V could not be used (Gyulkhandanyan et al., 2012)), or PAC1 substituted as an alternative marker of integrin αIIbβ3 activation where sample resting is likely to occur (Frelinger, 2018). The robust marker of CD62P remained sensitive to activation over the time points tested, although basal expression significantly increased over time. This highlights that when comparing donors, it is vital assays are initiated at the same time point to minimise basal activation, which could be misinterpreted as having clinical significance, where basal activation could be considered a clinical biomarker. This increase in basal CD62P suggests that some platelets are degranulating, by both a small amount (noting small MFI increases) and not all cells (noting percentage positive). Both annexin V basal and stimulated expression increased over time, but this is likely due to reduction in the inhibition of

the apoptotic pathways at 4.5 hours *ex vivo*, if longer time points were examined it is probable more platelets would become apoptotic and functional responses continue to decline (Sperling et al., 2019, Sodergren et al., 2016).

The platelet medium which assays will be performed in is an important consideration. The data presented here suggested that for activation, whole blood is optimal. However, contradictions for the use of whole blood may include fluorescent dyes, chemical inhibitors or agonists which are incompatible with any system other than washed cells in a buffered suspension. Fibrinogen binding, counter-intuitively, appears to substantially increase on the surface of washed platelets, however when MFI is compared with percent positive cells, it is apparent that there is a significant loss of sensitivity. This is clearly demonstrated by the EDTA control which can no longer prevent binding, suggesting that most of the signal appears to be non-specific binding or no longer calcium dependent/integrin $\alpha IIb\beta 3$ mediated. Where washed platelets might regularly be assayed, it would be practical to exchange anti-fibrinogen for PAC1, which would detect integrin activation without the need for fibrinogen to be present and eliminate this anomaly and restore assay sensitivity (Frelinger, 2018). Although CD62P retains capacity for activation within washed platelets, there is a high basal activation from the physical stresses of isolation, as a result percent positive cells loses sensitivity as a marker of activation. Finally, annexin V binding to phosphatidylserine appears to increase in PRP and further in washed platelets. It appears that in washed platelets, platelets are pre-disposed to become procoagulant, this could be due to increased agonist availability, however as it has previously been demonstrated that the number of phosphatidylserine positive cells should not change based on agonist availability (Sodergren and Ramstrom, 2018). In support of this, this phenomena was also observed in later experiments when annexin V and TMRE were assayed together, again the number of PS positive cells exceeding the typically accepted ~35%.

Finally, we considered the effect of storage of fixed and probed samples. In many instances, it is not feasible to acquire samples immediately, although based on our findings we recommend that samples are acquired promptly. Notably here, and in contrast to our other results presented here, fibrinogen binding remains robust but both CD62P and annexin V are diminished by storage. Previous work by Atar et al. has suggested CD62P is stable up to 5 days, however they used different concentrations of paraformaldehyde (2% versus 0.9%) and based their observations on basal expression whereas our samples were stimulated, greatly increasing the window to detect a decrease (Atar et al., 2010). Furthermore, although there is a considerable decrease in CD62P MFI in our data, the number of positive cells remained consistent (data not shown). Where samples are required to be stored, it may be prudent to freeze samples immediately to add further protection against degradation. Regardless, we recommend that where possible samples are run for cytometry acquisition as soon as feasible, or in cases where this is not possible delays are universally applied to all samples to reduce any errors within data.

Here we have described several comparisons of pre-acquisition parameters within the control of the platelet biologist. In summary, we determined that when performing platelet activation assays in re-calcified systems, assays should be performed on citrated blood drawn into evacuated tubes; sample preparation should be begun immediately after the blood is drawn or when this is not possible started at a consistent time point after blood acquisition, and samples must be acquired immediately or stored for standard time frames. As a result, we followed these strictures in subsequent studies.

3.8.2 PGI$_2$ and platelet subpopulations

Signalling downstream of elevated cAMP is known to regulate multiple aspects of platelet function including calcium mobilisation, integrin $\alpha_{IIb}\beta3$ activity and the actin

cytoskeleton (Raslan and Naseem, 2014). The aim of this series of experiments was to determine if distinct platelet functions showed differential sensitivity to inhibition by PGI_2, using multiparameter fluorescent flow cytometry as a model assay. A pro-coagulant platelet subpopulation has been characterised and the three-dimensional structure, stimulation conditions and functions of the pro-coagulant PS positive platelet subpopulation has been previously described (Heemskerk et al., 2013, Agbani and Poole, 2017). However, several unresolved discrepancies between studies are evident, in particular, the difference in the expression of active integrin αIIbβ3 or fibrinogen binding on PS positive platelets has remained unresolved, despite publications on this subject (Agbani and Poole, 2017, Topalov et al., 2012, Choo et al., 2017). A combination of multicolour flow cytometry assays, validated with the pre-analytical considerations study, was used and multidimensional data analysis algorithms applied, variants of which have been previously applied to CyTOF platelet data (Blair et al., 2018) but not fluorescent flow cytometry data, and this facilitated both a novel and objective approach.

Using a four-parameter assay, fibrinogen-FITC, CD62P-PE, annexin V-APC and CD42b0BB700 we identified two subsets within the larger subpopulation of procoagulant platelets that could be differentiated by their ability to bind fibrinogen (PS^{hi}/FB^{hi} and PS^{hi}/FB^{lo}). This suggests that both sides of this ongoing discussion as to whether PS positive platelets bind to fibrinogen are correct. This PS^{hi} characterisation supports a previous study that also identified two PS populations, which were distinguished primarily by Ca^{2+} signalling, this group also demonstrated a difference in PAC-1 binding, but intriguingly they suggested there were no differences in fibrinogen binding (Topalov et al., 2012), in direct disagreement with our study. However, we further validated our findings using PAC1. The analytical approach with FIt-SNE allowed us to evaluate how these subsets were linked to other platelet surface markers. Under potent activatory conditions, CD62P was expressed on all platelets, but the highest expression of CD62P was concentrated in the

PS^{hi}/FB^{hi} subset, indicating that these platelets were "super-activated". Given the functional dichotomy of procoagulant and aggregatory platelets, the role of the intermediate subset that expresses both markers are unclear. However, they may represent a group of cells that act to integrate the two arms of platelet function or indeed may change in disease and represent a hyperactive/thrombotic platelet subset which can facilitate both platelet-rich thrombus formation and thrombin generation alone.

Having established the presence of three subsets of platelets upon strong activation, we wanted to understand how they were affected by cAMP signalling. First, in a screening experiment, we found that PGI$_2$ failed to fully inhibit mild agonist-induced CD62P expression on the blood platelets of 42 healthy individuals despite robust inhibition of fibrinogen binding. Further exploration with the subpopulation defining four colour assays revealed that PGI$_2$ prevented fibrinogen binding and PS exposure despite potent activation, ameliorating the generation of any procoagulant subsets. What emerged was a novel platelet population that was characterised by high CD62P expression (CD62P^{hi}/PS^{lo}/FB^{lo}). Further investigation using a separate multicolour assay for independent validation showed that this subset of platelets was also enriched in the expression of CD154 and CD63. To understand the wider physiological relevance of these findings we measured platelet-monocyte aggregates (PMA) in whole blood, as it is established to occur through CD62P-CD162 and potentially CD154-CD40. In these experiments, PMA was confirmed to be fibrinogen independent, and it was not significantly inhibited by PGI$_2$. This suggests that the resistant CD62P on the platelet surface is competent to support heterotypic cell-cell interactions. Thus, under physiological conditions of elevated cAMP, procoagulant and aggregatory subsets are diminished, yet an immunocompetent phenotype is maintained. This could represent a model for platelet monocyte aggregate formation without associated thrombotic activity.

The mechanism underpinning the ability of PGI_2 to modulate subset formation remains unclear. It is now established that the formation of PS^{hi} platelets requires a sustained increase in Ca^{2+} and subsequent mitochondrial depolarisation (Agbani and Poole, 2017). PGI_2 has been shown to regulate intracellular Ca^{2+} flux (Fung et al., 2012), which accounts for both PS exposure and integrin activation, there is a component of Ca^{2+} signalling that is resistant to PGI_2. We found that TMRE fluorescence, where a loss is associated with mitochondrial depolarisation (Choo et al., 2017), is protected by treatment with PGI_2, confirming that another component of the pathway driving the generation of procoagulant platelets is blocked by cAMP. This data also suggests that granule secretion under these conditions is independent of mitochondrial dysfunction and not wholly reliant on flux of Ca^{2+}. Previous studies have shown that cAMP-elevating agents can inhibit CD62P expression in weakly activated platelets, leading us to believe that cAMP causes global inhibition of platelet function. However, it has previously been shown that elements of Ca^{2+} in platelets are unaffected by supraphysiological concentrations of PGI_2 (Fung et al., 2012). Recently, clear differences in agonist-dependent platelet sensitivity have been shown in the presence of gradient doses of PGI_2 (Macwan et al., 2019). Indeed, in the cited study CD62P expression showed far greater resistance to PGI_2-mediated inhibition than fibrinogen-mediated aggregation in paired samples that were stimulated with only CRP-XL (Macwan et al., 2019), a finding that we are able to support and expand on using single cell analysis. In the context of our current study, CD62P resistance is not related to a difference in overall cAMP signalling in platelets as pVASP-s157 phosphorylation was elevated to the same degree in all subsets. Thus, our data, and that of others, suggests that a more nuanced mechanism must explain the inhibition of platelets by cAMP.

One caveat of non-imaging flow cytometry is that it cannot reveal the localisation of signalling molecules (Cossarizza et al., 2017). In many cells, cAMP modulates distinct aspects of cell function through the selective coupling of its signalling

complexes to specific substrates or regions within the cell (Raslan et al., 2015). However, much of the data regarding the role of cAMP in platelet function, including CD62P expression (Libersan et al., 2003), has been gained from *in vitro* studies using mimetics that act as global cAMP modulators or bypass AC, as well as pharmacological inhibitors that have off-target effects (Yan et al., 2009, Libersan et al., 2003). Previously there has been evidence of compartmentalisation of cAMP signalling (Raslan and Naseem, 2015, Raslan et al., 2015), with individual PKA isoforms targeting distinct components of activatory machinery and elements of Ca^{2+} signalling demonstrating resistance to PGI_2. Therefore, it is possible that cAMP signalling preferentially targets signalling mediators which lead to PS exposure and integrin activation, while secretory mechanisms are only partially inhibited in highly activated platelets. Thus, platelets could retain their immunomodulatory properties and continue to regulate vascular inflammation, or wound healing, despite the elevations in cAMP they experience during routine circulation, but this concept requires further study and we have only been able to hint at its existence.

Our data provides a novel glimpse into the complex regulation of platelets that occurs within the vasculature, where despite the constant barrage of inhibitory endothelial PGI_2 and nitric oxide (Mitchell et al., 2008), platelets can become activated and form thrombi. Our model may initially suggest that PGI_2 is able to fully block haemostasis, but several points must be considered. Firstly, haemostasis will often occur outside the direct effect of endothelial-derived PGI_2 (Cho and Allen, 1978). Furthermore, *in vivo*, the core and shell model of thrombus formation would promote platelet activation at the core, where PGI_2 is excluded leading to a reduction in cAMP signalling (Stalker et al., 2013). Additionally, a recent model of platelet adhesion resolved with microfluidic studies proposed that thrombus formation was initiated by the GP1b(CD42)-IX-V complex binding to vWF in conjunction with CD62P interacting with endothelial PSGL1 prior to subsequent arrest and activation via integrin outside-in signalling, GPVI and thromboxane synthesis (Coenen et al., 2017). This suggests

that the CD42 complex and CD62P may be enough to initiate haemostasis and promote tethering, a model which supports our findings of expression of CD42 and resistant CD62P in the presence of vascular inhibition.

The observation that granule secretion is resistant to PGI$_2$ may have importance in the context of cardiovascular disease. Platelet hyperactivity in several cardiovascular diseases manifests as increased circulating levels of platelet-monocyte complexes, sCD62P, sCD154 (Wang et al., 2007) and PF4 (Gresele et al., 2011), all of which are granule-dependent processes. However, it has been difficult to explain the observations in patients, since short-lived haemostatic agonists are unlikely to mimic sustained levels of activation in platelets that circulate in patients with cardiovascular diseases. Where perhaps what is happening, is that short-lived haemostatic agonists are inducing granule secretion with the majority of thrombotic activity suppressed by tonic inhibition. Furthermore, many platelet studies do not look at activation in physiological conditions, where platelets are continually bathed in PGI$_2$ and NO. Our data might suggest that PS and integrin αIIbβ3 are maintained at near basal levels by exposure to PGI$_2$ after transient platelet activation, but CD62P remains elevated where it can then mediate heterotypic cellular interactions that are important for vascular inflammation, and degranulation permits the release of soluble ligands such as sCD62P or sCD154, and the secretion of growth factors that contribute to the resolution of injury. It may be important to determine if the level of CD62P resistance or indeed the ratio of PS^{hi}/FB^{lo} and PS^{hi}/FB^{hi} subsets change in disease cohorts, as this might prove to be a valuable clinical biomarker of platelet hyperactivity. Such an approach may be particularly pertinent since many states of cardiovascular disease are associated with hyposensitivity to PGI$_2$ (Magwenzi et al., 2015, Knebel et al., 2015, Hishinuma et al., 2001).

In summary, we have identified and characterised novel platelet subsets, which reveal themselves only in the presence of both activatory and inhibitory agonists. Stimulatory conditions lead to the generation of PS^{lo}/FB^{hi}, PS^{hi}/FB^{lo} and PS^{hi}/FB^{hi}

subsets. After PGI$_2$ treatment, however, these subsets are replaced primarily by platelets expressing CD62P, which we demonstrate allows the continued interaction of platelets with monocytes.

3.8.3 Reversible platelet activation

The previous work focussed on examining platelet activation post-inhibitory stimulation, which drives a potent remodelling of the activated platelet phenotype. However, what is less well understood is the effect of inhibition post-activation. Although this has previously been explored in static systems, as opposed to systems in suspension, there is evidence of a phenotype which is predominantly remodelling of the actin cytoskeleton by endothelial inhibitors after activation (Atkinson et al., 2018, Yusuf et al., 2017). Therefore, we sought to replicate this finding in our models. The physiological relevance of this question can be justified, as, within the vasculature, there will be regions of the vascular system, likely capillary beds, that have reduced endothelial surface area and are at much lower shear and therefore produce less inhibitory PGI$_2$ and NO. Platelets will circulate through these capillary beds and return to the venous and finally arterial vasculature where they will then again be exposed to greater levels of PGI$_2$ and NO, suggesting platelets may have to respond to fluctuations in inhibitory signalling in the circulation. Therefore, we hypothesise that within the healthy controls tested here, platelets will have the capacity to reduce expression of activation markers. We applied four-parameter whole blood fluorescent flow cytometry to this question.

We adapted our previously used four-colour assay to measure fibrinogen binding, CD62P, CD63 and CD42b expression and stimulated platelets for 20 minutes prior to 2 minutes treatment with PGI$_2$, followed by fixation. Under these conditions, we found a marked reduction in expression of all markers when compared to mock treated. Critically, we found no recovery of CD42b expression, which was already

shed and could not be returned to the surface (Bodnar et al., 2002). The reduction in marker expression was most significant with transient expression at lower doses of SFLLRN. While CD42b did not change with post-inhibition, fibrinogen binding demonstrated the largest post-activation inhibition mediated reduction, suggesting that integrin $\alpha_{IIb}\beta3$ may be able to be turned back off, although this experiment requires further repeats and validation by PAC1, to confirm this observation. It would also be valuable to examine both the cAMP response after 20 minutes of stimulation and the calcium flux, both can also be performed by fluorescent flow cytometry. The granule markers CD62P and CD63 demonstrate small decreases with post-activation inhibition, whether this is recycling or shedding we cannot currently comment, although fractionation experiments could be used to determine if membrane bound receptors return to the cytoplasm, or fluorescence live cell microscopy could be used to track the movement of these receptors when stimulated with an inhibitor.

In addition to this, a further observation was made from the pVASP-s157, CD62P and CD42b assay we performed as part of the previous study. Here we were able to demonstrate that basal CD62P expression was consistently inhibited and returned to background by the addition of PGI$_2$. While not designed to examine this question initially, it was a model of addition of PGI$_2$ post (basal) stimulation, of note this was a reversion from very weak stimulation where CD62P positive cells was <20%. This may well further support the hypothesis that platelets are able to not only be prevented from activation by pre-exposure to PGI$_2$, but also have some capacity to be "switched off" with post-activation exposure to PGI$_2$, the pVASP-s157 experiments would be a valuable addition to measuring cAMP-PKA activity in cells treated with PGI$_2$ post stimulation. Although only a small exploration of this hypothesis, it suggests that there is some flexibility within platelets to reverse or diminish their activatory state post-stimulation. This provides a novel insight into how thrombi may be resolved once haemostasis has occurred, where weakly or transiently activated platelets at the

margin of the thrombus (Stalker et al., 2013) may return to circulation, or how platelets in the vasculature may respond to fluctuations in tonic inhibition.

Chapter 4
NLRP3 inflammasome activation and expression

4.1 INTRODUCTION

The inflammasomes are a broad group of large multimeric protein complexes with enzymatic activity which are related in their ability to drive an inflammatory response (Schroder and Tschopp, 2010). NLRP3 is a relatively unique inflammasome as it appears to play a role in many diseases, notably in several sterile inflammatory diseases including gout (Martinon et al., 2006), systemic lupus erythematosus (SLE) (Kahlenberg et al., 2013), cardiovascular disease (Yang et al., 2017b) and rheumatoid arthritis (Mathews et al., 2014). NLRP3 has been shown *in vitro* to respond to many agonists including the bacterial toxin nigericin, bacterial membrane component LPS, cellular stress signal ATP, gout derived monosodium urate crystals, atherosclerotic plaque cholesterol crystals, oxLDL and amyloid-β protein (Sheedy et al., 2013, Agostini et al., 2004). NLRP3 is suggested to respond to the wide variety of ligands as they are assumed to share common signalling node, where they converge on a regulator of activity, which is proposed to be mitochondrial ROS production (Zhou et al., 2011). While there is literature demonstrating other cells types respond to oxLDL and this drives NLRP3 activity, and that platelets respond to oxLDL which drives other pathways and that platelet NLRP3 can be activated by other agonists, there has been no exploration yet surrounding oxLDL and NLRP3 platelet activity. Here we attempt to characterise the platelet NLRP3 inflammasome and explore if oxLDL can drive inflammatory platelet activity mediated by this complex.

4.2 AIMS OF CHAPTER

- To measure platelet caspase-1 cleavage through the FLICA dye and fluorescent flow cytometry

- To assess expression of NLRP3 inflammasome components by biochemical analysis

4.3 FLUORESCENT MEASUREMENT OF CASPASE-1 ACTIVITY

Caspase-1 cleavage and subsequent activity can be used as a direct measure of NLRP3 inflammasome activity. This can be measured by immunoblotting for cleaved caspase-1 (P20/P10 subunits) (Lin et al., 2015) or by proprietary methods which rely on the specificity of caspases to unique amino acid sequences. Caspase-1 primarily targets, and has a high specificity for, the amino acid YVAD motif (Garcia-Calvo et al., 1998).

The assay employed here uses a cell permeable construct of the YVAD motif sandwiched between a fluorophore, FAM or a far-red 660nm dye and a FMK which forms a covalent bond with the enzyme once within close enough proximity (Bedner et al., 2000). This assay has been termed as fluorochrome-labelled inhibitors of caspases (FLICA) and for caspase-1 are based on the *fluorophore*-YVAD-FMK design. Therefore, FLICA assays allow specific activated caspases to be targeted, bound to covalently, and tagged with a fluorescent probe.

Here, the FLICA assay was set up to detect caspase-1 cleavage in human and murine washed platelets to assess their NLRP3 inflammasome activity in a high throughput and quantitative manner.

4.3.1 Calcium is required for detection of caspase-1 cleavage

This assay was established using washed platelets to allow activation of platelets in an otherwise cell and plasma free system, as initial attempts in whole blood appeared to be not compatible with the FLICA dye (data not shown). Experiments using washed platelets are normally performed in modified Tyrode's buffer, which does not contain calcium. We first examined whether the inclusion of extracellular calcium was required to detect caspase-1 cleavage. At the time, this was based on the single previous report of detection of caspase-1 cleavage by FLICA in platelets in a complete media, M199, which included extracellular calcium (Hottz et al., 2013).

Calcium was also assumed to be required for NLRP3 activation due to previous biochemical studies that determined that the influx of calcium from extracellular pools was vital for NLRP3 inflammasome activity and therefore caspase-1 cleavage (Murakami et al., 2012).

In a single experiment, we were able to reproduce these previous findings and demonstrate a significant increase in fluorescent signal. Washed platelets were incubated with nigericin (20 µM) in the presence or absence of extracellular calcium (2 mM). In the absence of extracellular calcium nigericin failed to increase FLICA signal above basal (Figure 45). In contrast the presence of Ca^{2+} led to a significant increase in signal (p=<0.005). As a result, all subsequent assays were performed with the inclusion of calcium (2 mM).
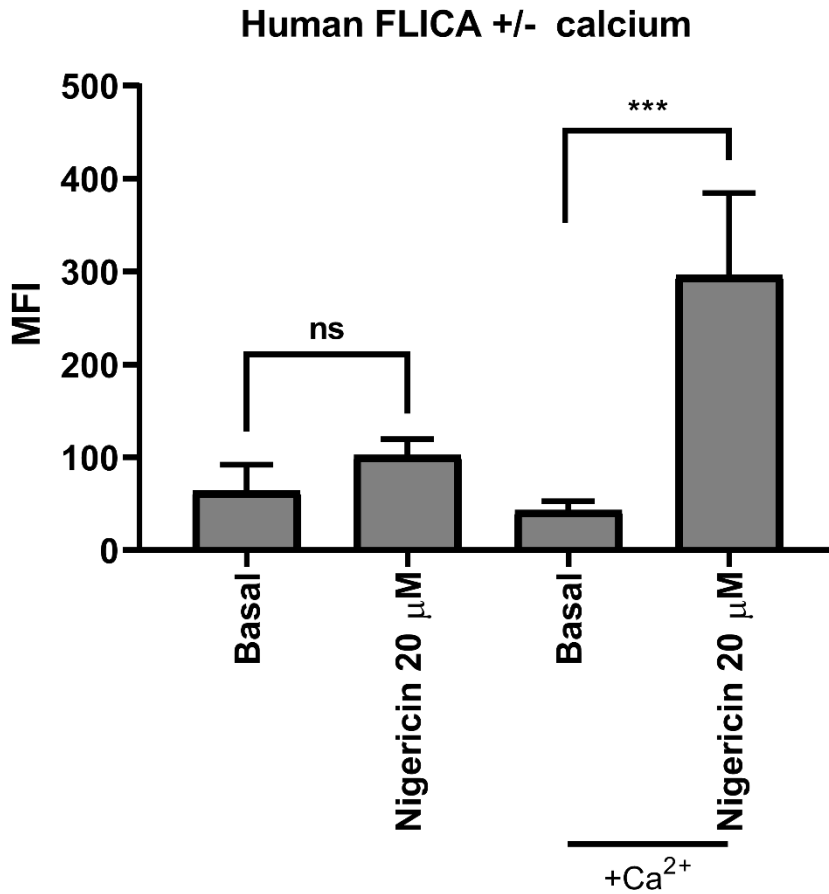
Figure 45. FLICA in human washed platelets +/- calcium. Human washed
platelets ($2x10^6$/well) in the presence and absence of $CaCl_2$ (2 mM) treated with
or without nigericin (20 µM) for 30 minutes then incubated with 1x FLICA-green
for 60 minutes followed by fixing, washing and acquisition. (One-way ANOVA
vs. relative basal, ***<0.005, error shown as standard deviation, n=3)

4.3.2 FLICA titrations and optimal conditions

As the basis for this assay is a cell-permeant fluorescent dye, we performed titrations to determine optimal dose and incubation time. Each dilution and time point were compared with a basal sample at a matched concentration and time, this comparison allows a comment on the sensitivity of each assay condition as oppose to asking simply which dye condition is brightest, which often leads to excessive background binding and therefore anomalously high basal signal. Calculating fold over control allows the condition with the highest fold increase, and therefore optimal window for detection of changes, to be selected.

Data are presented as fold increase over relative basal (same concentration/timepoint) to account for the additional background signal that more dye will induce. All 60-minute timepoints induced only a 2-fold increase, while at 40 minutes the increases ranged from 2 to 4-fold. 40 minutes incubation with 1x dye presented a fold increase of 4 over relative control (Figure 46). Therefore, we determined that 1x dye, or 5 µM, incubated for 40 minutes post stimulation then followed by fixation provided the optimal window for signal to be measured.

FLICA dye dose and time
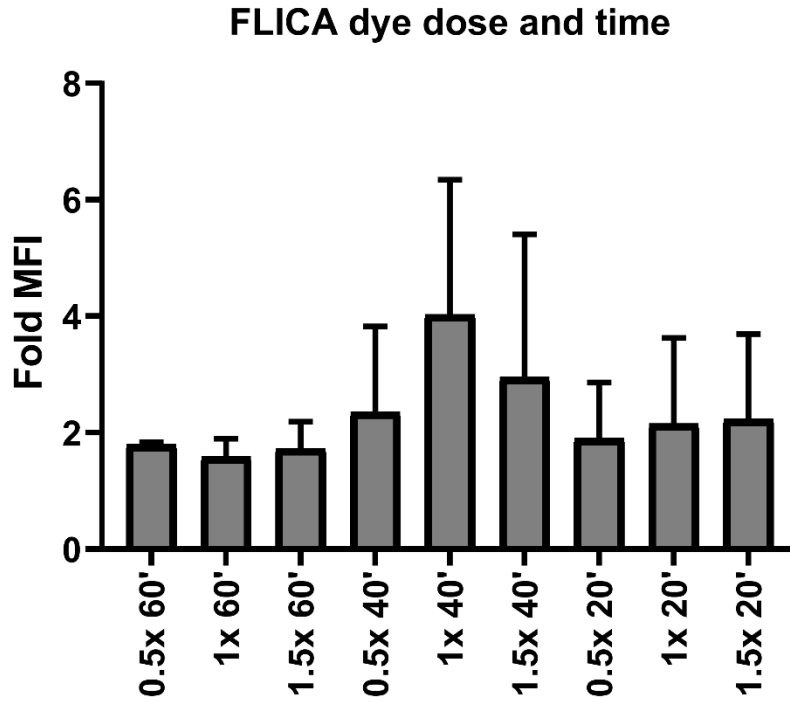
Figure 46. FLICA in human washed platelets at a range of dye doses and incubation times. Human washed platelets ($2x10^6$/well) + 2 mM $CaCl_2$ treated with or without nigericin 5 µM for 15 minutes then incubated with designated dose of FLICA-green for designated time followed by fix, wash and acquisition. (error shown as standard deviation, n=2-5)

Beyond optimal dye dose and incubation time, we also optimised the conditions for appropriate fixation and washing of the samples. Fixation can both improve adherence and stability of a probe or conversely mask epitopes and diminish signal. Washing samples should generally improve signal: noise ratio, however in the case of weakly bound probes positive signal may also be lost. Therefore, we confirmed optimal conditions for this assay.

First, we compared three different fixation conditions; fixed and washed, unfixed and washed, unfixed then washed and fixed. In each instance we compared basal with a dose response of nigericin (2, 5 and 10 µM) and there was a dose dependent increase in signal in all conditions. Comparing the three conditions at maximal treatment (nigericin 10 µM) the MFI values were 6364.8, 4771.5 and 4133.6 for fixed/washed, unfixed/washed and unfixed/washed/fixed respectively. There was a reduced basal signal when washing pre-fix 824.8 but not post-fix 1237.7, suggesting that early fixation does drive some increase in background signal, however the increased retention of positive signal outweighed this caveat. From this we determined that fixation prior to washing provided the largest signal (Figure 47). Fixing of the samples has the additional advantage of providing a distinct halt point in time course experiments.

Secondly, we compared fixed and washed platelets with unwashed platelets. Here we demonstrated that washing after fixation significantly reduced excess binding of the dye and increases resolution and sensitivity of the assay. After washing the increase in MFI from basal to nigericin treatment (10 µM), there was a 2.6-fold increase, compared to 1.6-fold increase without washing (Figure 47). Therefore, we determined that fixed and then washed cells are optimal for signal resolution and sensitivity in the FLICA assay when measured by flow cytometry.
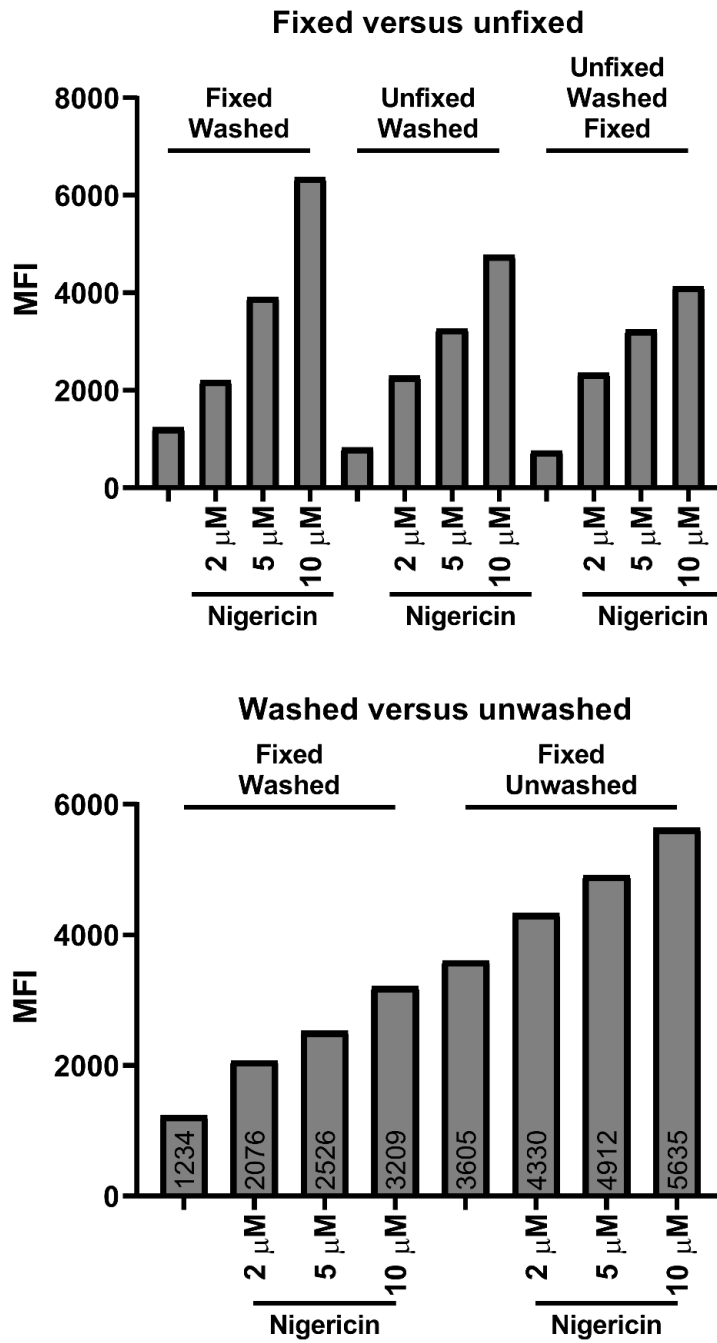
Figure 47. FLICA fixed versus unfixed and washed versus unwashed. Human washed platelets (2 x 10^{6}/well) + 2 mM CaCl$_2$ treated with or without nigericin (2 – 10 μM) for 20 minutes followed by 1x FLICA-green for 40 minutes followed by varied combinations of fixation and washing protocols followed by acquisition. (n=1)

4.3.3 Nigericin dose response

Nigericin is a potassium ionophore (Perregaux and Gabel, 1994, Estradao et al., 1967), and is a known canonical activator of the NLRP3 inflammasome (Tang et al., 2017). It was used as a positive control ligand in all FLICA experiments. To validate assay sensitivity and determine the optimal concentrations of nigericin a dose response experiment was performed using concentrations surrounding those commonly cited in the literature (Liu et al., 2017).

Incubation of platelets with nigericin (2, 5 and 10 µM) led to a concentration dependent increase in FLICA signal. While there was a response at all doses of nigericin, it was significantly different to basal (987.4±61) at 5 µM (3531.2±1495, $p<0.01$) and 10 µM (4445.5±1972, $p<0.005$), but not at 2 µM (2396±1137) (Figure 48). This data further demonstrated the natural variation within the assay, assumed to be due to variation across a normal cohort of healthy donors, mixed in age, gender, ethnicity, BMI and other lifestyle factors. This variation suggests that within a normal population, platelets are primed for NLRP3 inflammasome activity at varying states and therefore demonstrates a wide variety of responses. Nevertheless, it is important to note that while all donors and treatments do demonstrate an increase over basal, it is solely the size of increase which is variable.
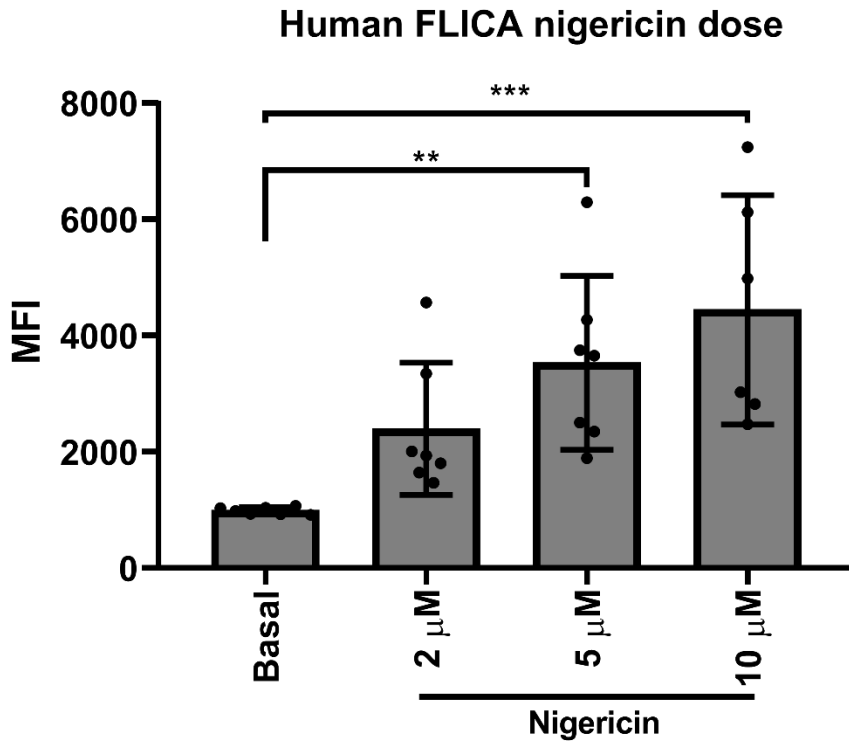
Figure 48. FLICA in human washed platelets, nigericin dose response. Human washed platelets (2 x 10⁶/well) + 2 mM CaCl₂ treated with or without nigericin (2 – 10 µM) for 20 minutes followed by 1x FLICA-green for 40 minutes followed by fix, wash, wash and acquisition. (One-way ANOVA vs. basal, **<0.01 and ***<0.005, error shown as standard deviation, n=7)

4.3.4 OxLDL and caspase-1 cleavage

Typically, NLRP3 inflammasome activity is considered in the context of various diseases, both sterile and unsterile, with priming and activation driven by DAMPs and PAMPs dependent on the disease in question. We have previously published that platelets respond to oxLDL, a DAMP which is known to be significantly upregulated in cardiovascular disease (Berger et al., 2019a, Berger et al., 2019b, Magwenzi et al., 2015, Wraith et al., 2013). Furthermore, oxLDL has been shown to drive NLRP3 inflammasome activity in other cells types including macrophages (Liu et al., 2014). Hence the aims of this section were to examine if oxLDL could drive caspase-1 cleavage alone or potentiate caspase-1 cleavage following stimulation with nigericin at a low dose (2 µM), since we previously showed a low dose induces a consistent but small increase over basal which provides a suitable window to observe potentiation of signal (Figure 48).

Basal caspase-1 cleavage was demonstrated to be low (968.0±63), and in response to nigericin (2 µM) there was a small but statistically non-significant increase in signal (2566.4±1346). Incubation of platelets with oxLDL and nLDL did not cause a significant increase in FLICA response above basal (724.9±31 and 845.4±32 respectively). However, pre-treatment of platelets with oxLDL (50 µg/mL) for 10 minutes, but not nLDL, significantly potentiated nigericin (2 µM) induced caspase-1 cleavage from 8116.9±7092 vs. 1399.9±364 (p<0.01) (Figure 49). Interestingly we found that only 3 of 5 platelet donors were sensitive to the effects of oxLDL.

Given the variability of the response, we repeated these experiments with different batches of ox/nLDL, but also employed a distinct FLICA-red dye. Here we were able to demonstrate findings consistent with those previously observed, nigericin (2 µM) induced a significant increase in MFI over basal (12,588.8±1513 and 3133.0±1309 respectively, p<0.001), while oxLDL significantly potentiated the response induced by nigericin (2 µM) (31,941.1±5139, p<0.0001). Vitally nLDL (12,194.2±3048) was no

different to nigericin (2 μM) (12,588.8±1513). We included an additional condition of maximal dose nigericin (10 μM) and found the level of caspase-1 cleavage induced by this strong stimulus was substantially exceeded by nigericin (2 μM) when pre-treated with oxLDL (50 μg/mL) (18,910.7±4606 and 31,941.1±5139 respectively) (Figure 49). Here we again demonstrate a significant potentiation of caspase-1 cleavage induced by oxLDL treatment, confirming our prior observations with different donors, LDL preparations and dye conjugate.

This data also suggests that FLICA-red is potentially more sensitive than FLICA-green, although the same trends were observed in both assays. The significant difference between basal and nigericin (2 μM) observed in FLICA-red but not green is indicative of this improvement in assay sensitivity.
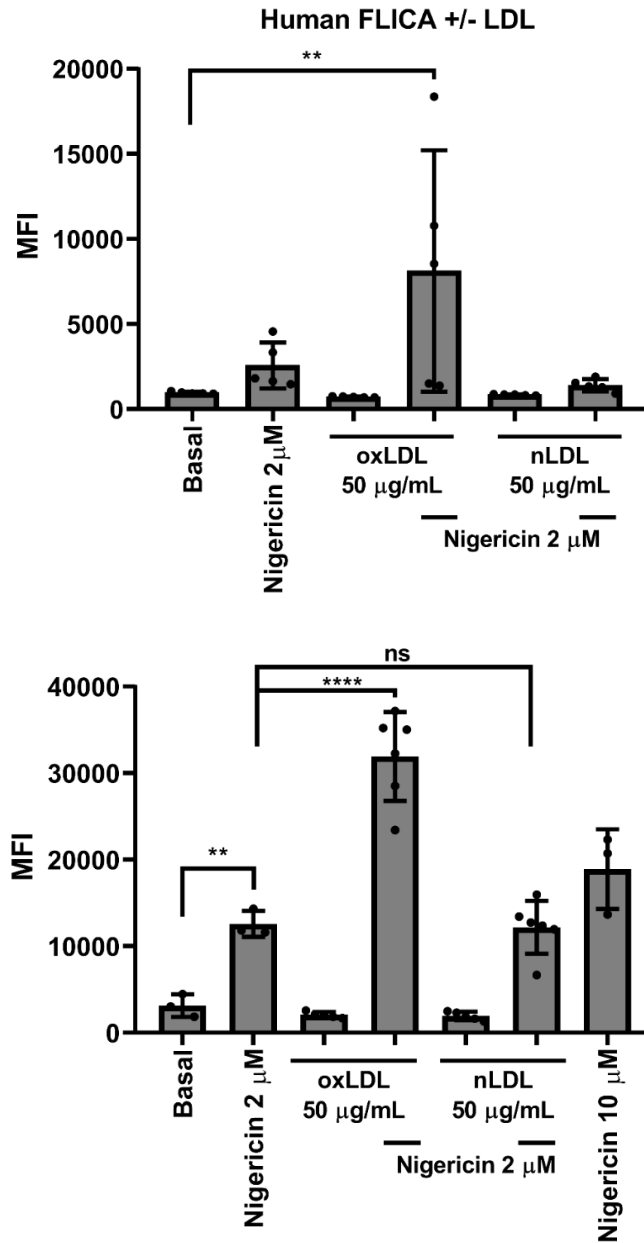
Figure 49. LDL treatment of human washed platelets. Human washed platelets (2×10^6/well) + 2 mM $CaCl_2$ treated with or without ox/nLDL (50 µg/mL) for 10 minutes, then incubated with or without nigericin (2 µM) for 20 minutes followed by 1x FLICA-green (upper) or 1x FLICA-red (lower) for 40 minutes followed by fix, wash, wash and acquisition. (One-way ANOVA vs. basal, ns=non-significant, **<0.01, ****<0.0001, error shown as standard deviation; Green n=5; Red n=3 with LDL conditions in 2 duplicates with different LDL preparations)

4.3.5 oxLDL potentiation, CD36 inhibitors and ROS scavenger screen

Following on from our previous key observation that oxLDL primes the NLRP3 inflammasome for activation in washed platelets, we sought to understand the pathway through which this process may occur. Here we applied several inhibitors and scavengers/chelators to investigate this pathway. We primarily targeted ROS, which oxLDL is known to induce in platelets (Berger et al., 2019b), calcium which our previous observations suggested was vital and then the primary platelet oxLDL receptor CD36 and downstream signalling apparatus (Wraith et al., 2013). N-acetyl-cysteine (NAC) was used as a ROS scavenger, BAPTA-AM as an intracellular calcium chelator, EDTA as an extracellular calcium chelator, FA6-152 as a CD36 blocking antibody with control IgG, BAY61 to block Syk, PP2 to block Src family kinases, PP3 as an analogue control and a DMSO vehicle control.

Treatment with nigericin (2 µM) increased FLICA MFI to 3568.4±1290 which was potentiated by oxLDL to 29,287.4±4980, this was again a large increase over nigericin alone or nigericin pre-treated with nLDL. We were then able to demonstrate that NLRP3 inflammasome activation and potentially oxLDL priming were ablated completely by the addition of the ROS scavenger NAC, as was the nigericin and nLDL control. In the oxLDL experiments, FLICA MFI was reduced from 29,287.4±4980 to 1060.75±313 ($p < 0.0001$) by the presence of the antioxidant NAC (Figure 50). We again reiterated our previous observation of the requirement of calcium for caspase-1 cleavage in platelets with the chelators BAPTA-AM (intracellular) and EDTA (extracellular), these reduced FLICA MFI from 29,287.4±4980 (oxLDL/nigericin) to 2372.7 and 2474.8 respectively. Finally, blockade of CD36, Src family kinases or Syk had no effect (Figure 50). This suggests that other receptors may be involved. While we were unable to explore these here, there is literature evidence that oxLDL can drive NLRP3 through CD36/TLR4/6 complexes in other cells, and evidence that oxLDL can ligate CD36/TLR2/TLR6 on platelets driving hyperactivity (Stewart et al., 2010, Biswas et al., 2017).
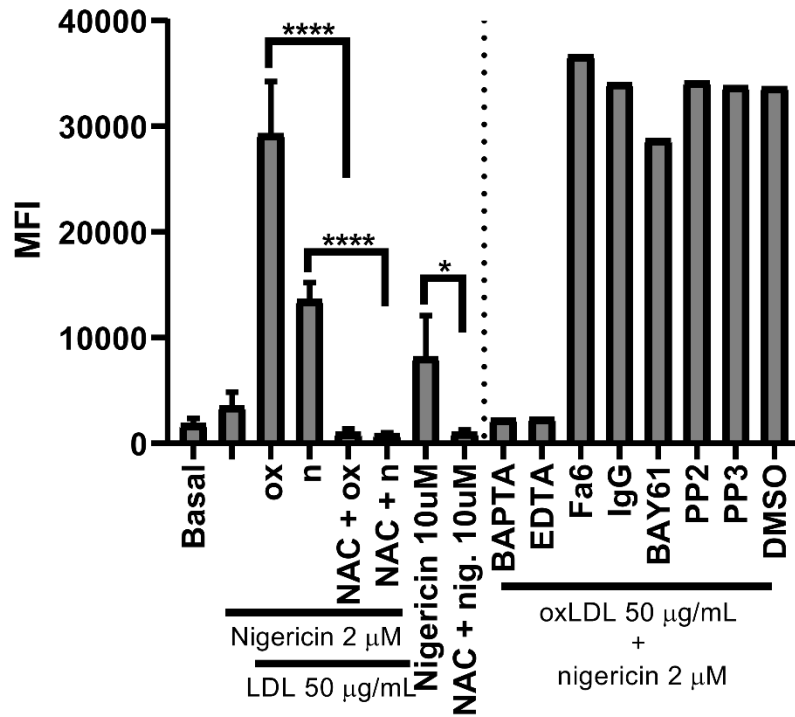
Figure 50. FLICA-red in human washed platelets +/- LDL, scavengers, chelators and CD36 signalling inhibitors. Human washed platelets (2 x 10^6/well) + 2 mM CaCl$_2$ treated with or without designated inhibitors (NAC 5 mM, BAPTA 20 µM, EDTA 10 mM, Fa6/IgG 5 µg/mL, BAY61 5 µM, PP2/PP3 20 µM, DMSO 0.1% (v/v)) for 20 minutes, then incubated with or without ox/nLDL (50 µg/mL) for 10 minutes then nigericin (2 – 10 µM) for 20 minutes followed by 1x FLICA-red for 40 minutes followed by fix, wash, wash and acquisition. (One-way ANOVA vs. inhibited sample, *<0.05 and ****<0.0001, error shown as standard deviation, n=1(CD36 signalosome), 3(all other measurements))

4.3.6 NLRP3 inhibition by MCC950

While previous results have highlighted a novel role for oxLDL in the potentiation of NLRP3 inflammasome activity measured by caspase-1 cleavage, the FLICA assay has lacked a negative control peptide or a control to specifically target and block NLRP3. To measure this we sought to apply the highly specific compound inhibitor of NLRP3, MCC950 (Coll et al., 2015). This inhibitor has been widely applied both *in vitro* and *in vivo* (Coll et al., 2019, van der Heijden et al., 2017) and has also been used in platelets to some effect (Vogel et al., 2018a). We stimulated washed platelets with a mid-range dose of nigericin (5 µM) and compared this against a range of doses of MCC950 pre-treated samples (Figure 51). On stimulation with nigericin (5 µM) MFI increased to 1281±1562 from 168.8±51 at basal, although there was large error in these experiments primarily to a very strong responder. When treated with maximal dose of MCC950 (10 µM) MFI remained comparable to nigericin alone at 603±412 due to the error (Figure 51). We were not able to demonstrate any significant differences in treated samples, however the variability in the nigericin alone treated samples results in it not being significantly different to the basal condition (which mimics 100% inhibited) either, a lower dose of nigericin was used here to prevent there being excessive activation preventing the inhibitor functioning, however repetition with a higher dose of nigericin may provide a larger window of observation. In order to pursue that possibility, this was later repeated on oxLDL potentiated samples where the window for inhibition considerably exceeds any nigericin alone treatments (Figure 55, Figure 56). Nevertheless, there are not any significant trends of inhibition emerging, while the literature suggests this inhibitor has a high efficacy (Coll et al., 2015).
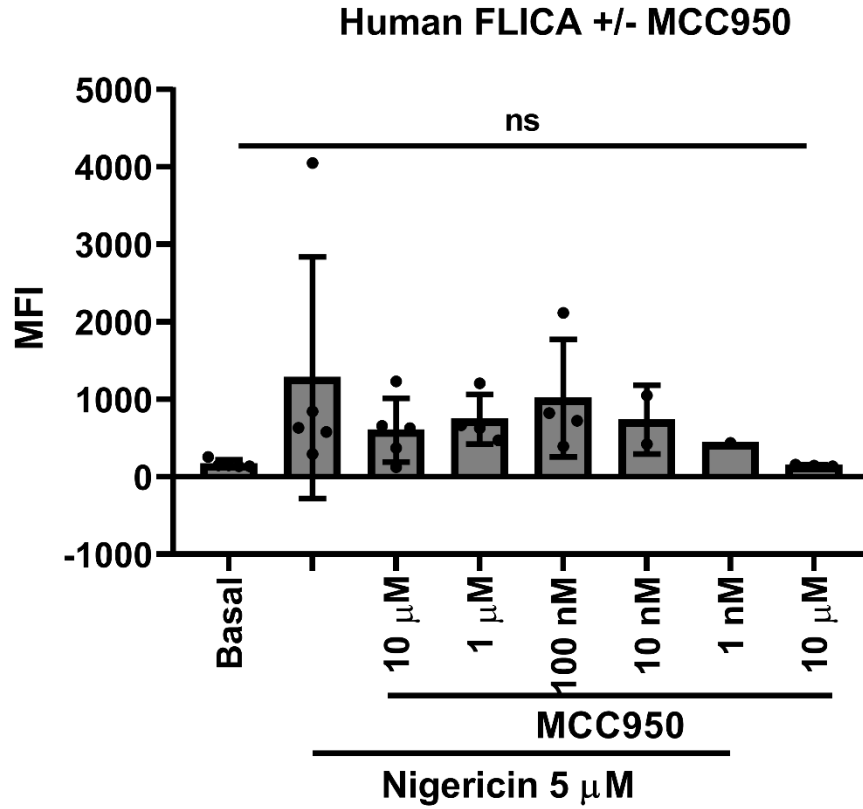
Figure 51. FLICA-green in human washed platelets +/- MCC950. Human washed platelets (2×10^6/well) + 2 mM $CaCl_2$ treated with or without MCC950 (1 nM – 10 µM) for 30 minutes, then incubated with nigericin (5 µM) for 20 minutes followed by 1x FLICA-green for 40 minutes followed by fix, wash, wash and acquisition. (One-way ANOVA vs. basal, ns=non-significant, error shown as standard deviation, n=1-5)

4.3.7 Correlation of FLICA signal with CD62P

To further understand mechanist elements of what may be occurring within the platelets concurrent to caspase-1 cleavage, we developed an assay to simultaneously measure both FLICA-green and a marker of α-granule secretion (CD62P-PE) against a dose response of nigericin (1 – 10 µM) and a low/high dose of the thrombin mimetic and PAR1 peptide agonist SFLLRN (1 and 10 µM). These two agonists act as positive controls for each marker respectively and allow a comparison of how each marker responds to a specific agonist targeted against the other pathway.

Incubation of platelets with nigericin (0 – 10 µM) led to a concentration dependent increase in caspase-1 cleavage. However, this was associated with increased expression of CD62P on the platelet surface, suggesting the platelets are activated and have undergone degranulation (Figure 52). Although this cannot be the exclusive conclusion, as loss of membrane stability would allow antibody entry into the platelet, similar to a detergent permeabilisation step, and therefore intracellular staining of pools of CD62P would be detected. While the expression of CD62P at maximal dose of nigericin (10 µM) (28,043) was similar only to low dose SFLLRN (1 µM) (32,094.7), it was increased over basal (784.4). Furthermore, SFLLRN (10 µM) (4216.3) was shown to induce caspase-1 cleavage to a similar level compared to low dose nigericin (2 µM) (3922.1) over basal (1329.4) (Figure 52).

We also explored if nigericin is able to induce platelet aggregation by LTA, as the prior indication was that it did possibly drive platelet activation. However, nigericin did not induce aggregation up to 15 minutes, only a linear decrease in turbidity, potentially agglomeration or platelet death (Figure 53). Notably there was no shape change or aggregates in the nigericin treated cuvette (19%) and tirofiban an inhibitor of the integrin $\alpha_{IIb}\beta3$, did not attenuate the effect of nigericin (22%) suggesting it is not typical platelet aggregation and is independent of any fibrinogen: integrin

interactions. In support of this inducing platelet death, samples treated with nigericin analysed by flow cytometry also consistently demonstrated a reduced concentration of cells when compared with basal despite all tubes being initially loaded with 2×10^6 platelets (data not shown).
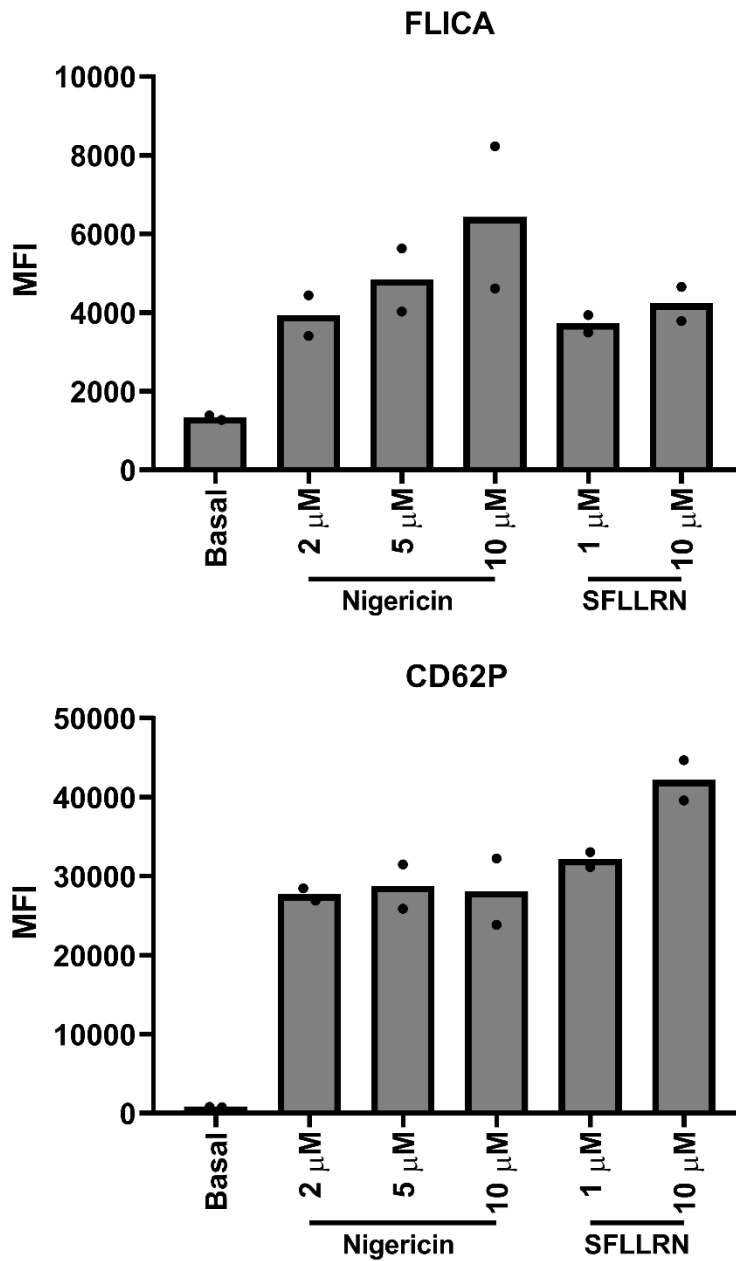
FLICA

CD62P

Figure 52. Correlation of FLICA-green binding with platelet activation. Human washed platelets (2×10^6/well) + 2 mM $CaCl_2$ incubated with nigericin (1 – 10 μM) or SFLLRN (1 or 10 μM) for 20 minutes followed by co-staining with 1x FLICA-green and CD62P-PE for 40 minutes followed by fix, wash, wash and acquisition. (n=2)
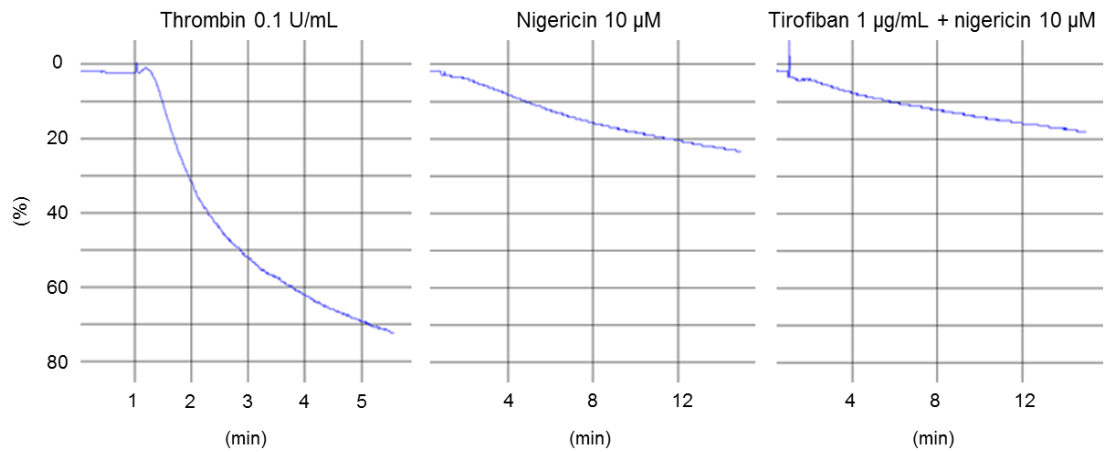
Figure 53. Nigericin induces linear clearance of platelet solution that is aggregation independent. Human washed platelets (2.5×10^8/mL) were stimulated with 0.1U/mL or 10 μM nigericin +/- 1 μg/mL tirofiban and trace was observed for aggregation for up to 15 minutes by light transmission aggregometry. (Thrombin alone and nigericin alone are representative of n=3)

4.3.8 Transgenic murine caspase cleavage

Our previous observations suggested a wide variation across healthy human donors with respect to caspase-1 activation. Having also demonstrated that oxLDL can potentiate this response, we sought to assess if basal activity changed with cardiovascular disease, where oxLDL has been shown to be increased (Ramos-Arellano et al., 2014). To do this we translated the FLICA assay into a murine model to allow further exploration with genetically modified or diet induced models of obesity. We first repeated our previous experiment, to demonstrate extracellular calcium was required for the FLICA assay to detect caspase-1 cleavage in murine samples. Calcium was reconstituted to 2.5 mM, to mirror the calcium concentrations found within murine blood (Otto et al., 2016). This basic question was first explored as it fulfils two early questions, namely; does the assay translate to murine models, and is the mechanism conserved with human platelets, *i.e.,* calcium dependent. Here we were able to reiterate our previous findings from humans in a murine model and confirm that calcium is a requirement for murine platelet caspase-1 cleavage (Figure 54).

Due to the variation in response to nigericin we saw across the normal human population, we hypothesised this could be a phenotype driven by lifestyle and environmental changes which may be commonly observed within a normal cohort of individuals. To explore this question, we tested this theory in wild type C57/Bl6 and ApoE$^{-/-}$ murine platelets. ApoE$^{-/-}$ models are known to progress to early atherosclerosis and demonstrate a strong phenotype of vascular inflammation on chow diet (Getz and Reardon, 2006). Wild type (WT) mice alone showed an increase over basal (318.3) when treated with nigericin (5 µM) (1344.8) but not with ATP (5 mM) (229.7). Basal caspase-1 cleavage was not different between the two groups and unexpectedly when stimulated with a mid-dose of nigericin (5 µM) the C57/Bl6 platelets demonstrated a greater caspase-1 cleavage than the platelets from the ApoE$^{-/-}$ animals (1344.8 compared to 944.2). We also stimulated with ATP, which is

another canonical stimulator of NLRP3 activity, and this showed no increase in MFI above basal at a maximal dose (Figure 54). Therefore, assuming parallels between murine models of atherosclerosis and human cardiovascular disease, this is not regulating NLRP3 activity of platelets in these models and suggests that factors beyond hyperlipidaemia must be inducing the natural variation.

Murine FLICA +/- calcium

FLICA murine KO
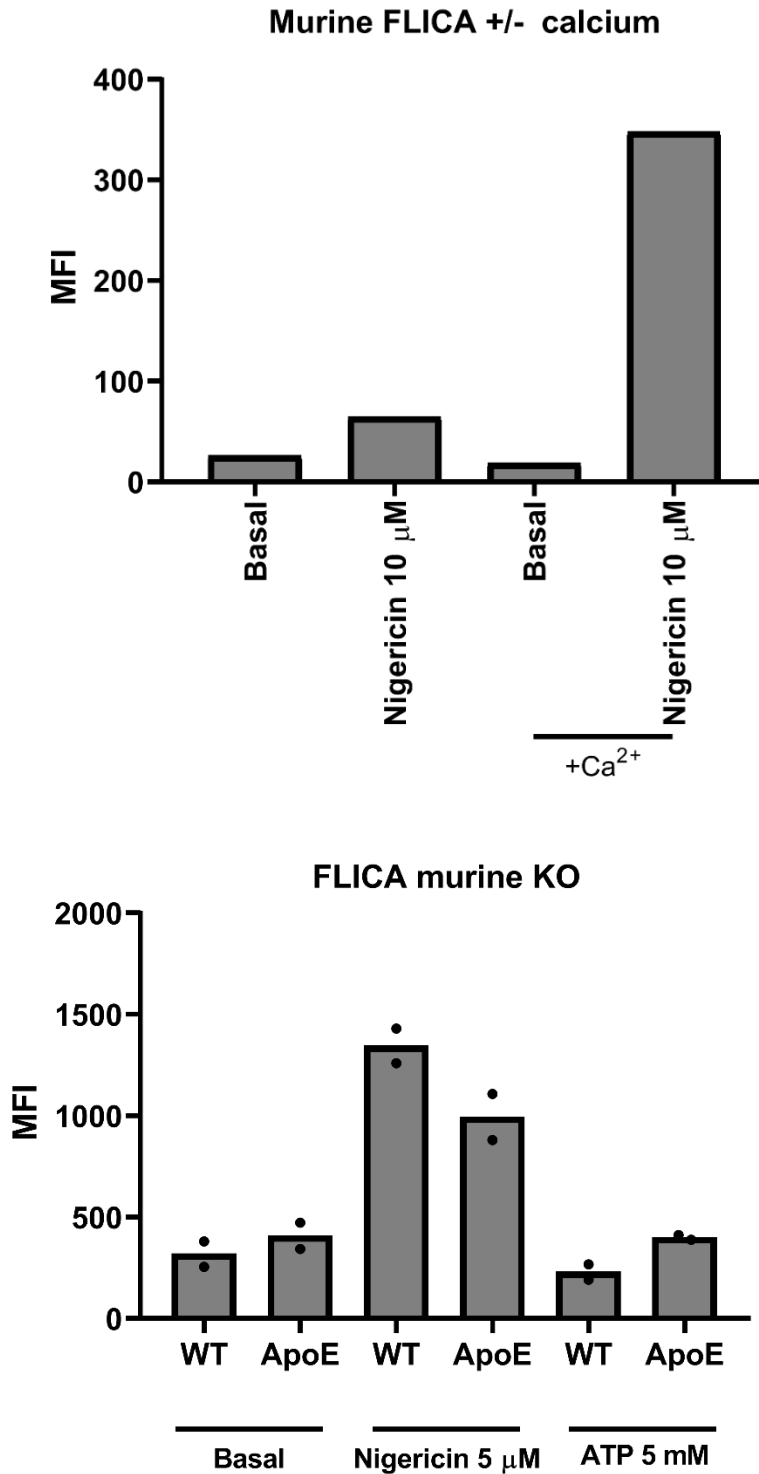
Figure 54. FLICA in murine washed platelets +/- calcium. (Upper) Murine washed platelets (2x10^6/well) +/- 2.5 mM CaCl$_2$ treated with or without nigericin 10 µM for 15 minutes then incubated with 1x FLICA-green for 60 minutes followed by fix, wash and acquisition (n=1). (Lower) As prior but cells were treated with or without nigericin 5 µM or ATP 5 mM for 15 minutes. (n=2)

4.3.9 Specificity and validation of the FLICA assay

Although we had made several novel and extremely reproducible observations including; (i) oxLDL is able to significantly potentiate caspase-1 cleavage, (ii) the requirement for ROS and (iii) requirement for extracellular calcium for caspase-1 cleavage in platelets, a key inhibitor of NLRP3, MCC950 (Coll et al., 2015), was unable to this block signal. This led to several concerns of the specificity of the FLICA dye, as without a negative control the signal could not be confirmed as a true marker of caspase-1 cleavage. This was further supported by literature that has previously demonstrated that FLICA will bind with a low specificity to apoptotic cells and cannot be outcompeted by unlabelled peptide controls, although these studies were not performed in platelets (Pozarowski et al., 2003, Darzynkiewicz and Pozarowski, 2007). A series of experiments were performed to explore the specificity of the dye and events which occur concurrently to FLICA dye binding in platelets.

Using mirrored conditions across four assays we explored other events occurring simultaneously to caspase-1 cleavage. The assays applied included; (i) mitoSOX to detect mitochondrial superoxide, (ii) Annexin V binding to detect apoptosis or coagulant platelet formation, (iii) TMRE to measure mitochondrial polarisation and formation of mitochondrial pores, and (iv) FLICA-red. MitoSOX at basal gave an MFI of 486 and when treated with nigericin (2 µM) alone or with oxLDL (50 µg/mL) this increased to 1962.6 and 1534.3 respectively. The positive control of antimycin A (100 µM) (1188.9) surprisingly produced less mitochondrial superoxide than nigericin alone. Annexin V binding at basal was low (1011) and when treated with nigericin (2 µM) alone or with oxLDL (50 µg/mL) this increased to 4680.1 and 4161.1 respectively, the positive control of SFLLRN/CRP-XL (20 µM/10 µg/mL) was comparable at 4014.2. TMRE binding at basal was bright (1859.1) suggesting normally polarised mitochondria, when treated with nigericin (2 µM) alone or with oxLDL (50 µg/mL) this decreased to 357.7 and 407.7 respectively. FLICA bound as previously demonstrated, with low basal, a mild increase with low dose nigericin (2

μM) and significant potentiation with oxLDL (50 μg/mL) from 10,335.3 to 35,278.9 respectively. The inhibitor MCC950 (1000 nM) did not drive a large reduction in the signal when cleavage was induced with nigericin and oxLDL together (31,787.3) (Figure 55). Through comparisons across each assay, we were able to determine that concurrent to caspase-1 cleavage detected by the FLICA-red assay, mitochondrial superoxide is significantly increased, PS is exposed on the outer leaflet of the phospholipid membrane and the mitochondria are depolarised (Figure 55). These are many hallmarks of apoptotic cells and suggests that the FLICA-red assay may be binding non-specifically to apoptotic platelets – potentiated by oxLDL and driven by nigericin.

To further understand if the binding of FLICA-red mirrored PS exposure we tested these two parameters with a series of inhibitors; basal, nigericin alone, nigericin pre-treated with MCC950, glyburide (Lamkanfi et al., 2009), mitoTEMPO, NAC, EDTA or vehicle control. As expected nigericin (2 μM) increased FLICA-red binding (2402.0 to 5899.5), and consistent with previous data was blocked by the ROS scavenger NAC (2291.4), and calcium chelator EDTA (2791.9) (Figure 56). In contrast, NLRP3 inhibitors MCC950, the ATP channel inhibitor glyburide and the mitochondrial superoxide scavenger mitoTEMPO were without effect and all showed comparable values to nigericin alone (5795.5, 9772.0 and 7102.5 respectively). Importantly, these effects were almost identical to PS exposure measured by annexin V binding, where nigericin (2 μM) induced a significant increase in surface PS over basal (1432.9 to 14,698.1) and only NAC and EDTA reduced signal (2369.0 and 255.8 respectively) (Figure 56). In conjunction, this may suggest that this treatment is killing the platelets, but in a calcium and ROS dependent manner, which suggests mitochondria may be the common node here. Finally, the specificity of the FLICA-dye was validated with z-YVAD-FMK, an identical peptide to FLICA's FAM-YVAD-FMK, but without a fluorophore conjugate (Pozarowski et al., 2003). Using concentrations ranging from

50x less to 200-fold excess no demonstrable competitive inhibition of FLICA-green's binding to nigericin stimulated platelets across two donors (Figure 57).

Taken together, we used two different dyes and a range of inhibitors that have been shown to modulate the activity of the NLRP3 inflammasome and were unable to see any change in response. While the numbers of experiments are not high, the data suggested that the signal measured by FLICA may indeed be non-specific to apoptotic cells and so further experiments in this system were not pursued.
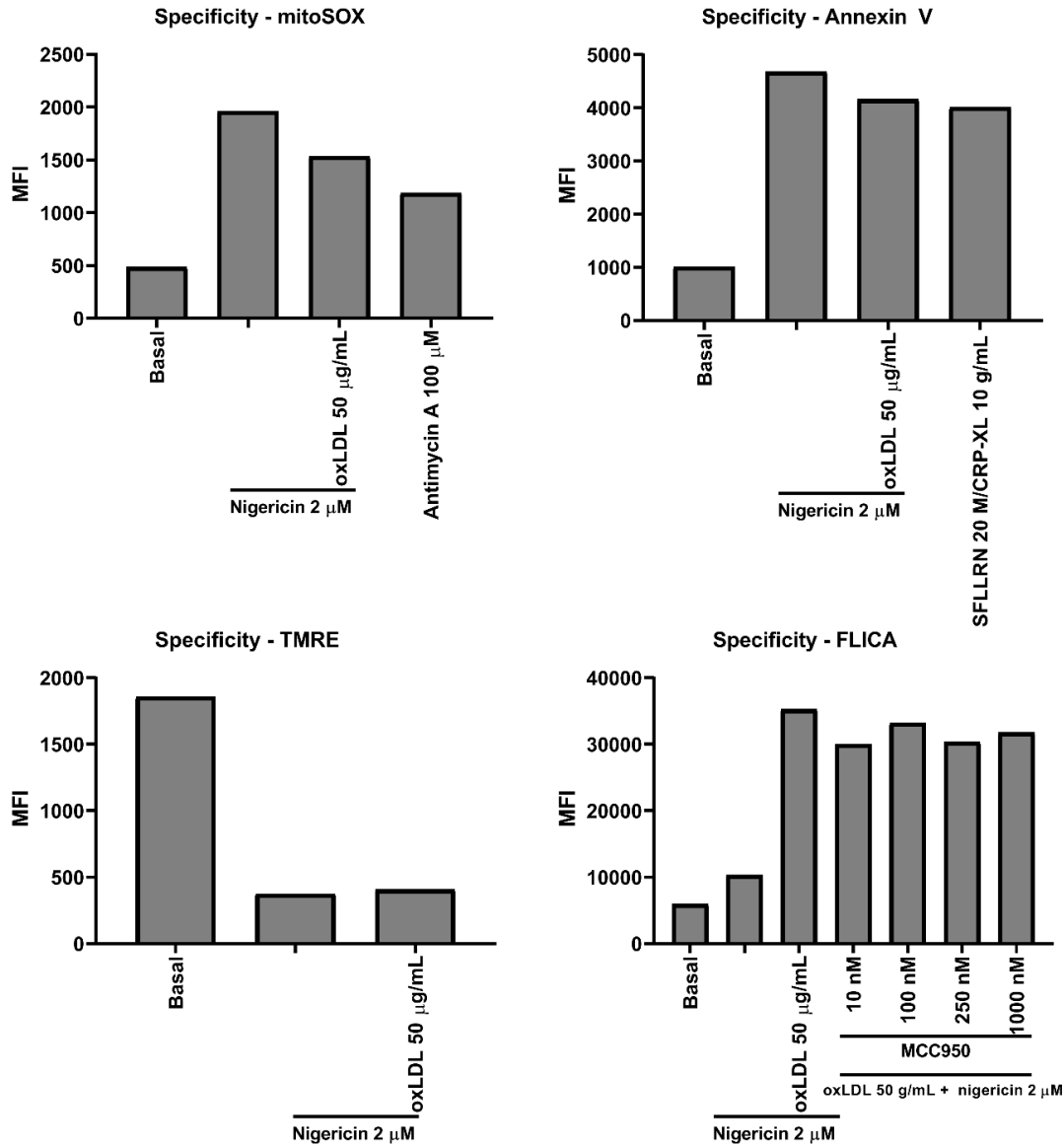
Figure 55. Specificity of the FLICA reagent to caspase-1 cleavage, marker screen. Four assays in washed human platelets were performed under identical conditions on the same donor to understand what events may occur simultaneous to FLICA dye binding. mitoSOX was used to detect mitochondrial superoxide, Annexin V to detect phosphatidylserine exposure, TMRE to detect mitochondrial membrane potential and FLICA-green to detect caspase-1 cleavage. All assays used human washed platelets (2×10^6/well) + 2 mM $CaCl_2$. All dyes were used as described. oxLDL was pre-incubated for 10 minutes prior to nigericin addition for a total time course of 60 minutes prior to sample acquisition or fixation (n=1)
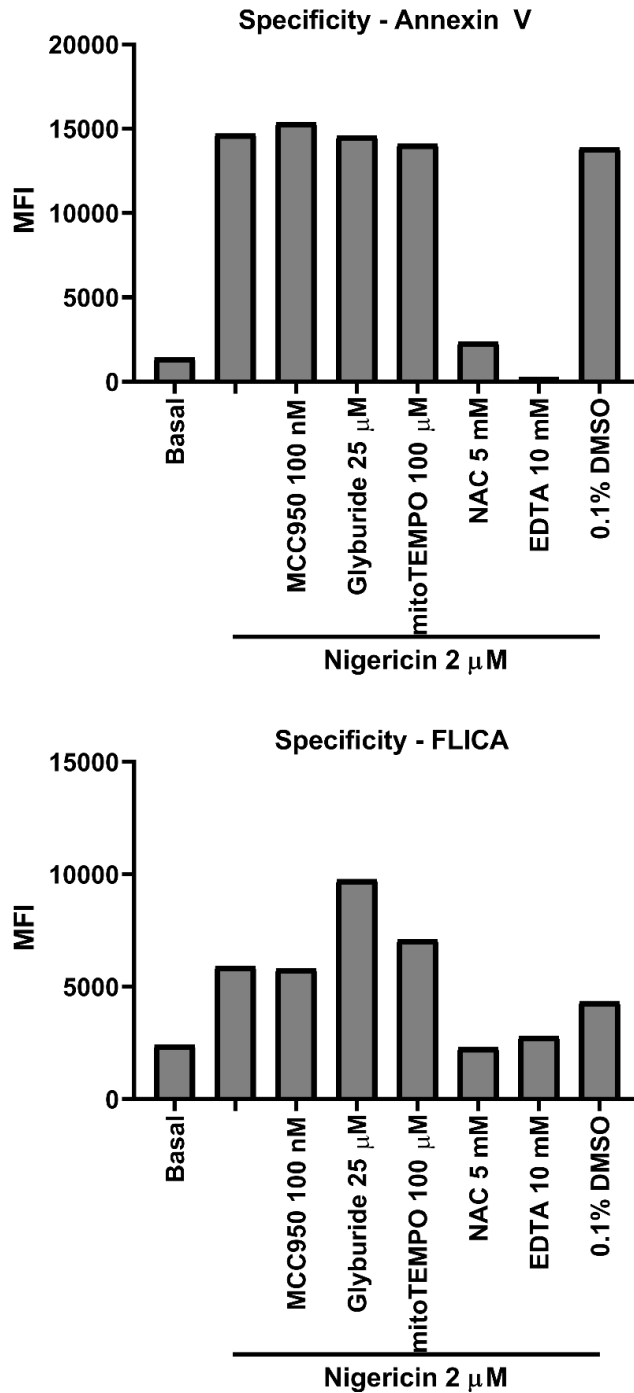
Figure 56. Specificity of the FLICA reagent to caspase-1 cleavage, inhibitor screen. Two assays were performed under identical conditions on the same donor to understand the relationship between phosphatidylserine exposure and FLICA binding. All assays used human washed platelets (2×10^6/well) + 2 mM $CaCl_2$. All dyes were used as described, FLICA-red was used, and inhibitors were incubated for 30 minutes prior to addition of nigericin (2 µM) for a total time of 60 minutes. (n=1)
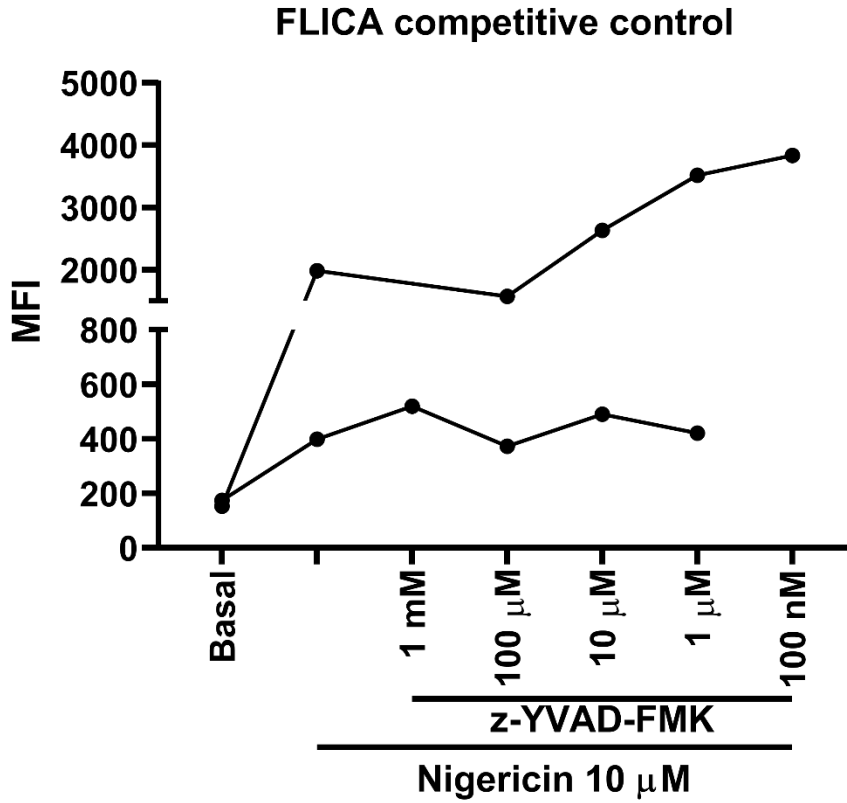
Figure 57. Inability to outcompete FLICA dye binding by unlabelled z-YVAD-FMK peptide. Human washed platelets (2 x 10^{6}/well) + 2 mM $CaCl_2$ treated with or without z-YVAD-FMK (100 nM – 100 μM) for 30 minutes, then incubated with nigericin (10 μM) for 20 minutes followed by 1x FLICA-green for 40 minutes followed by fix, wash, wash and acquisition. (n=2, plotted as individual data sets)

4.4 PROTEIN EXPRESSION, IMMUNOBLOTS AND IMMUNOPRECIPTATIONS

In order to perform cross validation of FLICA data, immunoblotting experiments were performed for components of the NLRP3 inflammasome including NLRP3, ASC, caspase-1, gasdermin D and IL-1β (Schroder and Tschopp, 2010). Although NLRP3 activity in platelets has been measured, primarily by FLICA it is worth noting, there has been little convincing evidence of expression in any published papers to date, with the majority relying on immunofluorescence (Vogel et al., 2018a) or flow cytometry (Hottz et al., 2013), with the first report of detection by immunoblot appearing in 2019 (Vats et al., 2019).

4.4.1 NLRP3 immunoblot and immunoprecipitation

Here we immunoprecipitated (IP) NLRP3 from human washed platelet lysate using two antibodies raised against NLRP3, monoclonal (anti-cryopyrin 6F12) and polyclonal (anti-cryopyrin H66). Whole cell lysate, immunoprecipitated monoclonal antibody (mAb), immunoprecipitated polyclonal antibody (pAb), IgG and inputs were immunoblotted using both anti-cryopyrin 6F12 and H66 antibody. The IP using anti-cryopyrin H66 led to the detection of bands at 110 kDa and 140 kDa respectively (Upper, **Figure 58**). The proposed molecular weight of NLRP3 is 110 kDa, suggesting that NLRP3 was potentially identified under these conditions. In contrast, no NLRP3 was detected in the whole cell lysate or immunoprecipitating with anti-cryopyrin 6F12, which made this less conclusive, where typically a second antibody would act to validate findings. The lack of a positive control sample and potential PBMC contamination in a standard washed platelet preparation also weakens the possibility of expression. Intriguingly the Coomassie stain of the same membrane suggests the presence of a 110 kDa band in both immunoprecipitate elutions.

We also immunoblotted for NLRP3 on human washed platelet lysate with the extensively published CRYO-2 antibody clone. As part of this study, we validated the

antibody against positive control lysates from immortalised THP1 and HL60 cell lines. While a band was detected in both positive controls at ~110 kDa, the predicted molecular weight of NLRP3, no band was detected at that weight in the platelet lysates from three separate donors although we were able to detect the ~140 kDa band which was immunoprecipitated previously alongside several other protein bands at <100 kDa (Figure 58).
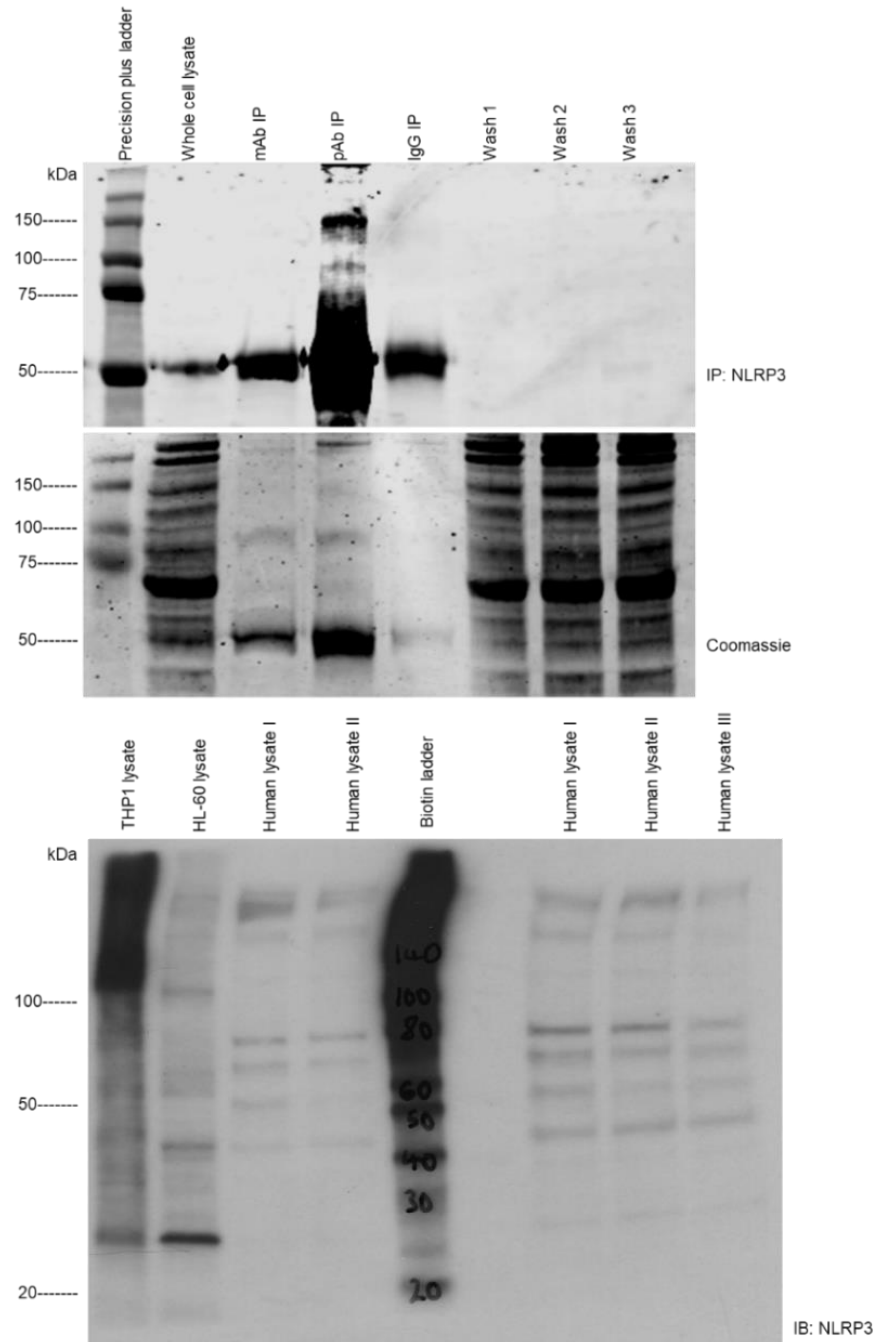
Figure 58. Immunoprecipitation and immunoblot of NLRP3. (Upper) NLRP3 was immunoprecipitated from human washed platelet lysate with either a monoclonal (6F12) or polyclonal (H66) anti-cryopyrin (Santa Cruz) antibody as shown. The immunoprecipitate was washed, lysed and underwent SDS-PAGE and western blot. The blot was probed with anti-NLRP3 (6F12) mAb 1/1000 in 5% milk followed by anti-mouse-680nm 1/20,000 and anti-NLRP3 (H66) pAb 1/1000 in 5% milk followed by anti-mouse-800nm 1/20,000. The blot is composite of both secondary detections, NLRP3 only detected in pAb lysate by pAb probe. Detection was by fluorescence using an Odyssey LiCor. (Lower) Immunoblot, human washed platelet lysate was separated with SDS-PAGE and probed with anti-NLRP3 (CRYO-2, Adipogen) at 1/1000 in 5% milk followed by anti-mouse-HRP 1/10,000. Detected by ECL. Representative of 3 blots.

4.4.2 ASC immunoblot and immunoprecipitation

ASC is a 22 kDa protein which bridges NLRP3 and caspase-1 through its pyrin domain and CARD domain respectively (Matsushita et al., 2009). ASC forms filaments which amplify the signal from NLRP3 and results in caspase-1 recruitment (Dick et al., 2016). In the first instance, ASC was detected by immunoblot of whole cell lysates of multiple human and murine donors and was demonstrated to be expressed in 3 human and 3 murine donors at 20 kDa (Upper, Figure 59). In the second instance ASC was immunoprecipitated from human washed platelet lysate using a monoclonal antibody raised against ASC, note that the dominant bands in the IP are immunoglobulin heavy and light chain (50 and 25 kDa respectively) (Lower, Figure 59). In both sets of experiments, the detected ASC band was clear, suggesting this is specific antibody recognition, but at 20 kDa rather than 22 kDa, as typically described in the literature and also demonstrated here as blotted from THP1 and HL60 cells. Of note, ASC was immunoblotted and immunoprecipitated from multiple donors exclusively at a molecular weight of 20 kDa. However, there are shortened isoforms of ASC previously described in other cells which may lack a hinge domain and therefore be constitutively active (Matsushita et al., 2009), and are known to be 20 kDa. Here we have described, that human and murine platelets predominantly express a shortened isoform of the NLRP3 adaptor protein ASC.
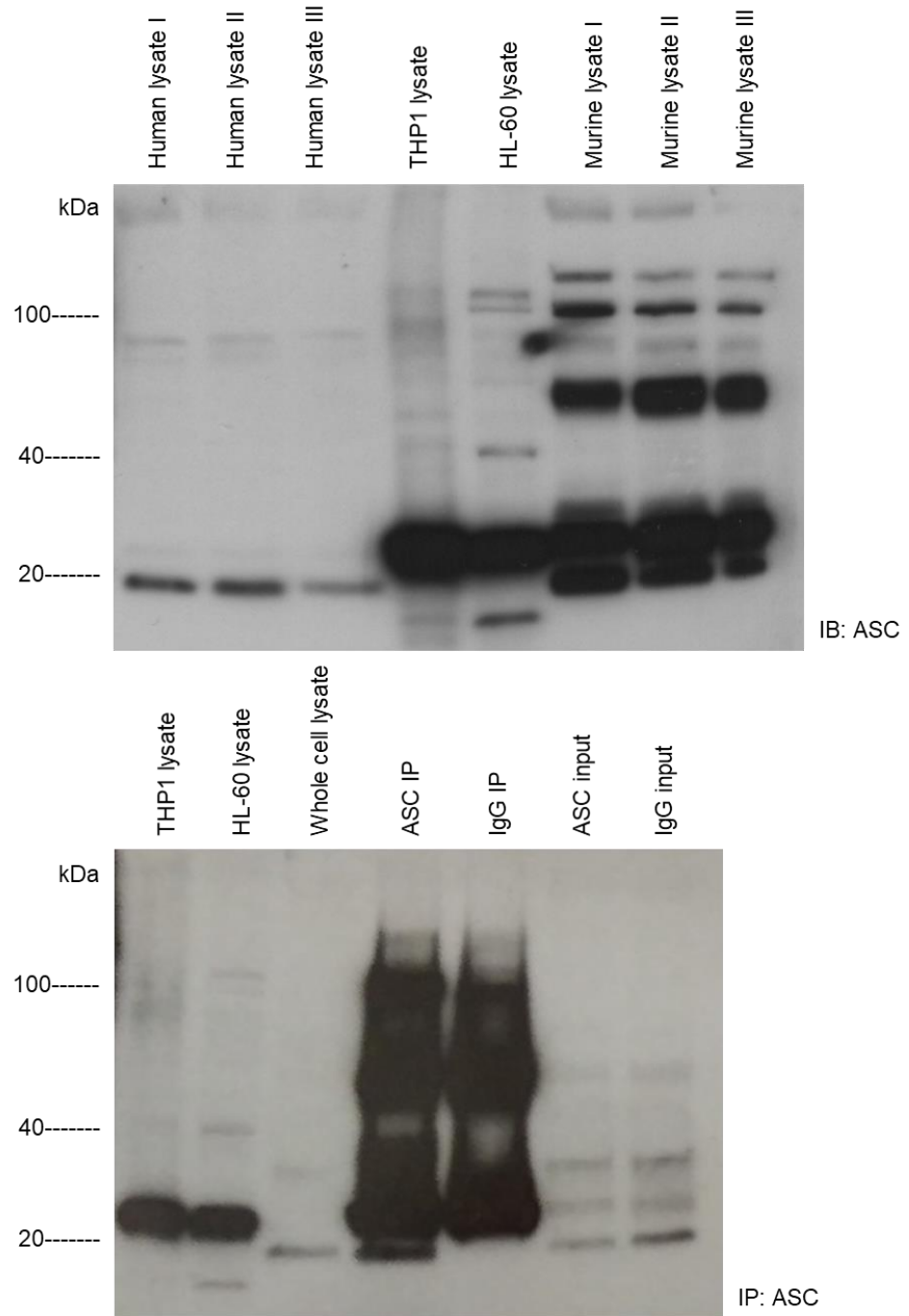
Figure 59. Immunoblot and immunoprecipitation of ASC. (Upper) human washed platelet lysate was separated with SDS-PAGE and probed with anti-ASC (F9, mAb) at 1/250 in 5% milk followed by anti-mouse-HRP 1/10,000, representative of 3 blots. (Lower) the ASC (F9, mAb) immunoprecipitate was washed, lysed and underwent SDS-PAGE and western blot. The blot was probed with anti-ASC (F9, mAb) 1/250 in 5% milk followed by anti-mouse-HRP 1/10,000. Developed by ECL onto x-ray film.

4.4.3 Identification of caspase-1 and cleavage products

Caspase-1 is a thiol protease which belongs to the inflammatory caspases sub-group (Miao et al., 2011). Upon inflammasome activation, recruited caspase-1 undergoes self-cleavage which forms two subunits, P20 and P10, these form an active enzymatic tetramer which cleaves at the amino acid motif YVAD (Garcia-Calvo et al., 1998).

Here, using two antibodies, we first try to determine the presence of caspase-1 in washed platelet lysate and compare these with two leukocyte lysates THP1 and HL-60 used as positive controls. We validated that the antibody detects bands between 50 and 40 kDa, which covers the range of major caspase-1 isoforms; α (50 kDa), β/γ (40-45 kDa) and δ (<40 kDa) (Alnemri et al., 1995) (Upper left, Figure 60). Using the HL-60 as a positive control we next immunoblotted platelet lysates and detected a dominant band at 45 kDa, which would suggest that platelets may express primarily a caspase-1 β isoform (Upper right, Figure 60).

When caspase-1 is activated, it undergoes cleavage, therefore we sought to immunoblot for cleavage products, ranging from 10-20 kDa, encompassing P20 and P10 subunits (Broz et al., 2010). Washed platelets were stimulated with thrombin (10 U/mL), ATP (5 mM) or nigericin (1 and 10 µM) for 15 and 30 minutes and caspase-1 cleavage evaluated. Under these conditions, only nigericin was able to induce cleavage with a band detected at 15 kDa (Lower, Figure 60). This is consistent with previous FLICA data, which detected caspase-1 cleavage was optimal after treatment with nigericin (Figure 48), with only a mild increase for the thrombin mimetic SFLLRN (Figure 52).
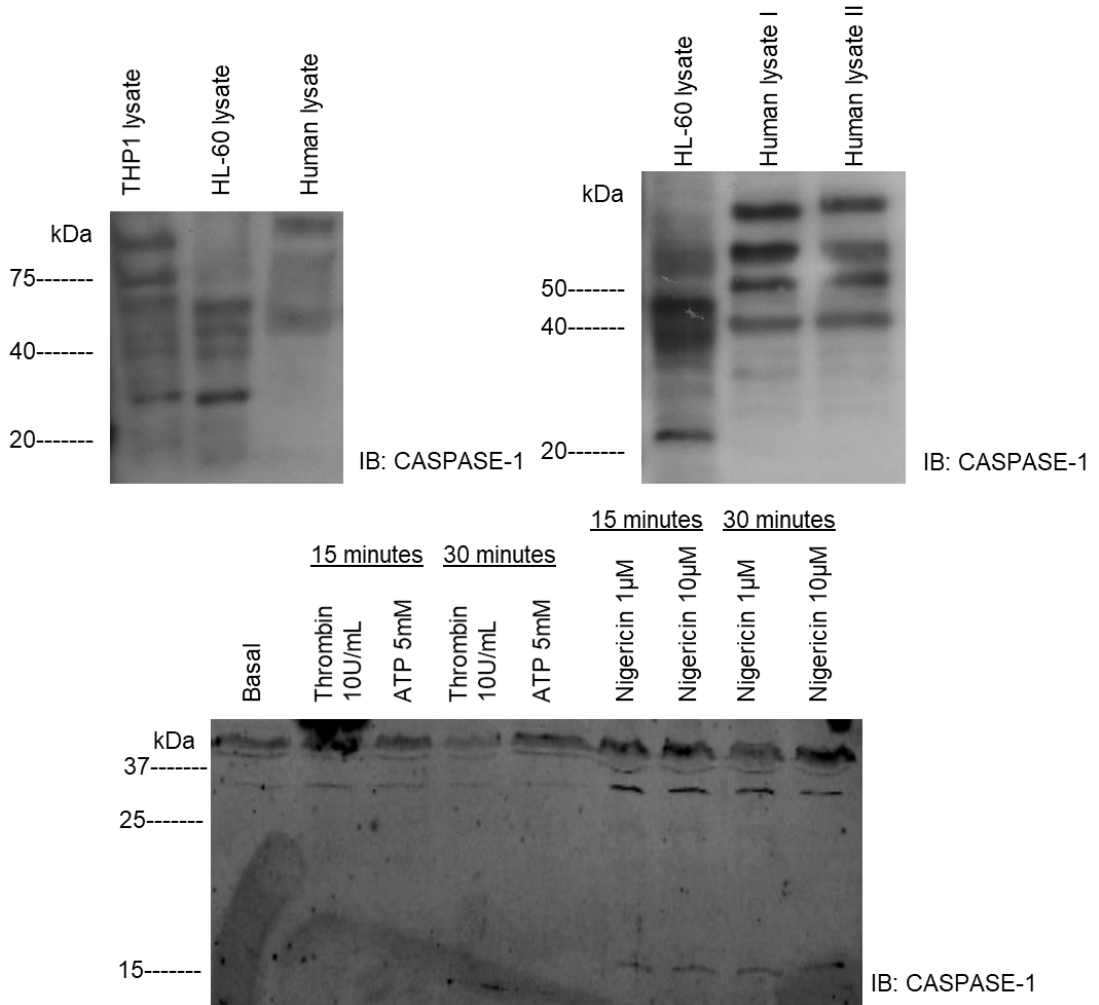
Figure 60. Immunoblots of caspase-1. Human washed platelet lysate untreated or treated as indicated was separated with SDS-PAGE and probed with anti-caspase-1 CST2225S (upper 2 blots) or SCBT mAb (16F468) (lower blot) in 5% milk followed by anti-rabbit-HRP (upper blots) or anti-mouse-IR800 (lower blot) and then developed by enhanced chemi-luminescence onto x-ray film or fluorescence on Odyssey LiCor respectively. Cleavage blot representative of n=4.

4.4.4 Identification of Gasdermin D

Gasdermin D is a 55 kDa protein cleaved by caspase-1. In canonical inflammasome activation it is responsible for pore formation which induces pyroptosis and releases IL-1β (Liu et al., 2016) and in non-canonical activation it is part of the caspase-11 feedback loop leading to potassium efflux dependent NLRP3 activation (Ringel-Scaia et al., 2016).

Here gasdermin D was detected by immunoblot from three human donors washed platelet lysate using a monoclonal antibody raised against gasdermin D. Comparing THP1 lysate to human washed platelet lysate from three separate donors, there was a prominent band at the predicted 55 kDa and a second band at 40 kDa which is shared by both cell lines (Figure 61), suggesting it may be non-specific or a cleavage product of the pore forming domain or repressor domain. This novel observation confirms that human platelets express gasdermin D and may represent a novel pathway for secretion of intracellular cargo. To examine this further, gasdermin D cleavage products after caspase-1 activation should be immunoblotted for, where they should represent a pore-forming domain and repressor domain.
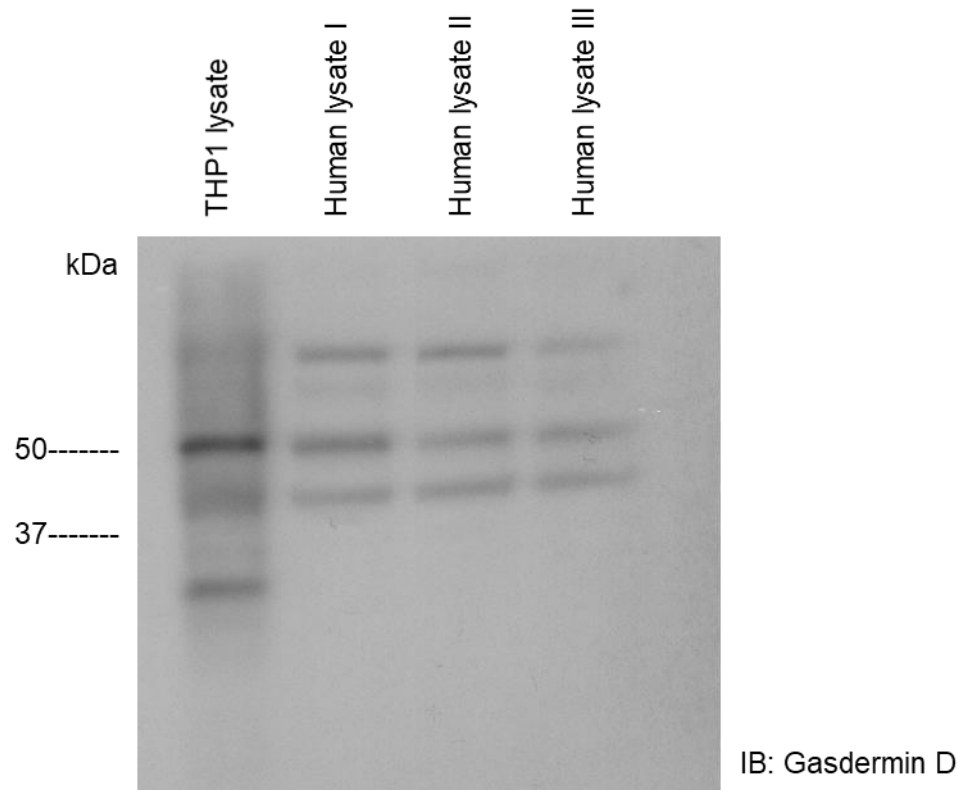
Figure 61. Immunoblot of Gasdermin D. Human washed platelet lysate was separated with SDS-PAGE and probed with anti-gasdermin D (mAb) at 1/500 in 5% milk followed by anti-mouse-HRP 1/10,000. Developed by enhanced chemi-luminescence onto x-ray film.

4.4.5 Interleukin 1-beta immunoblot

IL-1β is the final cleavage product of NLRP3 inflammasome activation and is the systemic effector of the pathway. On an initial signal, pro-IL-1β (p37) is produced via transcriptional priming and accumulates within the cell, prior to cleavage by caspase-1 into bio-active IL-1β (p17) which can then act beyond the cell and drive inflammation (Perregaux and Gabel, 1994, Grebe et al., 2018).

Here we screen human washed platelet lysate treated with several agonists for expression of IL-1β using two separate antibodies, anti-IL-1β P420B pAb and 5C10 mAb to ensure confidence in findings. Using the HL-60 lysate both clones bound to a distinct band at approximately 40 kDa. In contrast, this was not detected in THP1 lysate. This discrepancy is likely as the HL60 lysate is generated from cells pre-treated with LPS while the THP1 was not, and as described LPS acts as a priming signal and drive IL-1β accumulation within the cell. There is also a remarkable difference in specificity of antibody when comparing the pAb with the mAb. Even with the highly specific mAb, from this donor, the washed platelets demonstrated no detectable IL-1β under any of the conditions of stimulation or priming used (Figure 62).
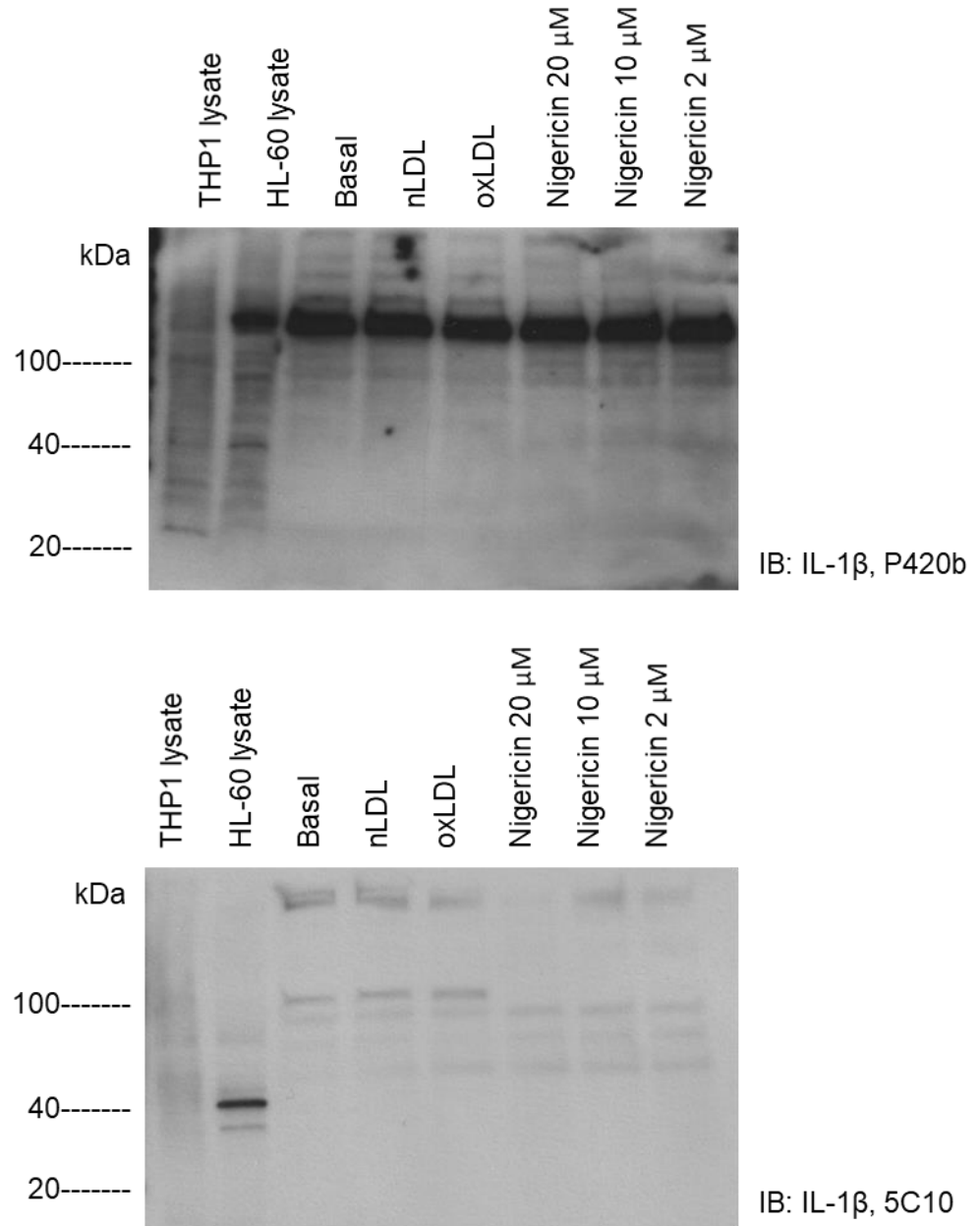
Figure 62. Immunoblot of IL-1β. Human washed platelet lysate was left untreated or treated with the indicated agonist (30 minutes) and was separated with SDS-PAGE and probed with anti-IL-1β (SCBT 5C10 mAb or TF P420b pAb) at 1/500 in 5% milk followed by anti-mouse/rabbit-HRP 1/10,000. Developed by ECL onto x-ray film.

4.5 DISCUSSION

4.5.1 FLICA and NLRP3 inflammasome activity

The first section of data in this chapter concerned the FLICA assay, which fluorescently labels active caspase-1 (Bedner et al., 2000). We used this to attempt to pull apart mechanistic elements and novel ligands which may drive activation of the platelet NLRP3 inflammasome, first described in 2013 (Hottz et al., 2013). Initially we were able to show that the canonical NLRP3 activating ligand, nigericin (Perregaux and Gabel, 1994), could drive a significant increase in FLICA signal in the presence of (plasma levels of) calcium (Murakami et al., 2012), this was an important basis for the study, as it suggested that known aspects of NLRP3 biology described in other cells was reproducible in platelets. We next sought to understand if oxLDL may drive or potentiate caspase-1 cleavage in platelets, as it has been shown to have other effects on platelets including ROS production (Berger et al., 2019b), disinhibition (Magwenzi et al., 2015, Berger et al., 2019a) and activation (Wraith et al., 2013, Yang et al., 2017a) and in macrophages, oxLDL has been shown to drive NLRP3 activation (Liu et al., 2014). While we were unable to demonstrate an increase in FLICA signal when treated with oxLDL alone, oxLDL significantly potentiated a sub-maximal dose of the canonical activator nigericin. Vitally this effect was not observed if treated with nLDL. This suggests that in platelets, rather than directly activating the NLRP3 inflammasome, oxLDL may be functioning as a primer of complex recruitment, allowing for greater activation when stimulated. This hypothesis is in agreement with the literature, where oxLDL is proposed to have both a priming effect (transcriptional activity) and also an activatory effect via ROS production (Liu et al., 2014). Considering the potential for oxLDL to be present not only in atherosclerotic plaque, but in circulation (Ramos-Arellano et al., 2014), we can suggest that circulating oxLDL may priming platelets for NLRP3 activity.

Having demonstrated that oxLDL potentiated the effects of nigericin on caspase-1 cleavage as measured by FLICA, we sought to understand the mechanisms through which this occurs. In platelets, there are many studies which show oxLDL signals primarily through CD36 (Podrez et al., 2007, Wraith et al., 2013), which is highly expressed by human platelets (Burkhart et al., 2012). However, it is also known that other receptors may be involved in driving platelet-oxLDL interactions. To look at other mechanisms through which this effect could be transduced we included the general ROS scavenger N-acetyl cysteine (NAC) and the calcium chelators EDTA (extracellular) and BAPTA (intracellular). OxLDL is known to induce ROS in platelets (Magwenzi et al., 2015), and also induce calcium release via PLCγ2 (Berger et al., 2019b), which is a key mediator of both platelet activation (Begonja et al., 2005) and also NLRP3 (Ye et al., 2017, Liu et al., 2014). Interestingly we were able to demonstrate both that this increase in signal was wholly reliant on ROS, and again reiterated the importance of calcium. As the inhibitors also blocked the positive control of nigericin alone, it cannot be confirmed if they also selectively inhibit oxLDL potentiation or instead block all nigericin driven NLRP3 activity. Since NAC also completely blocks the activation of caspase-1 by high dose nigericin (10 μM) suggesting it blocks an upstream event, it cannot be assumed that NAC is targeting only downstream of oxLDL rather it is either only blocking all NLRP3 activity or simultaneously blocking the potentiation caused by oxLDL. To dissect the role of CD36 in the transduction of the oxLDL signal, we applied inhibitors against several aspects of the pathway targeting the receptor itself and downstream kinases using previously published inhibitors (Magwenzi et al., 2015, Wraith et al., 2013). We applied FA6-152 as a CD36 blocking antibody, BAY61 to block Syk and PP2 to block Src family kinases. These inhibitors were shown to not have any significant effects on the FLICA signal after treatment with nigericin and oxLDL. There was a minor decrease in signal after treatment with BAY61, which based on Fa6 and PP2 not inhibiting response would suggest it was not affecting CD36 signalling, therefore as

Syk has been previously shown to be involved in the regulation of ASC recruitment, this may be the pathway through which this reduction was mediated (Lin et al., 2015). Nevertheless, together this suggests that oxLDL is not signalling through CD36 to potentiate caspase-1 activity. However, as these studies on the CD36 signalosome lack repeats, it is important that the experiments are later repeated to validate these observations.

Having found a reproducible phenotype, where oxLDL heavily potentiated the cleaved caspase-1 signal, we wanted to verify this, as it was a larger increase than anticipated. Therefore we adjusted our strategy to attempt to blockade NLRP3 with the specific inhibitory compound MCC950, which has been shown to inhibit the NLRP3 inflammasome with a high specificity (Coll et al., 2019, Coll et al., 2015). We chose to pursue this method, as the FLICA assay does not have an intrinsic control to account for non-specific binding and a well published inhibitor (MCC950) could provide a negative control for this purpose. As was demonstrated several times, this inhibitor, at a wide range of doses failed to inhibit FLICA signal. This surprising result suggested that; (i) NLRP3 is not present in platelets and the caspase-1 cleavage being measured is downstream of an alternative mediator, or (ii) the FLICA dye is binding non-specifically and potentially an alternative event is being measured. Platelet proteomic studies have demonstrated no other inflammasome complexes present in human or murine platelets, bar NLRX1 (Burkhart et al., 2012, Zeiler et al., 2014), which does not signal through caspase-1 as it lacks both a pyrin domain to recruit ASC, or a CARD domain to recruit caspase-1 (Allen, 2014). We were therefore concerned that we were inducing platelet apoptosis and pursued several assays to measure events which are hallmarks of death pathways.

Having demonstrated that the signal we induce is insensitive to MCC950, we sought further validation of the assay. We pursued the use of a competitive unlabelled YVAD-motif control and screened our optimal stimulation conditions against assays for mitochondrial ROS, mitochondrial membrane potential and phosphatidylserine

exposure. Here we were able to demonstrate, in agreement with previous literature (Pozarowski et al., 2003), that an unlabelled peptide cannot outcompete FLICA binding at large molar excess. We further demonstrated that under identical conditions, where FLICA binding is high, that apoptotic hallmarks such as PS exposure, loss of mitochondrial membrane potential and mitochondrial ROS are all induced. Critically MCC950 was confirmed as unable to block FLICA binding, but the data also suggested that PS exposure may not be downstream of inflammasome activation, which was similarly unperturbed by the inhibitor, again indicative of apoptosis. While pyroptosis, or inflammatory cell death (Miao et al., 2011) is a well described phenomena of NLRP3 activity the inability of blockade of FLICA signal by specific inhibitors and the relative similarities to apoptosis observed suggest the peptide may be binding non-specifically to apoptotic/pyroptotic platelets (Pozarowski et al., 2003, Darzynkiewicz and Pozarowski, 2007). Potassium efflux is also suggested to be vital to NLRP3 activation, we tested whether an excess of extracellular potassium could block FLICA binding (Tang et al., 2017) but again, we could demonstrate no blockade of signal (data not shown). Further to this, we tested nigericin on the classical platelet assay of LTA. This demonstrated no aggregation but did induce a linear clearance of platelet suspension which was not dependent on fibrinogen binding, suggesting this may be cell death. This was also supported by an observation in cellular concentrations when samples were analysed by flow cytometry, where those samples treated with nigericin took considerably longer to acquire an equivalent number of cells in comparison to basal samples. While LTA demonstrated no functional response CD62P expression did appear to be induced by nigericin treatment. This observation is in agreement with literature suggesting that NLRP3 activity in platelets can be induced by traditional platelet agonists thrombin and collagen, of which SFLLRN is a thrombin mimetic (Murthy et al., 2017). Furthermore, we can show that the K+ ion flux driven by nigericin is possibly able to induce α-granule secretion, however confirmation with additional marker PAC1 would

provide validation that this is complete activation. PAC1 would be insensitive to changes in membrane permeability, as CD62P staining might be, as it instead detects the active conformation of the integrin $\alpha_{IIb}\beta3$. There is a likelihood that if the cells are truly becoming apoptotic, the CD62P antibody may be simply entering the cell to detect total CD62P rather than exposure of the protein on the surface.

While there are concerns over the specificity of FLICA as a readout of NLRP3 activity within the literature (Darzynkiewicz and Pozarowski, 2007), we have applied several control experiments to our model in washed human platelets. We can summarise that FLICA signal is robustly increased by the known NLRP3 activator nigericin and we show that oxLDL significantly potentiates this and nLDL does not, however, we are unable to block this effect with MCC950 (Coll et al., 2015), glyburide (Lamkanfi et al., 2009), competitive peptide controls (Pozarowski et al., 2003) or potassium efflux blockade (Tang et al., 2017). Remarkably the ROS scavenger NAC (Ye et al., 2017) and calcium (Murakami et al., 2012) are shown to be vital to this signal, but the FLICA signal also co-exists with several apoptotic markers. The importance of ROS and calcium concurrent with markers of apoptosis and mitochondrial dysfunction may suggest that nigericin is perturbing mitochondrial stability leading to apoptosis. Ultimately, while we may be reading caspase-1 cleavage, under the current conditions we cannot be sure that this is the case and several factors point to the treatment inducing platelet death, although again this may be pyroptosis (Miao et al., 2011). This study requires further validation, preferably by alternative methods such as immunoblot for cleaved caspase-1 or ELISA for secreted IL-1β. Additionally the use of NLRP3 knockout murine models to avoid relying on chemical inhibition would significantly enhance the study and overcome the limitations of biochemical inhibitors.

4.5.2 NLRP3 inflammasome expression

Another important consideration is the expression of NLRP3 and associated components in platelets. The human platelet proteome reports the presence of only ASC and gasdermin D (Table 9), with copy numbers of both proteins presumed not to exceed 1500 per cell (Burkhart et al., 2012), the murine platelet proteome also reports that only ASC and gasdermin D are present (Table 10) (Zeiler et al., 2014). However, it must be noted that these proteomic studies were performed on healthy donors, or wild type mice, and there is a strong argument for inflammatory protein complexes being upregulated in a diseased state, and therefore not present in healthy donors. However, it is of some concern to this argument of inflammatory reprogramming, that in individuals with dengue virus infection, where platelet NLRP3 activity was initially described (Hottz et al., 2013), the same group later reported no NLRP3 detectable by proteomics (Trugilho et al., 2017). In contrast with this, the transcriptome of both human and murine platelet RNA reports the presence of all components; NLRP3, ASC, caspase-1, IL-1β and gasdermin D (Table 11), although none are ranked within the 3000 most common transcripts (Rowley et al., 2011). These negative reports could be attributed to a lack of protein presence in the healthy donors assayed or low copy numbers of these proteins or transcripts, below detection thresholds. In support of this, the human proteome does not detect the presence of TLRs, but their expression has been evidenced by traditional biochemistry and functional studies both *in vivo* and *in vitro* (Biswas et al., 2017, Fung et al., 2012, Damien et al., 2015, Vogel et al., 2018a, Vogel et al., 2018b, Rex et al., 2009).

Table 9. Protein name, accession code, confidence of signal and estimated copy number for each component of the NLRP3 inflammasome in human platelets (Burkhart et al., 2012).

Protein	Accession	Confidence (%)	Copy number
NLRP3	Q96P20	-	-
ASC	Q9ULZ3	100	1,000
Caspase-1	P29466	-	-
Gasdermin D	P57764	100	1,500
IL-1β	P01584	-	-

Table 10. Protein name, accession code and estimated copy number for each component of the NLRP3 inflammasome in murine platelets (Zeiler et al., 2014).

Protein	Accession	Copy number (+/- variation)
NLRP3	Q8R4B8	-
ASC	Q9EPB4	3,743 +/- 1,375
Caspase-1	P29452	-
Gasdermin D	Q9D8T2	308 +/- 111
IL-1β	P10749	-

Table 11. Protein name, genecard symbol and relative expression rank in the transcriptome for each component of the NLRP3 inflammasome (Rowley et al., 2011).

Protein	Symbol	Human rank	Murine rank
NLRP3	NLRP3	5913	10955
ASC	PYCARD	3005	4178
Caspase-1	CASP1	3365	6354
Gasdermin D	GSDMD	4114	9645
IL-1β	IL1B	4972	5773

We attempted to assess the expression of NLRP3 inflammasome components by protein biochemistry; immunoprecipitation and immunoblot. We were able to immunoprecipitate a clear NLRP3 band, however this migrated at a molecular weight different to that predicted from the literature by roughly 30 kDa. The data indicated that immunoblotting confidently detected three potential components of this complex

including ASC, caspase-1 and gasdermin D. While efforts to detect caspase-1 cleavage, IL-1β and NLRP3 were challenging.

The above data was then compared and summarised in a single table to compare expression of NLRP3 inflammasome complex proteins by different methods including open access proteomics, transcriptomics and our own protein biochemistry of platelet lysates. In summary, only ASC and gasdermin D are present across all three studies (Burkhart et al., 2012, Zeiler et al., 2014, Rowley et al., 2011), including our own (Table 12).

Table 12. NLRP3 inflammasome complex components presence based on proteomic data (Burkhart et al., 2012), transcriptomic data (Rowley et al., 2011) and own immunoblots and immunoprecipitations. += present, -=not-present, ~=further validation and X=not tested.

Protein	Proteome (h)	Transcript (h)	Lysate (h)	Proteome (m)	Transcript (m)	Lysate (m)
NLRP3	-	+	~	-	+	✕
ASC	+	+	+	+	+	+
Caspase-1	-	+	+	-	+	✕
Gasdermin D	+	+	+	+	+	✕
IL-1β	-	+	-	-	+	✕

A novel finding made here was that platelets express primarily a spliced transcript of ASC (Matsushita et al., 2009), which is suggested to be constitutively active or play regulatory roles in NLRP3 activity depending on the spliced variant expressed (Bryan et al., 2010). What is known is that ASC recruitment is a vital step in NLRP3 activity (Dick et al., 2016), one could hypothesise, that if ASC is able to oligomerise without NLRP3, NLRP3 itself may not be required in platelets to activate ASC CARD domains and recruit caspase-1, potentially explaining why the MCC950 did not work in this model. Further studies are required on the capacity of platelet ASC to oligomerise, and this can be pursued by both CHAPS cross-linked immunoblotting for oligomers or light microscopy for ASC puncta (Dick et al., 2016). We also identified that platelets

express gasdermin D, a novel finding that has not previously been described but which requires further work, as if confirmed, gasdermin D pore formation could well represent a novel node of cargo trafficking available to platelets (Liu et al., 2016), particularly if as some literature suggests platelet NLRP3 is activated by typical platelet agonists (Murthy et al., 2017, Qiao et al., 2018). The fact that several components of the pathway are present would suggest that; (i) there is some capacity to enact NLRP3 like activity via a novel pathway, (ii) an alternative and as of yet undetected NLR complex exists, where a recent proteomic study detected NLRP2 (Trugilho et al., 2017), (iii) the NLRP3 inflammasome is present in platelets and detection and inhibition remains a challenge. However, without the confirmation of the NLRP3 inflammasome in this study, these suggested points currently remain speculation.

Our findings here raise some discrepancies when compared with the literature currently surrounding the NLRP3 inflammasome in platelets. Where several platelet NLRP3 papers all provide functional evidence of NLRP3 activity (Hottz et al., 2013, Murthy et al., 2017, Qiao et al., 2018, Vogel et al., 2018a, Vogel et al., 2018b) and there is also prior evidence of platelets cytokines downstream of NLRP3, IL-1β (Brown et al., 2013, Nhek et al., 2017), or IL-18 (Allam et al., 2017). Furthermore, activation of the inflammasome in platelets, in our study and others, has been measured primarily using the FLICA assay. In comparison with our own work, the effects of MCC950 on platelet inflammasome activity have been small in the literature (Vogel et al., 2018a). However, there has been little evidence of protein expression by immunoblot of NLRP3 bar a single report (Vats et al., 2019), which has routinely been shown in leukocytes, and indeed in almost all leukocyte NLRP3 papers since the field was started (Agostini et al., 2004). Instead, platelet studies have typically used fluorescent flow cytometry (Hottz et al., 2013) or fluorescent microscopy (Vogel et al., 2018a), which intrinsically have fewer controls than traditional protein detection by immunoblot.

Chapter 5
Mitochondrial dysfunction under lipid stress

5.1 INTRODUCTION

Platelets are metabolically active cells and demand for energy production increases on activation (Aibibula et al., 2018). Therefore a decreased mitochondrial activity leads to platelets which are hyporesponsive (Baaten et al., 2018). Beyond the requirement of functional mitochondria for effective platelet haemostatic activity, mitochondria have been implicated as key regulators of NLRP3 activity in other cell types (Zhou et al., 2011) and also in platelets (Hottz et al., 2013). Platelet mitochondria also regulate the procoagulant platelet phenotype – where mitochondrial depolarisation driven by sustained calcium signalling is a key event in the pathway leading to phosphatidylserine exposure (Choo et al., 2017, Choo et al., 2012).

Mitochondrial superoxide anion ($O_2^{\bullet-}$) is produced from the electron transport chain and is reduced by manganese superoxide dismutase (Mn^+ SOD) to H_2O_2 which can leave the mitochondria into the cytoplasm. In the cytoplasm, H_2O_2 is broken down by catalase to produce H_2O and O_2 (Collins et al., 2012). Mitochondrial membrane potential can be diminished by excess mitochondrial ROS, and when membrane potential is lost, this further increases the rate of mitochondrial ROS production, leading to a snowball effect of mitochondrial dysfunction. These mitochondrial ROS can leak out of the mitochondria if the mitochondrial permeability transition pore is formed (Schulz et al., 2014). Mitochondria play a key role in many cellular signalling pathways (Tait and Green, 2012) and by measuring markers of mitochondrial stress we aim to link mitochondrial dysfunction to a functional platelet phenotype.

Mitochondrial function in platelets has previously been measured and shown to be implicated in several aspects of platelet function, including activation, ageing and necrosis (Gyulkhandanyan et al., 2012, Fidler et al., 2017, Zhao et al., 2017, Baaten

et al., 2018, Obydennyi et al., 2019, Zhang et al., 2019). Collagen-GPVI mediated platelet activation has been shown to be potentiated by hyperglycaemia driven by mitochondrial superoxide production (Yamagishi et al., 2001). In aged mice, mitochondria are changed in circulating platelets by parent megakaryocytes which are suggested to drive an age-associated hyperactivity phenotype (Davizon-Castillo et al., 2019). Furthermore, in Wiscott-Aldrich syndrome patients, platelets are shown to undergo mitochondrial-dependent necrosis on activation (Obydennyi et al., 2019). Understanding there is a key role for mitochondria in the regulation of many facets of platelet function, we sought to understand how oxLDL or lipid stress may be affecting platelet mitochondrial function. In other cell types oxLDL has been shown to affect mitochondrial function having several effects; driving mitochondria-dependent apoptosis in endothelial cells (Vindis et al., 2005), mitochondrial ROS production in endothelial cells (Chowdhury et al., 2010, Zmijewski et al., 2005), mitochondrial ROS production in macrophages (Asmis and Begley, 2003) and hyperpolarisation in enterocytes (Giovannini et al., 2002). This suggests a clear effect of oxLDL on metabolism in cells from multiple lineages, however, the effects of oxLDL on platelet or megakaryocyte metabolism has not been previously explored. Nevertheless, we have previously shown that ROS are produced in platelets in response to oxLDL (Magwenzi et al., 2015, Berger et al., 2019b), and that ROS signal from oxLDL treatment is sustained over several hours (Berger et al., 2019b), which is in contrast with the spike of ROS on GPVI activation (Walsh et al., 2014), suggesting that this divergence in ROS kinetics may control different platelet function.

To further understand the mechanisms of this pathway, several known pathways could be targeted to determine how oxLDL is transducing a signal to the mitochondria leading to the observed dysfunction. The first and most well described pathway through which oxLDL signals in platelets is via CD36. CD36 ligation with oxLDL has been shown to drive platelet activation via; Spleen tyrosine kinases (SYK) and Rho (Wraith et al., 2013), PLCγ2 and ROS (Berger et al., 2019b), disinhibition of NO via

NOX2 (Magwenzi et al., 2015), disinhibition of PGI$_2$ via PDE3a (Berger et al., 2019a), JNK (Chen et al., 2008) and ERK5 (Yang et al., 2017a). Recent studies in platelets have also now demonstrated a role for CD36 signalling in conjunction with other receptors, primarily Toll-like receptors (TLRs). This was first described in macrophages as being a CD36, TLR4 and TLR6 (Stewart et al., 2010) heteromeric complex, however it was then further described as a CD36, TLR2 and TLR4 (Chavez-Sanchez et al., 2014) complex. In platelets, oxLDL signalling has been suggested to be via a different heteromeric complex to that detailed above; CD36, TLR2 and TLR6 (Biswas et al., 2017). Other receptors on the platelet surface which may bind to oxLDL alongside CD36 include LOX1 and SRB1 (Levitan et al., 2010) and TLR2/4 in a heteromeric complex with CD36 (Biswas et al., 2017, Chavez-Sanchez et al., 2014). LOX1 has been shown to be expressed on the platelet surface downstream of activation (Chen et al., 2001). Importantly for this study, LOX1 has also been shown to directly drive mitochondrial dysfunction and release of mtDNA – in turn activating the NLRP3 inflammasome (Christ and Latz, 2014). Additionally, LOX1 has been suggested to target the mitochondrial enzyme arginase II (ARG2) via ROCK (Touyz, 2014). Furthermore, and in support of LOX1 activation related to modified LDL and metabolic defects, a recent clinical study has identified circulating soluble LOX1 as a marker of the metabolic syndrome (MetS) which further correlates with another modified LDL, carbamylated LDL (cLDL) (Stankova et al., 2019).

Therefore, within our system, we sought to understand how oxLDL, a key ligand in atherogenic lipid stress (Podrez et al., 2002a), may modulate mitochondrial biology, particularly in the context of mitochondrial superoxide production and mitochondrial membrane potential. We hypothesised that these observations may provide a functional link between oxLDL and the potentiation of FLICA/caspase-1 cleavage signal.

5.2 **AIMS OF CHAPTER**

- To measure platelet mitochondrial function in response to lipid stress

- To understand if platelet mitochondrial function changes in a model of diet-induced hyperlipidaemia

5.3 PLATELET MITOCHONDRIAL SUPEROXIDE

Previous FLICA findings suggested the potentiation of caspase-1 cleavage was driven by oxLDL but not by the control, nLDL. Furthermore, the data from section 4.3.5 (Figure 50) indicated that these effects were mediated by ROS and calcium. Both calcium and ROS are intrinsically related to modulating mitochondrial function and ROS are additionally produced by mitochondria (Tait and Green, 2012, Schulz et al., 2014). Therefore, we chose to examine whether oxLDL modulated mitochondrial biology, specifically mitochondrial superoxide production, a potent source of intracellular ROS.

A cell-permeant fluorescent probe assay which fluoresces when oxidised in mitochondria, mitoSOX, was established. This dye has previously been applied to measure platelet superoxide production (Hottz et al., 2013, Fidler et al., 2017), but platelet mitochondrial dysfunction in the context of lipid stress has not previously been measured.

5.3.1 MitoSOX titrations

The basis for this assay is a cell-permeant dye which fluoresces upon oxidation, and cell loading titrations were performed using the positive control antimycin A (AA; 100 µM), which blocks complex 3 of the electron transport chain leading to superoxide leak. Each dilution was compared with a basal sample at a matched concentration, this comparison allows a comment on the sensitivity. As before calculating fold over control allows the condition with the highest fold increase, and therefore optimal window for detection of changes to be selected. There was a consistent signal in basal samples which did not change when incubated with increasing amounts of mitoSOX dye. Antimycin A (100 µM) caused increased signal as a function of dye concentration and it was determined that 5 µM dye provided the optimal window for positive signal to be measured (Figure 63). This is a dose of the dye that has

previously been loaded into washed platelets to measure mitochondrial superoxide

(Fidler et al., 2017).
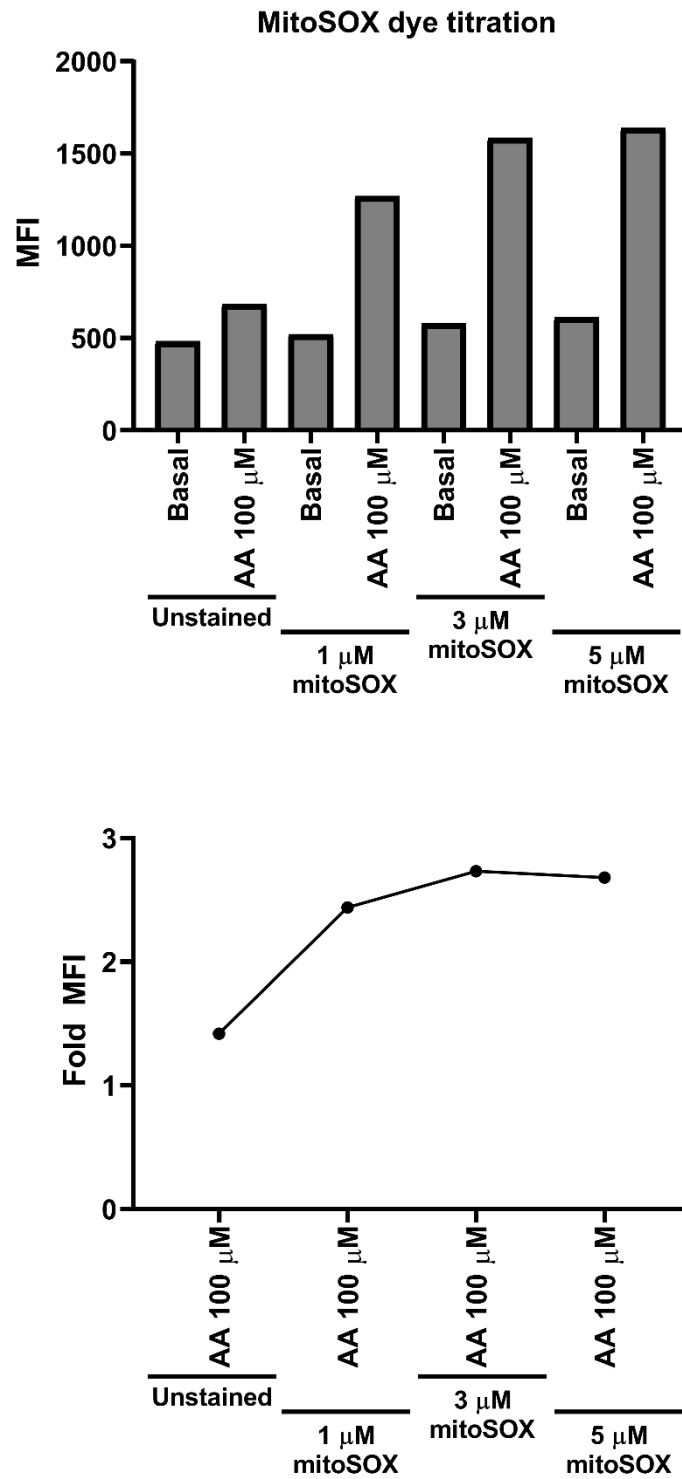
Figure 63. MitoSOX dye titration. Washed human platelets (2 x 10^{6}) were treated with or without antimycin A (100 μM) for 20 minutes prior to incubation with or without mitoSOX (1 – 5 μM) for 10 minutes. Samples were then diluted 10x in PBS and analysed by fluorescent flow cytometry. (n=1)

5.3.2 Antimycin A dose and time response

Antimycin A targets and blocks complex 3 of the mitochondrial electron transport chain (Potter and Reif, 1952). Blocking complex 3 is known to induce superoxide leak from the electron transport chain, therefore we can use this agonist as a positive control ligand for mitoSOX (Park et al., 2007). Here in washed human platelets, time and dose responses against antimycin A were performed to determine the sensitivity of the assay. At 0 minute basal, fluorescent signal was low, suggesting basal mitochondrial superoxide production in platelets was also low (569.1±23), and this was increased after 60 minutes of resting (730.4±86). Antimycin A (10 – 100 µM) caused a concentration dependent increase in superoxide generation when incubated for 60 minutes, with a significant increase over time matched basal observed at 50 and 100 µM (1229±374 and 1345±355 ($p < 0.05$) respectively) (Figure 64). Antimycin A (50 µM) also increased superoxide production in a time-dependent manner and outstripped basal at 60 minutes (730.4±86) after just 15 minutes with antimycin A (810.8±159) with maximal effects seen at 60 minutes (1117±263, $p < 0.005$, longest time tested) (Figure 64). This suggested the assay was sensitive to small changes in superoxide production at short time points and did not only detect changes at maximal dose/time.
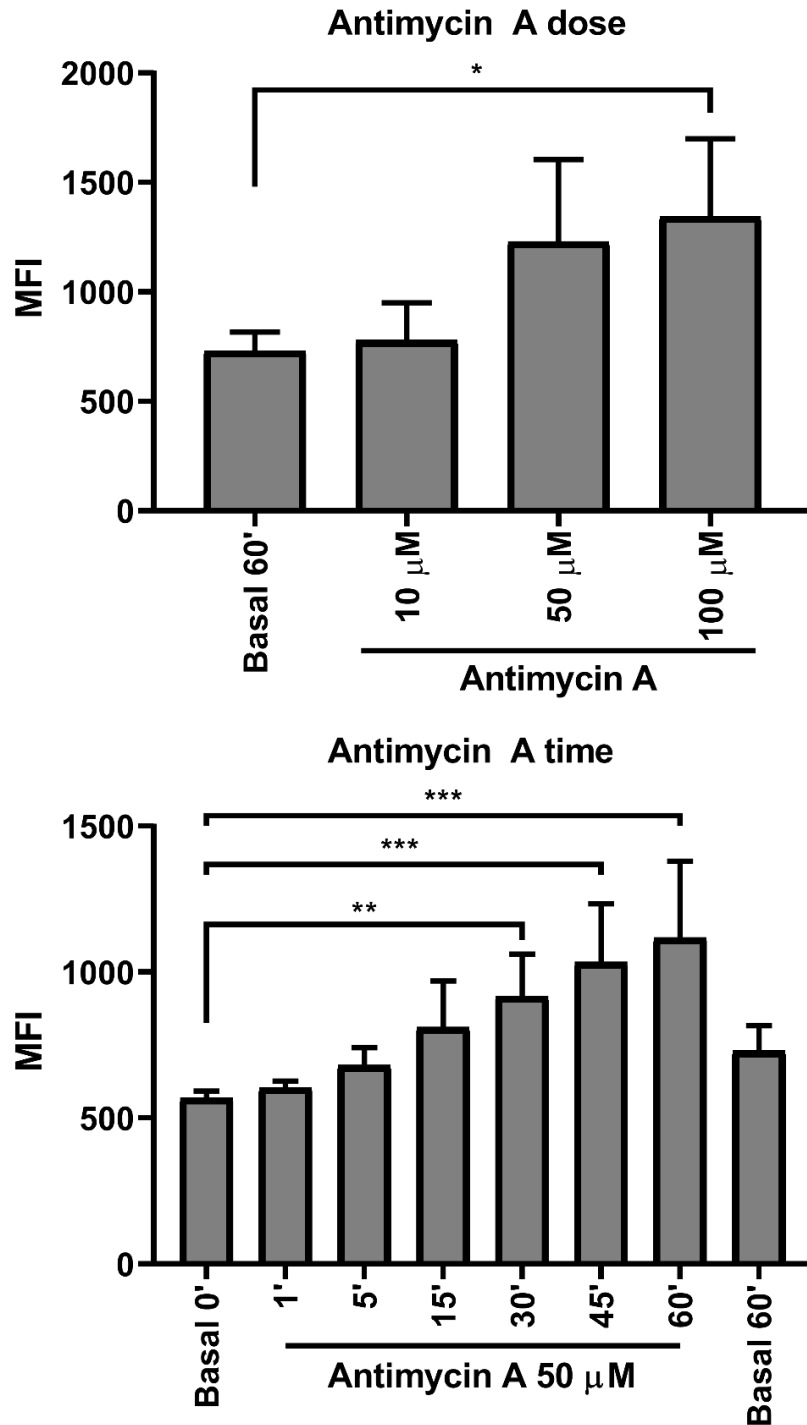
Figure 64. MitoSOX antimycin A dose and time response. Washed human platelets (2×10^6) were treated with or without antimycin A ($10 – 100$ µM) for 60 minutes or with or without antimycin A (50 µM) for $1 – 60$ minutes prior to incubation with mitoSOX (5 µM) for the final 10 minutes of incubation. Samples were then diluted 10x in PBS and analysed by fluorescent flow cytometry. (One-way ANOVA vs. basal sample, *<0.05, **<0.01 and ***<0.005, error shown as standard deviation, n=3-4)

5.4 OXIDISED LDL AND MITOCHONDRIAL SUPEROXIDE

5.4.1 OxLDL dose and time response

Having determined that the assay is sensitive over a wide range of time points and several doses of the positive control antimycin A, we next performed dose and time responses with oxLDL comparing it to basal and nLDL treated platelets. The mitoSOX probe was added 10 minutes prior to analysis, the assay was designed like this to avoid continued kinetic activation of the dye and false amplification of the signal. However, as part of this study we also explored if pre-incubation of the samples with the dye for 10 minutes followed by incubation with the agonist could improve the sensitivity of the assay through the amplification of superoxide signal (Figure 65).

Performing the assay with dye incubated for only 10 minutes prior to analysis, we used antimycin A as a positive control which was significantly increased over basal (1840 ± 412 vs. 634.9 ± 29, $p < 0.0001$) and confirmed the assay was functioning appropriately. We were then able to show that oxLDL (6.25 - 200 µg/mL) induced a dose-dependent increase in mitochondrial superoxide with maximal effects observed at 200 µg/mL (1055 ± 198, $p < 0.05$). In contrast, the signal at maximal dose of nLDL (617.6 ± 49) was not significantly different from basal. Although the difference in signal was not statistically significant at all doses of oxLDL, there was an obvious trend that as the concentration of added oxLDL increased so did the level of superoxide (Figure 66). There was also a time-dependent increase in mitochondrial superoxide when the concentration of added oxLDL was a constant (50 µg/ml). Again, increases in MFI were not statistically significant for all time points but nonetheless increase was seen after the shortest time point (674.7 ± 37), and significant increases were then observed after at 90 minutes (894.4 ± 115, $p < 0.05$) and 180 minutes (1037.0 ± 172, $p < 0.01$). Crucially, the control nLDL at 180 minutes was again not different from basal (634.6 ± 38) (Figure 66).
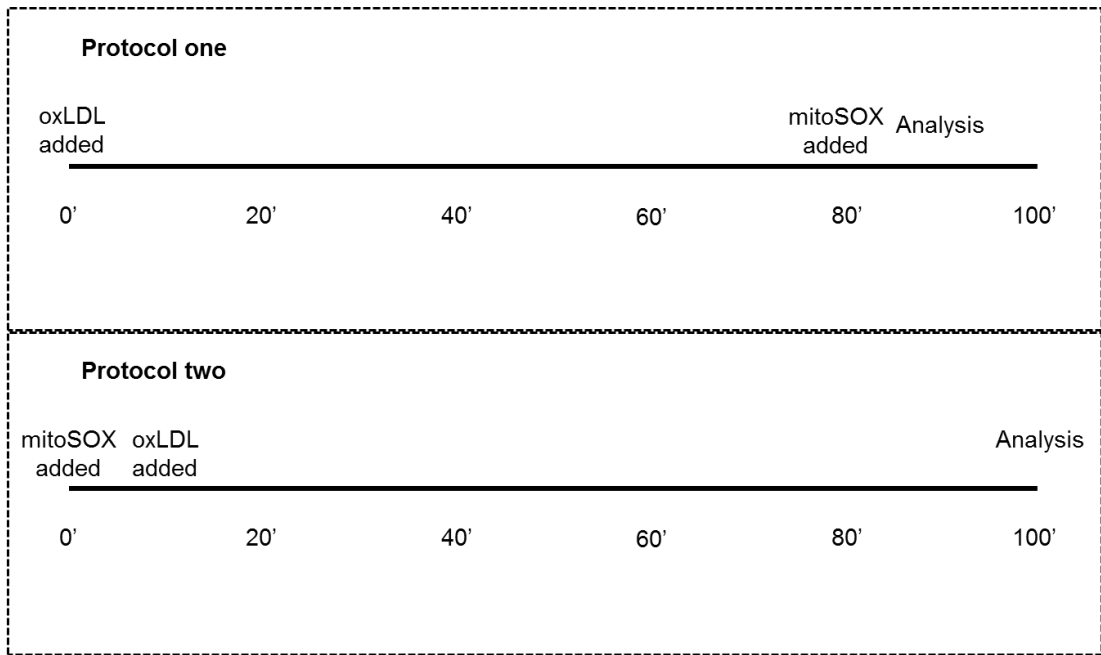
Figure 65. Timeline of two mitoSOX dye loading strategies. Two mitoSOX staining strategies were used in this study. Protocol one was used in Figure 66, and protocol two in Figure 67. A total oxLDL incubation of 90 minutes is used but the incubation of mitoSOX was varied.
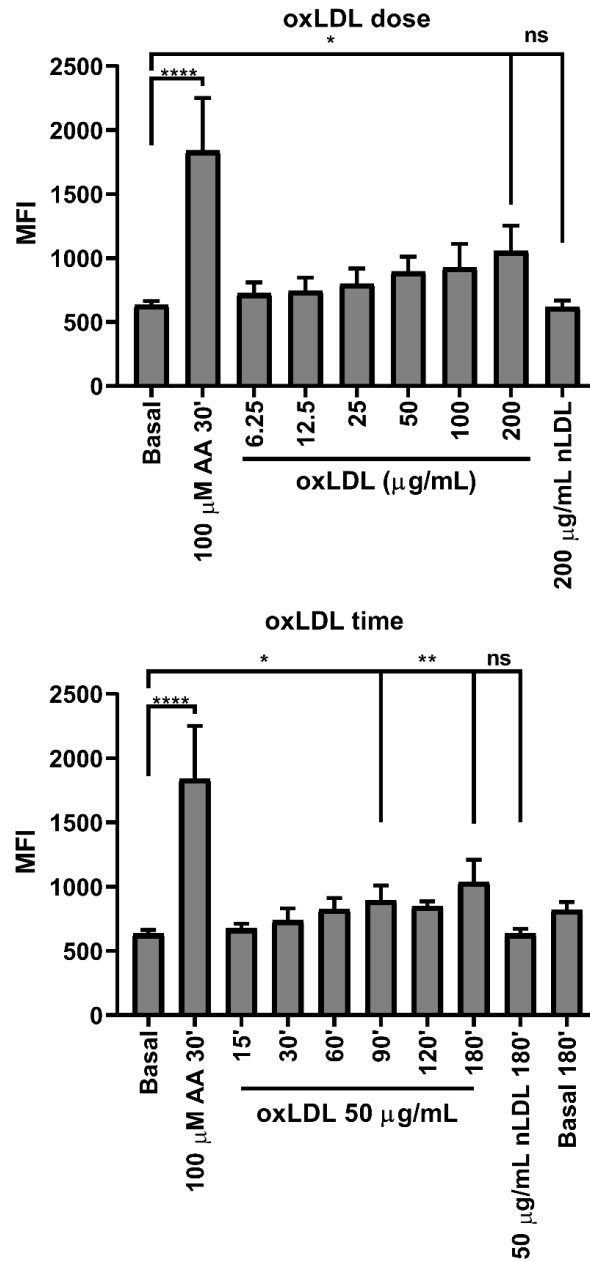
Figure 66. MitoSOX oxLDL dose and time response. Washed human platelets (2 x 10^{6}) were treated with oxLDL or nLDL (6.25 – 200 µg/mL) for 60 minutes or with oxLDL or nLDL (50 µg/mL) for 15 – 180 minutes prior to incubation with mitoSOX (5 µM) for the final 10 minutes of incubation. Antimycin A (100 µM, 30 minutes) was used as a positive control and stained in the same way. Samples were then diluted 10x in PBS and analysed by fluorescent flow cytometry. (One-way ANOVA vs. basal, ns=non-significant, *<0.05, **<0.01and ****<0.0001, error shown as standard deviation, n=3-11)

We repeated the previous experiment and explored if pre-incubation of the samples with the dye for 10 minutes followed by the agonist incubation would affect sensitivity (Figure 65). Under these conditions antimycin A (100 μM) again increased the MFI from 590.2±37 to 2111.2±623 (p=<0.0001) (Figure 67). Interestingly, the increase in MFI was not that different to that observed when mitoSOX was added at the assay endpoint (634.9±29 to 1840±412) (Figure 66), suggesting that assay performance was not affected by longer incubations with the dye and that the effects of antimycin A were likely maximal. In agreement with our previous findings oxLDL increased the level of superoxide in both a time and dose-dependent manner. OxLDL (200 μg/mL) increased MFI over nLDL (200 μg/mL) from 898.3±116 to 1498.7±78 (p=<0.05). Furthermore, at 120 minutes, oxLDL (50 μg/mL) increased MFI signal over nLDL (50 μg/mL) from 988.0±209 to 1576.0±296 (p=<0.05) (Figure 67). In comparison, when the dye was added for 10 minutes post agonist treatment (Figure 66), oxLDL (200 μg/mL) increased MFI over nLDL (200 μg/mL) from 617.6±49 to 1054.6±198 and at 120 minutes, oxLDL (50 μg/mL) increased MFI signal over nLDL (50 μg/mL) from 634.6±38 to 1037.2±172. Therefore, it was concluded that the differences between nLDL and oxLDL were greater when the dye was incubated for the duration of the experiment suggesting that this approach provided a better window of sensitivity. An additional advantage to using this incubation approach, is that it allows for the basal accumulation of superoxide to be assessed, here the basal superoxide signal was 590.2±37, 1025.0±282 and 1130.6±264 at 0, 90 and 120 minutes respectively, for reference background unstained signal was 487.0±2, importantly these basal signals were exceeded in all cases by oxLDL signal at the relative time points (Figure 67).
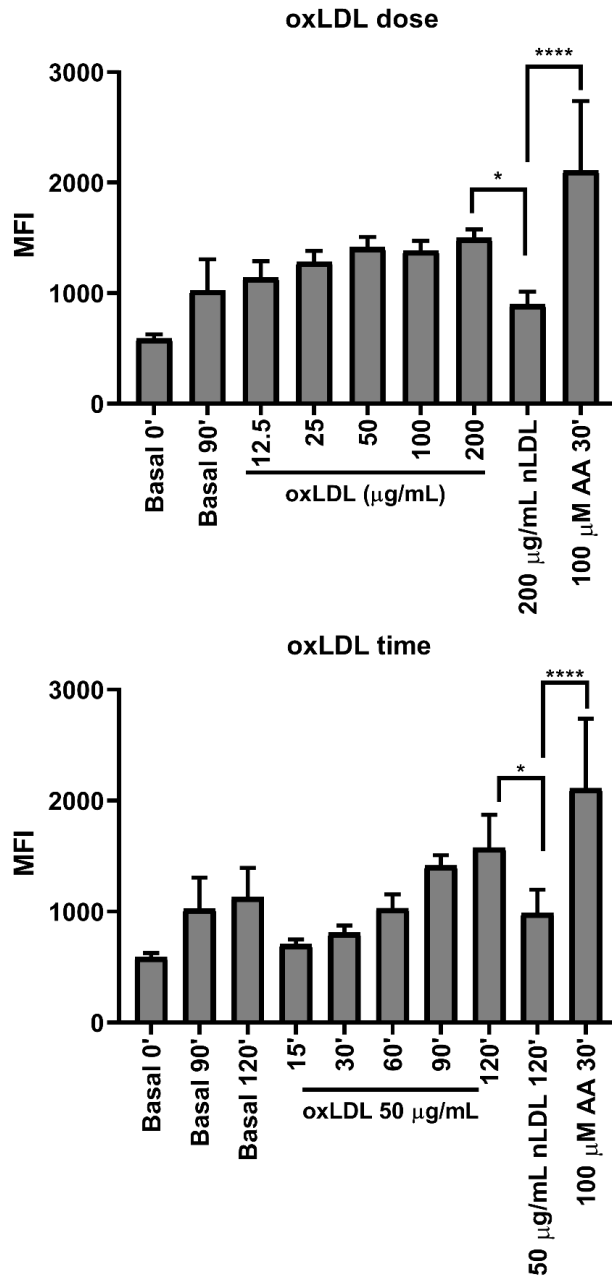
Figure 67. MitoSOX oxLDL dose and time response with assay redesign. Washed human platelets (2 x 10^6) were loaded with mitoSOX (5 µM) for 10 minutes and then treated with oxLDL or nLDL (12.5 – 200 µg/mL) for 60 minutes or with oxLDL or nLDL (50 µg/mL) for 15 – 120 minutes. Antimycin A (100 µM, 30 minutes) was used as a positive control and stained in the same way. Samples were then diluted 10x in PBS and analysed by fluorescent flow cytometry. (One-way ANOVA vs. nLDL, ns=non-significant, *<0.05 and ****<0.0001, error shown as standard deviation, n=3)

Having shown that using an assay design whereby the dye was incubated for the duration of the experiment is permissible and allows basal signal to be measured; the increased basal signal observed prompts the question of whether this assay design would allow the dye to be used as a kinetic measurement rather than the standard approach whereby single tubes are read at *x* time point and then discarded. Consequently, we compared a time response of oxLDL set up using single tubes for each condition, which were then read at *x* time point and discarded, against tubes read repeatedly for each increasing time point. Consistent with previous single tube with dye incubated throughout the time course, oxLDL (50 µg/mL) increased superoxide over time (30 – 120 minutes) which was elevated over matched basally treated time points (120 minutes) from 1130.6±264 to 1576±296 (Figure 68). Kinetic tubes also demonstrated an increase in MFI when comparing basal and oxLDL (50 µg/mL, 120 minutes) from 843.1±50 to 1526.4±143 respectively (Figure 68). The comparison between single and kinetic tubes demonstrated a similar increase in oxLDL treated superoxide signal, but the use of kinetic tubes also removed/reduced the increase in basal signal over time, where basal (120 minutes) in single tubes was 1130.6±264 and in kinetic tubes was 843.1±50.

This demonstrated that the assay could be used in a kinetic manner without the need for multiple tubes for each condition and suggested that a kinetic read ablates the error in increasing basal signal and also reduces intrinsic assay error as single tubes are read repeatedly eliminating tube-tube error. As a result, the sensitivity to measure an increase in superoxide stimulated by oxLDL was increased. Ultimately, we have shown that when dye is pre-loaded into the assay (protocol 2) and a kinetic process of measurements is used then optimal conditions are obtained.
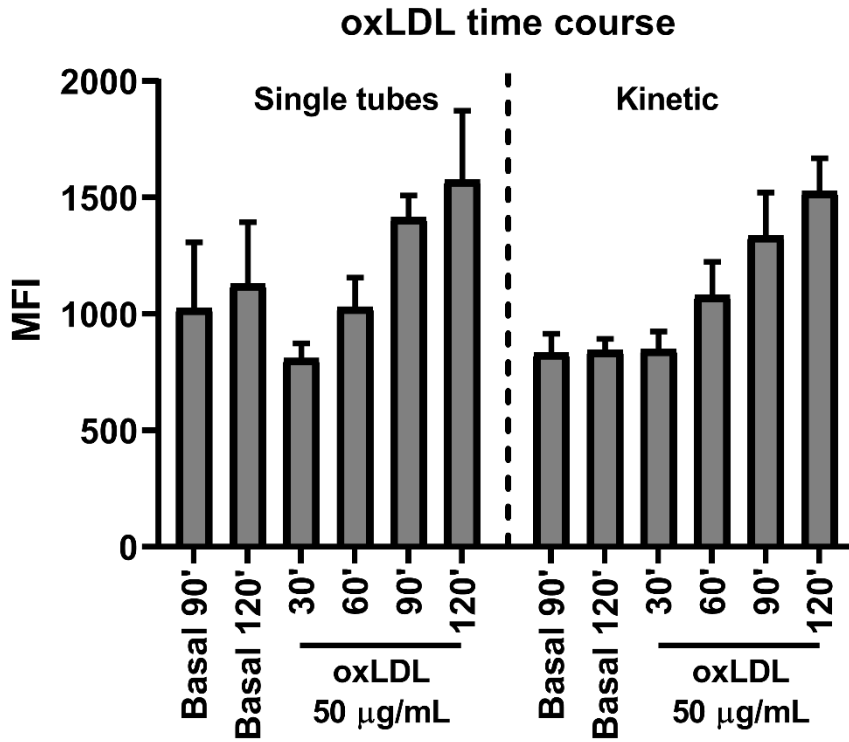
Figure 68. Single tubes versus kinetic reading. Washed human platelets (2 x 10^{6}) were loaded with mitoSOX (5 μM) for 10 minutes and then treated with oxLDL or nLDL (50 μg/mL) for 30 – 120 minutes. Antimycin A (100 μM, 30 minutes) was used as a positive control and stained in the same way. Samples were then diluted 10x in PBS and analysed by fluorescent flow cytometry, kinetic samples were single tubes from the earliest time point for each treatment that were then re-read at each subsequent time point. (Error shown as standard deviation, n=3)

5.4.2 ROS scavenger screen against oxLDL induced superoxide

The demonstration that oxLDL, but not nLDL, drove a time and dose-dependent increase in platelet mitochondrial superoxide is a novel finding. To understand this further and explore the mechanisms driving the process we used several pharmacological inhibitors to confirm the source of ROS.

We used oxLDL at a fixed dose and time point (50 µg/mL & 90 minutes) and pre-treated samples with two scavengers, the mitochondrial superoxide scavenger mitoTEMPO (mT, 100 µM) and the cytoplasmic ROS scavenger NAC (5 mM). Antimycin A (100 µM) caused a significant increase in MFI from 634.9±29 to 1839.7±412 which was significantly reduced to 952.9±107 by the presence of mitoTEMPO (p<0.0001), and therefore confirmed mitoTEMPO was an effective ROS scavenger (Figure 69). OxLDL (50 µg/mL, 90 minutes), caused a significant increase in MFI (894.4±115) over basal (634.9±29) (p<0.05) but this was not seen for nLDL (614.4±40) (Figure 69). In contrast to the effect of mitoTEMPO on antimycin A, attempts to scavenge oxLDL mediated superoxide demonstrated no significant decreases in MFI for oxLDL (894.4±115) compared to oxLDL + mitoTEMPO (774.5±125), with just a trend of reduction observed. Furthermore, the addition of NAC with oxLDL showed no difference in MFI (853.5±177), but as NAC scavenges cytoplasmic ROS and not mitochondrial superoxide this may mean it does not have access to the mitochondria. The inability of mitoTEMPO to cause a marked return to basal could be interpreted in several ways; (i) the superoxide signal from the oxLDL is false signal; (ii) the scavenging capacity of the mitoTEMPO is limited (superoxide is not returned to basal even with effective scavenging in antimycin A samples), or (iii) the mitoSOX assay is not sensitive enough to determine such subtle changes, where the increase over basal is already small (+260 a.u). However, with increased repetition of the experiment, the scavenging of oxLDL mediated superoxide would likely become more distinct. Considering the clear effects of oxLDL when compared

to the control nLDL and the non-return to basal of scavenged antimycin A superoxide,

an informed assumption suggests the issue is a combination of points ii and iii.
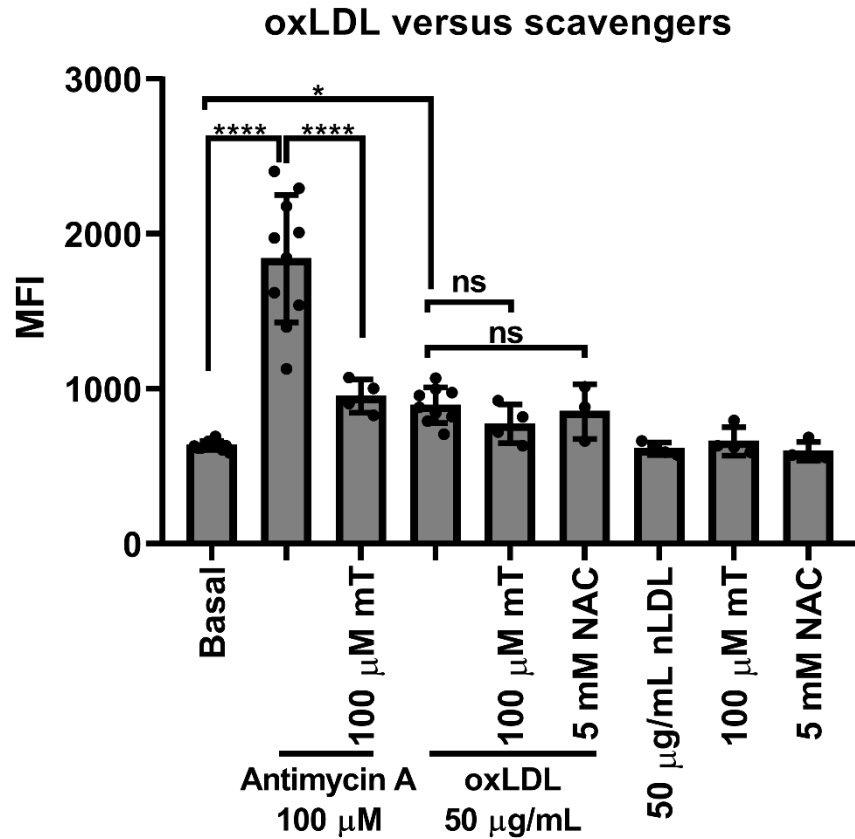
Figure 69. MitoSOX treated with ROS scavengers. Washed human platelets (2 x 10^6) were treated with oxLDL or nLDL (50 µg/mL) for 90 minutes prior to incubation with mitoSOX (5 µM) for the final 10 minutes of incubation. Antimycin A (100 µM, 30 minutes) was used as a positive control and stained in the same way. In some cases, samples were pre-incubated with mitoTEMPO (mT) (100 µM, 20 minutes) or N-acetyl-cysteine (5 mM, 20 minutes) prior to agonist addition. Samples were then diluted in PBS 10x and analysed by fluorescent flow cytometry. Individual donors are shown as superimposed points over each bar. (One-way ANOVA vs. shown, ns=non-significant, *<0.05 and ****<0.0001, error shown as standard deviation, n=3-11)

5.5 MURINE MITOCHONDRIAL SUPEROXIDE

5.5.1 Murine antimycin A dose and time

Having confirmed that superoxide production in mitochondria mediated by oxLDL is increased in human platelets, we next sought to replicate this study using a murine model. Here we wanted to validate the mitoSOX assay in murine platelets, so that we could later screen transgenic or diet-fed murine platelets. In washed wild type murine platelets, we performed time and dose responses against antimycin A.

Antimycin A (1 – 10 µM), caused a dose dependent increase in MFI, with maximal effects over basal observed at 10 µM (2016.2±137 vs. 1244.6±310, 10 µM vs. basal). Using a constant 10 µM concentration of antimycin A, a time dependent increase in superoxide production was observed with MFI increasing from 622.7±25 at basal to 931.9±65 after 1 minute ($p<0.05$) and 2295±159 after 60 minutes ($p<0.0001$) (Figure 70). The increase in superoxide occurred rapidly after just 1 minute of treatment and the MFI measured at every treated time points were significantly different to the basal at 0 minutes (Figure 70). Specifically, for time-matched comparison, the MFI at 60 minutes basal was 1244.6±310 and after 60 minutes of antimycin A treatment had increased to 2294.8±159 (Figure 70).
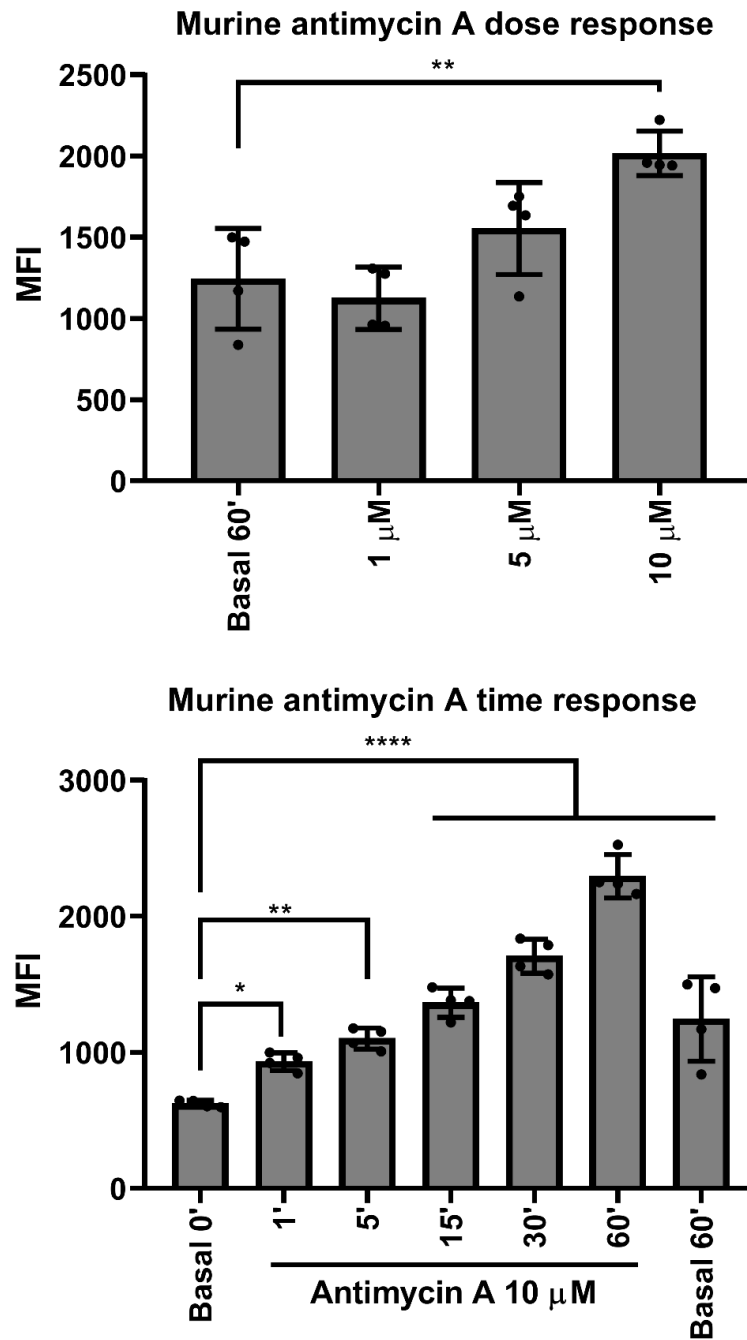
Figure 70. Murine mitoSOX antimycin A dose and time response. Washed murine platelets (2 x 10^6) were loaded with mitoSOX (5 µM) for 10 minutes and then treated with or without antimycin A (1 – 10 µM) for 60 minutes or with or without antimycin A (10 µM) for 1 – 60 minutes. Samples were then diluted 10x in PBS and analysed by fluorescent flow cytometry. Individual mice are shown as superimposed points over each bar. (One-way ANOVA vs. basal, *<0.05, **<0.01 and ****<0.0001, error shown as standard deviation, n=4)

5.5.2 Platelet mitochondrial superoxide in murine models of atherosclerosis

Having validated the applicability of the mitoSOX assay in wild type murine platelets we tested if platelet superoxide generation was altered in genetically instigated hyperlipidaemia. For this, we first compared wild type animals against the transgenic ApoE$^{-/-}$ model, where mice are spontaneously hyperlipidaemic, inflammatory and develop early atherosclerotic plaques (Getz and Reardon, 2006). MFI for mitoSOX increased from 710.2±78 for wild type murine platelets to 1135.8±308 for the ApoE-/- platelets (p<0.01) (Figure 71). Further investigation using a double knockout model deficient in GP91 a component of NOX2, ApoE/GP91$^{-/-}$ confirmed that basal superoxide was derived from mitochondrial sources, and not the cytoplasmic ROS generator NOX2 (Magwenzi et al., 2015). Similar to the ApoE, and in support of that observation, this double knockout also had increased platelet mitochondrial superoxide above wild type (1110.5±151) (p<0.05), indicating that NOX2 was not responsible for superoxide production under these conditions but the effects of ApoE knockout were conserved (Figure 71). This demonstrated that platelets from mice under lipid and inflammatory stress demonstrate increased basal superoxide.
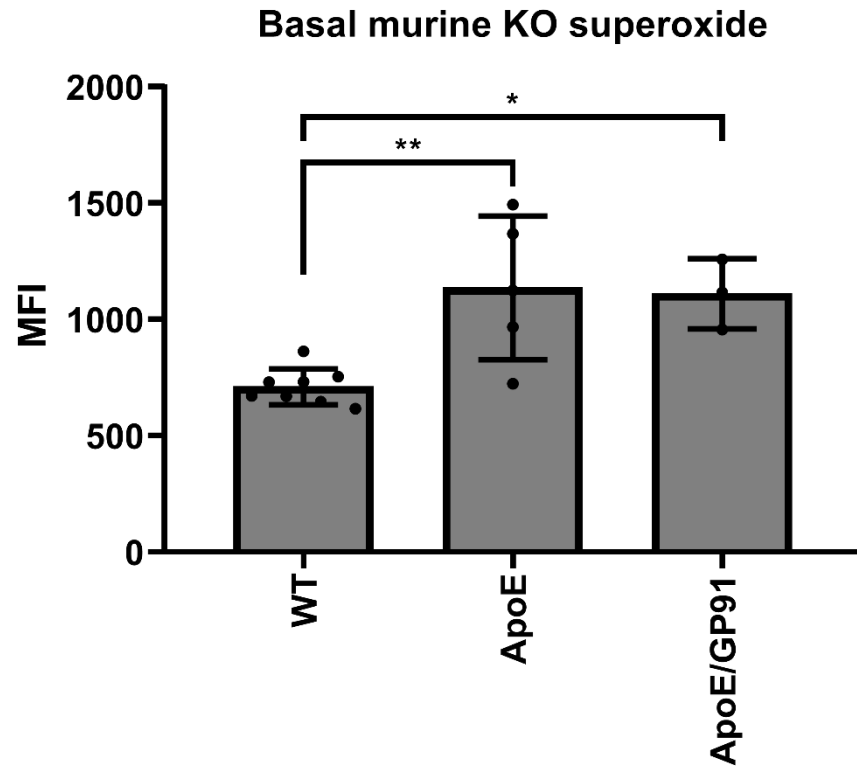
Figure 71. MitoSOX basal superoxide in murine models of atherosclerosis.
Washed murine platelets (2 x 10^6) were loaded with mitoSOX (5 µM) for 10 minutes. Samples were then diluted 10x in PBS and analysed by fluorescent flow cytometry. Individual mice are shown as superimposed points over each bar. (One-way ANOVA vs. basal, *<0.05 and **<0.01, error shown as standard deviation, n=3-8)

5.6 PLATELET MITOCHONDRIAL MEMBRANE POTENTIAL

Mitochondrial membrane potential can be used as a measure of the hyper-, normo- or hypopolarisation of the mitochondria (Joshi and Bakowska, 2011). Hypopolarisation is a collapse of the gradient across the mitochondria, this is often a pre-cursor to apoptosis. Hyperpolarisation describes an increase in the mitochondrial electrochemical gradient and may drive mitochondrial hyperactivity. Both events are likely to lead to an increased production of mitochondrial superoxide. Having shown that oxLDL can induce changes in mitochondrial function and drive superoxide production, we explored other measures of mitochondrial dysfunction to confirm these findings and further understand the involvement of oxLDL in mitochondrial superoxide formation. Specifically, we explored the effects of lipid stress on mitochondrial membrane polarisation.

5.6.1 TMRE titrations

TMRE is a dye which collects within mitochondria against an electrochemical gradient, therefore it can be used as a marker of mitochondrial hyperpolarisation or depolarisation (Joshi and Bakowska, 2011). TMRE is incompatible with whole blood and therefore must be used with washed cells. To optimise assay design for accurate discrimination between normally polarised platelet mitochondria and depolarised or hyperpolarised platelet mitochondria the dye was titrated to determine the optimum staining concentration. Here we determined that 50 nM of TMRE dye, staining 2 x 10^6 washed platelets was the optimum concentration compared to the FCCP (20 µM) control (Figure 72). This was determined based on the largest fold-decrease between the stained and the FCCP treated sample, where FCCP was used to induce depolarisation and therefore prevent TMRE accumulation and drive a decrease in TMRE signal (Toninello and Siliprandi, 1982). At 20 minutes incubation with 50 nM of dye, there was a 3-fold decrease in fluorescence. Comparatively, at excess levels

of dye, the higher concentration drove increased accumulation of the dye which then became insensitive to changes in mitochondrial membrane potential. For example, using 400 nM over 20 minutes resulted in only a 1.1-fold decrease.

In order to translate these findings to murine models of obesity, dyslipidaemia or genetic knockouts as previously used in mitoSOX studies, TMRE was also titrated in murine platelets. We determined that, in similarity to human samples, 50 nM of TMRE dye staining 2×10^6 washed platelets for 20 minutes was the optimal concentration over FCCP (20 µM) control demonstrating a 3-fold decrease in fluorescence when treated with FCCP (Figure 73).
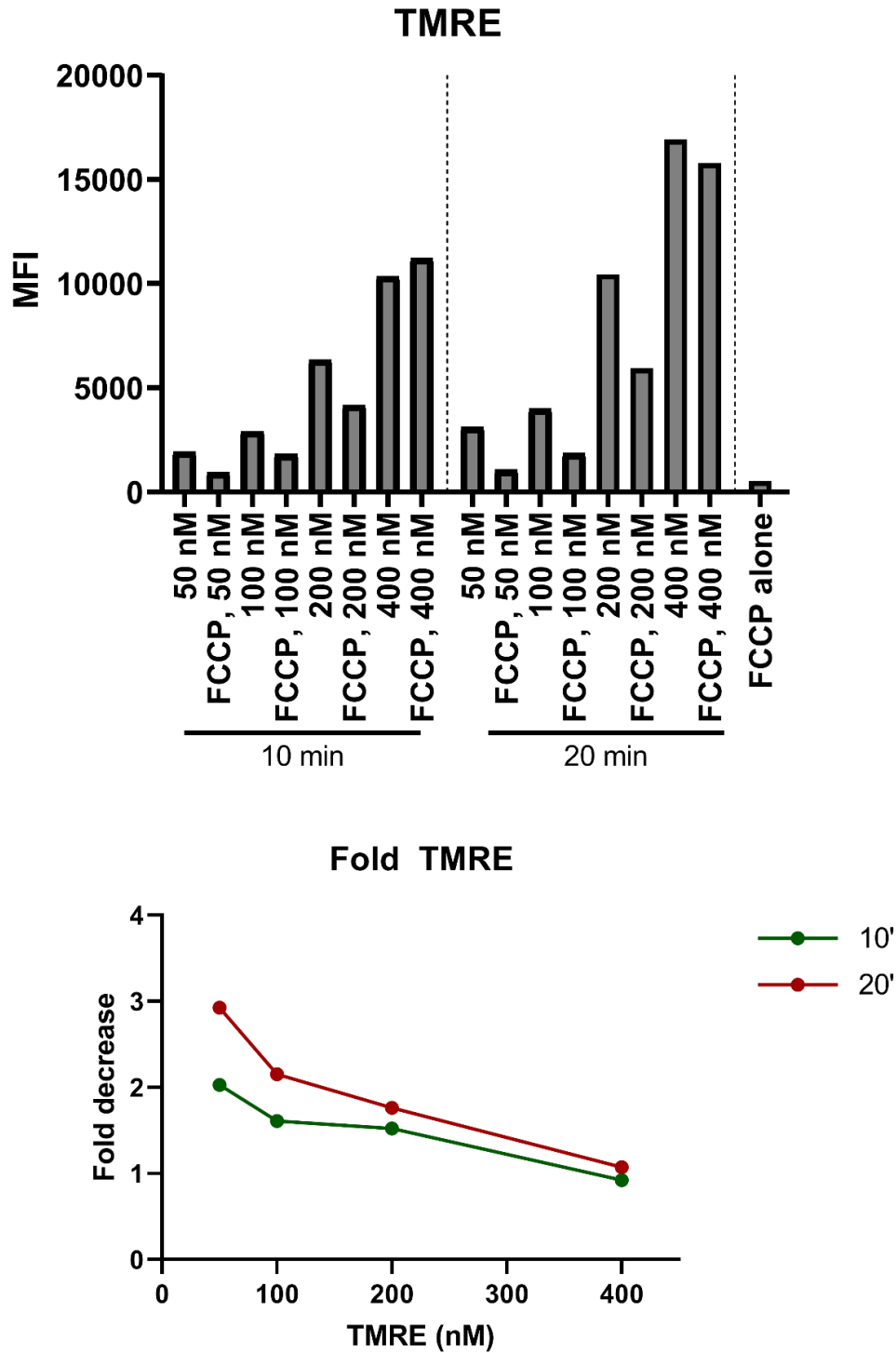
Figure 72. Titration of TMRE. Washed human platelets (2 x 10^{6}) were pre-treated with or without FCCP (20 µM) for 20 minutes and then stained with TMRE (50 – 400 nM) for 10 or 20 minutes. Samples were then diluted 10x in PBS and analysed by fluorescent flow cytometry. Total MFI and fold over matched control are shown. (n=1)
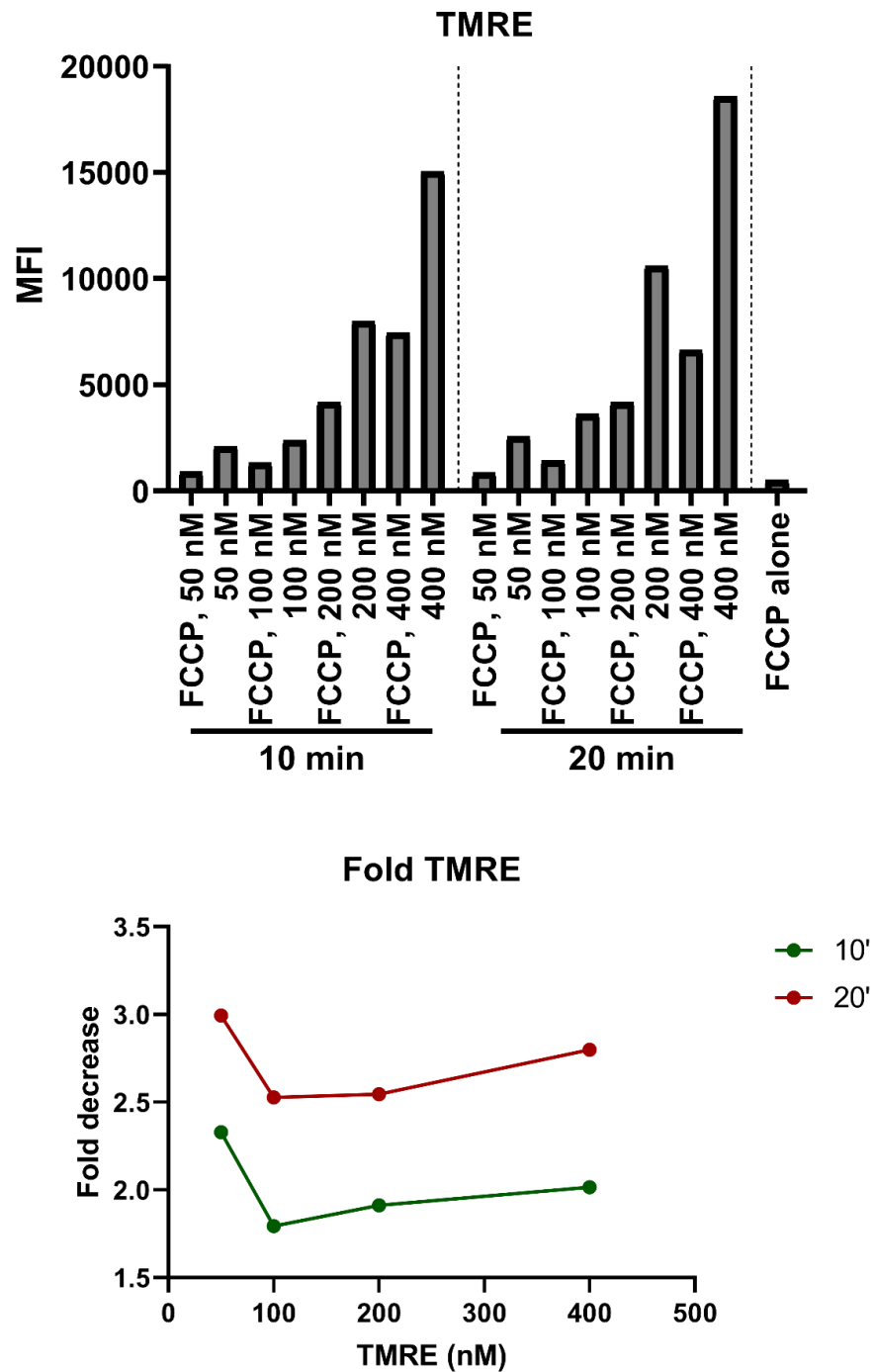
Figure 73. Murine TMRE titration. Washed murine platelets (2 x 10⁶) were pre-treated with or without FCCP (20 µM) for 20 minutes and then stained with TMRE (50 – 400 nM) for 10 or 20 minutes. Samples were then diluted 10x in PBS and analysed by fluorescent flow cytometry. Total MFI and fold over matched control are shown. (n=1)

5.6.2 OxLDL and mitochondrial membrane potential

Having confirmed that TMRE is an assay which is sensitive to changes in mitochondrial membrane potential in platelets, the next step was to identify if oxLDL influenced mitochondrial membrane potential in addition to superoxide production. Platelets ($2x10^6$ cells) were treated with oxLDL and nLDL (50 µg/ml) and changes in membrane potential were measured over time, including a 90-minute time point, which is comparable with the time point at which the majority of mitoSOX studies were performed.

FCCP (20 µM) caused a significant decrease in MFI, from 5451.5 to 580.1 after 90 minutes, which indicated a clear shift from normopolarised to hypopolarised mitochondria and loss of TMRE signal. This was observed for all time points where FCCP induced depolarisation of the platelet mitochondria. Furthermore, across the course of the experiment (0 – 180 min) basal polarisation decreased – although this did not reach the level of staining indicated as depolarised (FCCP treated) across time points tested (Figure 74). This steady loss of mitochondrial membrane potential could be explained by, or explain the short half-life of the washed platelet which typically begin losing function beyond 360 minutes of 37°C storage.

In contrast to FCCP, oxLDL significantly increased the TMRE signal at all time points measured over both basal (5451.5 to 9861.8, 90 minutes) and the control nLDL treated samples (5222.8), which suggests that oxLDL is driving significant mitochondrial hyperpolarisation in platelets. A key control was the dual FCCP/oxLDL treated sample, which demonstrated a total loss of fluorescent signal indicating that the increased MFI was neither autofluorescence of the LDL particles or binding of TMRE to LDL. After treatment with nLDL, polarisation remained consistent with time matched basal at 90 minutes but increased against time matched basal after 180 minutes. This suggested that at the longer time points nLDL could be maintaining some mitochondrial membrane potential, but vitally it did not exceed the initial basal

(0 minutes) MFI reading, which demonstrated nLDL does not drive hyperpolarisation while oxLDL convincingly does (Figure 74).
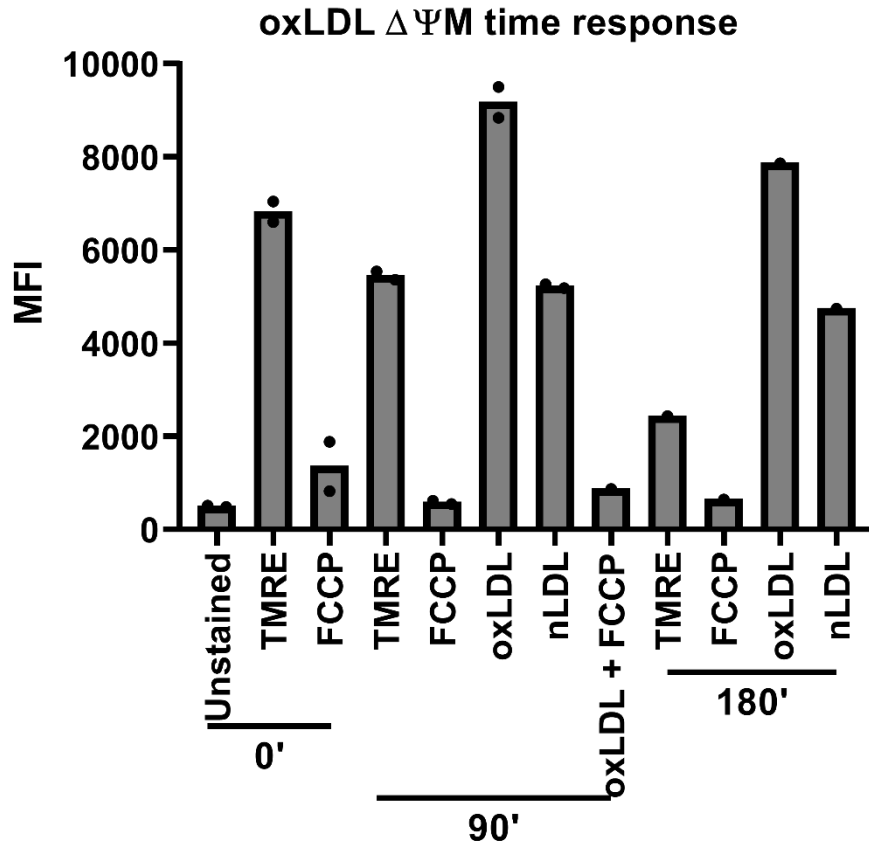
Figure 74. TMRE oxLDL time course. Washed human platelets (2 x 10^{6}) were pre-treated with or without FCCP (20 µM) for 20 minutes and/or treated with oxLDL or nLDL (50 µg/mL) for 0 – 180 minutes. Samples were then stained with TMRE (50 nM) for the final 20 minutes. Samples were then diluted 10x in PBS and analysed by fluorescent flow cytometry. Individual donors are shown as superimposed points over each bar. (n=1-2)

5.7 MURINE PLATELET MITOCHONDRIAL FUNCTION IN DIET-INDUCED OBESITY

In sections 5.4, 5.5 and 5.6, we concluded that oxLDL causes increased mitochondrial superoxide and mitochondrial membrane polarisation. Therefore, we sought to examine if western diet-induced obesity influenced murine platelet mitochondrial function. 8-week old C57/Bl6 mice were fed for up to 16 weeks with either normal chow or a western diet (WD) (45% fat). Several parameters were measured from these mice including; systemic changes such as weight, insulin resistance and glucose tolerance, and platelet function; mitochondrial superoxide, mitochondrial membrane potential, activation and platelet-monocyte interactions (activation and PMA data not shown). This approach allowed a deep phenotyping of the effects of obesity in C57/Bl6 mice caused by a prolonged western diet.

5.7.1 Systemic characteristics

We were able to measure several features to characterise the systemic phenotypes of these animals prior to platelet phenotyping. These included weight, post-prandial hyperglycaemia and insulin tolerance. This range of tests allowed an evaluation of the animal and diagnoses of obesity and/or type 2 diabetes which are both conditions likely to be induced by a western diet. C57/Bl6 mice fed a western diet put on weight at a greater rate than normal chow-fed animals and this was significantly different ($p<0.005$) at 11 weeks of feeding (Figure 75, weight). A test for post-prandial hyperglycaemia induced by fasted glucose bolus, or a glucose tolerance test (GTT) is a typical test for type 2 diabetes used in human diabetes and endocrine clinics. After 13 weeks of being fed a western diet (WD), fasting blood glucose was 7.7±1.3 mmol/L which was significantly higher than for normal chow (NC) fed mice (4.7±0.6 mmol/L). In addition WD showed a diminished reduction over time and remained more different to 0 minute basal at 120 minutes (14±1.8 mmol/L WD 120 minutes *vs*. 8±0.7 mmol/L NC 120), indicating that the mice are in a state of pre-diabetes (Figure

75, GTT). Insulin tolerance is another hallmark of cardiometabolic disease (Golia et al., 2014), and can be tested by an insulin tolerance test (ITT), where an injection of insulin is provided and response in blood glucose measured. After 13 weeks of feeding, the resting blood glucose was again demonstrably different between the two feeding regimes, with 10.6±1.3 mmol/L for NC and 13.6±1.6 mmol/L for the WD fed mice (p<0.005). However, there was no significant difference in response to insulin suggesting the mice are likely not diabetic (Figure 75, ITT).
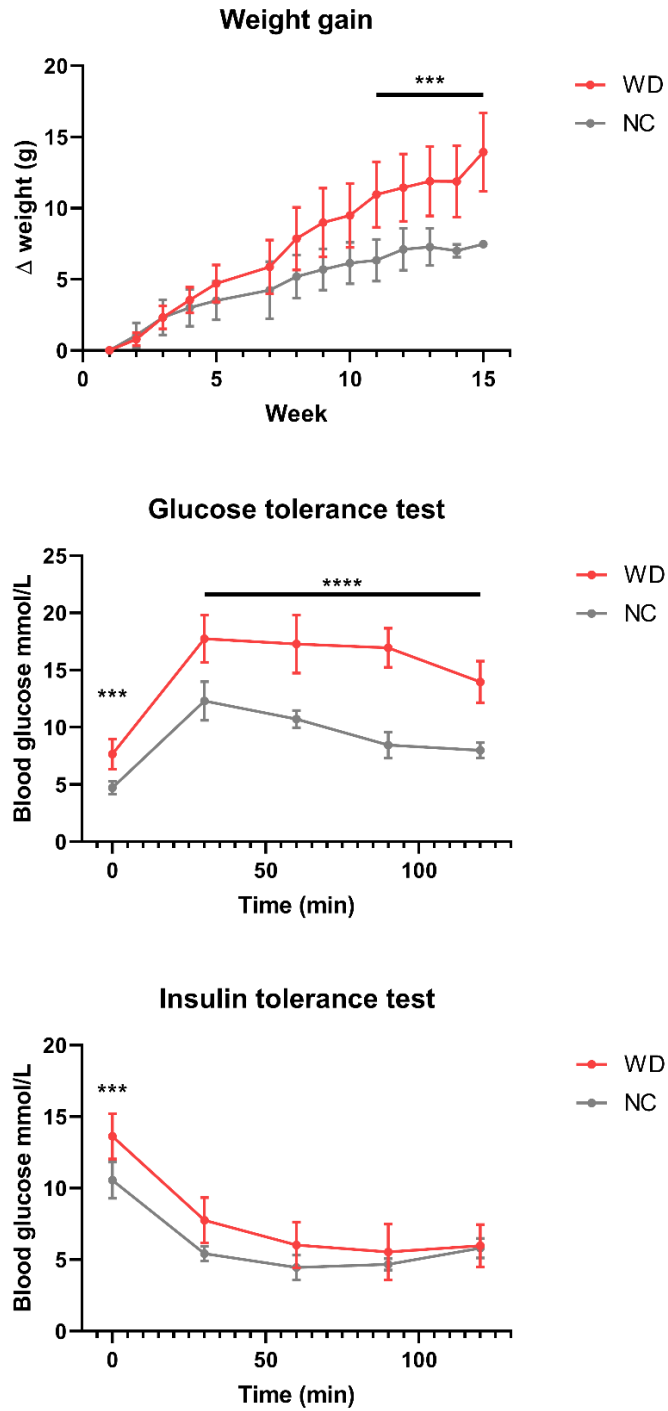
Figure 75. Analysis of systemic changes in a murine model on western diet. Murine delta (Δ) weight measured over 16 weeks of western diet feeding. Glucose tolerance test and insulin tolerance test, both done at 13 weeks western diet feeding. (Multiple T-tests with Holm-Sidak multiple comparisons, ***<0.005 and ****<0.0001, error shown as standard deviation, Weight NC n=3, WD n=4; GTT n=5; ITT NC n=4, WD n=5)

5.7.2 Platelet mitochondrial function in hyperlipidaemic mice

Platelet mitochondrial function was examined in both WD and normal chow fed mice after 8 and 16 weeks of feeding using the optimised mitoSOX and TMRE assays. There were no differences in mitoSOX at basal levels or in response to antimycin A (10 μM) between the two feeding regimes at 8 weeks (Figure 76, 8-week mitoSOX). After 16 weeks there was a trend that platelets from WD fed mice had a greater response to antimycin A, where NC platelet response was 2495.8±417 compared to 2906.4±465 from WD platelets, but this was not statistically significant (Figure 76, 16-week mitoSOX). Whilst a phenotype had been anticipated but not observed we can be confident in these results, since mitoSOX increased when treated with antimycin A and was scavenged by mitoTEMPO indicating the assay was functioning correctly.

When platelet mitochondrial polarisation was measured by TMRE, we again found no significant difference in fluorescence between the feeding regimes after 8 weeks (Figure 76, TMRE). At 16 weeks there was evidence of a small increase in basal mitochondrial membrane potential for the WD fed mice, from NC at 3668.5±643 to WD at 4129.5±456, but again this was not significant (Figure 76, 16-week TMRE).
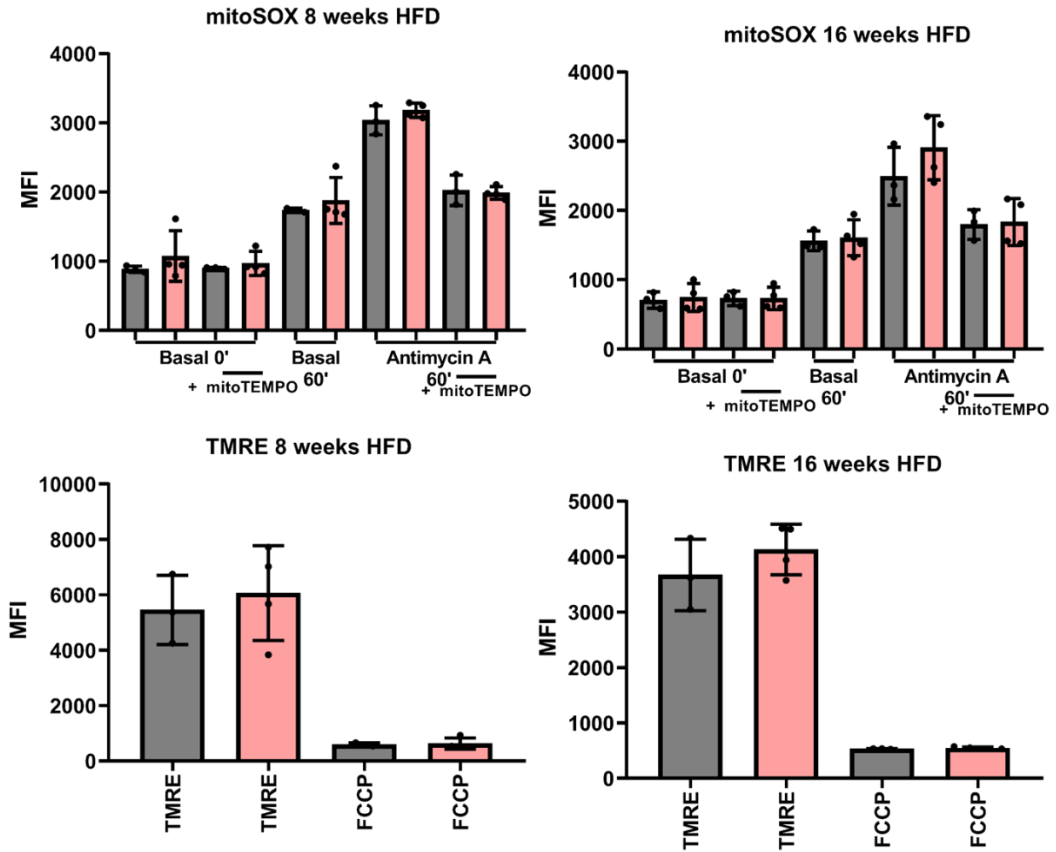
Figure 76. Mitochondrial superoxide and membrane potential in an 8 and 16-week fed DIO murine model. Grey bars, NC. Pink bars, WD. MitoSOX and TMRE staining were performed on murine washed platelets at 2x10⁶ per tube as previously described, mitoSOX was loaded prior to agonist addition. Treatments included positive control antimycin A, negative controls mitoTEMPO and FCCP for mitoSOX and TMRE respectively. Individual mice are shown as superimposed points over each bar. (Error shown as standard deviation, NC n=3, WD n=4)

5.8 DISCUSSION

While we did not pursue the NLRP3 inflammasome directly any further, primarily due to assay limitations and the requirement of murine knockout models, we were able to demonstrate that oxLDL had a distinct effect over nLDL on FLICA signal which was dependent on calcium and ROS (chapter IV). Calcium is key to the regulation of many cellular processes including mitochondrial function itself, and ROS are produced in platelets from several sources, but predominantly NADPH oxidases and the mitochondria (Schulz et al., 2014). Mitochondria are also involved in the regulation of inflammasome activity (Zhou et al., 2011) and were implicated in the initial observation regarding the platelet inflammasome (Hottz et al., 2013). Therefore, we explored what effects oxLDL may be having on mitochondrial metabolism and homeostasis in platelets, to this end we specifically measured mitochondrial superoxide production and mitochondrial membrane potential.

OxLDL, but not control nLDL, was found to induce platelet mitochondria to produce superoxide, detected by fluorescent mitoSOX. This is a novel finding and has never been observed before in platelets. Furthermore, a second new observation demonstrated that oxLDL stimulated increased mitochondrial membrane potential detected by fluorescent TMRE and maintained this polarisation over basal and control nLDL for up to 3 hours (longest time point measured). While not definitive, these two observations could suggest that the increased superoxide production is linked to the ability of oxLDL to induced mitochondrial hyperpolarisation. To determine the kinetics of the relationship between polarisation and superoxide production, co-incubation with oxLDL and mitoTEMPO followed by measurement of polarisation would suggest if polarisation occurred prior to superoxide production (and is therefore unaffected by scavenging) or is driven by changes in superoxide production (and is therefore protected by scavenging).

To explore the mechanistic aspects of oxLDL on mitochondrial superoxide production, we first applied the general ROS scavenger NAC and the mitochondrial specific scavenger mitoTEMPO. Here we were able to show that mitoTEMPO significantly reduced the superoxide produced by the positive control antimycin A, however it did not drive a significant reduction in oxLDL mitochondrial superoxide, although there was a trend towards a reduction in signal. It was possible that these observations were due to the small margin of increase induced by oxLDL, which reduced the opportunity to detect a significant inhibition of signal. Interestingly, mitoTEMPO never fully decreased the maximal effects of antimycin A of superoxide generation, and there is also the possibility that the scavenger is not able to fully deplete the mitochondria of superoxide. In a second approach, we found that oxLDL consistently induced hyperpolarisation of the mitochondria. Together we were able to confirm that oxLDL, through a currently unknown mechanism drives mitochondrial superoxide production and hyperpolarisation. The functional consequence of this mitochondrial dysfunction downstream of oxLDL remains unclear. However, there are suggestions in the literature that mitochondrial dysfunction is key to regulating NLRP3 inflammasome activity (Zhou et al., 2011, Hottz et al., 2013). Furthermore, oxLDL driven mitochondrial dysfunction is perhaps unlikely to affect platelet function itself, as several pathways for oxLDL driven platelet hyperactivity have been described and phenotypes rescued with no reference to mitochondrial superoxide (Berger et al., 2019a, Magwenzi et al., 2015, Wraith et al., 2013). In addition to this, a recent study has shown that platelet function is not perturbed by a superoxide dismutase 2 (SOD2/Mn$^+$ SOD) platelet specific knockout model either *in vitro* or *in vivo* (Fidler et al., 2017). These data in conjunction with the results described in this chapter suggest platelet mitochondrial dysfunction likely controls aspects of platelet function beyond (oxLDL-mediated) haemostatic function. In the future however, this work must all be repeated using the now optimised mitoSOX conditions, namely pre-loading of cells with the permeant superoxide dye followed by kinetic reading of each

treatment condition over time, as this has been shown to increase the sensitivity of the assay. A striking finding was the effect of oxLDL on mitochondrial membrane potential, therefore this study must be pursued and repeated, firstly to validate these findings and then to explore the pathways leading to this effect and also the outcomes of the mitochondrial hyperpolarisation.

While we were able to demonstrate that extracellular oxLDL treatment *in vitro* could drive a mitochondrial phenotype, we wanted to ask if this phenotype was also apparent in platelets from mice which were both inflammatory and hyperlipidaemic – a suitable environment for the production of circulating oxLDL (Kato et al., 2009). Therefore, we applied these experimental questions to murine platelets of the following genotypes. We compared wild-type C57/Bl6, ApoE [-/-] and ApoE/GP91 [-/-] mice, where ApoE knockouts are a model of hyperlipidaemia and atherosclerosis (Kirii et al., 2003), and GP91 are deficient in the major platelet source of cytoplasmic ROS, NOX2 (Magwenzi et al., 2015). Basal mitoSOX in C57/Bl6 mice was consistent across all animals tested. However, when compared with ApoE [-/-] and ApoE/GP91 [-/-] mice, there was a significant increase in superoxide in the mice under hyperlipidaemic stress. Furthermore, the inclusion of ApoE/GP91 [-/-] validated the model as independent of NOX2, which has been shown previously to be stimulated by oxLDL in platelets to produce ROS (Magwenzi et al., 2015). These differences in platelet mitochondrial biology between the transgenic mice requires further phenotyping and the inclusion of controls to scavenge superoxide. A further vital control to be pursued include a measurement of mitochondrial mass (Zhang et al., 2019), where this increase in signal from these murine platelets may potentially not caused by an increase in superoxide, but rather an increase in mitochondrial mass which in turn drives greater dye collection and therefore greater signal. Indeed, such a dramatic increase in platelet mitochondrial mass would be equally interesting in this context. These novel findings suggest that platelets circulating in murine models with

increased lipid stress, and likely circulating oxLDL (Kato et al., 2009), are metabolically and functionally different from a healthy donor C57/Bl6.

To examine our previous observation in transgenic mice further, we applied our experimental approach to western diet-fed C57/Bl6 mice at 8 and 16 weeks of western diet. This western diet model induces a hyperlipidaemic phenotype which is considerably milder than ApoE $^{-/-}$, particularly in terms of the inflammatory profile (Getz and Reardon, 2006). We were able to demonstrate that in the western diet-induced model of obesity, the C57/Bl6 mice put on weight at an increased rate over normal chow. Further analysis suggested that 11-weeks of feeding also showed increased resting blood glucose and diminished glucose tolerance but without marked insulin resistance. Beyond systemic changes to the mice, we also measured for changes in mitochondrial characteristics between the two groups at both 8 and 16 weeks of feeding using mitoSOX and TMRE to measure mitochondrial superoxide and membrane potential respectively. At both time points, 8 and 16-weeks, there were no significant differences between the normal chow and western diet-fed groups, although, at both stages there was a trend towards an increase in mitochondrial superoxide when stimulated with antimycin A and also increased basal mitochondrial membrane potential for the WD fed mice compared to the NC mice. Reassuringly these trends developed further when comparing them at 8 and 16-weeks. This pilot study has highlighted the critical difference between western diet induced models against transgenic models, suggesting that in less severe environments of only dietary pressure, platelets have a capacity to resist dysfunction. In interpretation, these results could point towards different phenotypes, for example; capacity for mitochondrial superoxide production is increased, mitochondrial membrane potential has increased, or tying the two together in a phenotype where mitochondrial mass has increased which in turns leads to a greater potential reading (due to there being more mitochondria to stain) and a greater superoxide production (as there is more mitochondrial surface area). Therefore this study would require

additional confirmation of mitochondrial mass changes, measured by either transmission electron microscopy (TEM) (Obydennyi et al., 2019) or fluorescent dye (Zhang et al., 2019). This study could also be further enhanced by understanding how mitochondrial function itself is changing in the presence of oxLDL, notably by the bioenergetic measurements of extracellular acidification rate and oxygen consumption rate as markers of glycolysis and oxidative phosphorylation respectively (Aibibula et al., 2018). The data in terms of increased platelet mitochondrial membrane potential in WD may tie in with a study in humans with cardiovascular disease, where monocytes bound to platelets were shown to have increased mitochondrial membrane potential (Vogel et al., 2015), although this could be from the platelets, monocyte or both cells, as the experiments in that study lacked the appropriate controls to confirm the source of changes in membrane potential (Vogel et al., 2015). Although we were unable to replicate the basal mitochondrial superoxide finding of the ApoE [-/-] models, the differences in systemic phenotype of the animals must be considered, where the knockout model is more severe (Getz and Reardon, 2006) – however it is likely a viable option to repeat this feeding study on animals with an ApoE [-/-] background to increase the potential for measuring a phenotype and repeat mitoSOX, and vitally measured mitochondrial membrane potential (TMRE) and add an additional marker of mitochondrial mass. The use of TEM (Obydennyi et al., 2019) and fluorescent dye (Zhang et al., 2019) to measure mass in conjunction would provide data on; mass, morphology, autophagy, fission and fusion simultaneously, all of which have the potential to be affected in a hyperlipidaemic environment (Dose et al., 2016). Alternatively, the relatively simple approach of continuing to use mitoSOX and TMRE but also measuring these by fluorescent microscopy would allow for mitochondrial mass and mitochondrial number to be evaluated.

In summary, we described that oxLDL, but not nLDL, can drive an increase in platelet mitochondrial superoxide and membrane potential. Furthermore, in murine models

of transgenic hyperlipidaemia, there is a phenotype of increased mitochondrial superoxide. However, in diet induced obesity models this is only mildly recapitulated and a trend towards increase mitochondrial superoxide and membrane potential. This work requires further exploration of mechanisms involved in the transduction of oxLDL signal, alongside other changes which may occur in the mitochondria by alternative methods and finally investigation into hyperlipidaemic human donors to measure if these modifications to platelet mitochondria are present.

Chapter 6
Conclusions and future studies

6.1 PLATELET REGULATION AND SUBPOPULATIONS

The application of novel multidimensional analysis to four parameter platelet fluorescent flow cytometry is a considerable innovation for platelet biologists. Typically, the majority of platelet fluorescent flow cytometry is done using single parameter assays, this not only limits the data rich potential of the technique, but it prevents true comparisons between markers on single cells and implicates a lack of platelet marker controls in each experiment. There are exceptions to this general statement, these include the very high parameter application of CyTOF (Blair and Frelinger, 2019, Blair et al., 2018) and other multicolour fluorescent flow cytometry studies (Reddy et al., 2018, Sodergren and Ramstrom, 2018), however the field is still immature compared to cellular immunology where up to 20 parameters are routinely applied (Cossarizza et al., 2017). Some groups are however publishing guidelines to both advance and standardise best practice in platelet cytometry (Spurgeon and Naseem, 2019, Frelinger, 2018, Welch et al., 2018, Ramstrom et al., 2016, Harrison, 2009, Harrison et al., 2011). The biggest innovation has undoubtedly come from the recent analysis of platelets by CyTOF, although the applications of CyTOF are powerful (Blair and Frelinger, 2019, Blair et al., 2018), a major caveat is the lack of accessibility to mass cytometers, therefore we sought to apply novel analytical techniques to fluorescent flow cytometry, an instrument that the majority of platelet biologists have access to. Since our initial study validated the potential of these analytical innovations paired with four parameter assays and resulted in the discovery of rare subpopulations of platelets, we believe this should stimulate the field to implement these techniques and continue to investigate and innovate modern assay design and analytical approaches.

Through the measurement of multiple markers simultaneously, we were not only able to describe subpopulations and define subsets within large subpopulations, but also

able to describe differences in PGI$_2$-cAMP regulation of aspects of platelet activation. Reassuringly a recent study, using single colour flow cytometry paired with LTA suggested there may well be differences in inhibition of different platelet markers of activation (Macwan et al., 2019). We took this further and demonstrated a dichotomy in granule secretion and integrin activity or PS exposure through four parameter assays with validation by alternative markers. We suggested this plays a role in the inhibitory vascular environment in allowing immunomodulatory platelet: monocyte interactions but preventing thrombotic platelet: platelet interactions. We further applied some mechanistic studies to confirm that PGI$_2$-cAMP protects mitochondria, preventing depolarisation upstream of PS exposure and that CD62P is expressed on the cell surface independent of robust inhibitory signalling indicated by pVASP-s157.

6.1.1 Future studies

While several approaches were taken to confirm that cAMP signalling was preserved and that CD62P is independent of cAMP-signalling further studies could describe the mechanism by which this occurs.

A primary question is how calcium signalling is regulated in the context of excess activation and inhibition. While aspects of calcium signalling are known to be independent of cAMP-signalling (Fung et al., 2012), it would be advantageous for this study if a calcium dye could be used to understand the flux of calcium and how this may compare under conditions where potent inhibition has blunted integrin $\alpha_{IIb}\beta3$ activity and inhibited PS exposure but where granule secretion has continued. Indeed, if residual calcium signal correlated with granule secretion that would suggest a mechanism of action and suggest granule secretion is less dependent on calcium than other hallmarks of platelet activation.

As the novel subset we described has previously been suggested to exist in murine platelets (Topalov et al., 2012) and was subsequently suggested to be a result of

platelet doublets (Choo et al., 2017) forming between PS^{hi} and integrin $\alpha_{IIb}\beta3^{hi}$ platelets, we validated this by a doublet gate based on the increase in pulse width of doublets. However, this could further be validated using a model treated with an antagonist of integrin $\alpha_{IIb}\beta3$ (tirofiban) which does not perturb calcium levels, though this would require that integrin $\alpha_{IIb}\beta3$ activity could still be detected by PAC1 (Frelinger, 2018) in the presence of inhibitors to distinguish the PS^{hi}/$\alpha_{IIb}\beta3^{hi}$ subset.

Future studies should also look to provide a full understanding of the mechanisms by which cAMP inhibition may be targeted to discrete aspects of activation. Based on previous literature the hypothesis would be that subcellular pools of cAMP are targeted to distinct machinery within the platelets (Wehbi and Tasken, 2016, Raslan et al., 2015, Raslan and Naseem, 2015). If PKA could be demonstrated to be associated with specific aspects of the cellular biology regulating integrin $\alpha_{IIb}\beta3$ and PS exposure but not granule secretion, this would demonstrate a definitive mechanism for this study.

Additionally, with modern iterations of *in vivo* imaging approaches (Imhof et al., 2016), it should be feasible to image platelets expressing CD62P in association with monocytes, vitally in the context of tonic endothelial inhibition. This would confirm that platelet: monocyte interactions can occur independently to active cAMP-signalling.

6.1.2 Summary of findings

In this chapter, several novel findings were described by the application of fluorescent flow cytometry. Platelet subpopulations using multidimensional FIt-SNE analysis were explored, applying this analysis for the first time to platelet fluorescent flow cytometry data. This allowed a detailed description of how PGI$_2$ controls the formation of platelet subpopulations and this further elucidated a dichotomy in how PGI$_2$-cAMP

regulates aspects of platelet function, most notably differences in granule secretion when compared with integrin activation and phosphatidylserine exposure.

- First application of multidimensional analysis to platelet FFC data

- Description of platelet subsets within PS^{hi} established by fibrinogen binding

- PGI$_2$ inhibition differentially targets fibrinogen binding, PS and granule secretion

- PGI$_2$ resistant CD62P facilitates platelet monocyte interactions

6.2 NLRP3 INFLAMMASOME ACTIVATION AND EXPRESSION

The first report of the NLRP3 inflammasome was published in 2004 (Agostini et al., 2004), and it was not until 2013 that is was shown to be present and functional in human platelets (Hottz et al., 2013). To date there have been a number of papers that have described a functional role for NLRP3 in platelet biology (Boone et al., 2019, Qiao et al., 2018, Vogel et al., 2018a, Vogel et al., 2018b, Murthy et al., 2017, Vogel et al., 2017, Vats et al., 2019). We measured NLRP3 activity in platelets using the FLICA assay which fluorescently labels activated caspases. Specifically, we measured caspase-1, as caspase-1 cleavage can be used as a marker of NLRP3 activity. We used this to measure NLRP3 activity downstream of oxLDL, which has not been examined in platelets before. Previously, in response to oxLDL, platelets have been shown to express markers of activation (Berger et al., 2019b, Wraith et al., 2013). Furthermore, oxLDL has been shown to drive NLRP3 activity in other cell types (Liu et al., 2014). We were able to describe a novel potentiation of caspase-1 cleavage by oxLDL treatment that was not seen in the nLDL control, and which was dependent on ROS and Ca^{2+} (Murakami et al., 2012). Additionally, preliminary studies here suggested it is not via the well described CD36-signalosome (Berger et al., 2019b, Wraith et al., 2013). However, due to a lack of responsiveness to NLRP3 inhibitors MCC950 (Coll et al., 2015) and glyburide (Lamkanfi et al., 2009) we were unable to validate this observation as a definite marker of caspase-1 cleavage. As a result, we pursued further questions regarding the validity of the assay and found it correlated with markers of apoptosis (Pozarowski et al., 2003).

Due to concerns over the validity of the FLICA observations we sought to identify the components of NLRP3 by immunoblot; NLRP3, ASC, caspase-1, gasdermin D and IL-1β (Schroder and Tschopp, 2010). We described a potential NLRP3 band by immunoprecipitation, a splice variant of ASC by immunoprecipitation and immunoblot (Matsushita et al., 2009), caspase-1 by immunoblot, gasdermin D by immunoblot and were unable to identify IL-1β in healthy donors. We cross-referenced this with

proteomic (Burkhart et al., 2012, Zeiler et al., 2014) and transcriptomic (Rowley et al., 2011) platelet studies, which are generally not supportive of NLRP3 inflammasome expression and suggest only ASC and gasdermin D are expressed at a protein level.

6.2.1 Future studies

The findings described in this chapter, while novel, are also potentially of great impact considering the presence of oxLDL in the vasculature and the literature supporting this finding. However, they require further validation, primarily due to assay limitations.

The single series of experiments, which would validate these observations beyond doubt, require transgenic murine models. Specifically, repetition of these studies in wild type murine models compared with NLRP3 knockout and CD36 knockout murine models respectively would confirm; the FLICA assay is correct/incorrect as there is no need for biochemical inhibitors of NLRP3, and the potential lack of involvement of the CD36-signalosome, again without the need for biochemical inhibitors of the receptor and signalling apparatus.

If transgenic models were available this would further allow for enhanced identification of the proteins by immunoprecipitation, as a comparison between wild type and transgenic models would immediately demonstrate the loss or otherwise of a protein band – thereby identifying that band as the protein in question. If the proteins could be confirmed by biochemical means that would allow further studies by co-immunoprecipitation (Shi et al., 2016) to understand the conditions under which the complex is assembled and potentially co-localisation studies by high-resolution microscopy.

This is also the first description of a spliced variant of ASC in platelets, this should also be explored. The size of the variant suggests it may lack a hinge domain and

therefore be constitutively active (Matsushita et al., 2009), further studies have also suggested that variants of ASC play important roles in the regulation of NLRP3 activity, both up and down regulation (Bryan et al., 2010). Therefore, additional immunoprecipitations of ASC should be performed, and mass spectrometry should be performed to confirm that this detected band is indeed a splice variant of ASC. In addition to this RT-PCR analysis of the platelet transcriptome would also suggest if a splice variant is also expressed at a transcriptional level, further supporting this protein observation. To highlight a functional role for a splice variant of ASC, cross-linked immunoblot assays should be performed to explore whether this splice variant of ASC is constitutively oligomerised in platelets, or indeed is even able to oligomerise.

This study also identified the pore forming protein gasdermin D, gasdermin D is known to be cleaved by caspase-1 to facilitate pyroptosis (Miao et al., 2011) and subsequent release of IL-1β (Liu et al., 2016). However, within platelets, which are cells packed with pro-thrombotic proteins, growth factors and chemokines, this may represent an additional pathway to the release of platelet contents on activation. In context, it has been shown that typical platelet activity does induce NLRP3 activity (Murthy et al., 2017, Qiao et al., 2018), which would in turn suggest that gasdermin D may be cleaved and pores formed in traditional platelet activation. Therefore, further biochemical studies over the capacity of gasdermin D to be cleaved in platelets and to form pores on the surface would suggest this is a hypothesis worth pursuing.

While there have been several publications on platelet NLRP3 there has been little mechanism described to date. Open questions remain regarding the recruitment and particularly the priming of the NLRP3 inflammasome in platelets (Schroder and Tschopp, 2010). While the role of transcriptional priming is a challenging avenue within platelets, where there is some evidence this may be able to occur (Denis et al., 2005), there is clear potential for non-transcriptional priming. Non-transcriptional

priming of NLRP3 has been shown in other cells and is driven by pathways common to platelets, namely phosphorylation of ASC by Syk (Lin et al., 2015), phosphorylation of NLRP3 by JNK1 (Song et al., 2017) or de-ubiquitination of ASC (Rodgers et al., 2014) or NLRP3 (Song et al., 2016). Additional studies into the mechanism of NLRP3 activity in platelets should be followed, with emphases on the post-translational modifications of NLRP3 components and how this may regulate function in platelets.

Finally, if the model can be validated, then the propensity for NLRP3 inflammasome activity should be measured in clinically relevant murine models such as ApoE (hyperlipidaemia) or streptozotocin (diabetes) to understand if activity changes, if so, clinical human cohorts are worth pursuing, as current studies suggest the NLRP3 inflammasome plays an important role in the progression of many human diseases (Ridker et al., 2011).

6.2.2 Summary of findings

Within this chapter the FLICA assay was applied to understand how oxLDL may regulate caspase-1 cleavage downstream of postulated NLRP3 activity. A significant effect of oxLDL on the potentiation of caspase-1 cleavage was demonstrated, where nLDL had no effect and chelation of calcium or scavenging of ROS blocked this potentiation effect. The effects of inhibitors against the CD36-signalosome were further examined and demonstrated no significant inhibition of potentiation. In addition, the expression of components of the NLRP3 inflammasome were measured by SDS-PAGE. The relative expression of each constituent was determined, and this described that ASC is expressed predominantly as a truncated form and for the first-time, expression of gasdermin D in human platelets.

- OxLDL potentiates FLICA signal
- Potentiation of oxLDL-caspase-1 cleavage is likely not through the CD36-signalosome

- An ASC isoform is expressed in human platelets

- Caspase-1 and GSDMD are expressed in human platelets

6.3 MITOCHONDRIAL DYSFUNCTION UNDER LIPID STRESS

OxLDL is known to induce mitochondrial dysfunction in other cells (Zmijewski et al., 2005, Giovannini et al., 2002, Vindis et al., 2005) and mitochondrial dysfunction is also known to play a key role in NLRP3 activity (Zhou et al., 2011). Therefore, as oxLDL is known to stimulate platelets (Berger et al., 2019b, Wraith et al., 2013) and we have made an observation of NLRP3 activity in platelets (chapter IV), we explored whether oxLDL may drive mitochondrial dysfunction in platelets. We were able to show that oxLDL, but not nLDL, drives both mitochondrial superoxide production and membrane potential, and this agrees with results from other cell types that demonstrate a similar phenotype in production of mitochondrial superoxide (Chowdhury et al., 2010, Zmijewski et al., 2005) and increased mitochondrial membrane potential (Giovannini et al., 2002). We further translated this hypothesis into western-diet fed (Getz and Reardon, 2006) and transgenic ApoE $^{-/-}$ murine models (Kato et al., 2009). We observed that the more severe transgenic model drove a significant increase in mitochondrial superoxide and diet-induced drove a small increase in superoxide and membrane potential in platelets, this agrees with literature demonstrating an increase in endothelial mitochondrial dysfunction in hyperlipidaemia (Yu et al., 2012).

6.3.1 Future studies

While the results within this chapter are preliminary, they highlight some changes to platelet mitochondrial metabolism in the context of hyperlipidaemia which should be pursued. However, prior to pursuing this, they must be validated.

The basic observations regarding increases in mitochondrial superoxide or mitochondrial membrane potential with oxLDL suggested there may be a phenotype *in vivo*, which was replicated in a severe model of hyperlipidaemia in ApoE animals. This observation should be repeated and additional controls to measure

mitochondrial mass should be used, as an increase in mass may have given false positive increase in signal of superoxide. These can be pursued by fluorescence microscopy, TEM or alternative mass dyes by fluorescent flow cytometry (Zhang et al., 2019). If mass does change, this must be accounted for, however it may be that the change in mass is an important finding. Further to this, the study could be expanded to examine other aspects of mitochondrial biology including oxygen consumption rate and extracellular acidification rate (Aibibula et al., 2018), to understand if oxLDL mitochondrial dysfunction also modulates basal metabolic rate.

Mechanistically, the pathway by which oxLDL may transduce mitochondrial dysfunction should be explored, as it may be via the well described CD36-signalosome (Chen et al., 2008, Wraith et al., 2013), alone or in heteromeric complexes with TLRs (Biswas et al., 2017), or via alternative LOX1 pathways (Holy et al., 2016). A combination of biochemical inhibitors targeting these pathways should be used before immunoblotting for tyrosine phosphorylation or IRAK phosphorylation for CD36 or TLR activity respectively to validate the inhibitors. The effects they have on oxLDL induced mitochondrial dysfunction could then be explored. LOX1 as an alternative oxLDL receptor should also be explored, as it has been demonstrated to transduce signal leading to mitochondrial dysfunction in other cell types (Christ and Latz, 2014).

If the findings can be validated and the mechanism understood, it would be vital that this finding was translated to a clinical hyperlipidaemic cohort, as the defects in platelet mitochondrial metabolism may drive hyperactivity, dysfunction, or indeed NLRP3 activity (Christ and Latz, 2014).

6.3.2 Summary of findings

In chapter V, how oxLDL may mediate superoxide production within platelet mitochondria was explored. This demonstrated that oxLDL, but not nLDL, drove

mitochondrial superoxide production and increased mitochondrial membrane potential in human platelets. This study was translated into murine models, in transgenic ApoE $^{-/-}$ a significant increase in basal superoxide was observed over wild type animal. In diet-induced obesity C57/Bl6 models a trend towards increased stimulated superoxide production and membrane potential was also measured.

- oxLDL induces mitochondrial superoxide production
- oxLDL drives a mitochondrial membrane potential increase
- Murine models of dyslipidaemia show increased mitochondrial superoxide and membrane potential

References

AGBANI, E. O. & POOLE, A. W. 2017. Procoagulant platelets: generation, function, and therapeutic targeting in thrombosis. *Blood,* 130**,** 2171-2179.

AGOSTINI, L., MARTINON, F., BURNS, K., MCDERMOTT, M. F., HAWKINS, P. N. & TSCHOPP, J. 2004. NALP3 forms an IL-l beta-Processing inflammasome with increased activity in Muckle-Wells autoinflammatory disorder. *Immunity,* 20**,** 319-325.

AIBIBULA, M., NASEEM, K. M. & STURMEY, R. G. 2018. Glucose metabolism and metabolic flexibility in blood platelets. *Journal of Thrombosis and Haemostasis,* 16**,** 2300-2314.

ALBERTS, B., JOHNSON, A., LEWIS, J., RAFF, M., ROBERTS, K. & WALTER, P. 2008. *Molecular Biology of the Cell (fifth edition),* Garland Science, Taylor & Francis Group.

ALLAM, O., SAMARANI, S., JENABIAN, M. A., ROUTY, J. P., TREMBLAY, C., AMRE, D. & AHMAD, A. 2017. Differential synthesis and release of IL-18 and IL-18 Binding Protein from human platelets and their implications for HIV infection. *Cytokine,* 90**,** 144-154.

ALLEN, I. C. 2014. Non-inflammasome forming NLRs in inflammation and tumorigenesis. *Frontiers in Immunology,* 5.

ALNEMRI, E. S., FERNANDESALNEMRI, T. & LITWACK, G. 1995. CLONING AND EXPRESSION OF 4 NOVEL ISOFORMS OF HUMAN INTERLEUKIN-1-BETA CONVERTING-ENZYME WITH DIFFERENT APOPTOTIC ACTIVITIES. *Journal of Biological Chemistry,* 270**,** 4312-4317.

ANAND, R., SHARMA, D. R., VERMA, D., BHALLA, A., GILL, K. D. & SINGH, S. 2013. Mitochondrial electron transport chain complexes, catalase and markers of oxidative stress in platelets of patients with severe aluminum phosphide poisoning. *Human & Experimental Toxicology,* 32**,** 807-816.

ANDRE, P. 2004. P-selectin in haemostasis. *British Journal of Haematology,* 126**,** 298-306.

ANGIOLILLO, D. J., FERNANDEZ-ORTIZ, A., BERNARDO, E., RAMIREZ, C., SABATE, M., JIMENEZ-QUEVEDO, P., HERNANDEZ, R., MORENO, R., ESCANED, J., ALFONSO, F., BANUELOS, C., COSTA, M. A., BASS, T. A. & MACAYA, C. 2005. Platelet function profiles in patients with type 2 diabetes and coronary artery disease on combined aspirin and clopidogrel treatment. *Diabetes,* 54**,** 2430-2435.

ASMIS, R. & BEGLEY, J. G. 2003. Oxidized LDL promotes peroxide-mediated mitochondrial dysfunction and cell death in human macrophages - A caspase-3-independent pathway. *Circulation Research,* 92**,** E20-E29.

ATAR, O. D., EISERT, C., POKOV, I. & SEREBRUANY, V. L. 2010. Stability validation of paraformaldehyde-fixed samples for the assessment of the platelet PECAM-1, P-selectin, and PAR-1 thrombin receptor by flow cytometry. *Journal of Thrombosis and Thrombolysis,* 30**,** 79-83.

ATKINSON, L., YUSUF, M. Z., ABURIMA, A., AHMED, Y., THOMAS, S. G., NASEEM, K. M. & CALAMINUS, S. D. J. 2018. Reversal of stress

fibre formation by Nitric Oxide mediated RhoA inhibition leads to reduction in the height of preformed thrombi. *Scientific Reports,* 8.

AYE, M. M., KILPATRICK, E. S., ABURIMA, A., WRAITH, K. S., MAGWENZI, S., SPURGEON, B., RIGBY, A. S., SANDEMAN, D., NASEEM, K. M. & ATKIN, S. L. 2014. Acute Hypertriglyceridemia Induces Platelet Hyperactivity That is Not Attenuated by Insulin in Polycystic Ovary Syndrome. *Journal of the American Heart Association,* 3.

BAATEN, C., MOENEN, F., HENSKENS, Y. M. C., SWIERINGA, F., WETZELS, R. J. H., VAN OERLE, R., HEIJNEN, H. F. G., TEN CATE, H., HOLLOWAY, G. P., BECKERS, E. A. M., HEEMSKERK, J. W. M. & VAN DER MEIJDEN, P. E. J. 2018. Impaired mitochondrial activity explains platelet dysfunction in thrombocytopenic cancer patients undergoing chemotherapy. *Haematologica,* 103**,** 1557-1567.

BACCARELLI, A. A. & BYUN, H. M. 2015. Platelet mitochondrial DNA methylation: a potential new marker of cardiovascular disease. *Clinical Epigenetics,* 7.

BALDRIGHI, M., MALLAT, Z. & LI, X. 2017. y NLRP3 inflammasome pathways in atherosclerosis. *Atherosclerosis,* 267**,** 127-138.

BEDNER, E., SMOLEWSKI, P., AMSTAD, P. & DARZYNKIEWICZ, Z. 2000. Activation of caspases measured in situ by binding of fluorochrome-labeled inhibitors of caspases (FLICA): Correlation with DNA fragmentation. *Experimental Cell Research,* 259**,** 308-313.

BEGONJA, A. J., GAMBARYAN, S., GEIGER, J., AKTAS, B., POZGAJOVA, M., NIESWANDT, B. & WALTER, U. 2005. Platelet NAD(P)H-oxidase-generated ROS production regulates alpha IIb beta 3-integrin activation independent of the NO/cGMP pathway. *Blood,* 106**,** 2757-2760.

BEHNKE, O. 1965. FURTHER STUDIES ON MICROTUBULES - A MARGINAL BUNDLE IN HUMAN AND RAT THROMBOCYTES. *Journal of Ultrastructure Research,* 13**,** 469-+.

BELKINA, A., CICCOLELLA, A., ANNO, R., HALPERT, E., SPIDLEN, J. & SNYDER-CAPPIONE, J. 2018. Automated Optimal Parameters For T-Distributed Stochastic Neighbor Embedding Improve Visualization And Allow Analysis Of Large Datasets. bioRxiv.

BENNETT, H. S. 1963. MORPHOLOGICAL ASPECTS OF EXTRACELLULAR POLYSACCHARIDES. *Journal of Histochemistry & Cytochemistry,* 11**,** 14-&.

BENZ, P. M., BLUME, C., SEIFERT, S., WILHELM, S., WASCHKE, J., SCHUH, K., GERTLER, F., MUNZEL, T. & RENNE, T. 2009. Differential VASP phosphorylation controls remodeling of the actin cytoskeleton. *Journal of Cell Science,* 122**,** 3954-3965.

BERGER, M., RASLAN, Z., ABURIMA, A., MAGWENZI, S., WRAITH, K. S., SPURGEON, B. E. J., HINDLE, M. S., LAW, R., FEBBRAIO, M. & NASEEM, K. M. 2019a. Atherogenic lipid stress induces platelet hyperactivity through CD36-mediated hyposensitivity to prostacyclin-; the role of phosphodiesterase 3A. *Haematologica.*

BERGER, M., WRAITH, K., WOODWARD, C., ABURIMA, A., RASLAN, Z., HINDLE, M. S., MOELLMANN, J., FEBBRAIO, M. & NASEEM, K. M. 2019b. Dyslipidemia-associated atherogenic oxidized lipids induce

platelet hyperactivity through phospholipase C gamma 2-dependent reactive oxygen species generation. *Platelets,* 30**,** 467-472.

BISWAS, S., ZIMMAN, A., GAO, D. T., BYZOVA, T. V. & PODREZ, E. A. 2017. TLR2 Plays a Key Role in Platelet Hyperreactivity and Accelerated Thrombosis Associated With Hyperlipidemia. *Circulation Research,* 121**,** 951-+.

BLAIR, P. & FLAUMENHAFT, R. 2009. Platelet alpha-granules: Basic biology and clinical correlates. *Blood Reviews,* 23**,** 177-189.

BLAIR, T. & FRELINGER, A. 2019. Platelet surface marker analysis by mass cytometry. *Platelets.*

BLAIR, T. A., MICHELSON, A. D. & FRELINGER, A. L. 2018. Mass Cytometry Reveals Distinct Platelet Subtypes in Healthy Subjects and Novel Alterations in Surface Glycoproteins in Glanzmann Thrombasthenia. *Scientific Reports,* 8.

BLANN, A. D., NADAR, S. K. & LIP, G. Y. H. 2006. The adhesion molecule P-selectin and cardiovascular disease (vol 24, pg 2166, 2003). *European Heart Journal,* 27**,** 501-501.

BODNAR, R. J., XI, X. D., LI, Z. Y., BERNDT, M. C. & DU, X. P. 2002. Regulation of glycoprotein Ib-IX-von Willebrand factor interaction by cAMP-dependent protein kinase-mediated phosphorylation at Ser(166) of glycoprotein Ib beta. *Journal of Biological Chemistry,* 277**,** 47080-47087.

BONACCIO, M., DI CASTELNUOVO, A., COSTANZO, S., DE CURTIS, A., DONATI, M. B., CERLETTI, C., DE GAETANO, G., IACOVIELLO, L. & INVESTIGATORS, M.-S. 2016. Age-sex-specific ranges of platelet count and all-cause mortality: prospective findings from the MOLI-SANI study. *Blood,* 127**,** 1614-1616.

BONAN, J. L., RINDER, H. M. & SMITH, B. R. 1993. DETERMINATION OF THE PERCENTAGE OF THIAZOLE ORANGE (TO)-POSITIVE, RETICULATED PLATELETS USING AUTOLOGOUS ERYTHROCYTE TO FLUORESCENCE AS AN INTERNAL STANDARD. *Cytometry,* 14**,** 690-694.

BOONE, B. A., MURTHY, P., MILLER-OCUIN, J. L., LIANG, X., RUSSELL, K. L., LOUGHRAN, P., GAWAZ, M., LOTZE, M. T., ZEH, H. J. & VOGEL, S. 2019. The platelet NLRP3 inflammasome is upregulated in a murine model of pancreatic cancer and promotes platelet aggregation and tumor growth. *Ann Hematol.*

BORN, G. V. R. 1962. AGGREGATION OF BLOOD PLATELETS BY ADENOSINE DIPHOSPHATE AND ITS REVERSAL. *Nature,* 194**,** 927-&.

BROWN, G. T., NARAYANAN, P., LI, W., SILVERSTEIN, R. L. & MCINTYRE, T. M. 2013. Lipopolysaccharide Stimulates Platelets through an IL-1 beta Autocrine Loop. *Journal of Immunology,* 191**,** 5196-5203.

BROZ, P., VON MOLTKE, J., JONES, J. W., VANCE, R. E. & MONACK, D. M. 2010. Differential Requirement for Caspase-1 Autoproteolysis in Pathogen-Induced Cell Death and Cytokine Processing. *Cell Host & Microbe,* 8**,** 471-483.

BRYAN, N. B., DORFLEUTNER, A., KRAMER, S. J., YUN, C., ROJANASAKUL, Y. & STEHLIK, C. 2010. Differential splicing of the apoptosis-associated speck like protein containing a caspase

recruitment domain (ASC) regulates inflammasomes. *Journal of Inflammation-London,* 7.

BURKHART, J. M., VAUDEL, M., GAMBARYAN, S., RADAU, S., WALTER, U., MARTENS, L., GEIGER, J., SICKMANN, A. & ZAHEDI, R. P. 2012. The first comprehensive and quantitative analysis of human platelet protein composition allows the comparative analysis of structural and functional pathways. *Blood,* 120**,** E73-E82.

BURKITT, M. J. 2001. A critical overview of the chemistry of copper-dependent low density lipoprotein oxidation: Roles of lipid hydroperoxides, alpha-tocopherol, thiols, and ceruloplasmin. *Archives of Biochemistry and Biophysics,* 394**,** 117-135.

BUTT, E., ABEL, K., KRIEGER, M., PALM, D., HOPPE, V., HOPPE, J. & WALTER, U. 1994. CAMP-DEPENDENT AND CGMP-DEPENDENT PROTEIN-KINASE PHOSPHORYLATION SITES OF THE FOCAL ADHESION VASODILATOR-STIMULATED PHOSPHOPROTEIN (VASP) IN-VITRO AND IN INTACT HUMAN PLATELETS. *Journal of Biological Chemistry,* 269**,** 14509-14517.

BUTT, E., GAMBARYAN, S., GOTTFERT, N., GALLER, A., MARCUS, K. & MEYER, H. E. 2003. Actin binding of human LIM and SH3 protein is regulated by cGMP- and cAMP-dependent protein kinase phosphorylation on serine 146. *Journal of Biological Chemistry,* 278**,** 15601-15607.

BUTT, E., IMMLER, D., MEYER, H. E., KOTLYAROV, A., LAASS, K. & GAESTEL, M. 2001. Heat shock protein 27 is a substrate of cGMP-dependent protein kinase in intact human platelets - Phosphorylation-induced actin polymerization caused by Hsp27 mutants. *Journal of Biological Chemistry,* 276**,** 7108-7113.

CARDENES, N., COREY, C., GEARY, L., JAIN, S., ZHARIKOV, S., BARGE, S., NOVELLI, E. M. & SHIVA, S. 2014. Platelet bioenergetic screen in sickle cell patients reveals mitochondrial complex V inhibition, which contributes to platelet activation. *Blood,* 123**,** 2864-2872.

CARR, A. C., MCCALL, M. R. & FREI, B. 2000. Oxidation of LDL by myeloperoxidase and reactive nitrogen species - Reaction pathways and antioxidant protection. *Arteriosclerosis Thrombosis and Vascular Biology,* 20**,** 1716-1723.

CATHCART, M. K., CHISOLM, G. M., MCNALLY, A. K. & MOREL, D. W. 1988. OXIDATIVE MODIFICATION OF LOW-DENSITY LIPOPROTEIN (LDL) BY ACTIVATED HUMAN-MONOCYTES AND THE CELL-LINES U937 AND HL60. *In Vitro Cellular & Developmental Biology,* 24**,** 1001-1008.

CHAN, H. C., KE, L. Y., CHU, C. S., LEE, A. S., SHEN, M. Y., CRUZ, M. A., HSU, J. F., CHENG, K. H., CHAN, H. C. B., LU, J., LAI, W. T., SAWAMURA, T., SHEU, S. H., YEN, J. H. & CHEN, C. H. 2013. Highly electronegative LDL from patients with ST-elevation myocardial infarction triggers platelet activation and aggregation. *Blood,* 122**,** 3632-3641.

CHAVEZ-SANCHEZ, L., GARZA-REYES, M. G., ESPINOSA-LUNA, J. E., CHAVEZ-RUEDA, K., LEGORRETA-HAQUET, M. V. & BLANCO-FAVELA, F. 2014. The role of TLR2, TLR4 and CD36 in macrophage activation and foam cell formation in response to oxLDL in humans. *Human Immunology,* 75**,** 322-329.

CHEEPALA, S. B., PITRE, A., FUKUDA, Y., TAKENAKA, K., ZHANG, Y. Y., WANG, Y., FRASE, S., PESTINA, T., GARTNER, T. K., JACKSON, C. & SCHUETZ, J. D. 2015. The ABCC4 membrane transporter modulates platelet aggregation. *Blood,* 126**,** 2307-2319.

CHEN, K., FEBBRAIO, M., LI, W. & SILVERSTEIN, R. L. 2008. A specific CD36-dependent signaling pathway is required for platelet activation by oxidized low-density lipoprotein. *Circulation Research,* 102**,** 1512-1519.

CHEN, M. Y., KAKUTANI, M., NARUKO, T., UEDA, M., NARUMIYA, S., MASAKI, T. & SAWAMURA, T. 2001. Activation-dependent surface expression of LOX-1 in human platelets. *Biochemical and Biophysical Research Communications,* 282**,** 153-158.

CHO, M. J. & ALLEN, M. A. 1978. CHEMICAL STABILITY OF PROSTACYCLIN (PGI2) IN AQUEOUS-SOLUTIONS. *Prostaglandins,* 15**,** 943-954.

CHOO, H. J., KHOLMUKHAMEDOV, A., ZHOU, C. Z. & JOBE, S. 2017. Inner Mitochondrial Membrane Disruption Links Apoptotic and Agonist-Initiated Phosphatidylserine Externalization in Platelets. *Arteriosclerosis Thrombosis and Vascular Biology,* 37**,** 1503-1512.

CHOO, H. J., SAAFIR, T. B., MKUMBA, L., WAGNER, M. B. & JOBE, S. M. 2012. Mitochondrial Calcium and Reactive Oxygen Species Regulate Agonist-Initiated Platelet Phosphatidylserine Exposure. *Arteriosclerosis Thrombosis and Vascular Biology,* 32**,** 2946-+.

CHOWDHURY, S. K. R., SANGLE, G. V., XIE, X. P., STELMACK, G. L., HALAYKO, A. J. & SHEN, G. X. 2010. Effects of extensively oxidized low-density lipoprotein on mitochondrial function and reactive oxygen species in porcine aortic endothelial cells. *American Journal of Physiology-Endocrinology and Metabolism,* 298**,** E89-E98.

CHRIST, A. & LATZ, E. 2014. LOX-1 and mitochondria: an inflammatory relationship. *Cardiovascular Research,* 103**,** 435-437.

CLARK, S. R., MA, A. C., TAVENER, S. A., MCDONALD, B., GOODARZI, Z., KELLY, M. M., PATEL, K. D., CHAKRABARTI, S., MCAVOY, E., SINCLAIR, G. D., KEYS, E. M., ALLEN-VERCOE, E., DEVINNEY, R., DOIG, C. J., GREEN, F. H. Y. & KUBES, P. 2007. Platelet TLR4 activates neutrophil extracellular traps to ensnare bacteria in septic blood. *Nature Medicine,* 13**,** 463-469.

COENEN, D. M., MASTENBROEK, T. G. & COSEMANS, J. 2017. Platelet interaction with activated endothelium: mechanistic insights from microfluidics. *Blood,* 130**,** 2819-2828.

COLL, R. C., HILL, J. R., DAY, C. J., ZAMOSHNIKOVA, A., BOUCHER, D., MASSEY, N. L., CHITTY, J. L., FRASER, J. A., JENNINGS, M. P., ROBERTSON, A. A. B. & SCHRODER, K. 2019. MCC950 directly targets the NLRP3 ATP- hydrolysis motif for inflammasome inhibition. *Nature Chemical Biology,* 15**,** 556-+.

COLL, R. C., ROBERTSON, A. A. B., CHAE, J. J., HIGGINS, S. C., MUNOZ-PLANILLO, R., INSERRA, M. C., VETTER, I., DUNGAN, L. S., MONKS, B. G., STUTZ, A., CROKER, D. E., BUTLER, M. S., HANEKLAUS, M., SUTTON, C. E., NUNEZ, G., LATZ, E., KASTNER, D. L., MILLS, K. H. G., MASTERS, S. L., SCHRODER, K., COOPER, M. A. & O'NEILL, L. A. J. 2015. A small-molecule inhibitor of the

NLRP3 inflammasome for the treatment of inflammatory diseases. *Nature Medicine,* 21**,** 248-+.

COLLINS, Y., CHOUCHANI, E. T., JAMES, A. M., MENGER, K. E., COCHEME, H. M. & MURPHY, M. P. 2012. Mitochondrial redox signalling at a glance. *Journal of Cell Science,* 125**,** 801-806.

COSSARIZZA, A., CHANG, H. D., RADBRUCH, A., AKDIS, M., ANDRA, I., ANNUNZIATO, F., BACHER, P., BARNABA, V., BATTISTINI, L., BAUER, W. M., BAUMGART, S., BECHER, B., BEISKER, W., BEREK, C., BLANCO, A., BORSELLINO, G., BOULAIS, P. E., BRINKMAN, R. R., BUSCHER, M., BUSCH, D. H., BUSHNELL, T. P., CAO, X. T., CAVANI, A., CHATTOPADHYAY, P. K., CHENG, Q. Y., CHOW, S., CLERICI, M., COOKE, A., COSMA, A., COSMI, L., CUMANO, A., DANG, V. D., DAVIES, D., DE BIASI, S., DEL ZOTTO, G., DELLA BELLA, S., DELLABONA, P., DENIZ, G., DESSING, M., DIEFENBACH, A., DI SANTO, J., DIELI, F., DOLF, A., DONNENBERG, V. S., DORNER, T., EHRHARDT, G. R. A., ENDL, E., ENGEL, P., ENGELHARDT, B., ESSER, C., EVERTS, B., DREHER, A., FALK, C. S., FEHNIGER, T. A., FILBY, A., FILLATREAU, S., FOLLO, M., FORSTER, I., FOSTER, J., FOULDS, G. A., FRENETTE, P. S., GALBRAITH, D., GARBI, N., GARCIA-GODOY, M. D., GEGINAT, J., GHORESCHI, K., GIBELLINI, L., GOETTLINGER, C., GOODYEAR, C. S., GORI, A., GROGAN, J., GROSS, M., GRUTZKAU, A., GRUMMITT, D., HAHN, J., HAMMER, Q., HAUSER, A. E., HAVILAND, D. L., HEDLEY, D., HERRERA, G., HERRMANN, M., HIEPE, F., HOLLAND, T., HOMBRINK, P., HOUSTON, J. P., HOYER, B. F., HUANG, B., HUNTER, C. A., IANNONE, A., JACK, H. M., JAVEGA, B., JONJIC, S., JUELKE, K., JUNG, S., KAISER, T., KALINA, T., KELLER, B., KHAN, S., KIENHOFER, D., KRONEIS, T., et al. 2017. Guidelines for the use of flow cytometry and cell sorting in immunological studies. *European Journal of Immunology,* 47**,** 1584-1797.

CROSLAND-TAYLOR, P. J. 1953. A DEVICE FOR COUNTING SMALL PARTICLES SUSPENDED IN A FLUID THROUGH A TUBE. *Nature,* 171**,** 37-38.

DAMIEN, P., COGNASSE, F., EYRAUD, M. A., ARTHAUD, C. A., POZZETTO, B., GARRAUD, O. & HAMZEH-COGNASSE, H. 2015. LPS stimulation of purified human platelets is partly dependent on plasma soluble CD14 to secrete their main secreted product, soluble-CD40-Ligand. *Bmc Immunology,* 16.

DARZYNKIEWICZ, Z. & POZAROWSKI, P. 2007. All that glitters is not gold: All that FLICA binds is not caspase. A caution in data interpretation - and new opportunities. *Cytometry Part A,* 71A**,** 536-537.

DAUB, K., SEIZER, P., STELLOS, K., KRAMER, B. F., BIGALKE, B., SCHALLER, M., FATEH-MOGHADAM, S., GAWAZ, M. & LINDEMANN, S. 2010. Oxidized LDL-Activated Platelets Induce Vascular Inflammation. *Seminars in Thrombosis and Hemostasis,* 36**,** 146-156.

DAVIZON-CASTILLO, P., MCMAHON, B., AGUILA, S., BARK, D., ASHWORTH, K., ALLAWZI, A., CAMPBELL, R. A., MONTENONT, E., NEMKOV, T., D'ALESSANDRO, A., CLENDENEN, N., SHIH, L., SANDERS, N. A., HIGA, K., COX, A., PADILLA-ROMO, Z.,

HERNANDEZ, G., WARTCHOW, E., TRAHAN, G. D., NOZIK-GRAYCK, E., JONES, K., PIETRAS, E., DEGREGORI, J., RONDINA, M. T. & DI PAOLA, J. 2019. TNF-alpha driven inflammation and mitochondrial dysfunction define the platelet hyperreactivity of aging. *Blood*.

DEFESCHE, J. C., GIDDING, S. S., HARADA-SHIBA, M., HEGELE, R. A., SANTOS, R. D. & WIERZBICKI, A. S. 2017. Familial hypercholesterolaemia. *Nature Reviews Disease Primers,* 3.

DENIS, M. M., TOLLEY, N. D., BUNTING, M., SCHWERTZ, H., JIANG, H. M., LINDEMANN, S., YOST, C. C., RUBNER, F. J., ALBERTINE, K. H., SWOBODA, K. J., FRATTO, C. M., TOLLEY, E., KRAISS, L. W., MCINTYRE, T. M., ZIMMERMAN, G. A. & WEYRICH, A. S. 2005. Escaping the nuclear confines: Signal-dependent Pre-mRNA splicing in anucleate platelets. *Cell,* 122**,** 379-391.

DICK, M. S., SBORGI, L., RUHL, S., HILLER, S. & BROZ, P. 2016. ASC filament formation serves as a signal amplification mechanism for inflammasomes. *Nature Communications,* 7.

DOLUNAY, A., SENOL, S. P., TEMIZ-RESITOGLU, M., GUDEN, D. S., SARI, A. N., SAHAN-FIRAT, S. & TUNCTAN, B. 2017. Inhibition of NLRP3 Inflammasome Prevents LPS-Induced Inflammatory Hyperalgesia in Mice: Contribution of NF-kappa B, Caspase-1/11, ASC, NOX, and NOS Isoforms. *Inflammation,* 40**,** 366-386.

DOSE, J., HUEBBE, P., NEBEL, A. & RIMBACH, G. 2016. APOE genotype and stress response - a mini review. *Lipids in Health and Disease,* 15.

EBBELING, L., ROBERTSON, C., MCNICOL, A. & GERRARD, J. M. 1992. RAPID ULTRASTRUCTURAL-CHANGES IN THE DENSE TUBULAR SYSTEM FOLLOWING PLATELET ACTIVATION. *Blood,* 80**,** 718-723.

ESCOLAR, G. & WHITE, J. G. 1991. THE PLATELET OPEN CANALICULAR SYSTEM - A FINAL COMMON PATHWAY. *Blood Cells,* 17**,** 467-485.

ESTRADAO, S., GRAVEN, S. N. & LARDY, H. A. 1967. POTASSIUM ION-DEPENDENT HYDROLYSIS OF ADENOSINE TRIPHOSPHATE INDUCED BY NIGERICIN IN MITOCHONDRIA. *Journal of Biological Chemistry,* 242**,** 2925-&.

ESTRUCH, M., RAJAMAKI, K., SANCHEZ-QUESADA, J. L., KOVANEN, P. T., OORNI, K., BENITEZ, S. & ORDONEZ-LLANOS, J. 2015. Electronegative LDL induces priming and inflammasome activation leading to IL-1 beta release in human monocytes and macrophages. *Biochimica Et Biophysica Acta-Molecular and Cell Biology of Lipids,* 1851**,** 1442-1449.

FEINGOLD, K. R., ANAWALT, B., BOYCE, A., CHROUSOS, G., DUNGAN, K., GROSSMAN, A., HERSHMAN, J. M., KALTSAS, G., KOCH, C., KOPP, P., KORBONITS, M., MCLACHLAN, R., MORLEY, J. E., NEW, M., PERREAULT, L., PURNELL, J., REBAR, R., SINGER, F., TRENCE, D. L., VINIK, A. & WILSON, D. P. 2000. Endotext.

FIDLER, T. P., ROWLEY, J. W., ARAUJO, C., BOUDREAU, L. H., MARTI, A., SOUVENIR, R., DALE, K., BOILARD, E., WEYRICH, A. S. & ABEL, E. D. 2017. Superoxide Dismutase 2 is dispensable for platelet function. *Thrombosis and Haemostasis,* 117**,** 1859-1867.

FRELINGER, A. L. 2018. Using flow cytometry to monitor glycoprotein IIb-IIIa activation. *Platelets,* 29**,** 670-676.

FRELINGER, A. L., GRACE, R. F., GERRITS, A. J., BERNY-LANG, M. A., BROWN, T., CARMICHAEL, S. L., NEUFELD, E. J. & MICHELSON, A. D. 2015. Platelet function tests, independent of platelet count, are associated with bleeding severity in ITP. *Blood,* 126**,** 873-879.

FRENETTE, P. S., DENIS, C. V., WEISS, L., JURK, K., SUBBARAO, S., KEHREL, B., HARTWIG, J. H., VESTWEBER, D. & WAGNER, D. D. 2000. P-selectin glycoprotein ligand 1 (PSGL-1) is expressed on platelets and can mediate platelet-endothelial interactions in vivo. *Journal of Experimental Medicine,* 191**,** 1413-1422.

FUNG, C. Y. E., JONES, S., NTRAKWAH, A., NASEEM, K. M., FARNDALE, R. W. & MAHAUT-SMITH, M. P. 2012. Platelet Ca2+ responses coupled to glycoprotein VI and Toll-like receptors persist in the presence of endothelial-derived inhibitors: roles for secondary activation of P2X1 receptors and release from intracellular Ca2+ stores. *Blood,* 119**,** 3613-3621.

GAERTNER, F., AHMAD, Z., ROSENBERGER, G., FAN, S. X., NICOLAI, L., BUSCH, B., YAVUZ, G., LUCKNER, M., ISHIKAWA-ANKERHOLD, H., HENNEL, R., BENECHET, A., LORENZ, M., CHANDRARATNE, S., SCHUBERT, I., HELMER, S., STRIEDNIG, B., STARK, K., JANKO, M., BOTTCHER, R. T., VERSCHOOR, A., LEON, C., GACHET, C., GUDERMANN, T., SCHNITZLER, M. M. Y., PINCUS, Z., IANNACONE, M., HAAS, R., WANNER, G., LAUBER, K., SIXT, M. & MASSBERG, S. 2017. Migrating Platelets Are Mechano-scavengers that Collect and Bundle Bacteria. *Cell,* 171**,** 1368-+.

GARCIA-CALVO, M., PETERSON, E. P., LEITING, B., RUEL, R., NICHOLSON, D. W. & THORNBERRY, N. A. 1998. Inhibition of human caspases by peptide-based and macromolecular inhibitors. *Journal of Biological Chemistry,* 273**,** 32608-32613.

GERRY, A. B., SATCHELL, L. & LEAKE, D. S. 2008. A novel method for production of lipid hydroperoxide- or oxysterol-rich low-density lipoprotein. *Atherosclerosis,* 197**,** 579-587.

GETZ, G. S. & REARDON, C. A. 2006. Diet and murine atherosclerosis. *Arteriosclerosis Thrombosis and Vascular Biology,* 26**,** 242-249.

GIBBINS, J. M. 2004. Platelet adhesion signalling and the regulation of thrombus formation. *Journal of Cell Science,* 117**,** 3415-3425.

GIOVANNINI, C., MATARRESE, P., SCAZZOCCHIO, B., SANCHEZ, M., MASELLA, R. & MALORNI, W. 2002. Mitochondria hyperpolarization is an early event in oxidized low-density lipoprotein-induced apoptosis in Caco-2 intestinal cells. *Febs Letters,* 523**,** 200-206.

GOLANSKI, J., PIETRUCHA, T., BAJ, Z., GREGER, J. & WATALA, C. 1996. Molecular insights into the anticoagulant-induced spontaneous activation of platelets in whole blood - Various anticoagulants are not equal. *Thrombosis Research,* 83**,** 199-216.

GOLEBIEWSKA, E. M. & POOLE, A. W. 2015. Platelet secretion: From haemostasis to wound healing and beyond. *Blood Reviews,* 29**,** 153-162.

GOLIA, E., LIMONGELLI, G., NATALE, F., FIMIANI, F., MADDALONI, V., PARIGGIANO, I., BIANCHI, R., CRISCI, M., D'ACIERNO, L.,

GIORDANO, R., DI PALMA, G., CONTE, M., GOLINO, P., RUSSO, M. G., CALABRO, R. & CALABRO, P. 2014. Inflammation and Cardiovascular Disease: From Pathogenesis to Therapeutic Target. *Current Atherosclerosis Reports,* 16.

GONZALEZ-PACHECO, H., VARGAS-ALARCON, G., ANGELES-MARTINEZ, J., MARTINEZ-SANCHEZ, C., PEREZ-MENDEZ, O., HERRERA-MAYA, G., MARTINEZ-RIOS, M. A., PENA-DUQUE, M. A., POSADAS-ROMERO, C. & FRAGOSO, J. M. 2017. The NLRP3 and CASP1 gene polymorphisms are associated with developing of acute coronary syndrome: a case-control study. *Immunologic Research,* 65**,** 862-868.

GREBE, A., HOSS, F. & LATZ, E. 2018. NLRP3 Inflammasome and the IL-1 Pathway in Atherosclerosis. *Circulation Research,* 122**,** 1722-1740.

GRESELE, P., FALCINELLI, E., LOFFREDO, F., CIMMINO, G., CORAZZI, T., FORTE, L., GUGLIELMINI, G., MOMI, S. & GOLINO, P. 2011. Platelets release matrix metalloproteinase-2 in the coronary circulation of patients with acute coronary syndromes: possible role in sustained platelet activation. *European Heart Journal,* 32**,** 316-325.

GRUNDLER, K., ANGSTWURM, M., HILGE, R., BAUMANN, P., ANNECKE, T., CRISPIN, A., SOHN, H. Y., MASSBERG, S. & KRAEMER, B. F. 2014. Platelet mitochondrial membrane depolarization reflects disease severity in patients with sepsis and correlates with clinical outcome. *Critical Care,* 18.

GUCLU, E., DURMAZ, Y. & KARABAY, O. 2013. Effect of severe sepsis on platelet count and their indices. *African Health Sciences,* 13**,** 333-338.

GYULKHANDANYAN, A. V., MUTLU, A., FREEDMAN, J. & LEYTIN, V. 2012. Markers of platelet apoptosis: methodology and applications. *Journal of Thrombosis and Thrombolysis,* 33**,** 397-411.

HARRISON, P. 2009. Assessment of platelet function in the laboratory. *Hamostaseologie,* 29**,** 25-31.

HARRISON, P. & CRAMER, E. M. 1993. PLATELET ALPHA-GRANULES. *Blood Reviews,* 7**,** 52-62.

HARRISON, P., MACKIE, I., MUMFORD, A., BRIGGS, C., LIESNER, R., WINTER, M., MACHIN, S. & BRITISH COMM STAND, H. 2011. Guidelines for the laboratory investigation of heritable disorders of platelet function. *British Journal of Haematology,* 155**,** 30-44.

HARRISON, P., ROBINSON, M. S., MACKIE, I. J. & MACHIN, S. J. 1997. Reticulated platelets. *Platelets,* 8**,** 379-83.

HEEMSKERK, J. W. M., MATTHEIJ, N. J. A. & COSEMANS, J. 2013. Platelet-based coagulation: different populations, different functions. *Journal of Thrombosis and Haemostasis,* 11**,** 2-16.

HEFFRON, S. P., MARIER, C., PARIKH, M., FISHER, E. A. & BERGER, J. S. 2018. Severe obesity and bariatric surgery alter the platelet mRNA profile. *Platelets***,** 1-8.

HISHINUMA, T., TSUKAMOTO, H., SUZUKI, K. & MIZUGAKI, M. 2001. Relationship between thromboxane/prostacyclin ratio and diabetic vascular complications. *Prostaglandins Leukotrienes and Essential Fatty Acids,* 65**,** 191-196.

HOFFMAN, M. & MONROE, D. M. 2001. A cell-based model of hemostasis. *Thrombosis and Haemostasis,* 85**,** 958-965.

HOFFMEISTER, K. M. & FALET, H. 2016. Platelet clearance by the hepatic Ashwell-Morrell receptor: mechanisms and biological significance. *Thrombosis Research,* 141**,** S68-S72.

HOLY, E. W., AKHMEDOV, A., SPEER, T., CAMICI, G. G., ZEWINGER, S., BONETTI, N., BEER, J. H., LUSCHER, T. F. & TANNER, F. C. 2016. Carbamylated Low-Density Lipoproteins Induce a Prothrombotic State Via LOX-1 Impact on Arterial Thrombus Formation In Vivo. *Journal of the American College of Cardiology,* 68**,** 1664-1676.

HOTTZ, E. D., LOPES, J. F., FREITAS, C., VALLS-DE-SOUZA, R., OLIVEIRA, M. F., BOZZA, M. T., DA POIAN, A. T., WEYRICH, A. S., ZIMMERMAN, G. A., BOZZA, F. A. & BOZZA, P. T. 2013. Platelets mediate increased endothelium permeability in dengue through NLRP3-inflammasome activation. *Blood,* 122**,** 3405-3414.

HUSKENS, D., SANG, Y., KONINGS, J., VAN DER VORM, L., DE LAAT, B., KELCHTERMANS, H. & ROEST, M. 2018. Standardization and reference ranges for whole blood platelet function measurements using a flow cytometric platelet activation test. *Plos One,* 13.

IMHOF, B. A., JEMELIN, S., BALLET, R., VESIN, C., SCHAPIRA, M., KARACA, M. & EMRE, Y. 2016. CCN1/CYR61-mediated meticulous patrolling by Ly6C(low) monocytes fuels vascular inflammation. *Proceedings of the National Academy of Sciences of the United States of America,* 113**,** E4847-E4856.

ITALIANO, J. E. & BATTINELLI, E. M. 2009. Selective sorting of alpha-granule proteins. *Journal of Thrombosis and Haemostasis,* 7**,** 173-176.

JOBE, S. M., WILSON, K. M., LEO, L., RAIMONDI, A., MOLKENTIN, J. D., LENTZ, S. R. & DI PAOLA, J. 2008. Critical role for the mitochondrial permeability transition pore and cyclophilin D in platelet activation and thrombosis. *Blood,* 111**,** 1257-1265.

JOSHI, D. C. & BAKOWSKA, J. C. 2011. Determination of Mitochondrial Membrane Potential and Reactive Oxygen Species in Live Rat Cortical Neurons. *Jove-Journal of Visualized Experiments.*

KAHLENBERG, J. M., CARMONA-RIVERA, C., SMITH, C. K. & KAPLAN, M. J. 2013. Neutrophil Extracellular Trap-Associated Protein Activation of the NLRP3 Inflammasome Is Enhanced in Lupus Macrophages. *Journal of Immunology,* 190**,** 1217-1226.

KAPPELMAYER, J. & NAGY, B. 2017. The Interaction of Selectins and PSGL-1 as a Key Component in Thrombus Formation and Cancer Progression. *Biomed Research International.*

KAR, N. S., ASHRAF, M. Z., VALIYAVEETTIL, M. & PODREZ, E. A. 2008. Mapping and characterization of the binding site for specific oxidized phospholipids and oxidized low density lipoprotein of scavenger receptor CD36. *Journal of Biological Chemistry,* 283**,** 8765-8771.

KATO, R., MORI, C., KITAZATO, K., ARATA, S., OBAMA, T., MORI, M., TAKAHASHI, K., AIUCHI, T., TAKANO, T. & ITABE, H. 2009. Transient Increase in Plasma Oxidized LDL During the Progression of Atherosclerosis in Apolipoprotein E Knockout Mice. *Arteriosclerosis Thrombosis and Vascular Biology,* 29**,** 33-U82.

KEMKES-MATTHES, B., FISCHER, R. & PEETZ, D. 2011. Influence of 8 and 24-h storage of whole blood at ambient temperature on prothrombin time, activated partial thromboplastin time, fibrinogen,

thrombin time, antithrombin and D-dimer. *Blood Coagulation & Fibrinolysis,* 22**,** 215-220.

KIRII, H., NIWA, T., YAMADA, Y., WADA, H., SAITO, K., IWAKURA, Y., ASANO, M., MORIWAKI, H. & SEISHIMA, M. 2003. Lack of interleukin-1 beta decreases the severity of atherosclerosis in ApoE-deficient mice. *Arteriosclerosis Thrombosis and Vascular Biology,* 23**,** 656-660.

KNEBEL, S. M., SPRAGUE, R. S. & STEPHENSON, A. H. 2015. Prostacyclin receptor expression on platelets of humans with type 2 diabetes is inversely correlated with hemoglobin A1c levels. *Prostaglandins & Other Lipid Mediators,* 116**,** 131-135.

KOUPENOVA, M., CLANCY, L., CORKREY, H. A. & FREEDMAN, J. E. 2018. Circulating Platelets as Mediators of Immunity, Inflammation, and Thrombosis. *Circulation Research,* 122**,** 337-351.

KUIJPERS, M. J. E., NIEUWENHUYS, C. M. A., FEIJGE, M. A. H., KLOOTS, W., GIESEN, P. L. A., JERLING, J. C., EGBRINK, M. & HEEMSKERK, J. W. M. 2005. Regulation of tissue factor-induced coagulation and platelet aggregation in flowing whole blood. *Thrombosis and Haemostasis,* 93**,** 97-105.

LADOR, A., LESHEM-LEV, D., SPECTRE, G., ABELOW, A., KORNOWSKI, R. & LEV, E. I. 2017. Characterization of surface antigens of reticulated immature platelets. *Journal of Thrombosis and Thrombolysis,* 44**,** 291-297.

LAEMMLI, U. K. 1970. CLEAVAGE OF STRUCTURAL PROTEINS DURING ASSEMBLY OF HEAD OF BACTERIOPHAGE-T4. *Nature,* 227**,** 680-&.

LAMKANFI, M., MUELLER, J. L., VITARI, A. C., MISAGHI, S., FEDOROVA, A., DESHAYES, K., LEE, W. P., HOFFMAN, H. M. & DIXIT, V. M. 2009. Glyburide inhibits the Cryopyrin/Nalp3 inflammasome. *Journal of Cell Biology,* 187**,** 61-70.

LAPETINA, E. G., LACAL, J. C., REEP, B. R. & VEDIA, L. M. Y. 1989. A RAS-RELATED PROTEIN IS PHOSPHORYLATED AND TRANSLOCATED BY AGONISTS THAT INCREASE CAMP LEVELS IN HUMAN-PLATELETS. *Proceedings of the National Academy of Sciences of the United States of America,* 86**,** 3131-3134.

LAWRENCE, W. G., VARADI, G., ENTINE, G., PODNIESINSKI, E. & WALLACE, P. K. 2008. Enhanced red and near infrared detection in flow cytometry using avalanche photodiodes. *Cytometry A,* 73**,** 767-76.

LEELATIAN, N., DIGGINS, K. E. & IRISH, J. M. 2015. Characterizing Phenotypes and Signaling Networks of Single Human Cells by Mass Cytometry. *Methods Mol Biol,* 1346**,** 99-113.

LEFRANCAIS, E., ORTIZ-MUNOZ, G., CAUDRILLIER, A., MALLAVIA, B., LIU, F. C., SAYAH, D. M., THORNTON, E. E., HEADLEY, M. B., DAVID, T., COUGHLIN, S. R., KRUMMEL, M. F., LEAVITT, A. D., PASSEGUE, E. & LOONEY, M. R. 2017. The lung is a site of platelet biogenesis and a reservoir for haematopoietic progenitors. *Nature,* 544**,** 105-+.

LENZ, M. L., HUGHES, H., MITCHELL, J. R., VIA, D. P., GUYTON, J. R., TAYLOR, A. A., GOTTO, A. M. & SMITH, C. V. 1990. LIPID HYDROPEROXY AND HYDROXY DERIVATIVES IN COPPER-

CATALYZED OXIDATION OF LOW-DENSITY-LIPOPROTEIN. *Journal of Lipid Research,* 31**,** 1043-1050.

LEV, E. I. 2016. Immature Platelets Clinical Relevance and Research Perspectives. *Circulation,* 134**,** 987-988.

LEVITAN, I., VOLKOV, S. & SUBBAIAH, P. V. 2010. Oxidized LDL: Diversity, Patterns of Recognition, and Pathophysiology. *Antioxidants & Redox Signaling,* 13**,** 39-75.

LHERMUSIER, T., CHAP, H. & PAYRASTRE, B. 2011. Platelet membrane phospholipid asymmetry: from the characterization of a scramblase activity to the identification of an essential protein mutated in Scott syndrome. *Journal of Thrombosis and Haemostasis,* 9**,** 1883-1891.

LI, J. L. Y., ZARBOCK, A. & HIDALGO, A. 2017. Platelets as autonomous drones for hemostatic and immune surveillance. *Journal of Experimental Medicine,* 214**,** 2193-2204.

LIBERSAN, D., ROUSSEAU, G. & MERHI, Y. 2003. Differential regulation of P-selectin expression by protein kinase A and protein kinase G in thrombin-stimulated human platelets. *Thrombosis and Haemostasis,* 89**,** 310-317.

LIN, Y. C., HUANG, D. Y., WANG, J. S., LIN, Y. L., HSIEH, S. L., HUANG, K. C. & LIN, W. W. 2015. Syk is involved in NLRP3 inflammasome-mediated caspase-1 activation through adaptor ASC phosphorylation and enhanced oligomerization. *Journal of Leukocyte Biology,* 97**,** 825-835.

LINDEN, M. D., FRELINGER, A. L., BARNARD, M. R., PRZYKLENK, K., FURMAN, M. I. & MICHELSON, A. D. 2004. Application of flow cytometry to platelet disorders. *Seminars in Thrombosis and Hemostasis,* 30**,** 501-511.

LINDERMAN, G. C., RACHH, M., HOSKINS, J. G., STEINERBERGER, S. & KLUGER, Y. 2019. Fast interpolation-based t-SNE for improved visualization of single-cell RNA-seq data. *Nature Methods,* 16**,** 243-245.

LITINSKIY, M. B., NARDELLI, B., HILBERT, D. M., HE, B., SCHAFFER, A., CASALI, P. & CERUTTI, A. 2002. DCs induce CD40-independent immunoglobulin class switching through BLyS and APRIL. *Nature Immunology,* 3**,** 822-829.

LIU, W. W., YIN, Y. L., ZHOU, Z. H., HE, M. & DAI, Y. L. 2014. OxLDL-induced IL-1beta secretion promoting foam cells formation was mainly via CD36 mediated ROS production leading to NLRP3 inflammasome activation. *Inflammation Research,* 63**,** 33-43.

LIU, X., PICHULIK, T., WOLZ, O.-O., DANG, T.-M., STUTZ, A., DILLEN, C., DELMIRO GARCIA, M., KRAUS, H., DICKHOFER, S., DAIBER, E., MUNZENMAYER, L., WAHL, S., RIEBER, N., KUMMERLE-DESCHNER, J., YAZDI, A., FRANZ-WACHTEL, M., MACEK, B., RADSAK, M., VOGEL, S., SCHULTE, B., WALZ, J. S., HARTL, D., LATZ, E., STILGENBAUER, S., GRIMBACHER, B., MILLER, L., BRUNNER, C., WOLZ, C. & WEBER, A. N. R. 2017. Human NACHT, LRR, and PYD domain-containing protein 3 (NLRP3) inflammasome activity is regulated by and potentially targetable through Bruton tyrosine kinase. *The Journal of allergy and clinical immunology*, 4, 1054-1067.

LIU, X., ZHANG, Z. B., RUAN, J. B., PAN, Y. D., MAGUPALLI, V. G., WU, H. & LIEBERMAN, J. 2016. Inflammasome-activated gasdermin D causes pyroptosis by forming membrane pores. *Nature,* 535**,** 153-158.

LOCKE, D., CHEN, H., LIU, Y., LIU, C. D. & KAHN, M. L. 2002. Lipid rafts orchestrate signaling by the platelet receptor glycoprotein VI. *Journal of Biological Chemistry,* 277**,** 18801-18809.

LOPEZ, J. A., DEL CONDE, I. & SHRIMPTON, C. N. 2005. Receptors, rafts, and microvesicles in thrombosis and inflammation. *Journal of Thrombosis and Haemostasis,* 3**,** 1737-1744.

LOWRY, O. H., ROSEBROUGH, N. J., FARR, A. L. & RANDALL, R. J. 1951. PROTEIN MEASUREMENT WITH THE FOLIN PHENOL REAGENT. *Journal of Biological Chemistry,* 193**,** 265-275.

LOYAU, S., DUMONT, B., OLLIVIER, V., BOULAFTALI, Y., FELDMAN, L., AJZENBERG, N. & JANDROT-PERRUS, M. 2012. Platelet Glycoprotein VI Dimerization, an Active Process Inducing Receptor Competence, Is an Indicator of Platelet Reactivity. *Arteriosclerosis Thrombosis and Vascular Biology,* 32**,** 778-U543.

MACWAN, A. S., BOKNÄS, N., NTZOUNI, M. P., RAMSTRÖM, S., GIBBINS, J. M., FAXÄLV, L. & LINDAHL, T. L. 2019. Gradient-dependent inhibition of stimulatory signaling from platelet G protein-coupled receptors. *Haematologica,* 1482-1492.

MAGWENZI, S., WOODWARD, C., WRAITH, K. S., ABURIMA, A., RASLAN, Z., JONES, H., MCNEIL, C., WHEATCROFT, S., YULDASHEVA, N., FEBBRIAO, M., KEARNEY, M. & NASEEM, K. M. 2015. Oxidized LDL activates blood platelets through CD36/NOX2-mediated inhibition of the cGMP/protein kinase G signaling cascade. *Blood,* 125**,** 2693-2703.

MANGANELLO, J. M., DJELLAS, Y., BORG, C., ANTONAKIS, K. & LE BRETON, G. C. 1999. Cyclic AMP-dependent phosphorylation of thromboxane A(2) receptor-associated G alpha(13). *Journal of Biological Chemistry,* 274**,** 28003-28010.

MANGANELLO, J. M., HUANG, J. S., KOZASA, T., VOYNO-YASENETSKAYA, T. A. & LE BRETON, G. C. 2003. Protein kinase A-mediated phosphorylation of the G alpha(13) switch I region alters the G alpha beta gamma(13)-G protein-coupled receptor complex and inhibits Rho activation. *Journal of Biological Chemistry,* 278**,** 124-130.

MARTIN, J. F., KRISTENSEN, S. D., MATHUR, A., GROVE, E. L. & CHOUDRY, F. A. 2012. The causal role of megakaryocyte-platelet hyperactivity in acute coronary syndromes. *Nature Reviews Cardiology,* 9**,** 658-670.

MARTINON, F., PETRILLI, V., MAYOR, A., TARDIVEL, A. & TSCHOPP, J. 2006. Gout-associated uric acid crystals activate the NALP3 inflammasome. *Nature,* 440**,** 237-241.

MATHEWS, R. J., ROBINSON, J. I., BATTELLINO, M., WONG, C., TAYLOR, J. C., EYRE, S., CHURCHMAN, S. M., WILSON, A. G., ISAACS, J. D., HYRICH, K., BARTON, A., PLANT, D., SAVIC, S., COOK, G. P., SARZI-PUTTINI, P., EMERY, P., BARRETT, J. H., MORGAN, A. W., MCDERMOTT, M. F. & BRAGGSS 2014. Evidence of NLRP3-inflammasome activation in rheumatoid arthritis (RA); genetic variants within the NLRP3-inflammasome complex in relation

to susceptibility to RA and response to anti-TNF treatment. *Annals of the Rheumatic Diseases,* 73**,** 1202-1210.

MATSUSHITA, K., TAKEOKA, M., SAGARA, J., ITANO, N., KUROSE, Y., NAKAMURA, A. & TANIGUCHI, S. 2009. A Splice Variant of ASC Regulates IL-1 beta Release and Aggregates Differently from Intact ASC. *Mediators of Inflammation,* 287387.

MEERSCHAERT, J. & FURIE, M. B. 1995. THE ADHESION MOLECULES USED BY MONOCYTES FOR MIGRATION ACROSS ENDOTHELIUM INCLUDE CD11A/CD18, CD11B/CD18, AND VLA-4 ON MONOCYTES AND ICAM-1, VCAM-1, AND OTHER LIGANDS ON ENDOTHELIUM. *Journal of Immunology,* 154**,** 4099-4112.

MEHTA, P., CUMMINGS, R. D. & MCEVER, R. P. 1998. Affinity and kinetic analysis of P-selectin binding to P-selectin glycoprotein ligand-1. *Journal of Biological Chemistry,* 273**,** 32506-32513.

MENCHE, D., ISRAEL, A. & KARPATKIN, S. 1980. PLATELETS AND MICROTUBULES - EFFECT OF COLCHICINE AND D2O ON PLATELET-AGGREGATION AND RELEASE INDUCED BY CALCIUM IONOPHORE A23187. *Journal of Clinical Investigation,* 66**,** 284-291.

MIAO, E. A., RAJAN, J. V. & ADEREM, A. 2011. Caspase-1-induced pyroptotic cell death. *Immunological Reviews,* 243**,** 206-214.

MICHELSON, A. D. 1994. PLATELET ACTIVATION BY THROMBIN CAN BE DIRECTLY MEASURED IN WHOLE-BLOOD THROUGH THE USE OF THE PEPTIDE GPRP AND FLOW-CYTOMETRY - METHODS AND CLINICAL-APPLICATIONS. *Blood Coagulation & Fibrinolysis,* 5**,** 121-131.

MITCHELL, J. A., ALI, F., BAILEY, L., MORENO, L. & HARRINGTON, L. S. 2008. Role of nitric oxide and prostacyclin as vasoactive hormones released by the endothelium. *Experimental Physiology,* 93**,** 141-147.

MOORE, K. L. 1998. Structure and function of P-selectin Glycoprotein ligand-1. *Leukemia & Lymphoma,* 29**,** 1-15.

MOORE, K. L., PATEL, K. D., BRUEHL, R. E., LI, F. G., JOHNSON, D. A., LICHENSTEIN, H. S., CUMMINGS, R. D., BAINTON, D. F. & MCEVER, R. P. 1995. P-SELECTIN GLYCOPROTEIN LIGAND-1 MEDIATES ROLLING OF HUMAN NEUTROPHILS ON P-SELECTIN. *Journal of Cell Biology,* 128**,** 661-671.

MORRELL, C. N., AGGREY, A. A., CHAPMAN, L. M. & MODJESKI, K. L. 2014. Emerging roles for platelets as immune and inflammatory cells. *Blood,* 123**,** 2759-2767.

MURAKAMI, T., OCKINGER, J., YU, J. J., BYLES, V., MCCOLL, A., HOFER, A. M. & HORNG, T. 2012. Critical role for calcium mobilization in activation of the NLRP3 inflammasome. *Proceedings of the National Academy of Sciences of the United States of America,* 109**,** 11282-11287.

MURTHY, P., DURCO, F., MILLER-OCUIN, J. L., TAKEDAI, T., SHANKAR, S., LIANG, X. Y., LIU, X., CUI, X. D., SACHDEV, U., RATH, D., LOTZE, M. T., ZEH, H. J., GAWAZ, M., WEBER, A. N. & VOGEL, S. 2017. The NLRP3 inflammasome and bruton's tyrosine kinase in platelets co-regulate platelet activation, aggregation, and in vitro thrombus formation. *Biochemical and Biophysical Research Communications,* 483**,** 230-236.

NASEEM, K. M., GOODALL, A. H. & BRUCKDORFER, K. R. 1997. Differential effects of native and oxidatively modified low-density lipoproteins on platelet function. *Platelets,* 8**,** 163-173.

NERGIZ-UNAL, R., LAMERS, M. M. E., VAN KRUCHTEN, R., LUIKEN, J. J., COSEMANS, J., GLATZ, J. F. C., KUIJPERS, M. J. E. & HEEMSKERK, J. W. M. 2011. Signaling role of CD36 in platelet activation and thrombus formation on immobilized thrombospondin or oxidized low-density lipoprotein. *Journal of Thrombosis and Haemostasis,* 9**,** 1835-1846.

NHEK, S., CLANCY, R., LEE, K. A., ALLEN, N. M., BARRETT, T. J., MARCANTONI, E., NWAUKONI, J., RASMUSSEN, S., RUBIN, M., NEWMAN, J. D., BUYON, J. P. & BERGER, J. S. 2017. Activated Platelets Induce Endothelial Cell Activation via an Interleukin-1 Pathway in Systemic Lupus Erythematosus. *Arteriosclerosis Thrombosis and Vascular Biology,* 37**,** 707-716.

OBERPRIELER, N. G. & TASKEN, K. 2011. Analysing phosphorylation-based signalling networks by phospho flow cytometry. *Cellular Signalling,* 23**,** 14-18.

OBYDENNYI, S. I., ARTEMENKO, E. O., SVESHNIKOVA, A. N., IGNATOVA, A. A., VARLAMOVA, T. V., GAMBARYAN, S., LOMAKINA, G. Y., UGAROVA, N. N., KIREEV, I. I., ATAULLAKHANOV, F. I., NOVICHKOVA, G. A., MASCHAN, A. A., SHCHERBINA, A. & PANTELEEV, M. 2019. Mechanisms of increased mitochondria-dependent necrosis in Wiskott-Aldrich syndrome platelets. *Haematologica,* 105-2.

OTTO, G. P., RATHKOLB, B., OESTEREICHER, M. A., LENGGER, C. J., MOERTH, C., MICKLICH, K., FUCHS, H., GAILUS-DURNER, V., WOLF, E. & DE ANGELIS, M. H. 2016. Clinical Chemistry Reference Intervals for C57BL/6J, C57BL/6N, and C3HeB/FeJ Mice (Mus musculus). *Journal of the American Association for Laboratory Animal Science,* 55**,** 375-386.

PALADE, G. E. 1953. AN ELECTRON MICROSCOPE STUDY OF THE MITOCHONDRIAL STRUCTURE. *Journal of Histochemistry & Cytochemistry,* 1**,** 188-211.

PARISE, L. V. 2016. Introduction to a review series: megakaryocytes to platelets in health and disease. *Blood,* 127**,** 1215-1215.

PARK, W. H., HAN, Y. W., KIM, S. H. & KIM, S. Z. 2007. An ROS generator, antimycin A, inhibits the growth of HeLa cells via apoptosis. *Journal of Cellular Biochemistry,* 102**,** 98-109.

PERREGAUX, D. & GABEL, C. A. 1994. INTERLEUKIN-1-BETA MATURATION AND RELEASE IN RESPONSE TO ATP AND NIGERICIN - EVIDENCE THAT POTASSIUM-DEPLETION MEDIATED BY THESE AGENTS IS A NECESSARY AND COMMON FEATURE OF THEIR ACTIVITY. *Journal of Biological Chemistry,* 269**,** 15195-15203.

PLOW, E. F. & MARGUERIE, G. 1982. INHIBITION OF FIBRINOGEN BINDING TO HUMAN-PLATELETS BY THE TETRAPEPTIDE "GLYCYL-L-PROLYL-L-ARGINYL-L-PROLINE. *Proceedings of the National Academy of Sciences of the United States of America-Biological Sciences,* 79**,** 3711-3715.

PODOPLELOVA, N. A., SVESHNIKOVA, A. N., KOTOVA, Y. N., ECKLY, A., RECEVEUR, N., NECHIPURENKO, D. Y., OBYDENNYI, S. I., KIREEV, II, GACHET, C., ATAULLAKHANOV, F. I., MANGIN, P. H. & PANTELEEV, M. A. 2016. Coagulation factors bound to procoagulant platelets concentrate in cap structures to promote clotting. *Blood,* 128**,** 1745-1755.

PODREZ, E. A., BYZOVA, T. V., FEBBRAIO, M., SALOMON, R. G., MA, Y., VALIYAVEETTIL, M., POLIAKOV, E., SUN, M., FINTON, P. J., CURTIS, B. R., CHEN, J., ZHANG, R., SILVERSTEIN, R. L. & HAZEN, S. L. 2007. Platelet CD36 links hyperlipidemia, oxidant stress and a prothrombotic phenotype. *Nature Medicine,* 13**,** 1086-1095.

PODREZ, E. A., POLIAKOV, E., SHEN, Z. Z., ZHANG, R. L., DENG, Y. J., SUN, M. J., FINTON, P. J., SHAN, L., FEBBRAIO, M., HAJJAR, D. P., SILVERSTEIN, R. L., HOFF, H. F., SALOMON, R. G. & HAZEN, S. L. 2002a. A novel family of atherogenic oxidized phospholipids promotes macrophage foam cell formation via the scavenger receptor CD36 and is enriched in atherosclerotic lesions. *Journal of Biological Chemistry,* 277**,** 38517-38523.

PODREZ, E. A., POLIAKOV, E., SHEN, Z. Z., ZHANG, R. L., DENG, Y. J., SUN, M. J., FINTON, P. J., SHAN, L., GUGIU, B., FOX, P. L., HOFF, H. F., SALOMON, R. G. & HAZEN, S. L. 2002b. Identification of a novel family of oxidized phospholipids that serve as ligands for the macrophage scavenger receptor CD36. *Journal of Biological Chemistry,* 277**,** 38503-38516.

POTTER, V. R. & REIF, A. E. 1952. INHIBITION OF AN ELECTRON TRANSPORT COMPONENT BY ANTIMYCIN-A. *Journal of Biological Chemistry,* 194**,** 287-297.

POZAROWSKI, P., HUANG, X., HALICKA, D. H., LEE, B., JOHNSON, G. & DARZYNKIEWICZ, Z. 2003. Interactions of fluorochrome-labeled caspase inhibitors with apoptotic cells: A caution in data interpretation. *Cytometry Part A,* 55A**,** 50-60.

PRETORIUS, E., ENGELBRECHT, M. J. & DUIM, W. 2012. Thromboembolic Ischemic Stroke and the Presence of Necrotic Platelets: A Scanning Electron Microscopy Investigation. *Ultrastructural Pathology,* 36**,** 19-22.

PY, B. F., KIM, M. S., VAKIFAHMETOGLU-NORBERG, H. & YUAN, J. Y. 2013. Deubiquitination of NLRP3 by BRCC3 Critically Regulates Inflammasome Activity. *Molecular Cell,* 49**,** 331-338.

QIAO, J. L., WU, X. Q., LUO, Q., WEI, G. Y., XU, M. D., WU, Y. L., LIU, Y., LI, X. Q., ZI, J., JU, W., FU, L., CHEN, C., WU, Q. Y., ZHU, S. Y., QI, K. M., LI, D. P., LI, Z. Y., ANDREWS, R. K., ZENG, L. Y., GARDINER, E. E. & XU, K. L. 2018. NLRP3 regulates platelet integrin alpha IIb beta 3 outside-in signaling, hemostasis and arterial thrombosis. *Haematologica,* 103**,** 1568-1576.

QUINTON, T. M., BROWN, K. D. & DEAN, W. L. 1996. Inositol 1,4,5-trisphosphate-mediated Ca2+ release from platelet internal membranes is regulated by differential phosphorylation. *Biochemistry,* 35**,** 6865-6871.

RAMOS-ARELLANO, L. E., MUNOZ-VALLE, J. F., DE LA CRUZ-MOSSO, U., SALGADO-BERNABE, A. B., CASTRO-ALARCON, N. & PARRA-ROJAS, I. 2014. Circulating CD36 and oxLDL levels are associated

with cardiovascular risk factors in young subjects. *Bmc Cardiovascular Disorders,* 14:54.

RAMSTROM, S., SODERGREN, A. L., TYNNGARD, N. & LINDAHL, T. L. 2016. Platelet Function Determined by Flow Cytometry: New Perspectives? *Seminars in Thrombosis and Hemostasis,* 42**,** 268-281.

RANDRIAMBOAVONJY, V., MANN, W. A., ELGHEZNAWY, A., POPP, R., ROGOWSKI, P., DORNAUF, I., DROSE, S. & FLEMING, I. 2015. Metformin reduces hyper-reactivity of platelets from patients with polycystic ovary syndrome by improving mitochondrial integrity. *Thrombosis and Haemostasis,* 114**,** 569-578.

RASLAN, Z., ABURIMA, A. & NASEEM, K. M. 2015. The Spatiotemporal Regulation of cAMP Signaling in Blood Platelets-Old Friends and New Players. *Frontiers in Pharmacology,* 6.

RASLAN, Z. & NASEEM, K. M. 2014. The control of blood platelets by cAMP signalling. *Biochemical Society Transactions,* 42**,** 289-294.

RASLAN, Z. & NASEEM, K. M. 2015. Compartmentalisation of cAMP-dependent signalling in blood platelets: The role of lipid rafts and actin polymerisation. *Platelets,* 26**,** 349-357.

REDDY, E. C., WANG, H., CHRISTENSEN, H., MCMILLAN-WARD, E., ISRAELS, S. J., BANG, K. W. A. & RAND, M. L. 2018. Analysis of procoagulant phosphatidylserine-exposing platelets by imaging flow cytometry. *Research and Practice in Thrombosis and Haemostasis,* 2**,** 736-750.

REX, S., BEAULIEU, L. M., PERLMAN, D. H., VITSEVA, O., BLAIR, P. S., MCCOMB, M. E., COSTELLO, C. E. & FREEDMAN, J. E. 2009. Immune versus thrombotic stimulation of platelets differentially regulates signalling pathways, intracellular protein-protein interactions, and alpha-granule release. *Thrombosis and Haemostasis,* 102**,** 97-110.

RIDKER, P. M., EVERETT, B. M., THUREN, T., MACFADYEN, J. G., CHANG, W. H., BALLANTYNE, C., FONSECA, F., NICOLAU, J., KOENIG, W., ANKER, S. D., KASTELEIN, J. J. P., CORNEL, J. H., PAIS, P., PELLA, D., GENEST, J., CIFKOVA, R., LORENZATTI, A., FORSTER, T., KOBALAVA, Z., VIDA-SIMITI, L., FLATHER, M., SHIMOKAWA, H., OGAWA, H., DELLBORG, M., ROSSI, P. R. F., TROQUAY, R. P. T., LIBBY, P., GLYNN, R. J. & GRP, C. T. 2017a. Antiinflammatory Therapy with Canakinumab for Atherosclerotic Disease. *New England Journal of Medicine,* 377**,** 1119-1131.

RIDKER, P. M., MACFADYEN, J. G., THUREN, T., EVERETT, B. M., LIBBY, P., GLYNN, R. J. & GRP, C. T. 2017b. Effect of interleukin-1 beta inhibition with canakinumab on incident lung cancer in patients with atherosclerosis: exploratory results from a randomised, double-blind, placebo-controlled trial. *Lancet,* 390**,** 1833-1842.

RIDKER, P. M., THUREN, T., ZALEWSKI, A., LIBBY, P. & GRP, C. S. 2011. Interleukin-1 beta inhibition and the prevention of recurrent cardiovascular events: Rationale and Design of the Canakinumab Anti-inflammatory Thrombosis Outcomes Study (CANTOS). *American Heart Journal,* 162**,** 597-605.

RINGEL-SCAIA, V. M., MCDANIEL, D. K. & ALLEN, I. C. 2016. The Goldilocks Conundrum: NLR Inflammasome Modulation of

Gastrointestinal Inflammation during Inflammatory Bowel Disease. *Critical Reviews in Immunology,* 36**,** 283-314.

RODGERS, M. A., BOWMAN, J. W., FUJITA, H., ORAZIO, N., SHI, M., LIANG, Q. M., AMATYA, R., KELLY, T. J., IWAI, K., TING, J. & JUNG, J. U. 2014. The linear ubiquitin assembly complex (LUBAC) is essential for NLRP3 inflammasome activation. *Journal of Experimental Medicine,* 211**,** 1331-1345.

ROSSAINT, J., KUHNE, K., SKUPSKI, J., VAN AKEN, H., LOONEY, M. R., HIDALGO, A. & ZARBOCK, A. 2016. Directed transport of neutrophil-derived extracellular vesicles enables platelet-mediated innate immune response. *Nature Communications,* 7.

ROWCZENIO, D. M., GOMES, S. M., AROSTEGUI, J. I., MENSA-VILARO, A., OMOYINMI, E., TROJERL, H., BAGINSKA, A., BAROJA-MAZO, A., PELEGRIN, P., SAVIC, S., LANE, T., WILLIAMS, R., BROGAN, P., LACHMANN, H. J. & HAWKINS, P. N. 2017. Late-Onset Cryopyrin-Associated Periodic Syndromes Caused by Somatic NLRP3 Mosaicism - UK Single Center Experience. *Frontiers in Immunology,* 8.

ROWLEY, J. W., OLER, A. J., TOLLEY, N. D., HUNTER, B. N., LOW, E. N., NIX, D. A., YOST, C. C., ZIMMERMAN, G. A. & WEYRICH, A. S. 2011. Genome-wide RNA-seq analysis of human and mouse platelet transcriptomes. *Blood,* 118**,** E101-E111.

SAGULENKO, V., THYGESEN, S. J., SESTER, D. P., IDRIS, A., CRIDLAND, J. A., VAJJHALA, P. R., ROBERTS, T. L., SCHRODER, K., VINCE, J. E., HILL, J. M., SILKE, J. & STACEY, K. J. 2013. AIM2 and NLRP3 inflammasomes activate both apoptotic and pyroptotic death pathways via ASC. *Cell Death and Differentiation,* 20**,** 1149-1160.

SALZER, U., CHAPEL, H. M., WEBSTER, A. D. B., PAN-HAMMARSTROM, Q., SCHMITT-GRAEFF, A., SCHLESIER, M., PETER, H. H., ROCKSTROH, J. K., SCHNEIDER, P., SCHAFFER, A. A., HAMMARSTROM, L. & GRIMBACHER, B. 2005. Mutations in TNFRSF13B encoding TACI are associated with common variable immunodeficiency in humans. *Nature Genetics,* 37**,** 820-828.

SCHRODER, K. & TSCHOPP, J. 2010. The Inflammasomes. *Cell,* 140**,** 821-832.

SCHULZ, E., WENZEL, P., MUNZEL, T. & DAIBER, A. 2014. Mitochondrial Redox Signaling: Interaction of Mitochondrial Reactive Oxygen Species with Other Sources of Oxidative Stress. *Antioxidants & Redox Signaling,* 20**,** 308-324.

SELVADURAI, M. V. & HAMILTON, J. R. 2018. Structure and function of the open canalicular system - the platelet's specialized internal membrane network. *Platelets,* 29**,** 319-325.

SHARMA, G. K. & TALBOT, I. C. 1986. PULMONARY MEGAKARYOCYTES - MISSING LINK BETWEEN CARDIOVASCULAR AND RESPIRATORY-DISEASE. *Journal of Clinical Pathology,* 39**,** 969-976.

SHEEDY, F. J., GREBE, A., RAYNER, K. J., KALANTARI, P., RAMKHELAWON, B., CARPENTER, S. B., BECKER, C. E., EDIRIWEERA, H. N., MULLICK, A. E., GOLENBOCK, D. T., STUART, L. M., LATZ, E., FITZGERALD, K. A. & MOORE, K. J.

2013. CD36 coordinates NLRP3 inflammasome activation by facilitating intracellular nucleation of soluble ligands into particulate ligands in sterile inflammation. *Nature Immunology,* 14**,** 812-820.

SHI, H. X., WANG, Y., LI, X. H., ZHAN, X. M., TANG, M., FINA, M., SU, L. J., PRATT, D., BU, C. H., HILDEBRAND, S., LYON, S., SCOTT, L., QUAN, J. X., SUN, Q. H., RUSSELL, J., ARNETT, S., JUREK, P., CHEN, D., KRAVCHENKO, V. V., MATHISON, J. C., MORESCO, E. M. Y., MONSON, N. L., ULEVITCH, R. J. & BEUTLER, B. 2016. NLRP3 activation and mitosis are mutually exclusive events coordinated by NEK7, a new inflammasome component. *Nature Immunology,* 17**,** 250-258.

SMITH, B. K., JAIN, S. S., RIMBAUD, S., DAM, A., QUADRILATERO, J., VENTURA-CLAPIER, R., BONEN, A. & HOLLOWAY, G. P. 2011. FAT/CD36 is located on the outer mitochondrial membrane, upstream of long-chain acyl-CoA synthetase, and regulates palmitate oxidation. *Biochemical Journal,* 437**,** 125-134.

SODERGREN, A. L. & RAMSTROM, S. 2018. Platelet subpopulations remain despite strong dual agonist stimulation and can be characterised using a novel six-colour flow cytometry protocol. *Scientific Reports,* 8.

SODERGREN, A. L., TYNNGARD, N., BERLIN, G. & RAMSTROM, S. 2016. Responsiveness of platelets during storage studied with flow cytometry - formation of platelet subpopulations and LAMP-1 as new markers for the platelet storage lesion. *Vox Sanguinis,* 110**,** 116-125.

SONG, H., LIU, B. Y., HUAI, W. W., YU, Z. X., WANG, W. W., ZHAO, J., HAN, L. H., JIANG, G. S., ZHANG, L. N., GAO, C. J. & ZHAO, W. 2016. The E3 ubiquitin ligase TRIM31 attenuates NLRP3 inflammasome activation by promoting proteasomal degradation of NLRP3. *Nature Communications,* 7:13727.

SONG, N., LIU, Z. S., XUE, W., BAI, Z. F., WANG, Q. Y., DAI, J., LIU, X., HUANG, Y. J., CAI, H., ZHAN, X. Y., HAN, Q. Y., WANG, H. X., CHEN, Y., LI, H. Y., LI, A. L., ZHANG, X. M., ZHOU, T. & LI, T. 2017. NLRP3 Phosphorylation Is an Essential Priming Event for Inflammasome Activation. *Molecular Cell,* 68**,** 185-197.

SPERLING, S., VINHOLT, P. J., SPROGOE, U., YAZER, M. H., FREDERIKSEN, H. & NIELSEN, C. 2019. The effects of storage on platelet function in different blood products. *Hematology,* 24**,** 89-96.

SPURGEON, B. E. J., ABURIMA, A., OBERPRIELER, N. G., TASKEN, K. & NASEEM, K. M. 2014. Multiplexed phosphospecific flow cytometry enables large-scale signaling profiling and drug screening in blood platelets. *Journal of Thrombosis and Haemostasis,* 12**,** 1733-1743.

SPURGEON, B. E. J. & NASEEM, K. M. 2018. High-Throughput Signaling Profiling in Blood Platelets by Multiplexed Phosphoflow Cytometry. *Methods Mol Biol,* 1812**,** 95-111.

SPURGEON, B. E. J. & NASEEM, K. M. 2019. Platelet Flow Cytometry: Instrument Setup, Controls, and Panel Performance. *Cytometry B Clin Cytom.*

STALKER, T. J., NEWMAN, D. K., MA, P., WANNEMACHER, K. M. & BRASS, L. F. 2012. Platelet signaling. *Handb Exp Pharmacol*, 59-85.

STALKER, T. J., TRAXLER, E. A., WU, J., WANNEMACHER, K. M., CERMIGNANO, S. L., VORONOV, R., DIAMOND, S. L. & BRASS, L.

F. 2013. Hierarchical organization in the hemostatic response and its relationship to the platelet-signaling network. *Blood,* 121**,** 1875-1885.

STANKOVA, T., DELCHEVA, G., MANEVA, A. & VLADEVA, S. 2019. Serum Levels of Carbamylated LDL and Soluble Lectin-Like Oxidized Low-Density Lipoprotein Receptor-1 Are Associated with Coronary Artery Disease in Patients with Metabolic Syndrome. *Medicina (Kaunas),* 55.

STEINBERG, D. 2009. The LDL modification hypothesis of atherogenesis: an update. *Journal of Lipid Research,* 50**,** S376-S381.

STELLOS, K., SAUTER, R., FAHRLEITNER, M., GRIMM, J., STAKOS, D., EMSCHERMANN, F., PANAGIOTA, V., GNERLICH, S., PERK, A., SCHONBERGER, T., BIGALKE, B., LANGER, H. F. & GAWAZ, M. 2012. Binding of Oxidized Low-Density Lipoprotein on Circulating Platelets Is increased in Patients With Acute Coronary Syndromes and Induces Platelet Adhesion to Vascular Wall In Vivo-Brief Report. *Arteriosclerosis Thrombosis and Vascular Biology,* 32**,** 2017-U626.

STEWART, C. R., STUART, L. M., WILKINSON, K., VAN GILS, J. M., DENG, J. S., HALLE, A., RAYNER, K. J., BOYER, L., ZHONG, R. Q., FRAZIER, W. A., LACY-HULBERT, A., EL KHOURY, J., GOLENBOCK, D. T. & MOORE, K. J. 2010. CD36 ligands promote sterile inflammation through assembly of a Toll-like receptor 4 and 6 heterodimer. *Nature Immunology,* 11**,** 155-U75.

STOCKER, R. & KEANEY, J. F. 2004. Role of oxidative modifications in atherosclerosis. *Physiological Reviews,* 84**,** 1381-1478.

STOKES, K. Y., CALAHAN, L., HAMRIC, C. M., RUSSELL, J. M. & GRANGER, D. N. 2009. CD40/CD40L contributes to hypercholesterolemia-induced microvascular inflammation. *American Journal of Physiology-Heart and Circulatory Physiology,* 296**,** H689-H697.

TAIT, S. W. G. & GREEN, D. R. 2012. Mitochondria and cell signalling. *Journal of Cell Science,* 125**,** 807-815.

TANG, T. T., LANG, X. T., XU, C. F., WANG, X. Q., GONG, T., YANG, Y. Q., CUI, J., BAI, L., WANG, J., JIANG, W. & ZHOU, R. B. 2017. CLICs-dependent chloride efflux is an essential and proximal upstream event for NLRP3 inflammasome activation. *Nature Communications,* 8.

TANG, W. H., STITHAM, J., JIN, Y., LIU, R. J., LEE, S. H., DU, J., ATTEYA, G., GLEIM, S., SPOLLETT, G., MARTIN, K. & HWA, J. 2014. Aldose Reductase-Mediated Phosphorylation of p53 Leads to Mitochondrial Dysfunction and Damage in Diabetic Platelets. *Circulation,* 129**,** 1598-1609.

TONINELLO, A. & SILIPRANDI, N. 1982. RESTORATION OF MEMBRANE-POTENTIAL IN MITOCHONDRIA DE-ENERGIZED WITH CARBONYL CYANIDE PARA-TRIFLUOROMETHOXYPHENYLHYDRAZONE (FCCP). *Biochimica Et Biophysica Acta,* 682**,** 289-292.

TOPALOV, N. N., YAKIMENKO, A. O., CANAULT, M., ARTEMENKO, E. O., ZAKHAROVA, N. V., ABAEVA, A. A., LOOSVELD, M., ATAULLAKHANOV, F. I., NURDEN, A. T., ALESSI, M. C. & PANTELEEV, M. A. 2012. Two Types of Procoagulant Platelets Are Formed Upon Physiological Activation and Are Controlled by Integrin

alpha(IIb)beta(3). *Arteriosclerosis Thrombosis and Vascular Biology,* 32**,** 2475-2483.

TOUYZ, R. M. 2014. Linking LOX-1 and Arginase II Through Mitochondria A Novel Paradigm in Endothelial Dysfunction. *Circulation Research,* 115**,** 412-414.

TRUGILHO, M. R. D., HOTTZ, E. D., BRUNORO, G. V. F., TEIXEIRA-FERREIRA, A., CARVALHO, P. C., SALAZAR, G. A., ZIMMERMAN, G. A., BOZZA, F. A., BOZZA, P. T. & PERALES, J. 2017. Platelet proteome reveals novel pathways of platelet activation and platelet-mediated immunoregulation in dengue. *Plos Pathogens,* 13.

TUCKER, K. L., SAGE, T. & GIBBINS, J. M. 2012. Clot retraction. *Methods Mol Biol,* 788**,** 101-7.

VAN DER HEIJDEN, T., KRITIKOU, E., VENEMA, W., VAN DUIJN, J., VAN SANTBRINK, P. J., SLUTTER, B., FOKS, A. C., BOT, I. & KUIPER, J. 2017. NLRP3 Inflammasome Inhibition by MCC950 Reduces Atherosclerotic Lesion Development in Apolipoprotein E-Deficient Mice. *Arteriosclerosis, thrombosis, and vascular biology.*

VAN DER MAATEN, L. & HINTON, G. 2008. Visualizing Data using t-SNE. *Journal of Machine Learning Research,* 9**,** 2579-2605.

VAN GASSEN, S., CALLEBAUT, B., VAN HELDEN, M. J., LAMBRECHT, B. N., DEMEESTER, P., DHAENE, T. & SAEYS, Y. 2015. FlowSOM: Using self-organizing maps for visualization and interpretation of cytometry data. *Cytometry Part A,* 87A**,** 636-645.

VAN HOUT, G. P. J., BOSCH, L., ELLENBROEK, G., DE HAAN, J. J., VAN SOLINGE, W. W., COOPER, M. A., ARSLAN, F., DE JAGER, S. C. A., ROBERTSON, A. A. B., PASTERKAMP, G. & HOEFER, I. E. 2017. The selective NLRP3-inflammasome inhibitor MCC950 reduces infarct size and preserves cardiac function in a pig model of myocardial infarction. *European Heart Journal,* 38**,** 828-836.

VARGA-SZABO, D., BRAUN, A. & NIESWANDT, B. 2009. Calcium signaling in platelets. *Journal of Thrombosis and Haemostasis,* 7**,** 1057-1066.

VARGAS, J. R., RADOMSKI, M. & MONCADA, S. 1982. THE USE OF PROSTACYCLIN IN THE SEPARATION FROM PLASMA AND WASHING OF HUMAN-PLATELETS. *Prostaglandins,* 23**,** 929-945.

VATS, R., BRZOSKA, T., BENNEWITZ, M. F., JIMENEZ, M. A., PRADHAN-SUNDD, T., TUTUNCUOGLU, E., JONASSAINT, J., GUTIERREZ, E., WATKINS, S. C., SHIVA, S., SCOTT, M., MORELLI, A. E., NEAL, M. D., KATO, G. J., GLADWIN, M. T. & SUNDD, P. 2019. Platelet Extracellular Vesicles Drive Inflammasome-IL1β-dependent Lung Injury in Sickle Cell Disease. *Am J Respir Crit Care Med*, 201:33-46.

VINDIS, C., ELBAZ, M., ESCARGUEIL-BLANC, I., AUGE, N., HENIQUEZ, A., THIERS, J. C., NEGRE-SALVAYRE, A. & SALVAYRE, R. 2005. Two distinct calcium-dependent mitochondrial pathways are involved in oxidized LDL-induced apoptosis. *Arteriosclerosis Thrombosis and Vascular Biology,* 25**,** 639-645.

VOGEL, S., ARORA, T., WANG, X. D., ALMEIDA, L. E., QUEZADO, Z. & THEIN, S. L. 2017. The NLRP3 Inflammasome in Platelets Is Upregulated in Sickle Cell Disease and Promotes Platelet Aggregation and In Vitro Thrombosis. *Blood,* 130:1, 113.

VOGEL, S., ARORA, T., WANG, X. D., MENDELSOHN, L., NICHOLS, J., ALLEN, D., SHET, A. S., COMBS, C. A., QUEZADO, Z. M. N. &

THEIN, S. L. 2018a. The platelet NLRP3 inflammasome is upregulated in sickle cell disease via HMGB1/TLR4 and Bruton tyrosine kinase. *Blood Advances,* 2**,** 2672-2680.

VOGEL, S., MURTHY, P., CUI, X., LOTZE, M. T., ZEH, H. J. & SACHDEV, U. 2018b. TLR4-dependent upregulation of the platelet NLRP3 inflammasome promotes platelet aggregation in a murine model of hindlimb ischemia. *Biochem Biophys Res Commun*, 614-619.

VOGEL, S., RATH, D., LU, J., CHATTERJEE, M., GEISLER, T. & GAWAZ, M. 2015. Elevated mitochondrial membrane potential of circulating monocyte-platelet aggregates in patients with coronary heart disease. *International Journal of Cardiology,* 181**,** 135-137.

VOGEL, S. & THEIN, S. L. 2018. Platelets at the crossroads of thrombosis, inflammation and haemolysis. *British Journal of Haematology,* 180**,** 761-767.

VOGLER, M., HAMALI, H. A., SUN, X. M., BAMPTON, E. T. W., DINSDALE, D., SNOWDEN, R. T., DYER, M. J. S., GOODALL, A. H. & COHEN, G. M. 2011. BCL2/BCL-X-L inhibition induces apoptosis, disrupts cellular calcium homeostasis, and prevents platelet activation. *Blood,* 117**,** 7145-7154.

VOLF, I., MOESLINGER, T., COOPER, J., SCHMID, W. & KOLLER, E. 1999. Human platelets exclusively bind oxidized low density lipoprotein showing no specificity for acetylated low density lipoprotein. *Febs Letters,* 449**,** 141-145.

VULLIAMY, P., GILLESPIE, S., ARMSTRONG, P. C., ALLAN, H. E., WARNER, T. D. & BROHI, K. 2019. Histone H4 induces platelet ballooning and microparticle release during trauma hemorrhage. *Proceedings of the National Academy of Sciences of the United States of America,* 116**,** 17444-17449.

WADHERA, R. K., STEEN, D. L., KHAN, I., GIUGLIANO, R. P. & FOODY, J. M. 2016. A review of low-density lipoprotein cholesterol, treatment strategies, and its impact on cardiovascular disease morbidity and mortality. *Journal of Clinical Lipidology,* 10**,** 472-489.

WALSH, T. G., BERNDT, M. C., CARRIM, N., COWMAN, J., KENNY, D. & METHAROM, P. 2014. The role of Nox1 and Nox2 in GPVI-dependent platelet activation and thrombus formation. *Redox Biology,* 2**,** 178-186.

WANG, J. H., ZHANG, S. Z., JIN, Y. P., QIN, G. M., YU, L. & ZHANG, J. N. 2007. Elevated levels of platelet-monocyte aggregates and related circulating biomarkers in patients with acute coronary syndrome. *International Journal of Cardiology,* 115**,** 361-365.

WANG, L., WU, Q., FAN, Z. J., XIE, R. F., WANG, Z. C. & LU, Y. 2017a. Platelet mitochondrial dysfunction and the correlation with human diseases. *Biochemical Society Transactions,* 45**,** 1213-1223.

WANG, Y. M., GAO, H. Y., SHI, C., ERHARDT, P. W., PAVLOVSKY, A., SOLOVIEV, D. A., BLEDZKA, K., USTINOV, V., ZHU, L., QIN, J., MUNDAY, A. D., LOPEZ, J., PLOW, E. & SIMON, D. I. 2017b. Leukocyte integrin Mac-1 regulates thrombosis via interaction with platelet GPIb alpha. *Nature Communications,* 8.

WEHBI, V. L. & TASKEN, K. 2016. Molecular Mechanisms for cAMP-Mediated immunoregulationin T cells - Role of Anchored Protein Kinase A Signaling Units. *Frontiers in Immunology,* 7.

WELCH, E. L., CROOKS, M. G. & HART, S. P. 2018. Agreement between blood draw techniques for assessing platelet activation by flow cytometry. *Platelets*, 1-5.

WHITE, J. G. 2004. Electron microscopy methods for studying platelet structure and function. *Methods Mol Biol,* 272, 47-63.

WILKINS, G. M. & LEAKE, D. S. 1994a. THE EFFECT OF INHIBITORS OF FREE-RADICAL GENERATING ENZYMES ON LOW-DENSITY-LIPOPROTEIN OXIDATION BY MACROPHAGES. *Biochimica Et Biophysica Acta-Lipids and Lipid Metabolism,* 1211, 69-78.

WILKINS, G. M. & LEAKE, D. S. 1994b. THE OXIDATION OF LOW-DENSITY-LIPOPROTEIN BY CELLS OR IRON IS INHIBITED BY ZINC. *Febs Letters,* 341, 259-262.

WRAITH, K. S., MAGWENZI, S., ABURIMA, A., WEN, Y. C., LEAKE, D. & NASEEM, K. M. 2013. Oxidized low-density lipoproteins induce rapid platelet activation and shape change through tyrosine kinase and Rho kinase-signaling pathways. *Blood,* 122, 580-589.

WRIGHT, S. D., WEITZ, J. I., HUANG, A. J., LEVIN, S. M., SILVERSTEIN, S. C. & LOIKE, J. D. 1988. COMPLEMENT RECEPTOR TYPE-3 (CD11B/CD18) OF HUMAN POLYMORPHONUCLEAR LEUKOCYTES RECOGNIZES FIBRINOGEN. *Proceedings of the National Academy of Sciences of the United States of America,* 85, 7734-7738.

XU, J., SHI, C., LI, Q., WU, J. J., FORSTER, E. L. & YEW, D. T. 2007. Mitochondrial dysfunction in platelets and hippocampi of senescence-accelerated mice. *Journal of Bioenergetics and Biomembranes,* 39, 195-202.

YAMAGISHI, S., EDELSTEIN, D., DU, X. L. & BROWNLEE, M. 2001. Hyperglycemia potentiates collagen-induced platelet activation through mitochondrial superoxide overproduction. *Diabetes,* 50, 1491-1494.

YAN, R., WANG, Z. C., YUAN, Y. H., CHENG, H. & DAI, K. S. 2009. Role of cAMP-dependent protein kinase in the regulation of platelet procoagulant activity. *Archives of Biochemistry and Biophysics,* 485, 41-48.

YANG, M., COOLEY, B. C., LI, W., CHEN, Y. L., VASQUEZ-VIVAR, J., SCOGGINS, N. O., CAMERON, S. J., MORRELL, C. N. & SILVERSTEIN, R. L. 2017a. Platelet CD36 promotes thrombosis by activating redox sensor ERK5 in hyperlipidemic conditions. *Blood,* 129, 2917-2927.

YANG, T. C., CHANG, P. Y. & LU, S. C. 2017b. L5-LDL from ST-elevation myocardial infarction patients induces IL-1 beta production via LOX-1 and NLRP3 inflammasome activation in macrophages. *American Journal of Physiology-Heart and Circulatory Physiology,* 312, H265-H274.

YE, X. C., ZUO, D. D., YU, L., ZHANG, L., TANG, J., CUI, C. C., BAO, L., ZAN, K., ZHANG, Z. H., YANG, X. X., CHEN, H., TANG, H., ZU, J., SHI, H. J. & CUI, G. Y. 2017. ROS/TXNIP pathway contributes to thrombin induced NLRP3 inflammasome activation and cell apoptosis in microglia. *Biochemical and Biophysical Research Communications,* 485, 499-505.

YE, Z. S., ZHONG, L., ZHU, S. N., WANG, Y. N., ZHENG, J., WANG, S. J., ZHANG, J. N. & HUANG, R. C. 2019. The P-selectin and PSGL-1 axis accelerates atherosclerosis via activation of dendritic cells by the TLR4 signaling pathway. *Cell Death & Disease,* 10.

YU, E., MERCER, J. & BENNETT, M. 2012. Mitochondria in vascular disease. *Cardiovascular Research,* 95**,** 173-182.

YUSUF, M. Z., RASLAN, Z., ATKINSON, L., ABURIMA, A., THOMAS, S. G., NASEEM, K. M. & CALAMINUS, S. D. J. 2017. Prostacyclin reverses platelet stress fibre formation causing platelet aggregate instability. *Scientific Reports,* 7.

ZEILER, M., MOSER, M. & MANN, M. 2014. Copy Number Analysis of the Murine Platelet Proteome Spanning the Complete Abundance Range. *Molecular & Cellular Proteomics,* 13**,** 3435-3445.

ZHANG, W., MA, Q., SIRAJ, S., NEY, P. A., LIU, J., LIAO, X., YUAN, Y., LI, W., LIU, L. & CHEN, Q. 2019. Nix-mediated mitophagy regulates platelet activation and life span. *Blood Adv,* 3**,** 2342-2354.

ZHAO, B., DIERICHS, R., LIU, B. & BERKES, P. 1994. GOLD-LABELED LOW-DENSITY LIPOPROTEINS BIND TO WASHED HUMAN PLATELETS. *Platelets,* 5**,** 113-120.

ZHAO, L. L., LIU, J., HE, C. Y., YAN, R., ZHOU, K. X., CUI, Q. Y., MENG, X. J., LI, X. D., ZHANG, Y., NIE, Y. M., HU, R. P., LIU, Y. C., ZHAO, L., CHEN, M. X., XIAO, W. L., TIAN, J. L., ZHAO, Y. X., CAO, L. J., ZHOU, L., LIN, A. N., RUAN, C. G. & DAI, K. S. 2017. Protein kinase A determines platelet life span and survival by regulating apoptosis. *Journal of Clinical Investigation,* 127**,** 4338-4351.

ZHARIKOV, S. & SHIVA, S. 2013. Platelet mitochondrial function: from regulation of thrombosis to biomarker of disease. *Biochemical Society Transactions,* 41**,** 118-123.

ZHOU, R. B., YAZDI, A. S., MENU, P. & TSCHOPP, J. 2011. A role for mitochondria in NLRP3 inflammasome activation. *Nature,* 469**,** 221-225.

ZMIJEWSKI, J. W., MOELLERING, D. R., LE GOFFE, C., LANDAR, A., RAMACHANDRAN, A. & DARLEY-USMAR, V. M. 2005. Oxidized LDL induces mitochondrially associated reactive oxygen/nitrogen species formation in endothelial cells. *American Journal of Physiology-Heart and Circulatory Physiology,* 289**,** H852-H861.

List of Abbreviations

ΔΨm	Mitochondrial membrane potential
αIIbβ3	Integrin alpha 2b beta 3
AC	Adenylyl cyclase
ACD	Acid-citrate dextrose
ADP	Adenosine diphosphate
AA	Antimycin A
APC	Allophycocyanin
APD	Avalanche photo-diode
ASC	Apoptosis-associated speck-like protein containing a CARD
ATP	Adenosine triphosphate
BB	Brilliant blue
BSA	Bovine serum albumin
Ca2+	Calcium ion
CARD	Caspase recruitment domain
cAMP	Cyclic adenosine monophosphate
cGMP	Cyclin guanosine monophosphate
Cu^{2+}	Copper ion
CVD	Cardiovascular disease
CyTOF	Mass cytometry by time-of-flight
DAMP	Danger-associated molecular pattern
DMSO	Dimethyl sulphoxide
ECL	Enhanced chemi-luminescence
EDTA	Ethylenediaminetetraacetic acid
FIIa	Thrombin
FCCP	Carbonyl cyanide-p-trifluoromethoxyphenylhydrazone
FFC	Fluorescent flow cytometry
FITC	Fluorescein
FIt-SNE	Fast Fourier Transform-accelerated Interpolation-based t-SNE
FLICA	Fluorochrome-labelled inhibitors of caspases
FSC	Forward scatter
GP1b-IX-V	Glycoprotein Ib-IX-V
GPVI	Glycoprotein VI

HRP	Horseradish peroxidase
IB	Immunoblot
IL-1β	Interleukin-1 beta
IP	Immunoprecipitation
IPR	Prostacyclin receptor
LDL	Low-density lipoprotein
LPS	Lipopolysaccharide
LTA	Light transmission aggregometry
Mg^{2+}	Magnesium ion
NAC	n-acetyl-cysteine
nLDL	Native low-density lipoprotein
NLRP3	Nacht-leucine rich repeat pyrin domain containing protein 3
NO	Nitric oxide
oxLDL	Oxidised low-density lipoprotein
PAGE	Polyacrylamide gel electrophoresis
PAMP	Pathogen-associated molecular pattern
PAR	Protease-activated receptor
PBMC	Peripheral blood mononuclear cell
PBS	Phosphate-buffered saline
PE	phycoerythrin
PDE	Phosphodiesterase
PerCP	Peridinin-Chlorophyll-protein
PGI_2	Prostaglandin I_2 (Prostacyclin)
PFD	Pore forming domain
PKA	Protein kinase A
PKC	Protein kinase C
PKG	Protein kinase G
PMN	Polymorphonuclear leukocyte
PPP	Platelet poor plasma
PRP	Platelet rich plasma
PYD	Pyrin domain
RD	Repressor domain
ROS	Reactive oxygen species

SD	Standard deviation
SDS	Sodium dodecyl sulphate
Ser	Serine
sGC	Soluble guanylyl cyclase
SOX	Superoxide
SSC	Side scatter
t-SNE	t-Stochastic Neighbourhood Embedding
TBS(-T)	Tris-buffered saline(-Tween 20)
TLR	Toll-like receptor
TMRE	Tetramethyl rhodamine ethyl ester
VASP	Vasodilator-stimulated phosphoprotein
vWF	Von Willebrand factor
WCL	Whole cell lysate
WP	Washed platelets